

Dissertation zur Erlangung des Doktorgrades
der Fakultät Chemie und Pharmazie
der Ludwig-Maximilians-Universität München

Understanding Spin Crossover: A Contribution

Wolfgang Manfred Bauer
aus
Landsberg am Lech

2011

Erklärung:

Diese Dissertation wurde im Sinne von § 13 Abs. 3 bzw. 4 der Promotionsordnung vom 29. Januar 1998 (in der Fassung der vierten Änderungssatzung vom 26. November 2004) von Frau Prof. Dr. Birgit Weber betreut.

Ehrenwörtliche Versicherung:

Diese Dissertation wurde selbständig, ohne unerlaubte Hilfe erarbeitet.

München, 14. April 2011

Wolfgang Bauer

Dissertation eingereicht am: 14. April 2011

1. Gutachter: Prof. Dr. B. Weber

2. Gutachter: Prof. Dr. D. Johrendt

Mündliche Prüfung am: 27. Mai 2011

Wenn du ein Problem hast, versuche es zu lösen.

Kannst du es nicht lösen, dann mache kein Problem daraus.

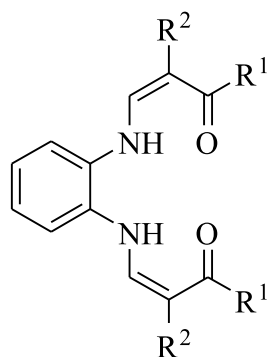
SIDDHARTHA GAUTAMA

Contents

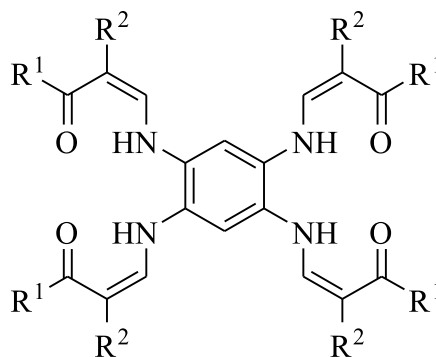
Contents.....	I
Abbreviations	III
1 Introduction	1
1.1 Thermal Spin Transition.....	2
1.2 Theoretical Aspects of the Spin Crossover	4
1.3 Detecting the Spin Crossover	7
2 Summary	9
2.1 The Ligand System.....	9
2.2 The Purposeful Design of Stepwise Spin Transitions	11
2.3 Spin Transitions in Solution	14
2.4 The Crystal Contact Index.....	15
2.5 The Solvent Effect.....	15
2.6 A New Model for the Explanation of Wide Hysteresis Loops	17
2.7 Synthesis of SCO Compounds in a Crystal Engineering-like Approach	19
2.8 References	21
3 Individual Contribution to Joint Publication.....	27
4 Two-Step <i>versus</i> One-Step Spin Transition in Iron(II) 1D Chain Compounds	33
4.1 Introduction	34
4.2 Results	38
4.3 Discussion	59
4.4 Conclusion.....	61
4.5 Experimental Section	62
4.6 References	66
4.7 Supporting Information	70
5 X-Ray Structure and Magnetic Properties of Dinuclear and Polymer Iron(II) Complexes.....	75
5.1 Introduction	76
5.2 Results and Discussion.....	78
5.3 Conclusion.....	85
5.4 Experimental Section	86
5.5 References	89
5.6 Supporting Information	91
6 X-Ray Structure and Magnetic Properties of Two New Iron(II) 1D Coordination Polymers with Bis(imidazolyle)-methane as Bridging Ligand	95
6.1 Introduction	95
6.2 Results and Discussion.....	97
6.3 Conclusion.....	102
6.4 Experimental Section	103
6.5 References	105
6.6 Supporting Information	108
7 Complete and Incomplete Spin Transitions in 1D Chain Iron(II) Compounds	111
7.1 Introduction	112
7.2 Results and Discussion.....	113
7.3 Conclusion.....	129
7.4 Experimental Section	130
7.5 References	132

7.6	Supporting Information	136
8	A Promising New Schiff Base-like Ligand for the Synthesis of Octahedral Iron(II) Spin Crossover Complexes	139
8.1	Introduction	139
8.2	Results and Discussion.....	140
8.3	Conclusion.....	146
8.4	Experimental Section	147
8.5	References	149
8.6	Supporting Information	151
9	Complete Two-Step Spin-Transition in a 1D Chain Iron(II) Complex with 110 K Wide Intermediate Plateau	153
9.1	Introduction	154
9.2	Results	156
9.3	Discussion	170
9.4	Conclusion.....	171
9.5	Experimental Section	172
9.6	References	175
9.7	Supporting Information	179
10	Influence of Hydrogen Bonding on the Hysteresis Width in Iron(II) Spin Crossover Complexes.....	181
10.1	Introduction	182
10.2	Results	184
10.3	Discussion	202
10.4	Conclusion.....	207
10.5	Experimental Section	208
10.6	References	212
10.7	Supporting Information	217
11	Unusual Stepped Spin Transitions at Iron(II) Coordination Polymers with zigzag-Structure	221
11.1	Introduction	221
11.2	Results	223
11.3	Conclusion.....	234
11.4	Experimental Section	235
11.5	References	238
11.6	Supporting Information	241
12	Increasing the Hysteresis Width of Iron(II) SCO Compounds in a Crystal Engineering-like Approach	243
12.1	Introduction	243
12.2	Results	246
12.2.1	The Ligand System H ₂ L1	247
12.2.2	The Ligand System H ₄ L2.....	256
12.2.3	The Ligand System H ₂ L3	260
12.3	Discussion	267
12.4	Conclusion.....	269
12.5	Experimental Section	270
12.6	References	278
12.7	Supporting Information	281

Abbreviations

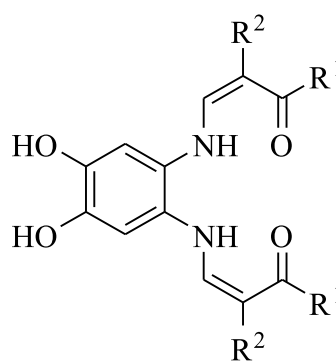


H₂L1



H₄L2

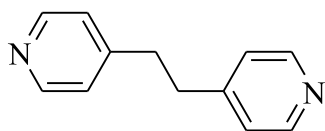
- a: R¹ = Me; R² = CO₂Et
 b: R¹ = Me; R² = COMe
 c: R¹ = Me; R² = CO₂Me
 d: R¹ = Me; R² = COPh
 e: R¹ = Ph; R² = CO₂Et



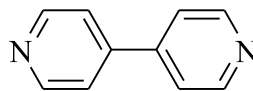
H₂L3

Scheme 1. Overview of the Schiff base-like tetradentate equatorial ligands discussed in this work and the used abbreviations.

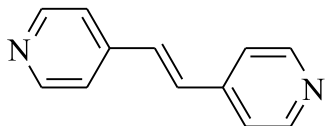
Abbreviations



1,2-Bis(4-pyridyl)ethane (bpea)



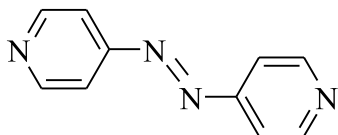
4,4'-Bipyridine (bipy)



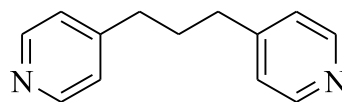
trans-1,2-Bis(4-pyridyl)ethylene (bpee)



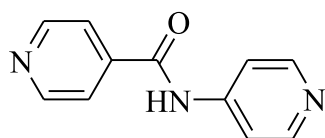
Bis(1-imidazolyle)methane (bimm)



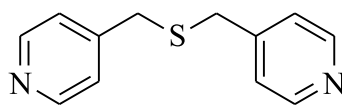
4,4'-Azopyridine (azpy)



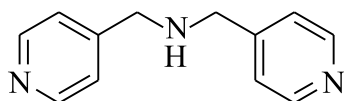
1,3-Bis(4-pyridyl)propane (bppa)



N-(4-Pyridyl)isonicotinamide (pina)



Bis(4-pyridylmethyl)sulfane (bpms)



Bis(4-pyridylmethyl)amine (bpma)

Scheme 2. Overview of the bidentate axial ligands discussed in this work and the used abbreviations.

Abbreviations

CCI	crystal contact index
DSC	differential scanning calorimetry
DTG	differential thermogravimetry
EXAFS	extended X-ray absorption fine structure
HS	high-spin
IP	intermediate plateau
IR	infrared spectroscopy
L_{ax}	axial ligand
L_{eq}	equatorial ligand
LIESST	light induced excited spin state trapping
LS	low-spin
MS	mass spectrometry
NMR	nuclear magnetic resonance
SCO	spin crossover
SQUID	superconducting quantum interference device
ST	spin transition
UV-Vis	ultraviolet-visible spectroscopy
γ_{HS}	molar high-spin fraction
k_B	Boltzmann constant
S	spin (quantum number)
$T_{1/2}$	spin transition temperature ($\gamma_{HS} = 0.5$)
χ_M	molar susceptibility

1 Introduction

The research on novel magnetic materials for application is confronted with two great challenges. On the one side, in the course of technological development in micro-electronics, the miniaturisation of the employed magnetic components plays an increasing role, which will certainly end up on the molecular scale.^[1] As miniaturisation with a top-down approach is limited by the spatial resolution of the lithography, the manufacturing of such materials follows the bottom-up approach, which uses the concepts of molecular self-assembly or molecular recognition to cause single molecules into some useful conformation.^[1,2] The current challenge in this field is to control the cluster size towards the levels required whilst retaining the magnetic/cooperative properties.^[1,3] On the other side, conventional inorganic magnetic materials (metals, oxides, alloys) are still unrivalled in many fields. Despite disadvantageous metallurgical manufacturing processes, their application-specific characteristics like magnetic saturation, the coercivity field or critical temperature can be modulated over a broad spectrum.^[4] Thus, the development of novel molecule-based magnetic materials does not primarily aim for optimising these magnetic characteristics, but for the combination of magnetic properties with interesting material properties from the technological point of view. Therefore, this field of research is focussed on the creation of a complete new branch of multifunctional magnetic materials.^[4] As an example, the combination of magnetic and optical properties envisions applications in the field of display devices.^[1,5]

Materials that show magnetic switching such as spin crossover (SCO), where multiple electronic states can be accessed through variation in external stimuli like temperature, pressure and light, have been identified as a viable class of materials for incorporation into devices and potential applications^[3]—in particular, when they show properties that depend on the history of the system, which results in hysteresis.^[6] This confers bistability on the system and thus a memory effect, which is of great interest as this aspect holds the potential for exploitation in display and memory device units,^[1,5] sensing devices^[7] and cold channel control units in food and medical storages.^[8] In this regard, a rapid development of multifunctional SCO materials has begun.^[9] The current stage of investigation is focused much on the interplay and synergic effects between SCO, magnetic coupling, liquid crystalline properties, host-guest interactions, non-linear optical properties, electrical

conductivity and ligand isomerisation,^[9,10,11] or is attended to the rational design of nano-structured SCO materials and their chemical and physical properties.^[12] However, the purposeful design and synthesis of such materials is still a great challenge for preparative chemists. Having this in mind, this work focuses not only on the synthesis and characterisation of new SCO compounds with interesting magnetic behaviour, but also on the development of new concepts to understand and explain the observed results.

1.1 Thermal Spin Transition

The thermal induced spin transition (ST, spin crossover, SCO) is one of the most fascinating and most extensively explored dynamic electronic structure phenomena in coordination chemistry and a very promising type of molecular magnet. SCO materials can be switched on the molecular level between two (or more) different electronic states, which can be easily detected by different means, as the switching process is associated with a change of the physical (magnetic, optical) properties.^[5,6] Similar as observed for ferromagnetic materials, the switching process may be accompanied by hysteresis effects, but in contrast, this is due to a spin state change of the SCO system, in the best of cases between the paramagnetic high-spin and diamagnetic low-spin state, instead of a re-orientation of the magnetisation. Besides temperature, other external physical parameters such as pressure, magnetic fields or electromagnetic radiation, here the most thoroughly investigated and most interesting phenomenon is the LIESST-effect,^[13] or chemical parameters such as counter-ions, substituent and solvent effects influence the spin transition. These aspects are well understood by now. A long time has passed by, since the first observation of a thermal spin crossover complex by Cambi *et al.* in 1931^[14] and the first characterisation of an iron(II) SCO complex in 1964.^[15] From then on, this field of research has experienced a lively development. One primary focus has been the nature of the cooperative interactions between the spin state changing complex molecules; these have been recognised as being responsible for special features of the spin transition characteristics such as temperature and abruptness of the transition and hysteresis effects.^[9a] However, the occurrence of hysteresis is to date hardly predictable and not yet fully understood. There are two principal explanations for the origin of hysteresis during a spin transition: the transition may be associated with a structural phase change in the lattice; or the intramolecular structural changes that occur along with a transition may be propagated throughout the solid to neighbouring molecules via a highly

effective cooperative interaction between the molecules.^[6c] The mode of this interaction is not always clear, but three principal strategies have been adopted in an attempt to generate it: (i) incorporation of aromatic moieties into the ligand structure which promote π - π -interactions through stacking throughout the lattice (this also includes van der Waals interactions): a 40 K wide hysteresis loop was reported due to π -stacking;^[16] (ii) incorporation of hydrogen bonding centres into the coordination environment allowing interaction either directly with other SCO centres or via anions or solvate molecules: a 70 K wide hysteresis loop was observed due to a two-dimensional hydrogen bonding network;^[17] (iii) linkage of the spin-active metal centres via covalent bonds to dinuclear systems or via covalent bridging molecules (linkers) to coordination polymers. This idea was suggested by Kahn *et al.*, in order to get control over the expansion of intermolecular interactions more efficiently compared to “non-covalent” interactions mentioned at (i) and (ii).^[18] This resulted in the synthesis and characterisation of several iron(II) SCO coordination polymers in the recent years, especially one-dimensional coordination polymers as well as dinuclear systems that exhibit *e.g.* a N_4O_2 -coordination sphere.^[19a]

The thermal spin crossover of single molecules in solution is always gradual and follows a Boltzmann distribution, as all packing effects are switched off.^[6c] In the solid state, such a spin transition curve can be observed, too, but extensive cooperative interactions give rise to various spin transition behaviours including the occurrence of hysteresis, as displayed in Figure 1.

Several chemical parameters influence the spin transition behaviour: non-coordinated counterions or solvent molecules incorporated in the crystal lattice may enhance or diminish cooperativity;^[20] the substitution of ligands or different substituents at the ligand may influence the ligand field strength, as could be shown on N_4O_2 -coordinated iron(II) compounds, for example;^[19] isotope effects have been observed upon partly deuteration of the investigated complexes.^[21] Moreover, the preparation of the sample can play a significant role: grinding of a crystalline compound may cause crystal defects which disturb the cooperative effects.^[22]

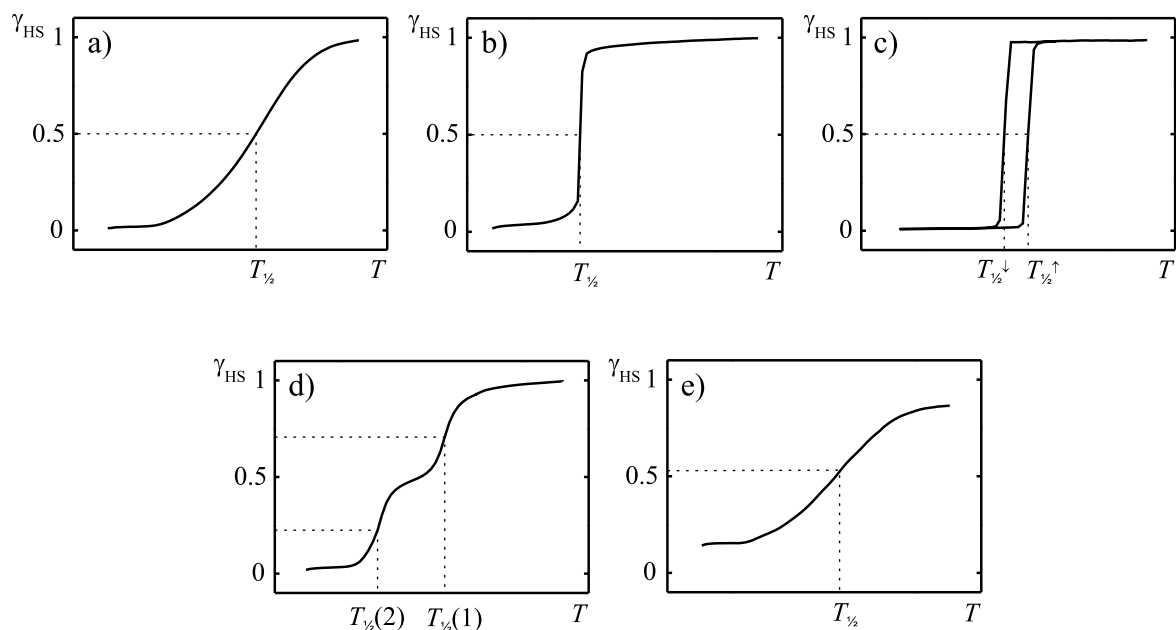


Figure 1. Schematic representation of the different types of thermal spin transition (high-spin fraction (γ_{HS}) vs. temperature (T)) observable in the solid state: a) gradual; b) abrupt; c) with hysteresis; d) stepwise; e) incomplete. The spin transition temperature $T_{1/2}$ is defined as the temperature at which 50% of the SCO-active complex molecules have changed their spin state.^[6e]

1.2 Theoretical Aspects of the Spin Crossover

In principal, spin crossover is feasible for ions with d^4 – d^7 electronic configuration and is observed for all these in octahedral coordinated complexes of first transition series ions.^[6e] In these cases, a spin state with maximum (low-spin, LS) and minimum (high-spin, HS) spin pairing is thinkable, depending in first approximation on the ligand field splitting energy Δ (or parameter $10Dq$) relative to the mean spin pairing energy P (HS: $\Delta \ll P$; LS: $\Delta \gg P$). Of the ions which do show typical spin crossover behaviour, the largest number of examples is found for the configuration d^6 and among these, iron(II) accounts for the vast majority: for Fe(II), on the one side, the low-spin d^6 -configuration has maximum ligand field stabilisation energy; on the other side, the relatively large Fe(II) ion induces a weaker ligand field in most ligands, contrary, for example, to the smaller Co(III) ion, at which the LS configuration is almost always adopted. Hence spin pairing is not so strongly favoured and it is possible to obtain relatively stable high-spin ($S = 2$) or low-spin ($S = 0$) complexes for a broad range of ligands.^[6e]

Whether a complex shows spin crossover or not, decisively depends on the ligand field strength. The Tanabe-Sugano-diagram^[23] of Fe(II) (Figure 2) displays that, for complexes with weak-field ligands, the HS- 5T_2 -state results as the ground state, which arises from the 5D -ground state of the free ion. With increasing $10Dq$ the energy of the LS- 1A_1 -state, which arises from the 1I -state of the free ion, is rapidly decreased compared to the 5T_2 -state. Thus, from a critical ligand field strength Δ_{crit} on, the LS- 1A_1 -state becomes the ground state, synonymic to Fe(II) complexes with strong field ligands

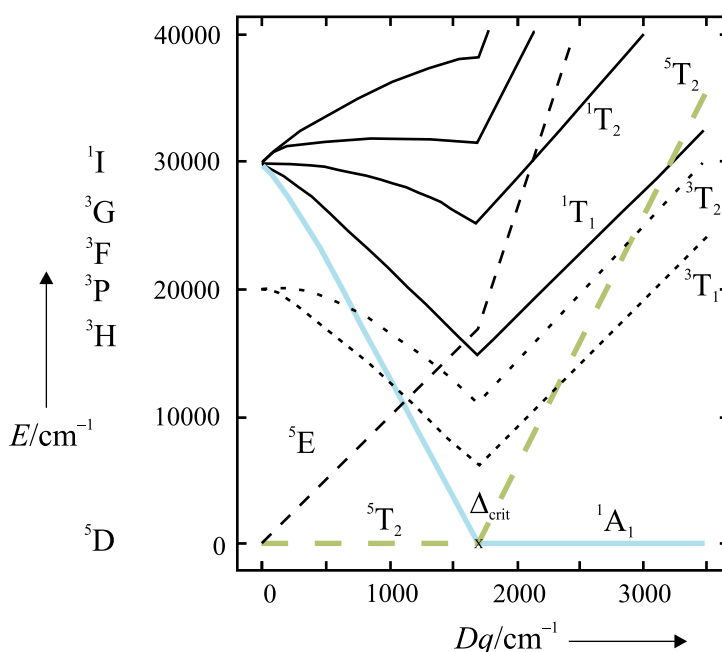


Figure 2. Tanabe-Sugano-diagram of an octahedral complex, calculated by using the Racah parameters^[24] of the free iron(II) ion according to Tanabe and Sugano,^[23] with the 5T_2 - (green) and the 1A_1 -state (blue) highlighted.

However, as the ligand field splitting depends not only on the properties of the ligand but also on the metal-to-ligand distance r , the electronic energies of the particular spin states have to be considered as a function of r (Figure 3). Independent of the ligand properties, the 5T_2 -potential well is shifted to a higher metal-to-ligand distance compared to the 1A_1 -potential well, as two electrons occupy the σ -anti-bonding e_g -orbitals in the HS state ($t_{2g}^4 e_g^2$ configuration), whereas the six d-electrons are situated in the σ -non-bonding t_{2g} -orbitals in the LS state (t_{2g}^6 configuration), which affects the bond lengths in a minor degree. X-Ray structural studies on SCO iron(II) complexes have shown that the spin state depending metal-to-donor atom bond length change amounts to significantly 5–10%.^[6] The vertical shifting of

both potential wells relative to each other, on the contrary, strongly depends on the properties of the ligand. Spin crossover is expected, when the zero-point energy difference of both states ($\Delta E_{\text{HL}}^0 = E_{\text{HS}}^0 - E_{\text{LS}}^0$) is in the order of magnitude of the thermal energy ($k_{\text{B}} T \approx \Delta E_{\text{HL}}^0 \approx 200 \text{ cm}^{-1}$ at $T = 295 \text{ K}$). In this case, at low temperatures, the ${}^1\text{A}_1$ -state of lowest enthalpy is the thermodynamically stable ground state. On the other side, at temperatures higher than a critical temperature T_{crit} , the ${}^5\text{T}_2$ -state becomes the thermodynamically stable state, as the entropy associated with the HS state is much larger than the entropy associated with the LS state and therefore the entropy gain overcomes the enthalpy loss.^[5a] In detail, approximately 25% of the total entropy gain accompanying the LS to HS change arises from the change in spin multiplicity. The major contribution originates from changes in the intramolecular vibrations.^[6e,25] Against this background, ranges for $10Dq^{\text{HS}}$ and $10Dq^{\text{LS}}$ can be specified, at which HS, LS or SCO complexes are expectable (Scheme 1).

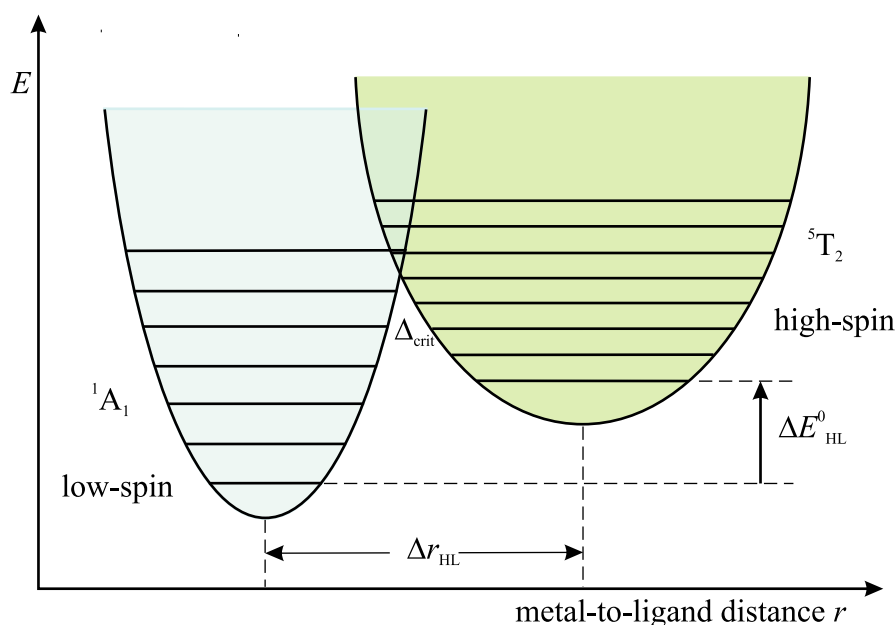


Figure 3. Schematic representation of the HS- ${}^5\text{T}_2$ - (green) and LS- ${}^1\text{A}_1$ -potential well (blue) for an octahedral iron(II) complex in dependence of the metal-to-ligand distance (r). The crossing point of both wells (Δ_{crit}) corresponds to the critical ligand field strength in the Tanabe-Sugano-diagram.

$10Dq^{\text{HS}} < 11000 \text{ cm}^{-1}$	HS complex
$10Dq^{\text{HS}} \approx 11500\text{--}12500 \text{ cm}^{-1}$ and $10Dq^{\text{LS}} \approx 19000\text{--}21000 \text{ cm}^{-1}$	spin crossover complex
$10Dq^{\text{LS}} > 21500 \text{ cm}^{-1}$	LS complex

Scheme 1. $10Dq$ -ranges at which HS, LS or SCO complexes are expectable.

1.3 Detecting the Spin Crossover

There are various methods and techniques to follow a spin transition. A complete overview of the experimental methods that are commonly used is provided by Table 1. Most of these methods are aimed at the temperature-dependent determination of the magnetic susceptibility,^[26] which reflects the momentary spin state in the value of the measured magnetic moment. Among these methods, the Gouy- and the Faraday-balance are the oldest examples, but both methods have become less important because they can only operate at ambient temperature. Modern methods like the Foner magnetometer (vibrating sample magnetometer) or the SQUID magnetometer use the effect of electromagnetic induction to determine the susceptibility depending on the temperature and the applied magnetic field. A SQUID is a very sensitive magnetometer, used to measure extremely weak magnetic fields. The basic principles of this device are related to superconductivity and quantum tunneling. Moreover, paramagnetic temperature-dependent NMR spectroscopy can be used to determine the magnetic susceptibility of a compound, especially in solution. However, the temperature range of this method is limited to the cold and boiling point of the solvent. The experimental NMR setup is known as the Evans-method,^[27] which compares the absolute shifting of the nuclei in a paramagnetic solution with a diamagnetic reference by using an external reference signal. For some complexes, the SCO in solution can be directly evaluated by interpretation of the temperature-dependence of their ^1H NMR chemical shifts, rather than interpreting the susceptibility.^[28,29]

Temperature-dependent X-ray structure analysis directly benefits from the structural changes following a spin transition and provides information on the metal-to-ligand bond lengths and angles within the inner coordination sphere of the central ion depending on its spin state.

A further important method, in particular for ^{57}Fe containing samples, is Mössbauer spectroscopy,^[30] which is based on the recoil-free resonant absorption and emission of gamma rays in solids. This method probes tiny changes in the energy levels of an atomic nucleus in response to its environment. The mainly observed types of interaction are the isomer shift, which provides information about the spin state and the oxidation state, and the quadrupole splitting, which is influenced by the spin state and the coordination sphere of the central ion. Due to the high energy and extremely narrow line widths of gamma rays, Mössbauer spectroscopy is one of the most sensitive techniques.^[31]

Heat capacity measurements (*e.g.* differential scanning calorimetry (DSC)) on SCO compounds provide important thermodynamic quantities, such as enthalpy or entropy changes accompanied with a spin transition, moreover, the transition temperature and the order of the transition.^[6e,25]

Table 1. Overview of the experimental methods most commonly used to follow a spin transition.

analytical method	characteristic value
Magnetic measurements	magnetic susceptibility (effective magnetic moment)
Calorimetry	heat capacity
Mössbauer spectroscopy	isomer shift, quadrupole splitting
NMR spectroscopy	paramagnetic chemical shift, magnetic susceptibility
Vibrational spectroscopy	metal-ligand vibrational wavenumber
UV-Vis spectroscopy	d-d/CT excitation energy
X-Ray structure analysis	metal-to-ligand distance
EXAFS measurements	metal-to-ligand distance

2 Summary

2.1 The Ligand System

This work deals with the synthesis and characterisation of new one-dimensional iron(II) SCO coordination polymers which exhibit an octahedral N_4O_2 -coordination sphere around the iron centres. On the one side, new tetradentate equatorial ligands were synthesised, which base on the Schiff base-like ligand system developed by Jäger *et al.*^[32] On the other side, new bidentate bipyridine and bisimidazole derivatives were synthesised which, offer the ability to link the complexes at the axial position to infinite 1D chains. Through specific variation of functional groups at the equatorial ligands (*e.g.* hydroxy groups, phenyl groups), it was possible to optimise the interactions between the chains (inter-molecular interactions, *e.g.* hydrogen bonds, π -stacking). These functional groups also influence the ligand field at the central atom, but this effect plays a minor role for the system presented here.^[19]

The free equatorial ligand offers two possible tautomeric structures with enol-imine functional groups or keto-enamine, respectively. Using the example of the newly developed ligand H_2L1c , it could be proven by 1H NMR-spectroscopy (Figure 4) and X-ray structure analysis (Figure 5) that the equilibrium is shifted to the keto-enamine structure.^[33] This is in contrast to classic Schiff base ligands like the salen ligand, for example. Upon coordination to a metal centre, the bond lengths of the conjugated π -system of the deprotonated ligand indicate a balance between both contributing structures and a delocalisation of the negative charge over the six-membered chelate ring.^[33]

Manifold combinations from a ligand pool, containing 9 axial and 9 equatorial partial newly developed ligands, allowed the synthesis of numerous SCO compounds with versatile spin transition behaviours: from gradual or abrupt, to stepwise and with thermal hysteresis. Through detailed investigation of the outcomes of magnetic measurements, X-ray structure analysis, Mössbauer spectroscopy, DSC and paramagnetic NMR spectroscopy in solution, new models were developed in this work to explain the formation of stepwise spin transitions and wide thermal hysteresis loops, as observed for some of the compounds presented. On the way to the purposeful synthesis of SCO materials and a better understanding and predictability of the SCO phenomenon, this is highly important.

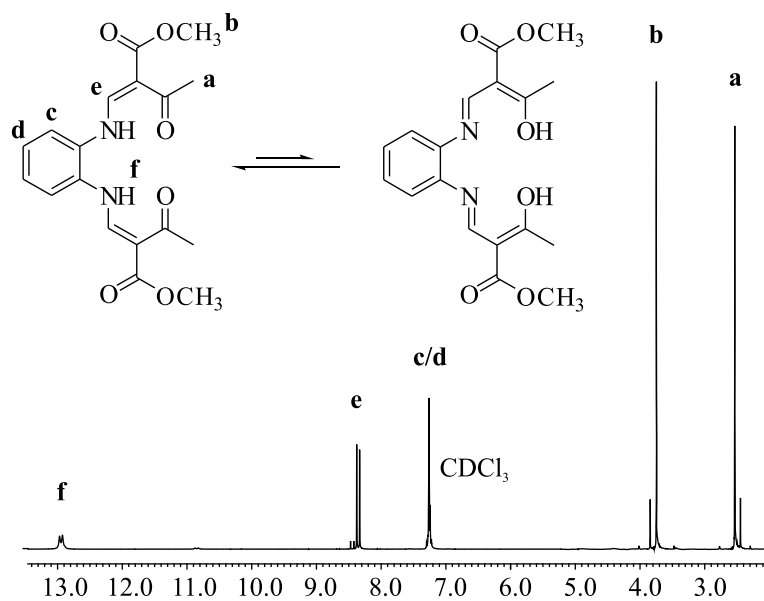


Figure 4. ^1H NMR spectrum (in CDCl_3) of the free equatorial ligand $\text{H}_2\text{L}1\text{c}$ with the signal assignment and the thinkable tautomeric structures “keto-enamine” (left) and “enole-imine” (right) given.

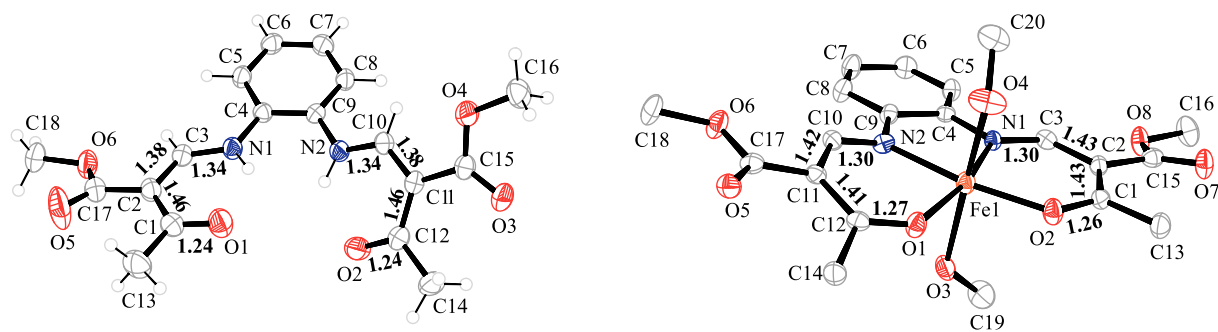


Figure 5. Molecular structures of the free equatorial ligand $\text{H}_2\text{L}1\text{c}$ and the corresponding iron(II) complex with methanol as axial ligands. For comparison the bond lengths [\AA] of the conjugated π -systems are given. The hydrogen atoms at the complex structure were omitted for clarity.

2.2 The Purposeful Design of Stepwise Spin Transitions

A quite often observed behaviour of 1D SCO coordination polymers synthesised so far, was a stepwise or incomplete spin transition with an intermediate plateau at 50% HS residue. Next to highly cooperative systems, stepwise transitions between three or more states attracted the interest of several research groups, because of the versatile switching possibilities.^[34] To date, three different models are discussed for describing stepwise spin transitions. The most common among these are systems that have multiple crystallographically distinct metal centres at all temperatures, which undergo the spin transition at different temperatures.^[29,35] Secondly, there are examples that undergo structural phase transition in which one unique metal site at high temperatures converts to two sites upon cooling through the first step.^[36,37] Lastly, and most often related to dinuclear complexes, this type of SCO is explained with the formation of [HS-HS], [HS-LS] and [LS-LS] spin pair states.^[34]

To define rules for the purposeful synthesis of 1D SCO materials with two-step spin transitions, these phenomenological models are not applicative. In this work, detailed investigations on one-dimensional SCO coordination polymers provided a decisive insight into the influence of covalent linkers on the spin transition properties. The outcomes of magnetic measurements led to the conclusion that no magnetic interactions are mediated over the bridging axial ligands,^[38] which is essential for the formation of spin pair states, as mentioned before. The results demonstrated in addition that covalent linkers do not have the ability to directly transmit elastic interactions within the crystal lattice, but indirectly, as the number of intermolecular contacts (hydrogen bonds, van der Waals interactions, π -stacking) is increased.^[19a] Moreover, they can be used to optimise the packing of the molecules in a crystal engineering-like approach.^[19a] The outcomes of X-ray structure analysis revealed that the type of spin transition correlates well with the “flexibility” of the bridging ligand and the resulting chain structure, as displayed in Figure 6: for rigid linker molecules like 4,4'-bipyridine, more often SCO compounds with hysteresis were detected, whereas flexible ligands like 1,3-bis(4-pyridyl)propane or bis(1-imidazolyl)methane, which result in the formation of pronounced zigzag chain structures, more likely led to stepwise spin transitions, even if all iron centres are crystallographically equivalent in the HS state.^[39] With regard to the plateau in the transition curve, the width of the step (culminating in incomplete spin transitions) is strongly dependant of the intensity of intermolecular contacts, as without the occurrence of significant interactions only gradual SCO were observed.^[39,40]

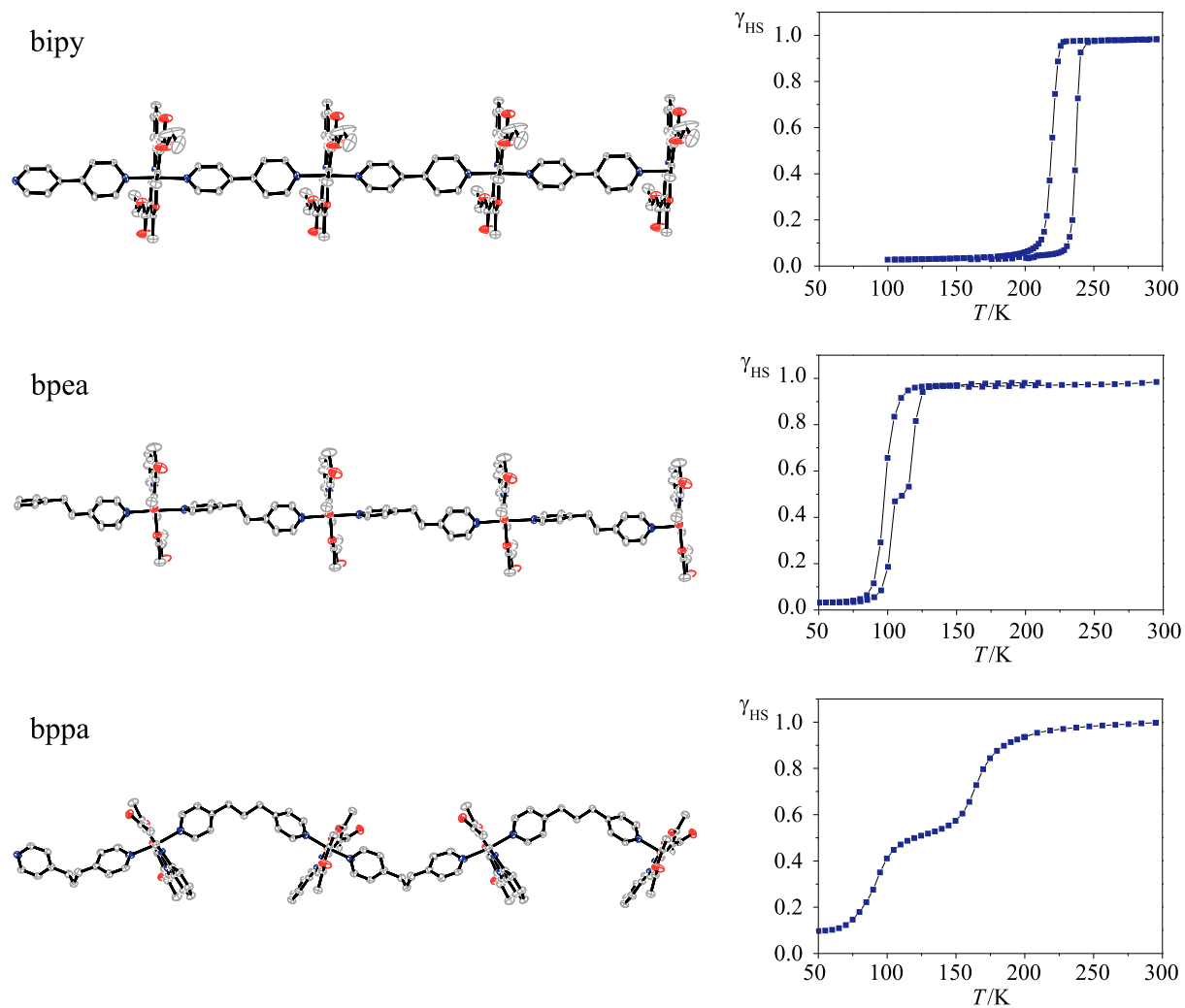


Figure 6. Excerpts of the chain structures and the corresponding magnetic measurements of compounds [FeL1b(bipy)] (top, ST with hysteresis), [FeL1b(bpea)] (middle, stepwise ST with hysteresis) and [FeL1b(bppa)] (bottom, stepwise ST).

2. Summary

The findings about the influence of the bridging ligand on the spin transition behaviour gathered in this work, allowed the development of a concept for the rational design of spin crossover materials with stepwise spin transition in 1D chain compounds: a HS to LS transition involves a relocation of the ligands towards the smaller LS molecule. If the distances of neighbouring metal centres within a chain structure cannot exactly follow the changes of the metal-to-ligand bond length at the LS centre due to restraining interactions (sterical hindrance), then the corresponding bonds at the neighbouring centres are elongated and thus the HS state is stabilised (Figure 7). For bridging ligands which lead to pronounced zigzag structure motives restraining interactions can be more easily imagined compared to linear chains.^[39]

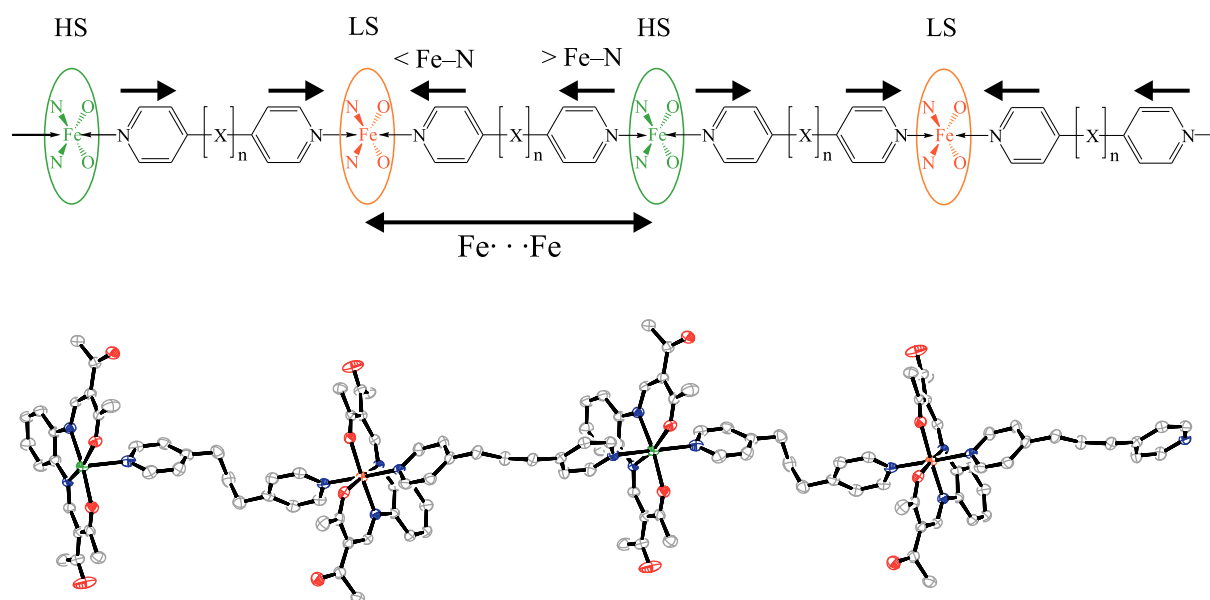


Figure 7. Top: schematic representation of the intrachain bond length changes upon SCO to illustrate the formation of stepwise spin transitions. Bottom: excerpt of a pronounced zigzag chain structure with alternating HS-LS centres along the chain (X = CH₂, n = 0-3).

2.3 Spin Transitions in Solution

The investigation of spin transitions in solution is a valuable tool to prove the influence of intermolecular interactions or covalent linkers on the spin transition temperature, as in solution all packing effects are switched off.^[28]

In this work, for the first time, the spin transition of two iron(II) SCO coordination polymers, which exhibit stepwise spin transitions in the solid state, was followed in solution by temperature-dependent paramagnetic ^1H NMR-spectroscopy.^[39] The outcomes for complex [FeL1a(bppa)] are shown in Figure 8. The signal assignment confirmed that all iron centres retain their octahedral coordination sphere and therefore, the 1D coordination polymers are still intact in solution. In comparison with the corresponding solid samples, the obtained transition temperatures are abundantly clearly shifted to higher temperatures. Moreover, both complexes show gradual spin transitions in solution. These huge differences in SCO behaviour demonstrated that the extent of cooperative interactions as well as the transition temperature is significantly influenced by packing effects, and the covalent linkers do not propagate the cooperative effects.^[39]

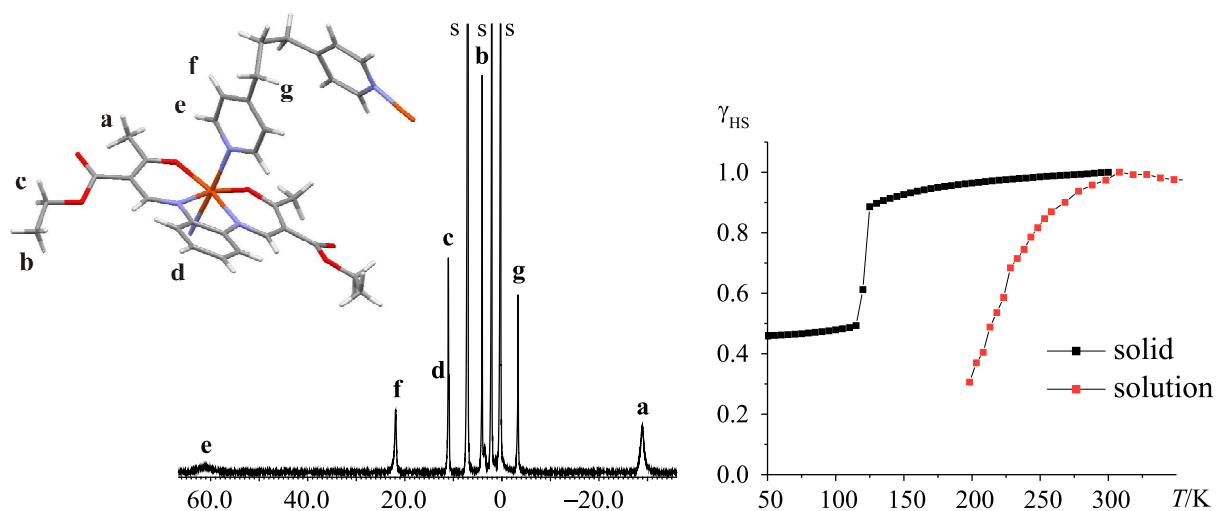


Figure 8. Left: ^1H NMR spectrum and signal assignment for iron(II) SCO coordination polymer [FeL1a(bppa)] in $[\text{D}_8]\text{toluene}$ at $75\text{ }^\circ\text{C}$ ($s = \text{solvent}$). Right: HS molar fraction vs. temperature for [FeL1a(bppa)] followed in solution and in the solid state.

2.4 The Crystal Contact Index

Aiming to quantitatively evaluate the influence of intermolecular interactions on spin crossover properties, the crystal contact index (CCI) was established, which correlates the sum of short contacts with the strength of the cooperative effect.^[40] It provides a good estimation to accompany the structural interpretation of spin transition properties obtained by X-ray structure analysis and, moreover, allows a qualitative comparison between the SCO behaviour of different materials. Therefore, the CCI values of several mononuclear and dinuclear SCO complexes as well as coordination polymers were tabulated.^[40] To some extent, the CCI can also be applied to other systems.

It was found that, up to spin transitions with small hysteresis loops, the above described correlation is in agreement with the model of elastic interactions mediating the structural rearrangements during the cooperative SCO in the solid phase. In the case of spin transition compounds with wider hysteresis loops the correlation fails, which indicates that there are additional mechanisms responsible for cooperative interactions. The CCI can also be used to estimate, if solvent molecules included in the crystal packing contribute to the cooperative effects or have dilution effects.^[40]

2.5 The Solvent Effect

The solvent effect describes the influence of molecules (solvent, ligand molecules or counterions), which are additionally intercalated into the crystal lattice besides the complex, on the spin transition behaviour. This effect is hardly predictable, as, on the one side, there are examples at which the transmission of elastic interactions is improved (positive effect),^[40,41] on the other side, it is well known that such molecules may have a dilution effect and by this inhibit intermolecular contacts (negative effect).^[42] The SCO coordination polymer [FeL1a(bpea)]^[39] is an example of a positive solvent effect: for the solvent-free sample, only a gradual spin transition was observed, whereas the methanol-containing sample (one methanol molecule per asymmetric unit hydrogen bonded to the equatorial ligand) exhibited a 27 K wide hysteresis loop.

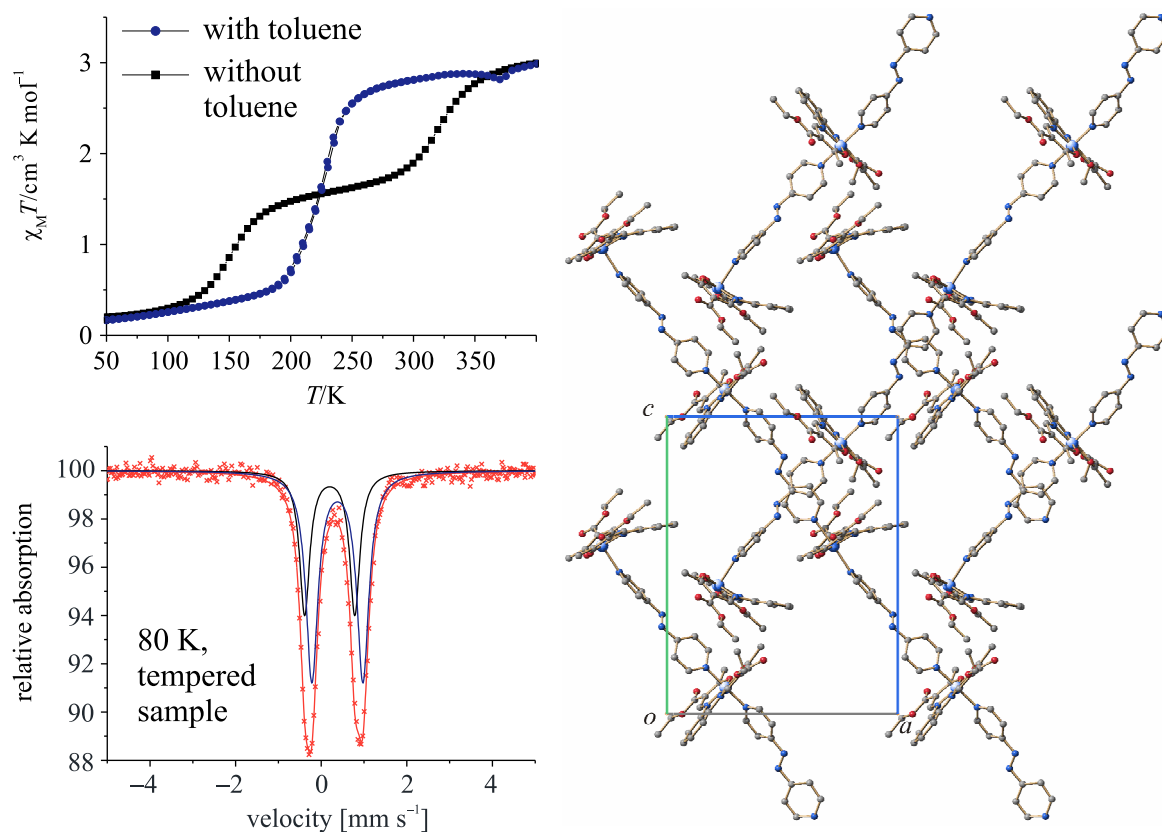


Figure 9. Top left: plot of the $\chi_M T$ product vs. T for the toluene-containing compound $[\text{FeL1a}(\text{azpy})]\cdot\text{tol}$ (blue circles) and the solvent-free sample after being tempered at 400 K (black squares). Bottom left: Mössbauer spectra of $[\text{FeL1a}(\text{azpy})]$ (temp) at 80 K consisting of a LS quadrupole split doublet (red) with a wide line width suggesting two (or more) nonequivalent iron centres (blue, black). Right: molecule packing of $[\text{FeL1a}(\text{azpy})]$ projected in the ac -plane.

An impressive example of a negative effect is the pair $[\text{FeL1a}(\text{azpy})]/[\text{FeL1a}(\text{azpy})]\cdot\text{tol}$ (tol = toluene),^[43] which was thoroughly investigated in this work: the solvent-free system showed a two-step SCO with 110 K wide intermediate plateau (IP) at $\gamma_{\text{HS}} = 50\%$, whereas the toluene-containing sample (one toluene molecule per asymmetric unit) showed a gradual SCO, as shown in Figure 9. However, after being heated to 400 K, the loss of the included toluene molecules resulted in a two-step spin transition very similar to the solvent-free sample. To the best of our knowledge, the 110 K wide IP of $[\text{FeL1a}(\text{azpy})]$ is the widest obtained so far for 1D coordination polymers. The related compound $[\text{FeL1c}(\text{azpy})]$ also provided a two-step SCO with 75 K wide IP.^[43] This led to the presumption that the bridging ligand 4,4'-azopyridine plays a decisive role regarding this phenomenon. The results of X-ray structure analysis and Mössbauer spectroscopy (Figure 9) for $[\text{FeL1a}(\text{azpy})]$ proved the presence of crystallographically distinct iron(II) centres, which are responsible for the occurrence of the

steps. A possible explanation for the broadness of the IP was found in the unusual molecule packing, as the one-dimensional chains are arranged in planar layers, rectangular to each other (Figure 9). This unusual arrangement leads to a very dense molecule packing with numerous short restraining interactions, similar as observed for zigzag chains^[39] and an interlocking of the polymer chains, which counter-act the relocation of the system following the SCO.

2.6 A New Model for the Explanation of Wide Hysteresis Loops

Various potential applications for SCO materials with wide thermal hysteresis loops around room temperature are thinkable.^[1,5,7,8] Therefore, it is very important to find an explanation for the occurrence of this phenomenon, as this is essential for a purposeful synthesis of such materials. The positive influence of hydrogen bonding in correlation with strong elastic interactions was never doubted and is well known in literature,^[44,45] but fuelled by the observation of a 2D network of hydrogen bonds being responsible for the 70 K wide hysteresis loop of compound [FeL1a(Him)₂]^[17], this field of research became a new impulse. Through ongoing research with this and two other compounds—an isostructural modification of [FeL1a(Him)₂] with 5 K wide hysteresis loop and the 1D coordination polymer [FeL1d[azpy]]·MeOH, which shows a 80 K wide hysteresis loop with methanol and a gradual SCO without methanol incorporated in the crystal lattice—a consistent model for the explanation of wide hysteresis loops and the role of hydrogen bonds was developed.^[46]

X-Ray structure analysis revealed that these compounds have two characteristics in common: firstly, an intermolecular network of hydrogen bonds for the transmission of cooperative effects and secondly, one oxygen atom of the Schiff base-like ligand involved in a hydrogen bond, which therefore simultaneously acts as hydrogen acceptor and as Lewis base for the iron(II) centre. Through substitution of all hydrogen atoms involved in hydrogen bonds by deuterium, an isotope effect was observed in all cases, which affected the width of the hysteresis loops as well as the transition temperatures (see Figure 10, left).^[46] In addition, the importance of hydrogen bonding is underlined by the outcomes of DSC measurements, as a considerable decrease of the entropy was observed upon deuteration. These findings demonstrated that, first of all, changes in the hydrogen bond network (often, but not necessarily, in line with a structural phase transition) affect the spin transition behaviour and, second of all, hydrogen bonds significantly influence the ligand field strength, if donor atoms

2. Summary

coordinated to the metal centre or atoms in conjugated systems with donor atoms, are involved.^[46]

Based on this information, a new model for the explanation of the wide thermal hysteresis loops of these compounds was suggested.^[46] According to that, a correlation between the structural changes upon spin transition, the hydrogen bond strength and the overall ligand field strength of the complex exists. Upon cooling, the structural changes result in a stabilisation of the LS state, as can be seen in Figure 10 (right). As a consequence, the energy gap between the LS and HS potential wells (ΔE_{HL}) increases and the transition temperature is shifted upwards upon heating. Of course, the same effects occur the other way round. Wide thermal hysteresis loops should be observed, if a large enough change in a hydrogen bond network involving donor atoms or atoms in conjugated systems with donor atoms is induced. Those changes can be associated with reversible structural phase transitions. This concept is a further step towards the purposeful design and application of SCO materials.

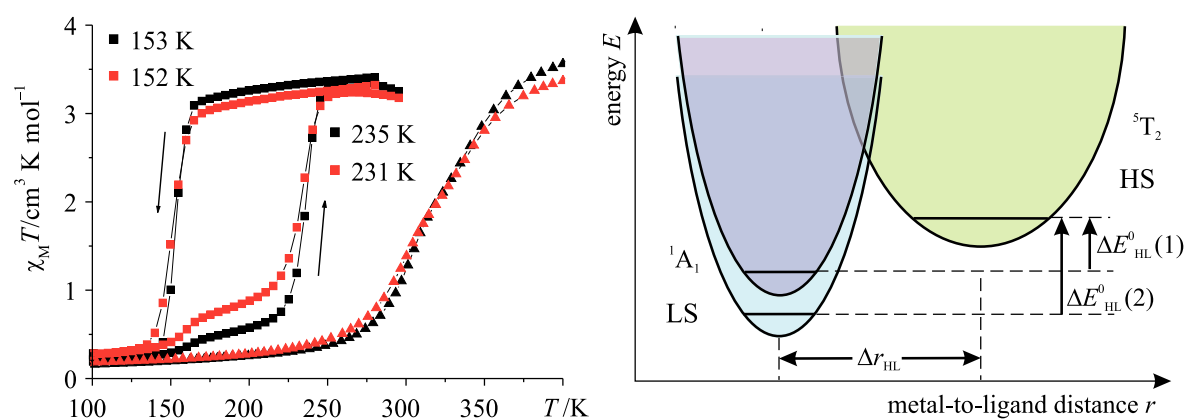


Figure 10. Left: plot of the $\chi_M T$ product vs. T for compound $[\text{FeL1d}(\text{azpy})]\cdot\text{MeOH}$ (black squares) and $[\text{FeL1d}(\text{azpy})]\cdot\text{CD}_3\text{OD}$ (red squares), indicating an isotope effect, and the gradual spin transition after tempering to 400 K (triangles). Right: schematic representation of the HS and LS potential wells before spin transition (LS dark blue) and after spin transition (LS light blue). Upon spin transition a change in the H-bond strength results in a different ligand field strength for the LS state and therefore a higher energy gap between the LS and HS state ($\Delta E_{\text{HL}}(1) \rightarrow \Delta E_{\text{HL}}(2)$).

2.7 Synthesis of SCO Compounds in a Crystal Engineering-like Approach

To get beyond the classical trial-and-error finding of SCO materials that exhibit a hysteresis loop, a general idea was to systematically improve the spin transition behaviour of our compounds by the means of cooperative effects, using the principals of coordination bonding, hydrogen bonding and network design in a crystal engineering-like approach. The developed synthesis strategy included to increase the covalent character of our SCO compounds step by step by increasing their intermolecular interactions.^[47] The principle of this idea is displayed in Figure 11: starting with the monomeric compound $[\text{FeL1b}(1\text{-meim})_2]$ ^[41] (1-meim = 1-methylimidazole), a 2 K wide hysteresis loop was observed due to a two-dimensional network of weak van der Waals interactions. The transition from a monomeric ligand system to a dimeric system led to an increased cooperativity, as compound $[\text{Fe}_2\text{L2b}(1\text{-meim})_4]\cdot 1\text{-meim}$ ^[41] shows a 21 K wide hysteresis loop due to a 3D network of short intermolecular contacts.

The implementation of covalent linker molecules, finally leading to the formation of 1D coordination compounds, which was the main part of this work, yielded in nearly 30 K wide hysteresis loops.^[39] Again the transmission of elastic interactions was improved as can be seen at compound $[\text{FeL1b}(\text{bipy})]$ (Figure 11): a multitude of short contacts between the chains were found to be responsible for a 18 K wide hysteresis loop.^[22,48] With introduction of specific variations at the axial (*e.g.* a peptide bond at the ligand *N*-(4-pyridyl)isonicotinamide)^[47] or equatorial ligands (hydroxy groups at the $\text{H}_2\text{L3}$ ligand system)^[49] it was possible to even intensify the formation of intermolecular interactions.^[47] This resulted in a nearly 90 K wide hysteresis for compound $[\text{FeL1b}(\text{pina})]\cdot x$ (MeOH), but unfortunately the mechanism is not yet fully understood at this example, and a 28 K wide hysteresis observed for compound $[\text{FeL3b}(\text{bpee})]\cdot (\text{bpee})(\text{MeOH})$.^[47] For both examples, no data from X-ray analysis were obtained so far.

The successful transition from mononuclear to dinuclear systems and one-dimensional coordination polymers finally led to the connection of dinuclear systems with suitable bidentate bridging ligands in order to get dimeric coordination polymers and thus further optimise the intermolecular interactions. With the newly synthesised compound $[\text{Fe}_2\text{L2a}(\text{bpee})]\cdot 1.5 \text{ tol}$, which exhibits a 34 K wide hysteresis loop and very likely a ladder-like 1D double-strand structure, we were able to show for the first time that this strategy can be expanded this far.^[47]

2. Summary

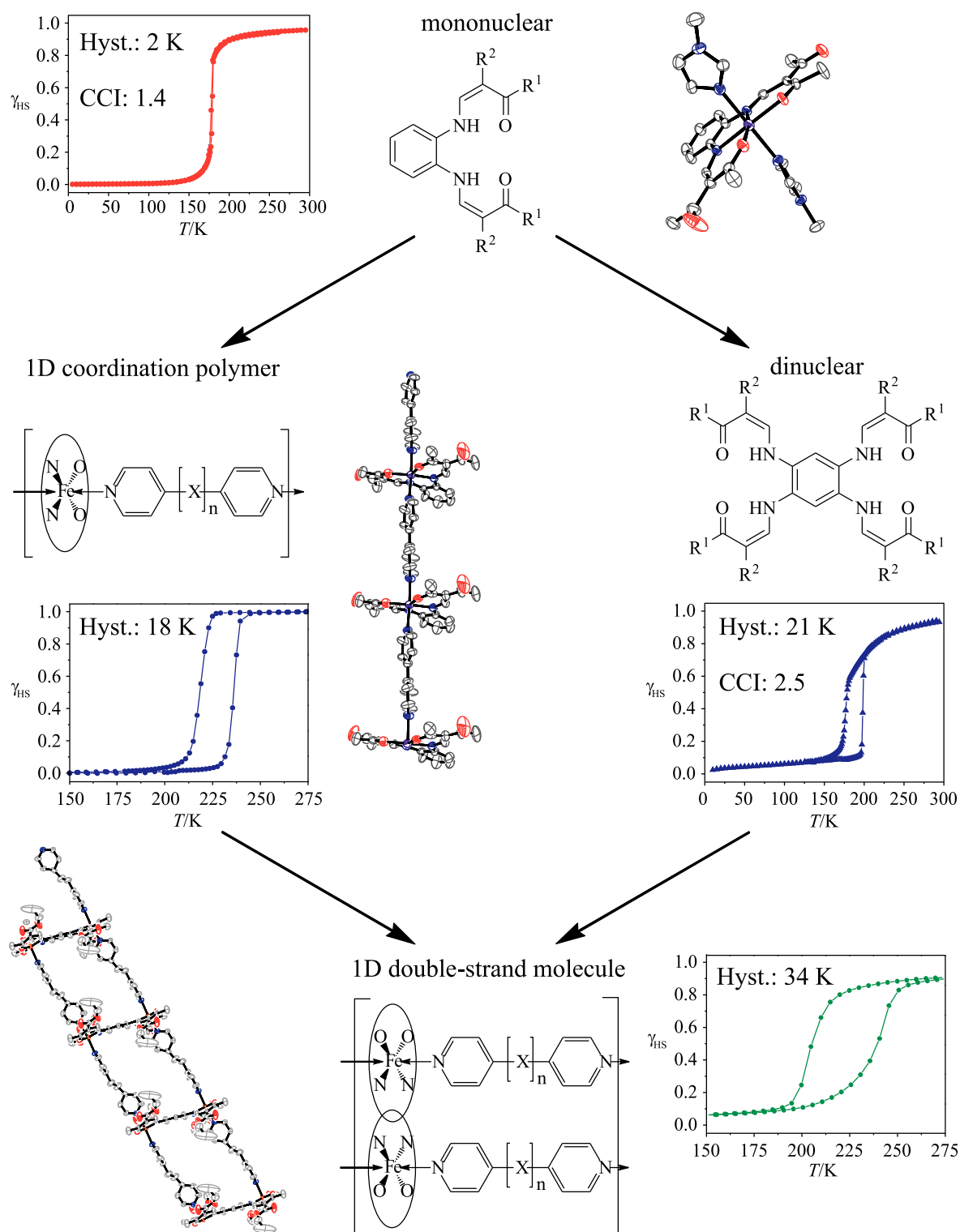


Figure 11. Transition from mononuclear to polynuclear systems. Schematic representation of the synthesis strategy to systematically increase the cooperativity of the iron(II) SCO compounds by increasing their covalent character in a crystal engineering-like approach.

2.8 References

- [1] J.-F. Létard, P. Guionneau, L. Goux-Capes, *Topics in Current Chemistry*, Vol. 235 (Eds.: P. Gülich, H.A. Goodwin), Springer, Wien, New York, **2004**, 221.
- [2] N. Nuraje, S. Mohammed, L. Yang, H. Matsui, *Angew. Chem.* **2009**, 121, 2584.
- [3] S.M. Neville, C. Etrillard, S. Asthana, J.-F. Létard, *Eur. J. Inorg. Chem.* **2010**, 282.
- [4] W. Plass, *Chem. Unserer Zeit* **1998**, 32, 323.
- [5] a) O. Kahn, C. Jay Martinez, *Science* **1998**, 279, 44; b) O. Kahn, C. Jay Martinez, J. Kröber, R. Claude, F. Grolière, *Patent* EP0666561, **1995**; c) J.-F. Létard, O. Nguyen, N. Daro, *Patent* FR0512476, **2005**; d) A. Galet, A.B. Gaspar, M.C. Munoz, G.V. Bukin, G. Levchenko, J.A. Real, *Adv. Mater.* **2005**, 17, 2949.
- [6] a) H.A. Goodwin, *Coord. Chem. Rev.* **1976**, 18, 293; b) E. König, *Struct. Bonding (Berlin)* **1991**, 76, 51; c) P. Gülich, A. Hauser, H. Spiering, *Angew. Chem. Int. Ed. Engl.* **1994**, 33, 2024, and references therein; d) P. Gülich, H.A. Goodwin (Eds.), *Spin Crossover in Transition Metal Compounds I–III*, *Topics in Current Chemistry*, Springer, Berlin, Heidelberg, New York, **2004**; e) P. Gülich, H.A. Goodwin (Eds.), *Topics in Current Chemistry*, Vol. 233, Springer, Wien, New York, **2004**, 1; f) J.A. Real, A.B. Gaspar, M.C. Munoz, *Dalton Trans.* **2005**, 2062; g) K. Nakano, N. Suemura, K. Yoneda, S. Kawata, S. Kaizaki, *Dalton Trans.* **2005**, 740; h) O. Sato, J. Tao, Y.-Z. Zhang, *Angew. Chem.* **2007**, 119, 2200; *Angew. Chem. Int. Ed.* **2007**, 46, 2152; i) J.A. Kitchen, S. Brooker, *Coord. Chem. Rev.* **2008**, 252, 2072; j) K.S. Murray, *Eur. J. Inorg. Chem.* **2008**, 3101; k) M.A. Halcrow, *Coord. Chem. Rev.* **2009**, 2059; l) S. Brooker, J.A. Kitchen, *Dalton Trans.* **2009**, 7331; m) C.J. Kepert, *Aust. J. Chem.* **2009**, 62, 1079; n) K.S. Murray, *Aust. J. Chem.* **2009**, 62, 1081; o) A.B. Koudriavtsev, W. Linert, *J. Struct. Chem.* **2010**, 51, 335.
- [7] Y. Garcia, V. Ksefontov, P. Gülich, *Hyperfine Interact.* **2002**, 139/140, 543.
- [8] Y. Garcia, V. Ksefontov, S. Mentior, M.M. Dîrtu, C. Gieck, A. Bhatthacharjee, P. Gülich, *Chem. Eur. J.* **2008**, 14, 3745.

- [9] a) A.B. Gaspar, V. Ksenofontov, M. Seredyuk, P. Gütllich, *Coord. Chem. Rev.* **2005**, 249, 2661; b) A.B. Gaspar, M. Seredyuk, P. Gütllich, *J. Mol. Struct.* **2009**, 924–926, 9.
- [10] a) M. Seredyuk, A.B. Gaspar, V. Ksenofontov, Y. Galyametdinov, M. Verdaguer, F. Villain, P. Gütllich, *Inorg. Chem.* **2008**, 47, 10232; b) M. Seredyuk, A.B. Gaspar, V. Ksenofontov, Y. Galyametdinov, J. Kusz, P. Gütllich, *Adv. Funct. Mater.* **2008**, 18, 2089; c) M. Seredyuk, A.B. Gaspar, V. Ksenofontov, Y. Galyametdinov, J. Kusz, P. Gütllich, *J. Am. Chem. Soc.* **2008**, 130, 1431.
- [11] a) J.A. Real, A.B. Gaspar, V. Niel, M.C. Muñoz, *Coord. Chem. Rev.* **2003**, 236, 121; b) A. Bousseksou, G. Molnár, J.A. Real, K. Tanaka, *Coord. Chem. Rev.* **2007**, 251, 1822.
- [12] a) I. Boldog, A.B. Gaspar, V. Martinez, P. Pardo-Ibanez, V. Ksenofontov, A. Bhattacharjee, P. Gütllich, J.A. Real, *Angew. Chem. Int. Ed. Engl.* **2008**, 47, 6433; b) S. Cobo, G. Molnar, J.A. Real, A. Bousseksou, *Angew. Chem. Int. Ed. Engl.* **2006**, 45, 5786; c) G. Molnár, S. Cobo, J.A. Real, F. Carcenac, E. Daran, C. Vieu, A. Bousseksou, *Adv. Mater.* **2007**, 19, 2163.
- [13] a) S. Decurtins, P. Gütllich, C.P. Köhler, H. Spiering, A. Hauser, *Chem. Phys. Lett.* **1984**, 105, 1; b) S. Decurtins, P. Gütllich, K.M. Hasselbach, A. Hauser, H. Spiering, *Inorg. Chem.* **1985**, 24, 2174.
- [14] L. Cambi, L. Szego, *Ber. Dtsch. Chem. Ges.* **1931**, 64, 2591.
- [15] W.A. Baker, H.M. Bobonich, *Inorg. Chem.* **1964**, 3, 1184.
- [16] a) J.-F. Létard, P. Guionneau, E. Codjvi, O. Lavastre, G. Bravic, D. Chasseau, O. Kahn, *J. Am. Chem. Soc.* **1997**, 119, 10861; b) J.-F. Létard, L. Capes, G. Chastanet, N. Moliner, S. Létard, J.-A. Real, O. Kahn, *Chem. Phys. Lett.* **1999**, 313, 115; c) H. Daubric, C. Cantin, C. Thomas, J. Kliava, J.-F. Létard, O. Kahn, *Chem. Phys. Lett.* **1999**, 244, 75; d) Z.J. Zhong, J.-Q. Tao, Z. Yu, C.-Y. Dun, Y.-J. Liu, X.-Z. You, *J. Am. Chem. Soc.* **1998**, 327; e) S. Hayami, Z.-Z. Gu, Y. Einaga, A. Fujishima, O. Sato, *J. Am. Chem. Soc.* **2001**, 123, 11644.
- [17] B. Weber, W. Bauer, J. Obel, *Angew. Chem.* **2008**, 120, 10252; *Angew. Chem. Int. Ed.* **2008**, 47, 10098.

- [18] a) O. Kahn, E. Codjovi, *Philos. Trans. R. Soc. London, Ser. A* **1996**, 354, 359; b) O. Kahn, Y. Garcia, J.-F. Létard, C. Mathonière, *NATO ASI Ser., Ser. C* **1998**, 518, 127.
- [19] B. Weber, *Coord. Chem. Rev.* **2009**, 253, 2432; b) B. Weber, E.-G. Jäger, *Eur. J. Inorg. Chem.* **2009**, 465.
- [20] a) P. Gütllich, Y. Garcia, H.A. Goodwin, *Chem. Soc. Rev.* **2000**, 29, 419; b) G.J. Halder, C.J. Kepert, B. Moubaraki, K.S. Murray, J.D. Cashion, *Science* **2002**, 298, 1762; c) V. Niel, A.L. Thompson, M.C. Munoz, A. Galet, A.E. Goeta, J.A. Real, *Angew. Chem. Int. Ed.* **2003**, 42, 3760; d) M. Nihei, L. Han, H. Oshio, *J. Am. Chem. Soc.* **2007**, 129, 5312.
- [21] a) K. Hosoya, T. Kitazawa, M. Takahashi, M. Takeda, J.-F. Meunier, G. Molnar, A. Bousseksou, *Phys. Chem. Chem. Phys.* **2003**, 5, 1682; b) P. Gütllich, H. Köppen, H.G. Steinhäuser, *Chem. Phys. Letters* **1980**, 74, 475.
- [22] B. Weber, E.S. Kaps, C. Desplanches, J.-F. Létard, *Eur. J. Inorg. Chem.* **2008**, 2963.
- [23] S. Sugano, Y. Tanabe, H. Kamimura, *Pure Appl. Phys.* **1970**, 33.
- [24] H.L. Schäfer, G. Gliemann, *Einführung in die Ligandenfeldtheorie*, Akademische Verlagsgesellschaft, Wiesbaden, **1980**, S. 462.
- [25] a) M. Sorai, S. Seki, *J. Phys. Soc. Jpn.* **1972**, 33, 575; b) M. Sorai, S. Seki, *J. Phys. Chem. Solids* **1974**, 35, 555.
- [26] H. Luecken, *Magnetochemie*, B.G. Teubner, Stuttgart, Leipzig **1999**.
- [27] a) D.F.J. Evans, *J. Chem. Soc.* **1959**, 2003; b) E.M. Schubert, *J. Chem. Educ.* **1992**, 69, 62.
- [28] B. Weber, F.A. Walker, *Inorg. Chem.* **2007**, 46, 6794.
- [29] B. Weber, C. Carbonera, C. Desplanches, J.-F. Létard, *Eur. J. Inorg. Chem.* **2008**, 1589.
- [30] U. Gonser (Eds.), *Mössbauer Spectroscopy*, Springer, New York, **1975**.
- [31] P. Gütllich, *Chem. Unserer Zeit* **1970**, 4, 133.
- [32] L. Wolf, E.-G. Jäger, *Z. Anorg. Allg. Chem.* **1966**, 346, 76.
- [33] W. Bauer, T. Ossiander, B. Weber, *Z. Naturforsch. B* **2010**, 65, 323.

- [34] a) J.A. Real, A.B. Gaspar, M.C. Munoz, P. Gülich, V. Ksenofontov, H. Spiering, *Topics in Current Chemistry*, Vol. 233 (Eds.: P. Gülich, H.A. Goodwin), Springer, Wien, New York, **2004**, 167; b) A.B. Gaspar, M.C. Munoz, J.A. Real, *J. Mater. Chem.* **2006**, 2522; c) A. Bousseksou, G. Molnar, J.A. Real, K. Tanaka, *Coord. Chem. Rev.* **2007**, 251, 1822.
- [35] a) Y. Garcia, O. Kahn, L. Rabardel, B. Chansou, L. Salmon, J.-P. Tuchagues, *Inorg. Chem.* **1999**, 38, 4663; b) G.S. Matouzenko, J.-F. Létard, S. Lecocq, A. Bousseksou, L. Capes, L. Salmon, M. Perrin, O. Kahn, A. Collet, *Eur. J. Inorg. Chem.* **2001**, 2935; c) W. Hibbs, P.J. van Koningsbruggen, A.M. Arif, W.W. Shum, J.S. Miller, *Inorg. Chem.* **2003**, 42, 5645; d) P. Poganiuch, S. Decurtins, P. Gülich, *J. Am. Chem. Soc.* **1990**, 112, 3270; e) L. Wiehl, *Acta Crystallogr., Sect. B* **1993**, 49, 289; f) R. Hinek, H. Spiering, D. Schollmeyer, P. Gülich, A. Hauser, *Chem. Eur. J.* **1996**, 2, 1427.
- [36] a) M. Mikami, M. Konno, Y. Saito, *Chem. Phys. Lett.* **1979**, 63, 566; b) N. Sasaki, T. Kambara, *Phys. Rev. B* **1989**, 40, 2442; c) A. Bousseksou, J. Nasser, J. Linares, K. Boukheddaden, F. Varret, *J. Phys. I* **1992**, 2, 1381; d) H. Spiering, T. Kohlhaas, H. Romstedt, A. Hauser, C. Bruns-Yilmaz, P. Gülich, *Coord. Chem. Rev.* **1999**, 190–192, 629.
- [37] a) V. Petrouleas, J.-P. Tuchagues, *Chem. Phys. Lett.* **1987**, 137, 21; b) D. Boinnard, A. Bousseksou, A. Dworkin, J.-M. Savariault, F. Varret, J.-P. Tuchaugues, *Inorg. Chem.* **1994**, 33, 271; c) K. Boukheddaden, J. Linares, H. Spiering, F. Varret, *Eur. Phys. J. B.* **2000**, 15, 317; d) D. Chernyshov, M. Hostettler, K.W. Törnroos, H.B. Bürgi, *Angew. Chem.* **2003**, 115, 3955; *Angew. Chem. Int. Ed.* **2003**, 42, 3825.
- [38] W. Bauer, B. Weber, *Inorg. Chim. Acta* **2009**, 362, 2341.
- [39] W. Bauer, W. Scherer, S. Altmannshofer, B. Weber, *Eur. J. Inorg. Chem.* **2011**, 2803.
- [40] T. M. Pfaffeneder, S. Thallmair, W. Bauer, B. Weber, *New J. Chem.* **2011**, 35, 691.
- [41] B. Weber, E. Kaps, J. Obel, K. Achterhold, F.G. Parak, *Inorg. Chem.* **2008**, 47, 10779.
- [42] a) H. Spiering, E. Meissner, H. Köppen, E.W. Müller, P. Gülich, *Chem. Phys.* **1982**, 68, 65; b) B. Weber, E. Kaps, C. Desplanches, J.-F. Létard, K. Achterhold, F.G. Parak, *Eur. J. Inorg. Chem.* **2008**, 4891.

- [43] W. Bauer, T. Pfaffeneder, K. Achterhold, B. Weber, *Eur. J. Inorg. Chem.* **2011**, DOI: 10.1002/ejic.201100224.
- [44] a) A.P. Summerton, A.A. Diamantis, M.R. Snow, *Inorg. Chim. Acta* **1978**, 27, 123; b) A. Bhattacharjee, V. Ksenofontov, K.H. Sugiyarto, H.A. Goodwin, P. Gütlich, *Adv. Funct. Mater.* **2003**, 13, 877; c) K.H. Sugiyarto, M.L. Scudder, D.C. Craig, H.A. Goodwin, *Aust. J. Chem.* **2000**, 53, 755; d) A. Bhattacharjee, J. Kusz, M. Zubko, H.A. Goodwin, P. Gütlich, *J. Mol. Struct.* **2008**, 890, 178; e) K.H. Sugiyarto, K. Weitzner, D.C. Craig, H.A. Goodwin, *Aust. J. Chem.* **1997**, 50, 869; f) T. Buchen, P. Gütlich, K.H. Sugiyarto, H.A. Goodwin, *Chem. Eur. J.* **1996**, 2, 1134.
- [45] B. Weber, J. Obel, D. Henner-Vásquez, W. Bauer, *Eur. J. Inorg. Chem.* **2009**, 5527.
- [46] B. Weber, W. Bauer, T. Pfaffeneder, M.M. Dîrtu, A.D. Naik, A. Rotaru, Y. Garcia, *Eur. J. Inorg. Chem.* **2011**, DOI: 10.1002/ejic.201100394.
- [47] This work, chapter 12, manuscript in preparation.
- [48] a) B. Weber, R. Tandon, D. Himsl, *Z. Anorg. Allg. Chem.* **2007**, 633, 1159.
- [49] B. Weber, J. Obel, *Z. Anorg. Allg. Chem.* **2009**, 635, 2474.

3 Individual Contribution to Joint Publication

The results presented in this thesis were obtained in collaboration with others and are published, accepted, submitted or are to be submitted as indicated below. In the following, the contributions of all co-authors to the publications are specified. The asterisk denotes the corresponding authors.

3.1. Chapter 4

This work is published in *Eur. J. Inorg. Chem.* **2011**, 2803–2818 with the title “**Two-Step versus One-Step Spin Transitions in Iron(II) 1D Chain Compounds**”.

Wolfgang Bauer, Wolfgang Scherer, Sandra Altmannshofer and Birgit Weber*

I synthesised, characterised or reproduced all complexes and ligands presented in this work, carried out the magnetic measurements and wrote the publication. Sandra Altmannshofer carried out the deep- and high-temperature X-ray structure analysis of one compound at the University of Augsburg. Wolfgang Scherer was involved in scientific discussions and correction of the manuscript. Birgit Weber carried out the paramagnetic NMR-experiments and was involved in scientific discussions and correction of the manuscript.

3.2. Chapter 5

This work is published in *Inorg. Chim. Acta* **2009**, 362, 2341–2346 with the title “**X-Ray Structure and Magnetic Properties of Dinuclear and Polymer Iron(II) Complexes**”.

Wolfgang Bauer and Birgit Weber*

I synthesised and characterised the iron(II) coordination polymers presented in this work and reproduced the other complexes, carried out the magnetic measurements and wrote the publication. Birgit Weber supervised this work and was involved in scientific discussions and correction of the manuscript.

3.3. Chapter 6

This work is published in *Z. Anorg. Allg. Chem.* **2010**, *636*, 183–187 with the title “**X-Ray Structure and Magnetic Properties of Two New iron(II) 1D Coordination Polymers with Bis(imidazolyle)methane as Bridging Ligand**”.

Toni Pfaffeneder, Wolfgang Bauer and Birgit Weber*

Toni Pfaffeneder wrote the publication. As his supervising tutor I controlled and supported the syntheses and characterisations of the ligands and complexes presented in this work. Moreover, I carried out the magnetic measurements and was involved in scientific discussions. Birgit Weber supervised this work, wrote the introduction and was involved in scientific discussions and correction of the manuscript.

3.4. Chapter 7

This work is published in *New J. Chem.* **2011**, *35*, 691–700 with the title “**Complete and Incomplete Spin Transitions in 1D Chain Iron(II) Compounds**”.

Toni Pfaffeneder, Sebastian Thallmair, Wolfgang Bauer and Birgit Weber*

Toni Pfaffeneder wrote the publication. As supervising tutor of Toni Pfaffeneder and Sebastian Thallmair I controlled and supported the syntheses and characterisation of the ligands and complexes presented in this work and reproduced the experimental results, carried out the magnetic measurements and was involved in the scientific discussion. Birgit Weber wrote the introduction, parts of the discussion and the conclusion section of this work and supervised the correction of the manuscript.

3.5. Chapter 8

This work is published in *Z. Naturforsch. B* **2010**, *65*, 323–328 with the title “**A Promising New Schiff Base-like Ligand for the Synthesis of Octahedral Iron(II) Spin Crossover Complexes**”.

Wolfgang Bauer, Tanja Ossiander and Birgit Weber*

I wrote the publication and carried out the magnetic measurements. As supervising tutor of Tanja Ossiander I controlled and supported the syntheses and characterisations of all ligands and complexes presented in this work. Birgit Weber supervised this work and was involved in scientific discussions and correction of the manuscript.

3.6. Chapter 9

This work is published in *Eur. J. Inorg. Chem.* **2011**, DOI: 10.1002/ejic.201100224 with the title **“Complete Two-Step Spin-Transition in a 1D Chain Iron(II) Complex with 110 K wide Intermediate Plateau”**.

Wolfgang Bauer, Toni Pfaffeneder, Klaus Achterhold and Birgit Weber*

I synthesised and characterised the ligands and complexes presented in this work by myself or supported Toni Pfaffeneder as his supervising tutor, carried out the magnetic measurements and wrote the publication. Klaus Achterhold carried out the Mössbauer measurements at the TU Garching and helped interpreting the results. Birgit Weber supervised this work, helped interpreting the Mössbauer spectra and was involved in scientific discussions and correction of the manuscript.

3.7. Chapter 10

This work is published in *Eur. J. Inorg. Chem.* **2011**, DOI: 10.1002/ejic.201100394 with the title **“Influence of Hydrogen Bonding on the Hysteresis Width in Iron(II) Spin Crossover Complexes”**.

Birgit Weber*, Wolfgang Bauer, Toni Pfaffeneder, Marinela M. Dîrtu, Anil D. Naik, Aurelian Rotaru and Yann Garcia*

I wrote the experimental section and parts of the result section (magnetic measurements, X-ray structure analysis), carried out the magnetic measurements and synthesised and characterised the complexes presented in this work by myself or supported Toni Pfaffeneder as his supervising tutor. Moreover, I was involved in scientific discussions and correction of the manuscript. Marinela M. Dîrtu and Anil D. Naik carried out the DSC measurements at the Université Catholique de Louvain. Yann Garcia interpreted the DSC and FORC

measurements and wrote these sections in the manuscript. Moreover, he was involved in scientific discussions and correction of the manuscript. Aurelian Rotaru of the "Stefan cel Mare" University helped interpreting the FORC measurements. Birgit Weber wrote the discussion and conclusion sections of the manuscript and supervised this work.

3.8. Chapter 11

This work is to be submitted with the title "**Unusual Stepped Spin Transitions at Iron(II) Coordination Polymers with zigzag-Structure**".

Wolfgang Bauer and Birgit Weber*

I synthesised and characterised all compounds and ligands presented in this work, carried out the magnetic measurements and wrote the manuscript. Birgit Weber supervised this work and was involved in scientific discussions and correction of the manuscript.

3.9. Chapter 12

This work is to be submitted with the title "**Increasing the Hysteresis Width of Iron(II) SCO Compounds in a Crystal Engineering-like Approach**".

Wolfgang Bauer and Birgit Weber*

I synthesised, characterised or reproduced all complexes in this work, carried out the magnetic measurements and wrote the manuscript. Birgit Weber supervised this work and was involved in scientific discussions and correction of the manuscript.

4 Two-Step versus One-Step Spin Transition in Iron(II) 1D Chain Compounds

Wolfgang Bauer,^[a] Wolfgang Scherer,^[b] Sandra Altmannshofer^[b,c] and Birgit Weber^{*,[a,d]}

[a] Center for Integrated Protein Science Munich at the Department Chemie und Biochemie, Ludwig-Maximilians- Universität München, Butenandtstr. 5–13 (Haus F), D-81377 München, Germany

[b] Universität Augsburg, Institut für Physik, Lehrstuhl für Chemische Physik und Materialwissenschaften, 86135 Augsburg, Germany

[c] Georg-August-Universität Göttingen, Institut für Anorganische Chemie, Tammannstraße 4, 37077 Göttingen, Germany

[d] Inorganic Chemistry II, Universität Bayreuth, Universitätsstraße 30, NW I, 95440 Bayreuth, Germany. Fax: +49-92155-2157, E-mail: weber@uni-bayreuth.de

Dedicated to Professor Peter Klüfers on the Occasion of his 60th Birthday

Keywords: Iron, N,O ligands, Magnetism, X-Ray structure, Spin Crossover

Published in: *Eur. J. Inorg Chem.* **2011**, 2803–2818.

Abstract: Eleven iron(II) 1D coordination polymers with the general formula $[\text{FeL}_{\text{eq}}(\text{L}_{\text{ax}})] \cdot \text{solvent}$ were synthesised and characterised, where $\text{L}_{\text{eq}} = \{\text{diethyl } (E,E)\text{-}2,2'\text{-}[1,2\text{-phenyl-bis(iminomethylidene)]bis[3-oxobutanoate] } (2\text{-})\text{-}N,N',O^3,O^{3'}\}$ (L1) and $\{3,3'\text{-}[1,2\text{-phenyl-bis(iminomethylidene)]bis[pentane-2,4-dione] } (2\text{-})\text{-}N,N',O^2,O^{2'}\}$ (L2); $\text{L}_{\text{ax}} = 4,4'\text{-bipyridine}$ (bipy), 1,2-bis(4-pyridyl)ethane (bpea) and 1,3-bis(4-pyridyl)propane (bppa) and solvent = MeOH, EtOH and toluene (tol). $[\text{FeL1}(\text{bpea})] \cdot \text{MeOH}$ (**3**·MeOH) shows an abrupt one-step spin crossover with thermal hysteresis (27 K) and $[\text{FeL2}(\text{bppa})] \cdot \text{MeOH}$ (**2**·MeOH), $[\text{FeL2}(\text{bpea})]$ (**4**), $[\text{FeL2}(\text{bpea})] \cdot 0.25 \text{ MeOH}$ (**4**·0.25 MeOH) and $[\text{FeL1}(\text{bipy})] \cdot \text{MeOH}$ (**5**·MeOH) show a two-step spin transition with an IP at $\chi_{\text{HS}} \approx 0.5$ (IP is intermediate plateau and χ_{HS} is high-spin mol fraction) and up to 50 K wide hysteresis loops (**5**·MeOH).

[FeL1(bppa)] (**1**), [FeL2(bppa)]·EtOH (**2**·EtOH) and [FeL1(bpea)]·1.5 tol (**3**·1.5 tol) show an abrupt incomplete spin transition that stops at $\chi_{\text{HS}} \approx 0.5$; for [FeL1(bppa)]·0.25 MeOH (**1**·0.25 MeOH) and [FeL1(bpea)] (**3**) the spin transition is gradual and incomplete. The X-ray crystal structures of six complexes were determined (**1**, **2**·MeOH, **3**·MeOH, **3**·1.5 tol, **4**·0.25 MeOH, and **5**·MeOH). In the case of **4**·0.25 MeOH the crystal structures for the HS and LS states were determined; for compounds **1**, **2**·MeOH and **3**·1.5 tol the crystal structures of the HS state and at the IP were investigated. For all complexes, the iron(II) centre is located in a distorted octahedral coordination sphere. Each axially coordinated ligand “connects” two iron(II) centres, which results in the formation of extended 1D chains with varying structures from linear (bipy) over steplike (bpea) to zigzag (bppa). Analysis of the intermolecular interactions reveals that the hysteresis width depends on both the stiffness of the axial ligand and the number of intermolecular contacts, while zigzag chains support stepwise spin transitions.

4.1 Introduction

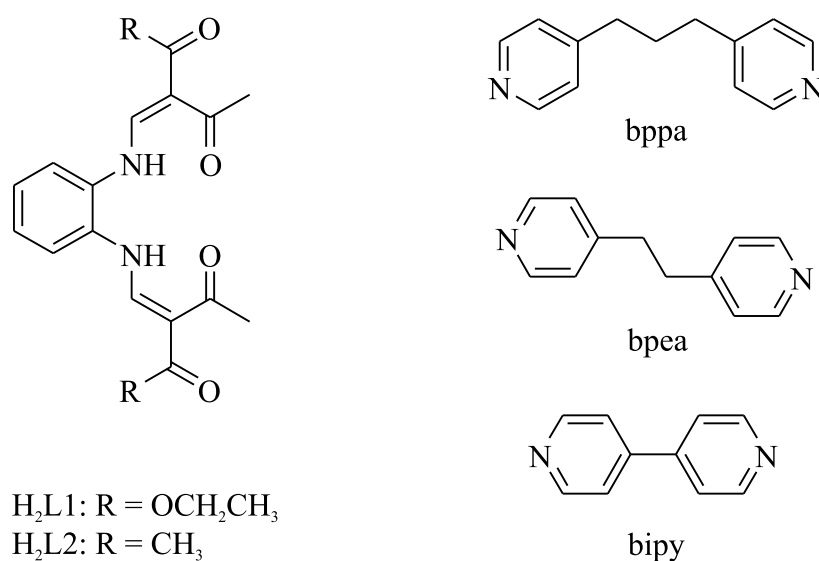
The bistability of spin transition complexes (spin crossover, SCO) is one of the most promising characteristics for new electronic devices in molecular memories and switches as it may be controlled by different physical perturbations such as temperature, pressure or light.^[1,2] Of the possible types of spin transition (gradual, abrupt, with hysteresis, stepwise, incomplete), much of the interest is focused on the bistability in highly cooperative systems (hysteresis or memory effect) as such compounds can exist in two different electronic states depending on the history of the system. Various examples in the literature^[1,3] as well as in our group^[4] demonstrate that the control over intermolecular interactions is a central point for the control of cooperative interactions. With regard to this we recently characterised an iron(II) spin crossover complex with a 70 K wide thermal hysteresis loop around room temperature based on a 2D network of hydrogen bonds between the complex molecules.^[5] Next to highly cooperative systems, stepwise transitions between three or more states have attracted the interest of several research groups, because of the versatile switching possibilities.^[6] This type of SCO is most frequently obtained for dinuclear complexes and explained with the formation of [HS-HS], [HS-LS] and [LS-LS] spin pair states (where HS and LS represent the local high-spin and low-spin states of the dinuclear species with $S = 2$ and $S = 0$ for d^6), which could be directly monitored, for example, by Mössbauer spectroscopy and switched selectively by

different wavelengths.^[34] Results from DFT calculations agree with the conclusion of the phenomenological model, that the enthalpy of the [HS-LS] state must be lower than the average enthalpy of the [LS-LS] and the [HS-HS] states to create conditions for a two-step transition (assuming that in the [HS-HS] and [LS-LS] state both iron centres are equivalent).^[7] Another possibility for having a multistep spin transition is attributed to two (or more) different spin crossover sites, each undergoing a transition at different temperatures.^[8] Finally, there are examples of mononuclear complexes with a unique crystallographic iron(II) site where two nonequivalent iron(II) sites appear upon cooling as a result of a crystallographic phase transition. In these cases, the effects of ferromagnetic-type long-range and antiferromagnetic-type short-range interactions of an elastic origin are responsible for steps in the transition curve.^[9,10] The most frequently used tool to assign SCO compounds with stepwise spin transitions to one of the three possibilities is X-ray structure analysis. The most obvious case (and also the most common one) is to have multiple crystallographic distinct metal centres at all temperatures. The often very subtle differences between the SCO sites are most likely the reason for the observed stepwise spin transitions. This also accounts for dinuclear complexes. The compound $[\text{Fe}(\text{NCS})_2(\text{ddpp})]_2 \cdot 4(\text{CH}_2\text{Cl}_2)$ (with $\text{ddpp} = 2,5\text{-}(\text{di-}2\text{-pyridylamine})\text{pyridine}$) was the first example of a dinuclear complex where an ordered [HS-LS] state was observed at the intermediate-plateau (IP) temperature. However, this compound has two nonequivalent iron sites at all temperatures, which is most likely the reason for the stepwise spin transition.^[11] Recently, the first examples of a 1D polymeric material undergoing a two-step spin transition were presented by Neville, Murray and co-workers.^[12] Of the two compounds presented, results from X-ray analysis reveal that one ($[\text{Fe}(\text{NCS})_2(\text{bdpp})]$, with $\text{bdpp} = 4,6\text{-bis}(2',2''\text{-pyridyl})\text{prazine}$) has two distinct iron(II) centres at each temperature with ordered, alternating HS and LS sites at the intermediate-plateau temperatures. In contrast to this, the second compound ($[\text{Fe}(\text{NCSe})_2(\text{bdpp})]$) has one unique iron(II) centre at each temperature with an averaged HS/LS character at the IP temperature. For both possibilities, a clear assignment to one of the types of stepwise spin transitions is difficult, and the reason for the step in the transition curve cannot be given without doubt.^[12]

One of the major goals in spin crossover research is to develop rules that allow the synthesis of spin crossover materials with predictable properties. Detailed magnetic and structural analyses of spin crossover systems in combination with a comparison between the different

systems are necessary to reach this point. The system investigated by our group is highly suitable for performing systematic investigations on structure-property relationships. The octahedral coordination sphere around the iron(II) centre is generated by an Schiff base-like N_2O_2 coordinating ligand that occupies the equatorial plane. With pyridine- or imidazole-derivatives at the axial sites, SCO behaviour is observed quite frequently.^[13] The replacement of the monodentate pyridine by bidentate ligands such as 4,4'-bipyridine (bipy), 1,2-bis(4-pyridyl)ethane (bpea) or 1,3-bis(4-pyridyl)propane (bppa) results in the formation of 1D coordination polymers with the general formula $[FeL_{eq}(L_{ax})] \cdot \text{solvent}$. A schematic representation of the ligands discussed in this work is given in Scheme 1. The combination of two equatorial and three axial ligands in different solvents leads to a series of 13 compounds, summarised in Table 1, of which the pair $[FeL_2(\text{bipy})]$ (**6**)/ $[FeL_2(\text{bipy})] \cdot 0.25 \text{ MeOH}$ (**6**·0.25 MeOH) is already published.^[14]

Detailed analyses of the structures and the magnetic properties of the remaining 11 compounds and comparisons with known 1D chain SCO materials allow the development of a first concept on how spin crossover materials with stepwise spin transitions can be designed rationally and to confirm already existing ideas about cooperative interactions in chain compounds.

**Scheme 1.** Schematic representation of the ligands discussed in this work.**Table 1.** Overview of the compounds discussed in this work with the used abbreviations.

L _{ax} /L _{eq}	bppa	bpea	bipy
H ₂ L1	[FeL1(bppa)] (1) ^[a] [FeL1(bppa)]·0.25 MeOH (1 ·0.25 MeOH) ^[b]	[FeL1(bpea)]·1.5 tol (3 ·1.5 tol) ^[a] [FeL1(bpea)] (3) ^[b] [FeL1(bpea)]·MeOH (3 ·MeOH) ^[c]	[FeL1(bipy)] (5) ^[b] [FeL1(bipy)]·MeOH (5 ·MeOH) ^[c]
H ₂ L2	[FeL2(bppa)]·EtOH (2 ·EtOH) ^[d] [FeL2(bppa)]·MeOH (2 ·MeOH) ^[b]	[FeL2(bpea)] (4) ^[b] [FeL2(bpea)]·0.25 MeOH (4 ·0.25 MeOH) ^[c]	[FeL2(bipy)] (6) ^{[b],[14]} [FeL2(bipy)]·0.25 MeOH (6 ·0.25 MeOH) ^{[c],[14]}

[a] Synthesised in or recrystallised from toluene; [b] synthesised in methanol; [c] crystals obtained by slow diffusion techniques in methanol; [d] synthesised in ethanol.

4.2 Results

Magnetic susceptibility studies of thermally induced SCO: The thermal dependence of the $\chi_M T$ product (χ_M is the molar susceptibility and T temperature) for all compounds measured is given in Figure 1. For purposes of completeness, the results of the magnetic measurements on compounds **6** and **6**·0.25 MeOH^[14] are given as well. Characteristic values of the susceptibility measurements are summarised in the Supplementary material. The room temperature $\chi_M T$ value of all compounds, with the exception of **5**·MeOH, are in the range of $3.25 \text{ cm}^3 \text{ K mol}^{-1}$, typical for an iron(II) complex in the HS state. For **5**·MeOH, the room temperature moment is $2.19 \text{ cm}^3 \text{ K mol}^{-1}$, which is significantly lower, but upon heating to 350 K, the moment increases to reach a value of $3.20 \text{ cm}^3 \text{ K mol}^{-1}$. Upon cooling (starting from the pure HS state), various types of spin transition can be observed for the compounds. A complete, one-step spin transition is observed for the previously published compound **6**, which is accompanied by an 18 K wide thermal hysteresis loop ($T_{1/2}^\downarrow = 219 \text{ K}$, $T_{1/2}^\uparrow = 237 \text{ K}$)^[14] and for **3**·MeOH, which is accompanied by an 27 K wide thermal hysteresis loop ($T_{1/2}^\downarrow = 155 \text{ K}$, $T_{1/2}^\uparrow = 182 \text{ K}$). For **1**·0.25 MeOH and **3**, the spin transition is gradual and incomplete, with remaining $\chi_M T$ products at 50 K of $1.09 \text{ cm}^3 \text{ K mol}^{-1}$ and $0.68 \text{ cm}^3 \text{ K mol}^{-1}$, respectively. All the other examples show either a two-step spin transition with an IP at $\chi_{\text{HS}} \approx 0.5$ (**2**·MeOH, **4**, **4**·0.25 MeOH, **5**·MeOH) or an incomplete spin transition that stops at $\chi_{\text{HS}} \approx 0.5$ (**1**, **2**, **2**·EtOH, **3**·1.5 tol). Compounds **5** and **6**·0.25 MeOH^[14] are HS in the entire temperature range investigated.

The spin transition behaviour of **5**·MeOH is more complex than those of the other examples: starting the magnetic measurement at room temperature, the $\chi_M T$ values decrease upon cooling, first gradually then more rapidly then again gradually from $2.19 \text{ cm}^3 \text{ K mol}^{-1}$ to attain a minimum value of $0.46 \text{ cm}^3 \text{ K mol}^{-1}$ at 175 K. The $T_{1/2}^\downarrow$ value is 255 K. Further cooling causes no significant decrease. The $\chi_M T$ value of $2.19 \text{ cm}^3 \text{ K mol}^{-1}$ indicates that approximately two thirds of the iron(II) sites are in the HS state at room temperature. Upon heating, the $\chi_M T$ values increase between 200 and 280 K to attain a maximum value of $1.76 \text{ cm}^3 \text{ K mol}^{-1}$, which indicates that half of the iron (II) sites are in the HS state. The $T_{1/2}^\uparrow(2)$ value of this step is 260 K. Above 280 K, the $\chi_M T$ values increase further to attain a maximum of $3.20 \text{ cm}^3 \text{ K mol}^{-1}$ at 350 K, indicative of iron(II) in the HS state. The $T_{1/2}^\uparrow(1)$ value of this step is 309 K. Between 245 and 300 K, the $\chi_M T$ values of the heating mode lie by an average

of $0.50 \text{ cm}^3 \text{ K mol}^{-1}$ lower than the values of the cooling mode. When starting the magnetic measurement at 350 K, the $\chi_{\text{M}}T$ values remain approximately constant upon cooling at $3.20 \text{ cm}^3 \text{ K mol}^{-1}$ down to 270 K. Between 270 and 225 K, the $\chi_{\text{M}}T$ values rapidly decrease to a first minimum at $1.75 \text{ cm}^3 \text{ K mol}^{-1}$. The $T_{1/2}^{\downarrow}(1)$ value of this step is 245 K. Between 225 and 190 K, the $\chi_{\text{M}}T$ values further decrease to $0.50 \text{ cm}^3 \text{ K mol}^{-1}$. The $T_{1/2}^{\downarrow}(2)$ value of the second step is 205 K. Below 190 K, the $\chi_{\text{M}}T$ values remain approximately constant. Upon heating, the $\chi_{\text{M}}T$ values increase rapidly between 200 and 250 K to attain a broad plateau at $1.80 \text{ cm}^3 \text{ K mol}^{-1}$. Here, the $\chi_{\text{M}}T$ values consequently lie lower than the values of the cooling mode. The $T_{1/2}^{\uparrow}(2)$ value of this step is 220 K. Between 250 and 295 K, the $\chi_{\text{M}}T$ values remain constant. Above 295 K, the $\chi_{\text{M}}T$ values increase rapidly to a maximum value of $3.20 \text{ cm}^3 \text{ K mol}^{-1}$ at 320 K. The $T_{1/2}^{\uparrow}(1)$ value of this step is 304 K, which results in a 50 K wide thermal hysteresis loop for the first step and 15 K for the second step. After the initial heating to 350 K, the hysteresis loop can be repeated several times. The varying curve progression for the first cycle and all following cycles can have different reasons. Obviously, the compound crystallises at room temperature in a mixed HS/LS state (approximately 60/40). Upon heating to 350 K the transition curves are shifted to lower temperatures and now a complete two-step spin transition is observed. The most likely explanation for this observation is a (partial) loss of the included methanol at 350 K. In order to check this theory, a TG analysis of compound **5**·MeOH was performed and the results are given in the Supplementary material. Upon heating up to 348 K, approximately 60% of the included methanol is lost, and for a complete removal of the solvent, heating above 373 K is necessary. Consequently, further heating of the SQUID sample to 400 K results in a complete loss of the crystal solvent, and a pure HS compound is obtained as for the separately prepared powder sample. These solvent effects are entirely contrary to the effects observed for the pair **6/6**·0.25 MeOH, where the solvent-free compound **6** shows a complete SCO, while the methanol-containing compound **6**·0.25 MeOH is always HS.^[14]

Solvent effects are well known for SCO compounds and a similar dependence can be observed for the other chain compounds in this study. For **2**·MeOH, upon heating to 400 K for 60 min, the included solvent is removed, and the transition temperature is shifted to lower temperatures (from 168 to 115 K) accompanied with the appearance of a 10 K wide hysteresis loop ($T_{1/2}^{\downarrow} = 110 \text{ K}$, $T_{1/2}^{\uparrow} = 120 \text{ K}$). As a consequence, the second step of the spin transition is shifted from 91 K to a temperature somewhere below 80 K and is now kinetically trapped.

This becomes obvious in the heating mode of the susceptibility measurements of the tempered sample **(2)**. A descent of the $\chi_{\text{M}}T$ value at 80 K is obtained when keeping the temperature constant for 60 min while the susceptibility was recorded every 5 min. As a result, the $\chi_{\text{M}}T$ values at 80 K drop over this period of time from $1.78 \text{ cm}^3 \text{ K mol}^{-1}$ down to $1.38 \text{ cm}^3 \text{ K mol}^{-1}$. In the case of **2**·EtOH ($T_{1/2} = 116 \text{ K}$, no hysteresis), the transition temperature does not change significantly upon the loss of ethanol, and a 10 K wide thermal hysteresis loop is observed as for the tempered methanol sample **(2)**. In contrast to this, the transition temperature of the first step of **4** (high-temperature step) is shifted to higher temperatures when going from the crystalline sample **4**·0.25 MeOH to the solvent-free powder sample **4**. This indicates that, in general, the influence of solvent effects on the SCO behaviour is difficult to predict without any further (structural) information. A strong dependence of the spin transition behaviour on included solvent molecules is also observed for the different compounds of **3**. The gradual incomplete spin transition of the solvent-free powder sample **3** can be explained with the absence of significant interchain interactions. This example demonstrates that interchain interactions are important for the observation of cooperative effects, as already suggested for compound **6**.^[14] For the two crystalline samples, a similar transition temperature is obtained, but the thermal hysteresis loop is more pronounced for **3**·MeOH (27 K , $T_{1/2}^{\downarrow} = 155 \text{ K}$, $T_{1/2}^{\uparrow} = 182 \text{ K}$) compared to **3**·1.5 tol (4 K , $T_{1/2}^{\downarrow} = 165 \text{ K}$, $T_{1/2}^{\uparrow} = 169 \text{ K}$). Additionally, the spin transition of **3**·MeOH is a complete one-step transition, while for **3**·1.5 tol it stops at $\gamma_{\text{HS}} \approx 0.5$.

4. Two-Step versus One-Step Spin Transition in Iron(II) 1D Chain Compounds

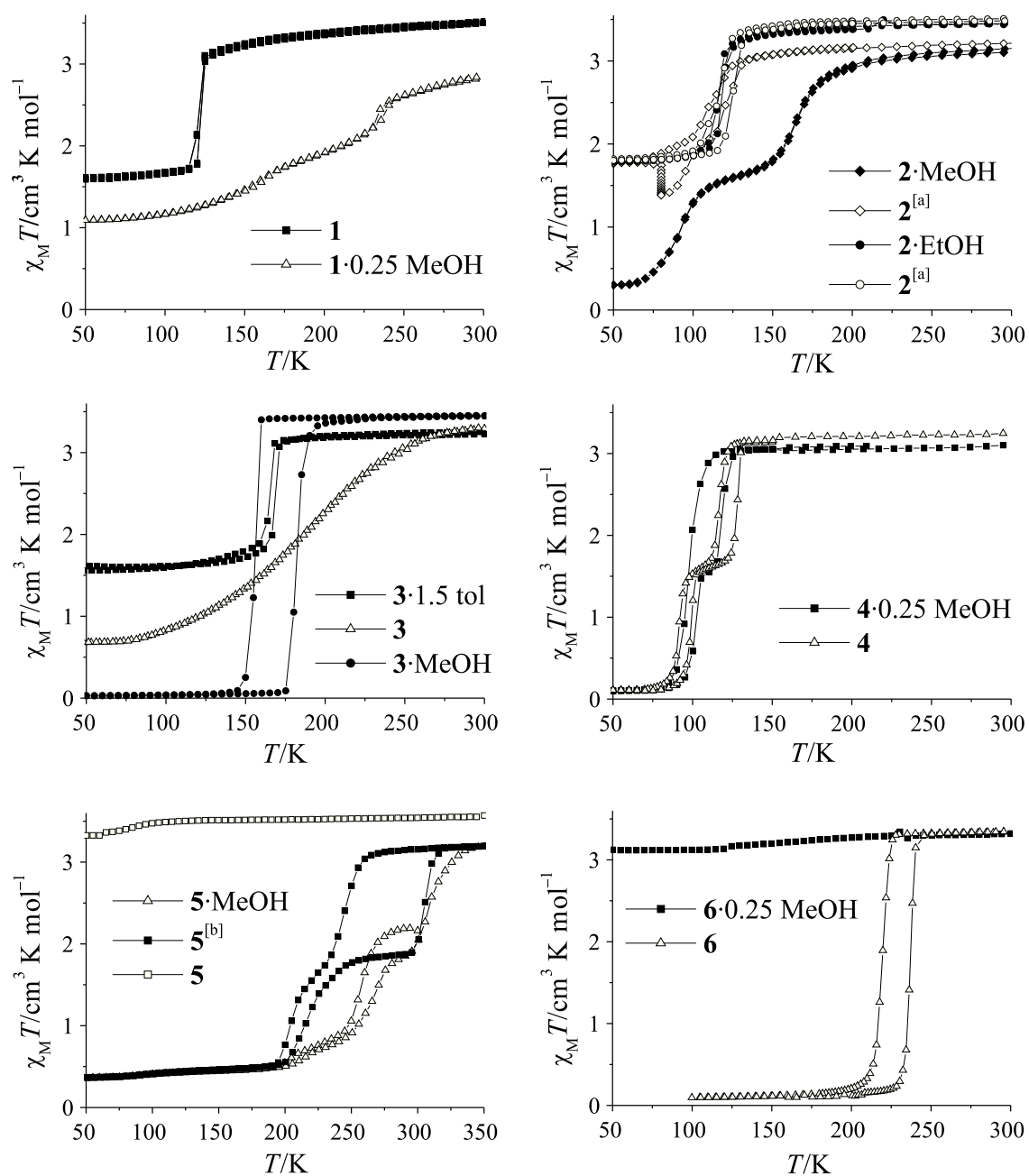


Figure 1. Plot of the $\chi_M T$ product vs. T for the different compounds discussed in this work. For completeness, the example of **6** and **6·0.25 MeOH**^[14] are given as well. [a] Tempered at 400 K for one hour; [b] heated to 350 K.

X-Ray structure analysis: Full single-crystal X-ray diffraction structure and refinement details have been obtained for the compounds $\mathbf{1}^{\text{HS}}$, $\mathbf{1}^{\text{HS-LS}}$, $\mathbf{2}^{\text{HS}}\cdot\text{MeOH}$, $\mathbf{2}^{\text{HS-LS}}\cdot\text{MeOH}$, $\mathbf{3}^{\text{HS}}\cdot\text{MeOH}$, $\mathbf{3}^{\text{HS}}\cdot 1.5 \text{ tol}$, $\mathbf{4}^{\text{HS}}\cdot 0.25 \text{ MeOH}$, $\mathbf{4}^{\text{LS}}\cdot 0.25 \text{ MeOH}$ and $\mathbf{5}^{\text{LS/LS}}\cdot\text{MeOH}$. In the case of $\mathbf{4}\cdot 0.25 \text{ MeOH}$, it was possible to determine the structure in the HS and LS states. For compounds $\mathbf{1}$, $\mathbf{2}\cdot\text{MeOH}$ and $\mathbf{3}\cdot 1.5 \text{ tol}$ (because of the low measurement quality of $\mathbf{3}^{\text{HS-LS}}\cdot 1.5 \text{ tol}$, the crystal structure can only be seen as a motif), it was possible to determine the molecule structure at $\chi_{\text{HS}} \approx 0.5$, in order to more clearly evaluate the reasons for the step in the transition curve. In the case of compound $\mathbf{3}\cdot\text{MeOH}$, the crystals crumbled while cooling down. The motif of the X-ray structure of $\mathbf{6}^{\text{HS}}\cdot 0.25 \text{ MeOH}$ was reported previously.^[14] The crystallographic data and refinement details are summarised in Supporting Information, Table S1.1–3. Selected bond lengths and angles within the first coordination sphere of the iron centre are summarised in Table 2. ORTEP drawings of the asymmetric units of the compounds are given in Figure 2.

In all complexes the iron(II) centres are located in distorted octahedral coordination spheres consisting of one equatorially coordinated tetradentate Schiff base-like ligand and two axially coordinated bis(monodentate) bridging ligands (bppa, bpea, bipy), bound through terminal 4-pyridyl groups. Each bridging ligand “connects” two iron(II) centres, which results in the formation of extended 1D chains as given in Figure 3. The average Fe-N/O bond lengths and angles are within the range reported previously for similar mononuclear,^[13] dinuclear^[15] and polymer^[14] HS and LS iron(II) complexes. For $\mathbf{3}^{\text{HS}}\cdot 1.5 \text{ tol}$, one ethoxy carbonyl side group of the equatorial ligand as well as one pyridyl ring of the axial ligand bpea are disordered.

The contents of the asymmetric units for all compounds, with the exception of $\mathbf{5}\cdot\text{MeOH}$, are made up of one crystallographically distinct iron(II) centre, when either the pure HS or LS state is expected, according to the results of the magnetic measurements. For compound $\mathbf{5}\cdot\text{MeOH}$, two crystallographically distinct iron(II) centres with slightly different crystallographic environments can be found. In the range of the IP, the asymmetric units are doubled and contain two crystallographically distinct iron centres, of which one can be assigned to iron(II) in the HS state (Fe1) and one to iron(II) in the LS state (Fe2).

4. Two-Step versus One-Step Spin Transition in Iron(II) 1D Chain Compounds

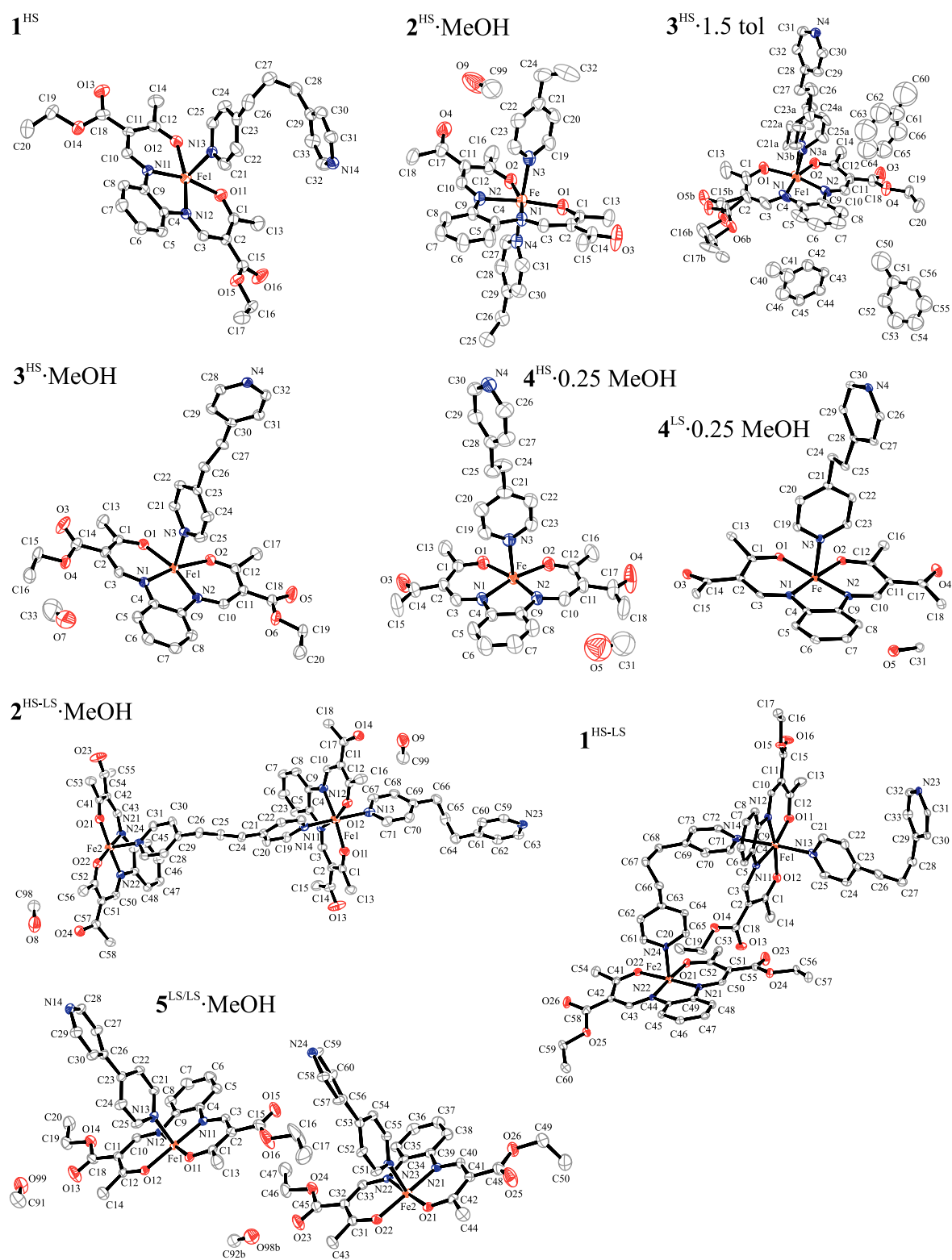


Figure 2. ORTEP drawing of the asymmetric units of the compounds discussed in this work, with the spin states of the iron(II) centres indicated at the top and the atom numbering scheme used in the text. The ellipsoids are shown with a 50% probability. Hydrogen atoms have been omitted for clarity.

4. Two-Step versus One-Step Spin Transition in Iron(II) 1D Chain Compounds

Table 2. Selected bond lengths [\AA] and angles [$^\circ$] within the first coordination sphere of the iron(II) complexes discussed in this work, with spin state S at temperature T .

compound	T/K	S	Fe-N _{eq}	Fe-O _{eq}	Fe-N _{ax}	O _{eq} -Fe-O _{eq}	N _{ax} -Fe-N _{ax}
1	200	2	2.091(2)	1.998(2)	2.253(3)	107.47(9)	177.82(8) ^[d]
			2.083(3)	2.012(2)	2.301(3) ^[d]		
	100	2	2.078(3)	1.994(2)	2.236(3)	106.92(8)	177.11(9)
			2.073(2)	2.007(2)	2.283(3)		
		0	1.902(2)	1.920(2)	2.000(2) ^[e]	89.09(9)	178.06(10) ^[e]
		1.908(3)	1.944(2)	2.011(2)			
2·MeOH	225	2	2.081(2)	2.013(2)	2.266(2)	109.64(6)	173.42(7)
			2.098(2)	2.011(1)	2.239(2)		
	125	2	2.066(3)	2.004(2)	2.238(3)	107.70(10)	172.64(11)
			2.075(3)	2.008(2)	2.221(3)		
		0	1.912(3)	1.948(2)	1.996(3) ^[f]	92.09(9)	174.55(11) ^[f]
		1.919(3)	1.948(2)	2.035(3)			
3·1.5 tol	200	2	2.094(4)	2.034(3)	2.218(4) ^[a]	110.98(13)	175.81(2) ^[a,g]
			2.115(4)	2.016(3)	2.285(5) ^[b]		169.23(2) ^[b,g]
					2.291(3) ^[g]		
		2 ^[c]	2.12/2.11	2.04/2.05	2.26/2.22	112.3	173.3
		0 ^[c]	1.91/1.89	1.96/1.95	2.00/2.00	90.1	176.5
3·MeOH	200	2	2.102(2)	2.013(2)	2.279(2)	109.80(6)	174.29(7) ^[h]
			2.091(2)	2.027(2)	2.256(2) ^[h]		
4·0.25 MeOH	293	2	2.087(2)	1.997(2)	2.259(2)	109.85(7)	176.47(8)
			2.083(2)	2.015(2)	2.293(2)		
			7	0	1.899(3)		
			1.892(2)	1.937(3)	2.032(3)		
5·MeOH	175	0	1.903(3)	1.926(3)	1.992(4)	87.90(11)	176.49(12) ^[i]
			1.909(3)	1.939(3)	1.996(4) ^[i]		
	175	0	1.901(3)	1.935(3)	1.981(4)	88.07(11)	176.78(12) ^[i]
			1.898(3)	1.939(3)	2.009(4) ^[i]		

[a] Related to N3A; [b] related to N3B; [c] values take from a structure motif due to low refinement quality; symmetry codes: [d] $-1 + x, \frac{1}{2} - y, -\frac{1}{2} + z$; [e] $-1 + x, y, z$; [f] $-1 + x, y, -1 + z$; [g] $x, y, -1 + z$; [h] $-1 + x, 1 + y, z$; [i] $1 + x, y, z$.

Compounds $\mathbf{1}^{\text{HS}}$ ($P2_1/c$) and $\mathbf{2}^{\text{HS}}\cdot\text{MeOH}$ ($C2/c$) crystallise in monoclinic space groups, and $\mathbf{3}^{\text{HS}}\cdot 1.5 \text{ tol}$ and $\mathbf{3}^{\text{HS}}\cdot\text{MeOH}$ in the triclinic space group $P\bar{1}$. For $\mathbf{1}^{\text{HS-LS}}$, $\mathbf{2}^{\text{HS-LS}}\cdot\text{MeOH}$ and $\mathbf{3}^{\text{HS-LS}}\cdot 1.5 \text{ tol}$, the change in the spin state at the iron(II) centres upon cooling can easily be followed by observing the O-Fe-O angle, the so-called bite of the equatorial ligand, which changes upon spin transition from about 110° in the HS state to about 90° in the LS state. Moreover, a characteristic shortening (ca. 10%) of the bond lengths occurs within the first coordination sphere. There are two different reasons for the change in the size of the asymmetric unit: for $\mathbf{2}^{\text{HS}}\cdot\text{MeOH}$, upon cooling to 125 K, the symmetry of the system is reduced from $C2/c$ to $P2_1/c$, half of the systematic extinctions observed at 225 K have vanished, as displayed in Figure 4. Consequently, the asymmetric unit of $\mathbf{2}^{\text{HS-LS}}\cdot\text{MeOH}$ consists of two crystallographically distinct iron(II) centres, as mentioned before. A one-dimensional chain of alternating HS and LS iron centres is formed as given in Figure 6. In contrast to this, at $\mathbf{1}^{\text{HS}}$ no change in the symmetry of the system is observed relative to $\mathbf{1}^{\text{HS-LS}}$, but an elongation of the unit cell along the a axis. Consequently, the cell volume is doubled from $3046(2) \text{ \AA}^3$ at 200 K to $5947(3) \text{ \AA}^3$ at 100 K. As in $\mathbf{2}^{\text{HS-LS}}\cdot\text{MeOH}$, a chain of alternating HS and LS iron centres is formed. The latter case is also true for $\mathbf{3}\cdot 1.5 \text{ tol}$, as no symmetry change is observed, but a duplication of the cell volume ($1966.5(4) \text{ \AA}^3$ at 200 K to $3861.2(3) \text{ \AA}^3$ at 130 K). It should be noted that the disorder of the equatorial and axial ligand disappears upon reaching the IP. For compound $\mathbf{4}\cdot 0.25 \text{ MeOH}$, it was possible to determine the X-ray structure in the HS and the LS state. In both cases, the compound crystallises in the triclinic space group $P\bar{1}$; unfortunately, we were not able to determine the X-ray structure at the plateau at 106 K. The bond lengths and angles around the iron(II) centre differ significantly at 298 and 7 K, highlighting the already discussed changes in spin state. Upon spin transition, the cell volume is reduced from $1427.8(5) \text{ \AA}^3$ at 298 K to $1328.4(8) \text{ \AA}^3$ at 7 K and the density rises from 1.337 g cm^{-3} to 1.436 g cm^{-3} . By considering the additional contribution of the thermal contraction, the observed change in the cell volume ($\Delta V/V = 7.2\%$, $\Delta V = 49.7 \text{ \AA}^3/\text{Fe}$) is in the range expected for an iron(II) SCO complex (contribution of the SCO itself: $\Delta V/V = 3.8\text{--}6\%$; $\Delta V = 25\text{--}35 \text{ \AA}^3/\text{Fe}$).^[1] Compound $\mathbf{5}\cdot\text{MeOH}$ also crystallises in the triclinic space group $P\bar{1}$. The asymmetric unit of $\mathbf{5}^{\text{LS/LS}}\cdot\text{MeOH}$ at 175 K is made up of two crystallographically distinct iron(II) centres that are both in the LS state, but with slightly geometrical differences within the inner coordination sphere caused by subtly different crystallographic environments of Fe1 and Fe2 as a result of incorporated solvent molecules.

Crystallographically distinct iron centres are the most likely reason for the step in the transition curve.

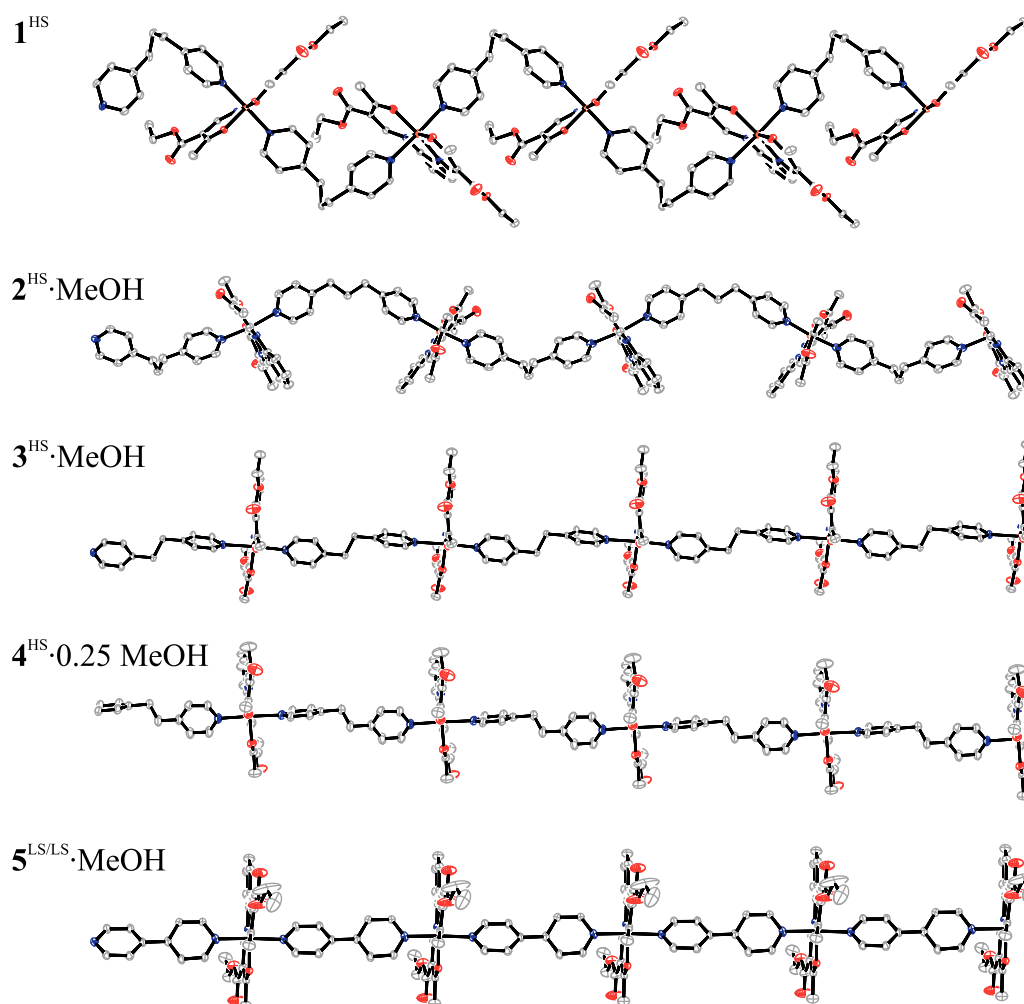


Figure 3. ORTEP drawing of the zigzag chain structure of compounds 1^{HS} and $2^{\text{HS}} \cdot \text{MeOH}$ with the axial bppa ligand, the steplike chain structure of $3^{\text{HS}} \cdot \text{MeOH}$ and $4^{\text{HS}} \cdot 0.25 \text{ MeOH}$ with the bpea ligand and the linear chain structure of $5^{\text{LS/LS}} \cdot \text{MeOH}$ with the bipy ligand.

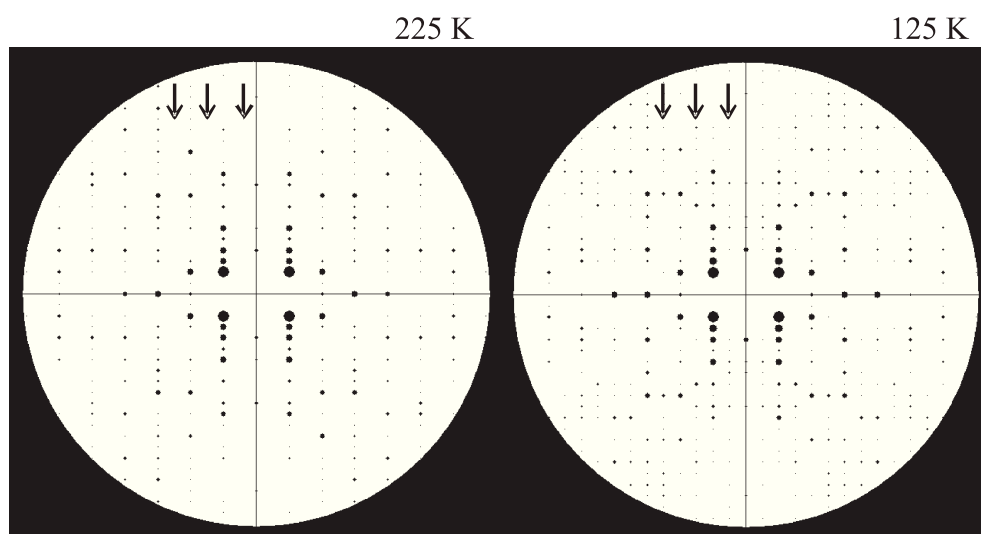


Figure 4. Reciprocal space $[0\ k\ l]$ section of compound **2**·MeOH at 225 K and 125 K represented with the Layer Program.

The step in the transition curve of compound **1** and **2**·MeOH is clearly related to the formation of an alternating [HS-LS] chain, and this may also be the case for **3**·1.5 tol; however, the order/disorder transition has to be kept in mind. For **1** and **2**·MeOH, the iron centres are clearly crystallographically equivalent in the HS state, while at the IP, two crystallographically distinct iron centres are obtained. This superstructure is only generated upon spin transition. Of the three already existing possibilities for the explanation of two-step spin transitions, two possibilities can be ruled out: the first one—two or more nonequivalent iron centres, can be excluded according to the results from X-ray structure analysis. The second possibility—the formation of energetically stable [HS-LS] pairs, is also not very likely. The formation of such pairs is associated with antiferromagnetic interactions between the neighbouring iron centres.^[7] Results from magnetic measurements on polymer HS iron(II) compounds of this ligand type show that the magnetic exchange interaction along the polymer chain is negligible.^[16] Hence, there is only the possibility of intermolecular interactions, generated through cooperative long-ranged (ferromagnetic-type) interactions or antiferromagnetic interactions between the HS and the LS sublattices. However, this model does not help us to define rules for the purposeful synthesis of 1D SCO materials with two-step spin transitions. Consequently, a new model is needed to explain the differences in the magnetic properties of the 1D chain compounds presented in this paper. A detailed comparison of intra- and interchain interactions is necessary to develop this model. Table 3 shows selected intra- and

interchain distances between the iron centres. Table 4 summarises intermolecular hydrogen bonds and short contacts, whereas in the Supplementary material detailed lists of intermolecular hydrogen bonds and short intermolecular contacts are given.

Table 3. Selected intra- ($\text{Fe}^{\cdot\cdot}\text{Fe}$) and interchain ($\text{Fe}^{\cdot\cdot}\text{Fe}^*$) iron(II) distances [\AA] of the coordination polymers discussed in this work.

compound	T/K	S	$\text{Fe}^{\text{HS}}\cdots\text{Fe}^{\text{HS}}$	$\text{Fe}^{\text{LS}}\cdots\text{Fe}^{\text{LS}}$	$\text{Fe}^{\text{HS}}\cdots\text{Fe}^{\text{LS}}$	$\text{Fe}^{\cdot\cdot}\text{Fe}^*$
1	200	2	10.01	/	/	8.25
	100	2/0	/	/	9.91/10.06	/
2 ·MeOH	225	2	13.14/13.80	/	/	8.55
	125	2/0	/	/	12.95/13.58	/
3 ·1.5 tol	200	2	13.85	/	/	13.96
3 ·MeOH	200	2	13.88	/	/	10.22
4 ·0.25 MeOH	293	2	13.83	/	/	8.68
	7	0	/	13.33	/	8.34
5 ·MeOH	175	0	/	11.10	/	7.56

In order to provide a better overview of the influence of packing effects on the spin transition properties, in the following, the differences in the crystal packing are compared by pairs with the different axial ligands as sort key.

The first pair of structures to be compared are the compounds with bppa as bridging ligand, namely **1** and **2**·MeOH (top of Figure 5). The infinite 1D chains of **1** propagate along $[2\ 0\ 1]$ for $\mathbf{1}^{\text{HS}}$ and $[1\ 0\ 0]$ for $\mathbf{1}^{\text{HS-LS}}$, a consequence from the symmetry change. The strong distortion of the axial bridging ligand results in the formation of zigzag chains. Between adjacent chains there is a multitude of short interactions, mainly between the ethoxy carbonyl side groups of the equatorial ligand and the CH groups of the axial ligand. Accompanied with the SCO, a change of the intrachain $\text{Fe}^{\cdot\cdot}\text{Fe}$ separation distance can be observed. One could expect this is to be due to the decrease in the Fe-L_{ax} distances from HS to LS. Along the $[\text{HS-HS}]$ chain of $\mathbf{1}^{\text{HS}}$, a $\text{Fe}^{\cdot\cdot}\text{Fe}$ separation distance of 10.01 \AA can be found which changes upon spin transition to the IP along $\mathbf{1}^{\text{HS-LS}}$ alternately to 9.91 and 10.06 \AA . Surprisingly, a shortening of

the $\text{Fe}^{\text{HS}} \cdots \text{Fe}^{\text{LS}}$ separation distance can only be seen for one chain link, whereas the other one is elongated, although at every second iron centre, the Fe-L_{ax} bond lengths decrease. A closer look reveals that the end-to-end distances of the strongly twisted bppa ligands elongate significantly from 6.98 Å at $\mathbf{1}^{\text{HS}}$ to 7.06/7.27 Å at $\mathbf{1}^{\text{HS-LS}}$. The bppa ligand can be thought to “compensate” the shortening of the Fe-L_{ax} distances, so that on average the chain length remains the same. The relative position of the iron centres and the equatorial ligands does not change, possibly because of the restraining interactions caused by the short contacts given in Table 4. The infinite 1D chains of $\mathbf{2}\cdot\text{MeOH}$ (HS and LS) propagate along the [1 0 1] direction. The distortion of the axial bridging ligand results also in the formation of zigzag chains, but with an angle of about 56° between the planes of neighbouring equatorial ligands, the distortion is weaker than in $\mathbf{1}$. Between the hydroxy hydrogen atom (H9) of the methanol molecule and the oxygen atom (O4) of one acetyl side group of the equatorial ligand, a hydrogen bond is formed. This is only of indirect importance; however, the oxygen atom as a strong H-bond acceptor is “occupied” and cannot form any kind of interchain interaction. Furthermore, a number of weak van der Waals contacts occur, mainly involving the second acetyl oxygen atom (O3), the methanol hydroxy oxygen atom (O9) and CH groups of the axial ligand. In the HS state, all hydrogen bonds are mediated by the methanol molecule, while in the HS/LS state, one additional direct contact is observed (see Table 4). By looking at the intrachain $\text{Fe} \cdots \text{Fe}$ separation distance, another situation can be observed for compound $\mathbf{2}\cdot\text{MeOH}$ relative to $\mathbf{1}$. Two differently elongated chain links can be found at $\mathbf{2}^{\text{HS}}\cdot\text{MeOH}$ (13.14 and 13.80 Å), which change significantly to 12.95 and 13.58 Å in $\mathbf{2}^{\text{HS-LS}}\cdot\text{MeOH}$ on the IP. The changes in the end-to-end distances of the bppa ligands ($\Delta = 0.04$ and 0.06 Å) are not as pronounced as observed for compound $\mathbf{1}$, thus the shortening of the Fe-L_{ax} distances are only marginally compensated. The more pronounced zigzag chain in the case of $\mathbf{1}$, in combination with the sterically more-demanding equatorial ligand L1 and the more direct (not mediated over the included methanol molecule) interchain interactions, results in the fact that the single chains of $\mathbf{1}$ are more strongly wedged together than in $\mathbf{2}\cdot\text{MeOH}$, as illustrated in Figure 5. Thus, the changes in the bond lengths expected upon spin transition cannot be as easily followed for $\mathbf{1}$ relative to $\mathbf{2}\cdot\text{MeOH}$, and the spin transition behaviour changes from a complete two-step transition ($\mathbf{2}\cdot\text{MeOH}$) to an incomplete spin transition for $\mathbf{1}$ that stops at the IP.

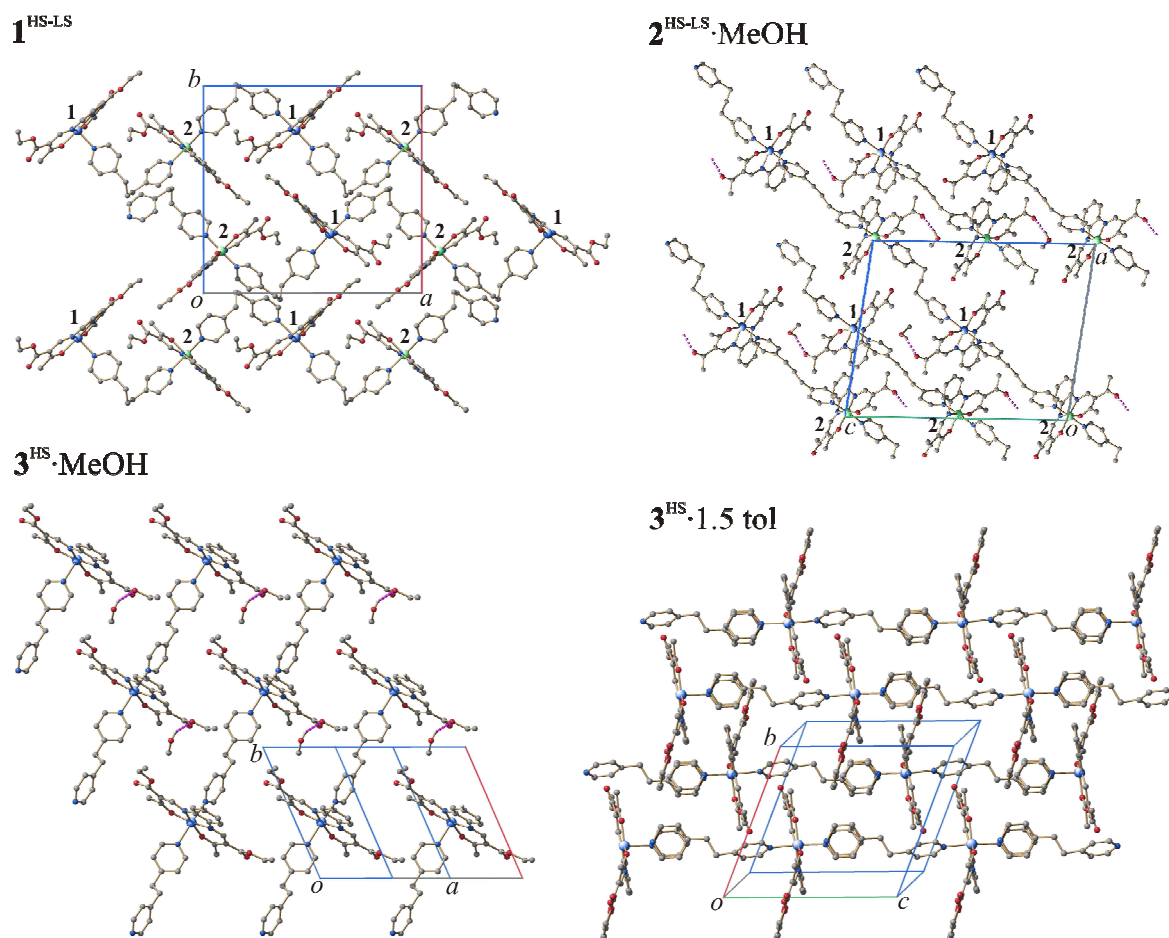


Figure 5. Plot of the crystal packing of the iron(II) coordination polymers **1**, **2**·MeOH, **3**·1.5 tol and **3**·MeOH. 1 and 2 refer to the different iron centres in the HS/LS state. Hydrogen bonds are shown as dashed lines. Hydrogen atoms are omitted for clarity.

The infinite 1D chains of **3**·MeOH and **3**·1.5 tol have the base vectors $[1\bar{1}0]$ and $[001]$, respectively (Figure 5, bottom). Because of the less-flexible ethyl bridge of the axial ligand bpea (instead of the propyl bridge of bppa), a stepped chain structure is observed for both compounds compared to the zigzag structure mentioned above. The intrachain Fe··Fe separation distances are almost identical: 13.88 Å (**3**·MeOH) and 13.85 Å (**3**·1.5 tol). The methanol molecule of **3**·MeOH is hydrogen bonded to one ethoxy oxygen atom (O4) of the equatorial ligand. The other carboxylate oxygen atoms and carbonyl oxygen atoms of the equatorial ligand form weak interactions with CH groups of the axial ligand of adjacent chains. These interactions together with the other short contacts are the most likely explanation for the 27 K wide hysteresis loop in this compound. The molecule packing of

3·1.5 tol has a lower density than that in **3**·MeOH (1.291 relative to 1.363 g cm⁻³), possibly because of the relatively huge disordered toluene molecules incorporated between the chains. This can also be seen by comparing the interchain Fe^{••}·Fe^{*} separation distances (Fe^{*} is the iron centre generated through the symmetry operation $-x, -y, -z$), which are significantly longer in **3**·1.5 tol (13.96 relative to 10.22 Å, Table 3). Consequently only a few interchain interactions can be found (see Table 4), mainly between both carbonyl oxygen atoms of the equatorial ligand and carbon-bonded hydrogen atoms of the axial ligand bpea. This satisfactorily explains the reduction in the hysteresis width when going from the methanol- to the toluene-containing sample. This pair also illustrates that it is important to compare all intermolecular contacts, as the number of hydrogen bonds is the same for both compounds. However, no explanation for the IP of **3**·1.5 tol can be derived from the crystal packing, as was possible for **1** and **2**·MeOH. Therefore, it can be assumed that the disorder observed in the HS structure is responsible for the incomplete spin transition with only 50% of the iron centres involved. The infinite 1D chains of **4**·0.25 MeOH (HS and LS) propagate along $[1 \bar{1} 0]$ with the same stepped structure observed for compounds **3**·MeOH and **3**·1.5 tol. Upon spin transition, the intrachain Fe^{••}·Fe distance is shortened about 0.50 Å, whereas the end-to-end distance of the axial bpea ligand is only shortened about 0.01 Å, which highlights the stiffness of bpea. In comparison with compound **3**, the solvent molecule seems to influence the SCO behaviour of compound **4** in a similar way, because, for both examples, the loss of methanol is accompanied with a decrease in the cooperativity when comparing the solvent-containing and the solvent-free sample. In contrast to compound **3**·MeOH with its full occupancy methanol molecule involved in strong hydrogen bonds, the structure of **4**·0.25 MeOH only contains a quarter occupancy methanol, which is furthermore not hydrogen bonded to one of the carbonyl oxygen atoms of the equatorial ligand. Therefore, both acetyl oxygen atoms of the equatorial ligand form nonclassical hydrogen bonds to adjacent chains involving the CH groups of the axial ligand, which explains the observed hysteresis loop, and are probably also responsible for the small IP in the heating mode.

The molecule structure of **5**^{LS/LS}·MeOH was determined at 175 K, thus all iron(II) centres are in the LS state. Because of the slightly different chemical surroundings as a result of an additional disordered methanol molecule, two complex molecules with nonequivalent iron(II) sites can be found in the asymmetric unit. The infinite 1D chains of compound **5**·MeOH run along $[1 0 0]$ and are totally linear because of the bridging ligand bipy. Adjacent chains are

arranged in a way that the ethoxy carbonyl side groups of the equatorial ligand point to each other. Consequently, many short intermolecular interactions can be observed. Every methanol molecule forms a hydrogen bond to a carboxylate oxygen atom of one of the equatorial ligands. However, whereas for Fe1, typical hydrogen bond values are found (H99 \cdots O13: 1.95 Å, see Table 4); in the case of Fe2, a significantly weaker hydrogen bond is observed (H98b \cdots O23: 2.32 Å, Table 4) and, additionally, the methanol molecule is disordered. This supports the results from the magnetic measurements and TG analysis, that, upon heating to 350 K, only one of the two methanol molecules is lost and two crystallographically different iron centres are obtained, which undergo spin transition at different temperatures. Short interactions are also observed between the remaining carboxylate oxygen atoms and CH groups of the axial ligand and the acetyl CH₃ groups of adjacent chains, as summarised in Table 4. In the magnetic measurements, different widths are observed for the two hysteresis loops, and the question arises whether this is reflected in the X-ray structure. In Figure 6, a top view of the packing of the chains in the crystal is given. The 1D chains of equivalent iron centres form layers along the *c* axis that alternate along the *b* axis. The summary of the intermolecular interactions given in Table 4 reveals that, between the chains of Fe1, more and shorter contacts are observed relative to the Fe2-Fe2 interactions. Between the layers (Fe1-Fe2 interactions), even fewer contacts are observed. Thus, the different hysteresis widths can be explained with differences in the number and strength of interchain contacts.

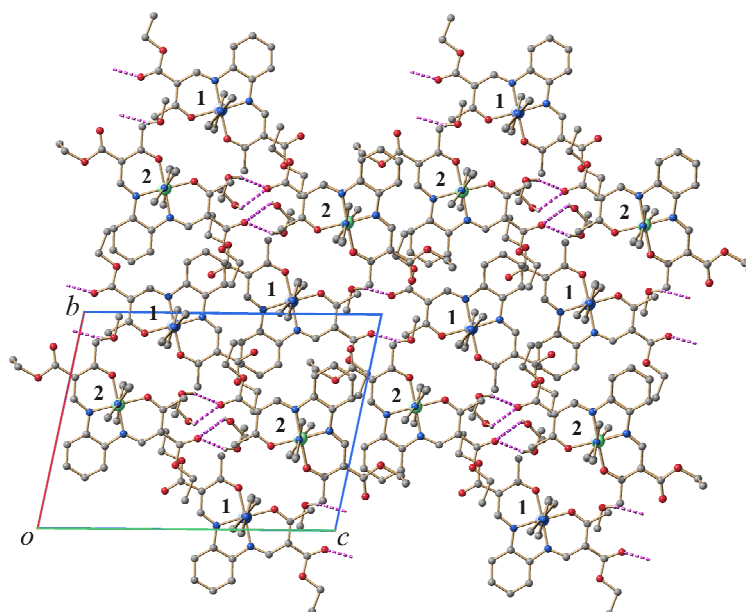


Figure 6. Top view of the crystal packing of the iron(II) coordination polymer **5**·MeOH. Hydrogen bonds shown as dashed lines. Hydrogen atoms are omitted for clarity. 1 and 2 refer to the different iron centres in the HS/LS state.

Table 4. Summary of intermolecular contacts per iron centre of the iron(II) coordination polymers discussed in this work. The number of contacts to solvent molecules is given in parentheses. For details about the hydrogen bonds with $d(D \cdots A) < R(D) + R(A) + 0.50 \text{ \AA}$, $d(H \cdots A) < R(H) + R(A) - 0.12 \text{ \AA}$, $D-H \cdots A > 100.0^\circ$ and for details about the short contacts with $\Delta = d(I \cdots J) - (R(I) + R(J))$ (sum of the van der Waals radii) see Supplementary material.

compound	H-Bond	$\Delta > 0.2 \text{ \AA}$	$\Delta = 0.20 - 0.1 \text{ \AA}$	$\Delta < 0.1 \text{ \AA}$	Σ (solvent)
1 ^{HS}	2		2	6	10
1 ^{HS-LS}	3		2	8.5	13.5
2 ^{HS} ·MeOH	(2)		1	4	5 (2)
2 ^{HS-LS} ·MeOH	(2)	0.5	3	9	12.5 (2)
3 ^{HS} ·1.5 tol	4		1 (1)	1 (1)	6 (2)
3 ^{HS} ·MeOH	3 (1)	1	2	9	15 (1)
4 ^{HS} ·0.25 MeOH	2	(1)	3 (3)	3 (3)	8 (7)
4 ^{LS} ·0.25 MeOH	2	(1)	2 (2)	12 (2)	16 (5)
5 ·MeOH ^[a]	2/1/0 (3)	0/0/1 (2)	3/0/1 (2)	2/4/1 (9)	7/5/3 (16)

[a] Distinguished between Fe1-Fe1/Fe2-Fe2/Fe1-Fe2 interactions and contacts to the solvent (MeOH).

Investigations in solution by using ^1H NMR spectroscopy: Variable-temperature NMR spectroscopy is a valuable tool to follow a spin transition in solution by interpretation of the temperature dependence of the ^1H NMR chemical shifts.^[15b] In order to prove the influence of the intermolecular interactions on the transition temperature and the appearance of a step during a SCO, compounds **1** and **3**·1.5 tol were dissolved in $[\text{D}_8]$ toluene, as, in solution, all packing effects are switched off. For all other compounds, the solubility in toluene was too low for measurement by this method and another solvent with similar properties (liquid range, non-coordinating) was not available. Before starting T -dependent measurements, it was important to verify that all iron centres retain their octahedral coordination sphere and therefore the 1D coordination polymers are intact in solution. This could be confirmed by the signal assignment, which is shown in Figure 7. The resonances of the equatorial ligand L1 appear in a similar region as reported previously for mononuclear iron(II) complexes of this ligand with different axial ligands (pyridine^[15b] and 4-cyanopyridine^[13c]). The signals are therefore assigned to the methyl group (a) and the ethyl group (b, c) of the substituents of the equatorial ligand. The signal at about 10 ppm with a relative intensity of 1 is assigned to the proton d of the phenylene ring. The signals of the two remaining protons of the equatorial ligand are not assigned. By considering the NMR spectra of this type of complex in pyridine,^[15b] the HC-N proton signal should be in the 400–500 ppm region of the spectrum, but it is very broad and therefore difficult to detect. The signal for the second proton of the phenylene ring is probably in the –5 to 5 ppm region of the spectrum, but is too broad to be detected because of additional signals from the solvent, impurities and the axial ligand. In each of the NMR spectra of **1** and **3**, in Figure 7, three remaining signals are observed, which belong to the axial ligands bppa and bpea. By assuming a chain structure, the bridging ligand bppa has a mirror plane in C26/C32, and four different signals are expected with the relative intensities of 2:2:2:1. If a *penta*-coordinated complex was to be considered (polymeric chain broken into monomers), seven different signals would be expected, each with the relative intensity of 1. As the chemical shift is strongly influenced by the paramagnetic iron centre, and this influence decreases rapidly with increasing distance from the metal centre (number of bonds), many of the signals would be expected in the diamagnetic region. In the case of complete dissociation, all the signals of the axial ligand would be expected in the diamagnetic region, which is not the case. For the remaining signals, a relative intensity of 2 is observed, which clearly proves the polymeric chain structure of the complex in solution. With regard to

the different line widths, signal g with the smallest line width is assigned to the CH₂ group farthest away from the paramagnetic centre, and signals e and f are assigned to the proton *ortho* (e) and *meta* (f) to the pyridine nitrogen. The last signal (C26/32) could not be assigned, probably because it is too weak and in the diamagnetic region of the spectrum. The same observation can be made for chain complex **3**. Here, only three signals with the relative intensities 2:2:2 are expected, by assuming an octahedral complex, as observed in the NMR spectra. The resonances appear in a similar region to those for the bppa ligand and are thus assigned the same way as shown in Figure 7.

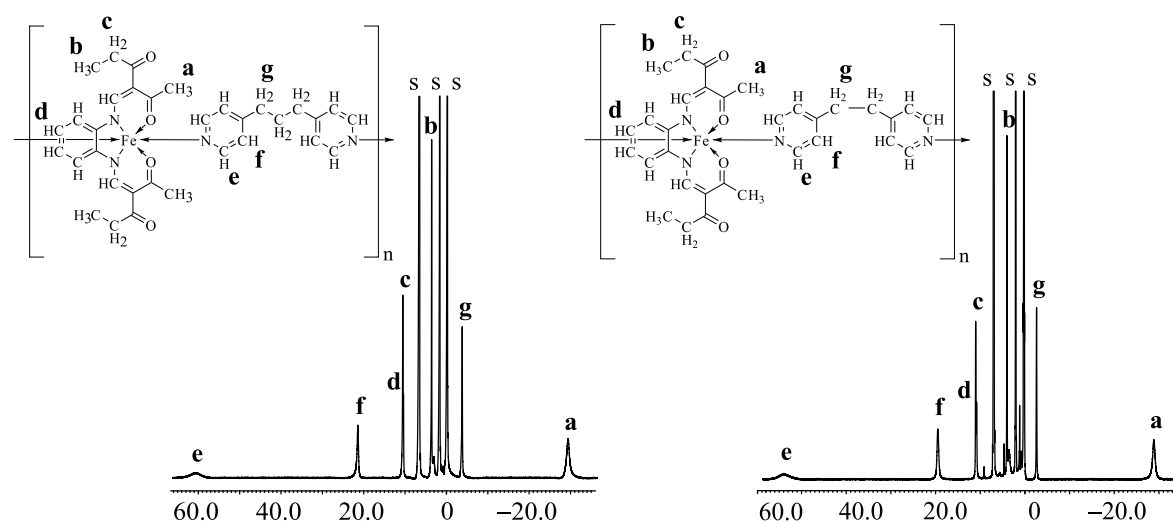


Figure 7. ¹H NMR spectra and signal assignment for complex **1** (left) and **3** (right) in [D₈]toluene at 348 K (s = solvent).

Figure 8 illustrates the shift of the NMR signals with temperature for complex **1**. In Figure 9, the isotropic shifts of the protons of the equatorial ligand are plotted vs. inverse temperature (Curie plot) for both complexes. Starting at 358 K, upon cooling, the NMR signals are shifted to the more paramagnetic regions of the spectra, thus showing Curie behaviour. This is confirmed by the nearly linear temperature dependence seen in the Curie plots in the high-temperature region ($T > 285$ K, $1/T < 3.5 \times 10^3$ K⁻¹). This behaviour is similar to that expected for pure HS complexes. Below this point, the isotropic shift tends to zero, which indicates the start of the spin transition, as reported previously for this type of SCO complex with pyridine as axial ligands.^[15b] From the ¹H signals of the NMR spectra shown in Figure 8, only signals a–d, f and g can be observed over the whole temperature range investigated. Of those signals,

only the chemical shifts of signals a–d, which are assigned to the equatorial ligand, show the described behaviour. The T -dependence of the chemical shifts of signals f and g, which are assigned to the axial ligand, is different; especially, in the high-temperature region no Curie behaviour is observed. The most likely reason for this is the possibility of the axial ligand to rotate freely around the z axis. Attempts to analyse this behaviour by using the T -dependent fitting program (TDF), applied successfully for the mononuclear complexes,^[15b] were not fruitful, and those resonances are not considered in the further discussion.

By assuming Curie behaviour for the high-spin species, the isotropic shift multiplied by the temperature is constant as long as the spin state does not change. A normalised plot of $\delta_{\text{iso}} T$ vs. T therefore reflects the high-spin mole fraction (χ_{HS}) of the complex as a function of temperature. In Figure 10, the transition curves of the averaged signals obtained in solution are compared with the results of the SQUID measurements in the solid state for both compounds. Because of the low solubility of both compounds at low temperature, only the beginning of the spin transition in solution could be detected by this method. Nevertheless, some trends can be observed as can be seen in Figure 10. When the transition curves of **1** and **3** obtained in solution are compared, both complexes show a gradual spin transition starting at similar temperatures of about 300 K. In the case of **1**, no indications for an abrupt SCO resting on a step as observed for the solid state analogue can be found. In comparison to the corresponding solid compounds (**1**, $T_{1/2} = 165$ K; **3**·1.5 tol, $T_{1/2} = 123$ K), the transition temperatures obtained in solution are clearly shifted to higher temperatures. These huge differences in SCO behaviour illustrate that the extent of cooperative interactions, as well as the transition temperature, is significantly influenced by packing effects.

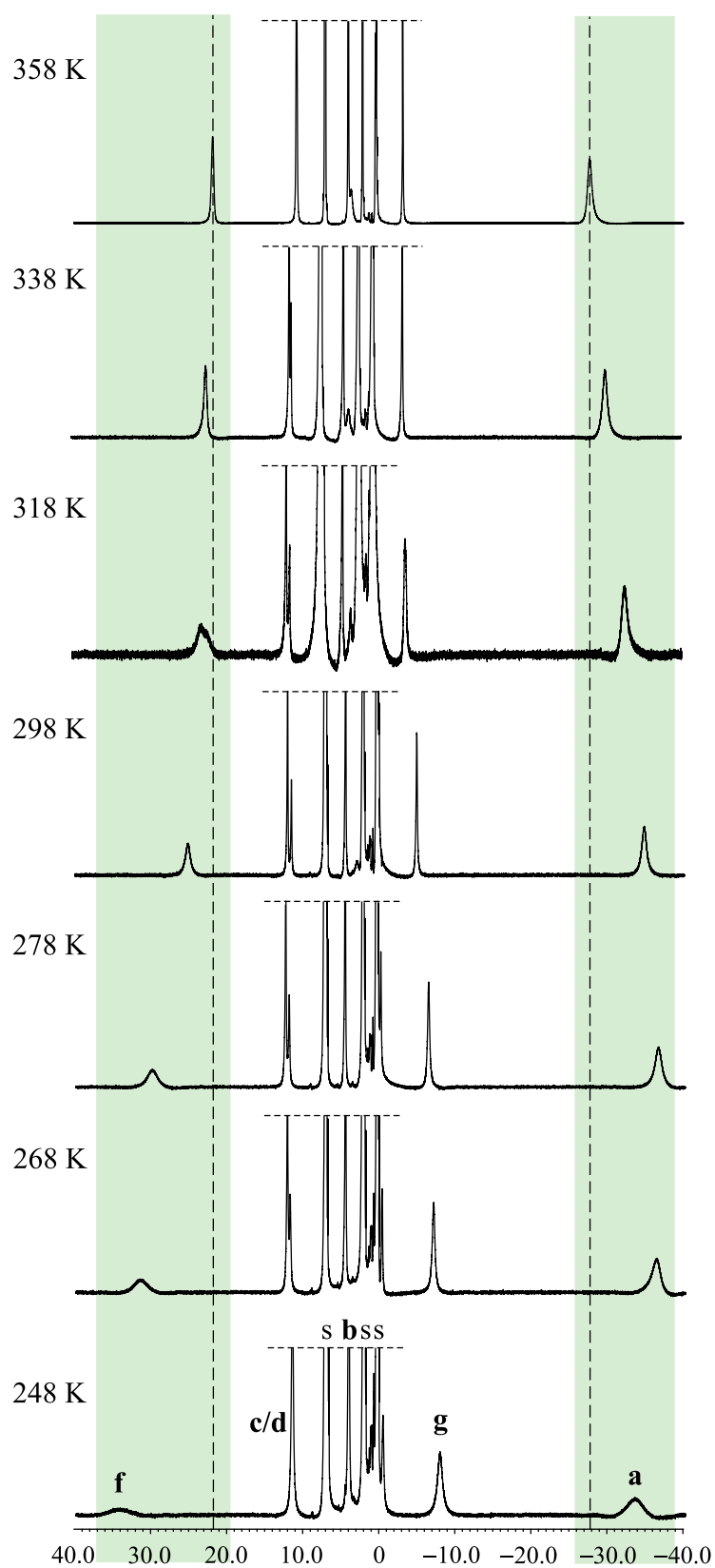


Figure 8. T -dependence of the chemical shifts of the ^1H signals a–d of complex **1** between 358–248 K (s = solvent). The relative position of the resonance of signals a and f at 358 K is tagged with a line to more clearly illustrate the T -dependent shift of the signal.

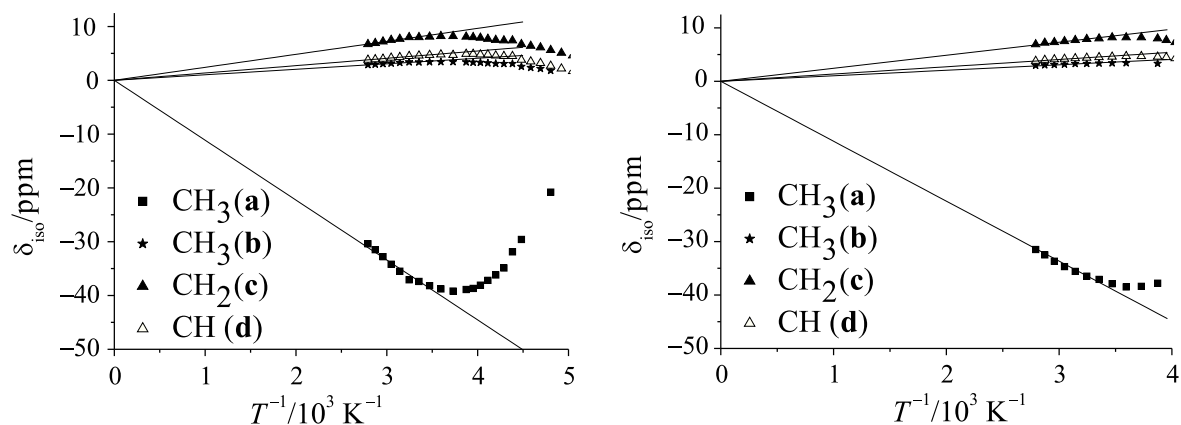


Figure 9. Chemical shifts δ_{iso} of the assigned ¹H signals of complex **1** (left) and **3** (right) plotted vs. inverse temperature.

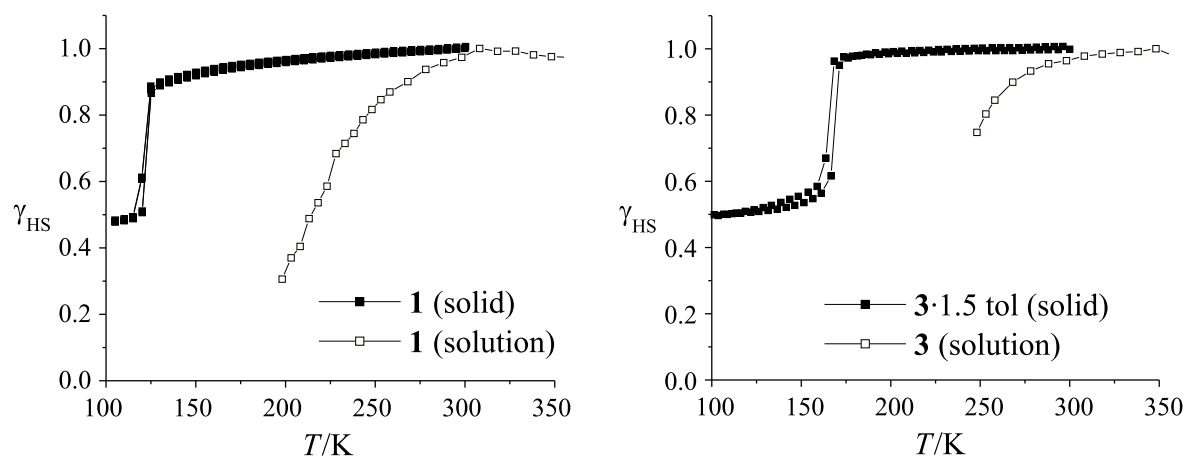


Figure 10. HS molar fraction γ_{HS} vs. T for complex **1** (left) and **3** (right) followed in solution and in the solid state.

4.3 Discussion

Different types of spin transition were obtained for the 13 compounds discussed in this work going from complete SCO to two-step SCO to incomplete SCO resting at the IP. In the same way, the cooperative interactions vary from gradual spin transition to up to 50 K wide thermal hysteresis loops. Some correlation can be found between the used axial bridging ligand, the width of the IP and the thermal hysteresis loop.

The width of the thermal hysteresis loop increases in the order $bppa < bpea < bipy$ for both equatorial ligands (L1: 0 K, 4 K, 58 K; L2: 10 K, 22 K, 18 K, always highest values considered). The occurrence of a thermal hysteresis loop correlates well with the flexibility of the used bridging ligand and the number of interchain contacts, especially weak hydrogen bonds. For the more rigid ligand 4,4'-bipyridine, wide thermal hysteresis loops are observed, while the flexible *bppa* ligand only leads to stepped transitions or small thermal hysteresis loops. This is in agreement with literature results where 1D chains with iron(II) ions linked by loose bridges (*e.g.* bis(tetrazole) bridges with flexible spacers)^[17] or ridged linkers without significant intermolecular interactions (*bpea*,^[18] *bipy*,^[19] dicyanamide^[20]) result in gradual SCO behaviour. Combinations of intermolecular and intramolecular interactions contribute to the cooperative mechanisms during the spin transition and thus wide hysteresis loops. It is important to note that a combination of both interaction pathways is necessary to observe wide hysteresis loops. On the one hand, ridged linkers with no significant intermolecular interactions result in gradual spin transitions. On the other hand, if the number of intermolecular contacts is in the same order of magnitude, as for the examples presented in this work, the more ridged linkers lead to wider hysteresis loops. This is in agreement with the analytical solution of 1D systems where width and shape of the hysteresis loop depends on the balance between long- and short range interactions.^[21]

In the case of two-step or incomplete spin transitions, two different reasons have to be distinguished. For **3**·1.5 *tol* and **5**·MeOH, crystallographically nonequivalent iron centres are clearly responsible for the incomplete/two-step spin transition. This is not the case for the other examples. Here, the width of the plateau ($T_{1/2}(1) - T_{1/2}(2)$) decreases in the order $bipy < bpea < bppa$ (L2: 0 K, 18 K, 77 K; L1: incomplete or disorder). With regard to the plateau in the transition curve, an interesting model was recently proposed by Koudriavtsev *et al.* for monomer complexes that can be transferred to our polymer systems. This quasi-chemical model uses specific molecular interactions for the description of stepwise or incomplete spin

transitions for mononuclear complexes.^[22] A HS \rightarrow LS transition in a pair of HS molecules with attractively interacting ligands (*e.g.* hydrogen bonds) involves a relocation of the ligands towards the smaller LS molecule. If the Fe \cdots Fe distances do not follow exactly the changes in Fe-L bonds in the LS species, then the corresponding bond in the HS partner is elongated and the HS state is thus stabilised.^[21] This principle can be very easily transferred to polymer chain compounds. In Figure 11 a schematic illustration of the proposed model is given.

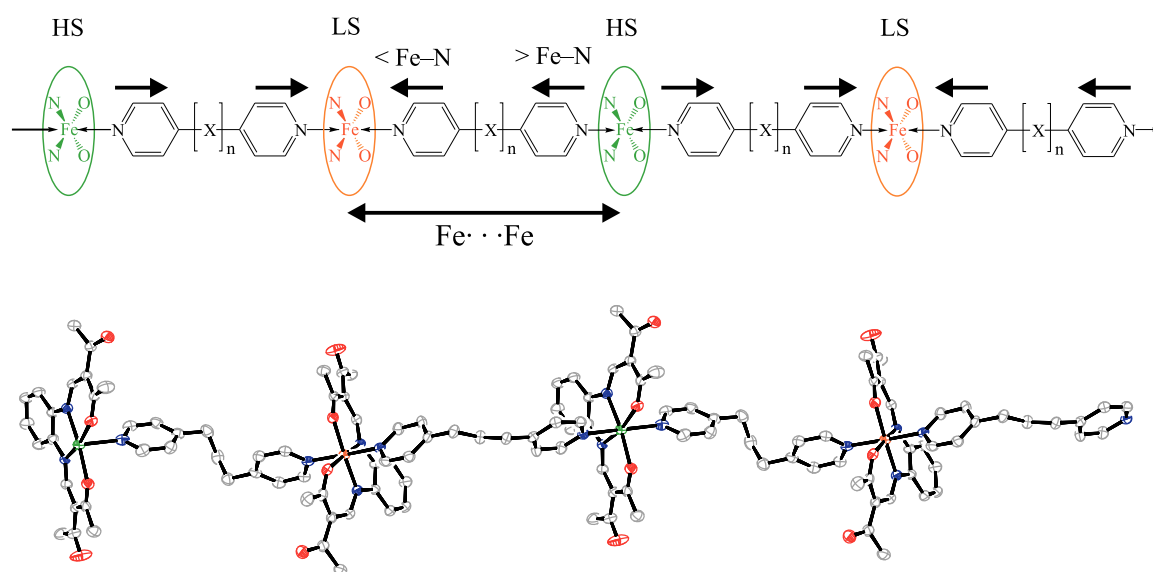


Figure 11. Schematic illustration of the model proposed for stepwise spin transitions ($X = \text{CH}_2$, $n = 0-3$).

The remaining question is why some of the compounds have one-step and others have two-step spin transitions; or in other words, are there factors that determine whether the Fe \cdots Fe distances can follow exactly the changes in Fe-L bonds or not. The pair **1** and **2**·MeOH gives an indication of which factors inhibit a change in the Fe \cdots Fe separation distance: a pronounced zigzag chain in combination with a number of interchain contacts results in an incomplete SCO for **1**. In the case of **2**·MeOH, the zigzag motive is less pronounced and less interchain contacts are observed, thus the second step can be observed. An even smaller step is observed for **4**·0.25 MeOH—the chain is nearly linear, the number of interchain contacts does not change significantly, and for the linear chain compound **6**, no steps in the transition curve are observed, although there are several interchain contacts that are responsible for the

thermal hysteresis loop. Thus, a pronounced zigzag structure of the 1D chain in combination with several interchain contacts result in stepwise spin transitions, even if all iron centres are equivalent in the HS state.

4.4 Conclusion

The synthesis and characterisation of several new 1D chain iron(II) spin crossover compounds is described in this paper. A comparison of the spin transition behaviour and the results from X-ray structure analysis lead to two conclusions for the rational design of spin crossover materials. The first, and to some extent already discussed, theory is that a combination of intermolecular and intramolecular interactions contributes to the cooperative mechanisms during the spin transition and thus to wide hysteresis loops. The second hypothesis is that a pronounced zigzag structure of the 1D chain in combination with several interchain contacts result in stepwise spins transitions, even if all iron centres are equivalent in the HS state. Further examples and further ongoing experiments, including photomagnetic investigations, DSC measurements and Mössbauer spectroscopy, are necessary to prove this theory. This work is already in progress and will be part of a subsequent publication.

4.5 Experimental Section

Magnetic measurements: Magnetic susceptibility data were collected by using a Quantum Design MPMSR-2 SQUID magnetometer under an applied field of 0.5 T over the temperature range 2–350 K in the settle mode. The samples were placed in gelatine capsules held within a plastic straw. The data were corrected for the diamagnetic magnetisation of the ligands by using tabulated Pascal's constants, and of the sample holder. The measurements were analysed by using the CGS system.

NMR spectroscopy: [D₈]toluene (D, 99.6%) was purchased from Euriso-top. The solvent was degassed with argon and stored over molecular sieves. The NMR samples were prepared under argon by using Schlenk techniques and locally-made sealing equipment. Saturated solutions of the iron(II) complexes were prepared and stored in sealed or air-tight 5 mm NMR tubes. The NMR spectra were recorded on a JEOL EX 400e spectrometer operating at 400.182 MHz equipped with a variable-temperature unit in the temperature range 198–358 K.

X-Ray structure determination: The intensity data were collected on an Oxford XCalibur diffractometer (**1**, **3**·MeOH), a Nonius Kappa CCD diffractometer (**2**·MeOH, **3**·1.5 tol, **5**·MeOH) and a Huber 4-circle diffractometer (**4**·0.25 MeOH) by using graphite-monochromated MoK_α radiation. The data were corrected for Lorentz and polarisation effects. The structures were solved by direct methods (SIR-97)^[23] and refined by full-matrix least-square techniques against F_0^2 (SHELXL-97).^[24] The hydrogen atoms were included at calculated positions with fixed displacement parameters. ORTEP-III^[25] was used for the structure representation, SCHAKAL-99^[26] to illustrate molecule packings. The crystallographic data are summarised in Supporting Information, Table S1.1–3. The quality of the data of **3**·1.5 tol in the mixed high-spin/low-spin state is inferior. We will therefore only be publishing the conformation of the molecule and the crystallographic data.

CCDC 793143 (**1**^{HS}), CCDC 793144 (**1**^{HS-LS}), CCDC 684269 (**2**^{HS}·MeOH), CCDC 684270 (**2**^{HS-LS}·MeOH), CCDC 973145 (**3**^{HS}·1.5 tol), CCDC 973146 (**3**^{HS}·MeOH), CCDC 973147 (**4**^{HS}·0.25 MeOH), CCDC 973149 (**4**^{HS-LS}·0.25 MeOH) and CCDC 973149 (**5**^{LS/LS}·MeOH) contain the supplementary crystallographic data for this paper. These data can be obtained free of charge from The Cambridge Crystallographic Data Centre *via* www.ccdc.cam.ac.uk/data_request/cif.

Synthesis: The syntheses of the iron(II) complexes were carried out under argon by using Schlenk tube techniques. All solvents were purified as described in the literature^[27] and distilled under argon. [FeL1(MeOH)₂] and [FeL2(MeOH)₂] were prepared as described in the literature.^[28] 1,3-Bis(4-pyridyl)propane and 1,2-bis(4-pyridyl)ethane were purchased from Sigma-Aldrich and used as received, 4,4'-bipyridine was purchased from Acros Organics and used as received.

[FeL1(bppa)] (1): [FeL1(MeOH)₂] (0.25 g, 0.49 mmol) and 1,3-bis(4-pyridyl)propane (0.98 g, 4.93 mmol) were dissolved in toluene (15 mL) and heated to reflux for 1 h. After cooling down to room temperature, a fine crystalline black precipitate had formed that was filtered off, washed with toluene (2 × 5 mL) and dried *in vacuo* (yield: 0.21 g, 67%). Crystals suitable for X-ray analysis formed in the mother liquor within a few weeks. IR (KBr): $\tilde{\nu}$ = 1679(s) cm⁻¹ (OC=O); MS (DEI-(+), 70 eV): *m/z* (%): 442 (71) [FeL1⁺], 198 (100) [bppa⁺]; elemental analysis calcd (%) for C₃₃H₃₆FeN₄O₆ (640.20): C 61.88, H 5.67, N 8.75; found: C 61.58, H 5.65, N 8.71.

[FeL1(bppa)]·0.25 MeOH (1·0.25 MeOH): [FeL1(MeOH)₂] (1.67 g, 3.30 mmol) and 1,3-bis(4-pyridyl)propane (3.27 g, 16.5 mmol) were dissolved in methanol (25 mL) and heated to reflux for 1 h. After cooling down to room temperature, a fine crystalline black precipitate had formed that was filtered off, washed with methanol (2 × 5 mL) and dried *in vacuo* (yield: 0.96 g, 46%). Elemental analysis calcd (%) for C_{33.25}H₃₇FeN₄O_{6.25} (648.52): C 61.58, H 5.75, N 8.64; found: C 61.53, H 5.73, N 8.68.

[FeL2(bppa)]·MeOH (2·MeOH): A mixture of [FeL2(MeOH)₂] (0.75 g, 1.96 mmol) and 1,3-bis(4-pyridyl)propane (1.94 g, 9.80 mmol) in methanol (10 mL) was heated to reflux for 1 hour. After cooling at 5 °C for 24 h, a crystalline black precipitate was obtained that was filtered off, washed with methanol (2 × 5 mL) and dried *in vacuo* (yield: 0.75 g, 62%). IR (KBr): $\tilde{\nu}$ = 1642(s) cm⁻¹ (C=O); MS (DEI-(+), 70 eV): *m/z* (%): 382 (64) [FeL2⁺], 367 (17) [FeL2⁺ - CH₃], 198 (89) [bppa⁺], 93 (100) [bppa⁺ - C₇H₈N]; MS (ESI): 778 (2) [FeL2⁺ + 2 bppa], 580 (4) [FeL2⁺ + bppa + H], 199 (100) [bppa⁺ + H]; elemental analysis calcd (%) for C₃₂H₃₆FeN₄O₅ (612.50): C 62.75, H 5.92, N 9.15; found: C 62.54, H 5.78, N 9.14.

[FeL2(bppa)]·EtOH (2·EtOH): A solution of [FeL2(MeOH)₂] (0.52 g, 1.36 mmol) and 1,3-bis(4-pyridyl)propane (1.35 g, 6.81 mmol) in ethanol (60 mL) was heated to reflux for 4 h. After cooling to room temperature, 2·EtOH was obtained in the form of fine black crystals

that were filtered off, washed with ethanol (2×5 mL) and dried *in vacuo* (yield: 0.44 g, 52%). IR (KBr): $\tilde{\nu} = 1643(\text{s}) \text{ cm}^{-1}$ (C=O); MS (DEI(+), 70 eV): m/z (%): 382 (96) [FeL2^+], 367 (27) [$\text{FeL2}^+ - \text{CH}_3$], 198 (100) [bppa⁺]; MS (ESI): 580 (4) [$\text{FeL2}^+ + \text{bppa}$], 199 (100) [bppa⁺ + H]; elemental analysis calcd (%) for $\text{C}_{33}\text{H}_{38}\text{FeN}_4\text{O}_5$ (626.52): C 63.26, H 6.11, N 8.94; found: C 63.15, H 5.92, N 9.12.

[FeL1(bpea)] (3): A solution of [$\text{FeL1}(\text{MeOH})_2$] (0.26 g, 0.51 mmol) and 1,2-bis(4-pyridyl)ethane (0.95 g, 5.13 mmol) in methanol (30 mL) was heated to reflux for 1 h. After cooling down to room temperature, a brown powder was obtained that was filtered off, washed with methanol (2×5 mL) and dried *in vacuo* (yield: 0.22 g, 69%). Elemental analysis calcd (%) for $\text{C}_{32}\text{H}_{34}\text{FeN}_4\text{O}_6$ (626.48): C 61.35, H 5.47, N 8.94; found: C 61.12, H 5.48, N 8.96.

[FeL1(bpea)]·MeOH (3·MeOH): Crystals of [$\text{FeL1}(\text{bpea})$] suitable for X-ray analysis were obtained from a slow diffusion process by using a Schlenk tube, which was, to a certain height, parcelled by a glass wall into two chambers. [$\text{FeL1}(\text{MeOH})_2$] (0.55 g, 1.09 mmol) was placed at the base of one chamber, and 1,2-bis(4-pyridyl)ethane (1.00 g, 5.43 mmol) was placed in the other chamber. Solvent methanol was carefully filled just as high to allow little diffusion between the chambers. After two weeks, 3·MeOH was obtained in form of black crystals. Elemental analysis calcd (%) for $\text{C}_{33}\text{H}_{38}\text{FeN}_4\text{O}_7$ (658.21): C 60.19, H 5.82, N 8.51; found: C 60.17, H 5.52, N 8.71.

[FeL1(bpea)]·tol (3·1.5 tol): A solution of [$\text{FeL1}(\text{MeOH})_2$] (0.22 g, 0.43 mmol) and 1,2-bis(4-pyridyl)ethane (0.81 g, 4.34 mmol) in toluene (15 mL) was heated to reflux for 1 h. After cooling down to room temperature, black crystals of 3·1.5 tol had formed which were filtered off, washed with toluene (2×5 mL) and dried *in vacuo* (yield: 0.20 g, 62%). IR (KBr): $\tilde{\nu} = 1688(\text{s}) \text{ cm}^{-1}$ (OC=O); MS (DEI(+), 70 eV): m/z (%): 442 (100) [FeL1^+], 184 (41) [bpea⁺]; elemental analysis calcd (%) for $\text{C}_{42.5}\text{H}_{46}\text{FeN}_4\text{O}_6$ (764.69): C 66.75, H 6.06, N 7.33; found: C 66.54, H 5.99, N 7.45.

[FeL2(bpea)] (4): [$\text{FeL2}(\text{MeOH})_2$] (0.57 g, 1.28 mmol) and 1,2-bis(4-pyridyl)ethane (2.35 g, 12.8 mmol) were dissolved in methanol (45 mL) and heated to reflux for 1 h. After cooling down to room temperature, a dark brown precipitate was obtained that was filtered off, washed with methanol (2×5 mL) and dried *in vacuo* (yield: 0.50 g, 69%). Elemental analysis

calcd (%) for $C_{30}H_{30}FeN_4O_4$ (566.43): C 63.61, H 5.34, N 9.89; found: C 64.09, H 5.60, N 10.18.

[FeL2(bpea)]·0.25 MeOH (4·0.25 MeOH): [FeL2(MeOH)₂] (0.62 g, 1.62 mmol) and 1,2-bis(4-pyridyl)ethane (1.49 g, 8.11 mmol) were dissolved in methanol (57 mL) and heated to reflux for 1 h. After cooling down to room temperature, a crystalline black precipitate was obtained that was filtered off, washed with methanol (2 × 5 mL) and dried *in vacuo* (yield: 0.49 g, 53%). Crystals of 4·0.25 MeOH suitable for X-ray analysis were obtained from a slow diffusion process by using methanol solutions of the pyridine (pyr) diadduct [FeL2(pyr)₂]^[13a] (0.15 g, 0.28 mmol) and of bpea (0.26 g, 1.41 mmol) at 50 °C. Elemental analysis calcd (%) for $C_{30.26}H_{31.06}FeN_4O_{4.26}$ (574.92): C 63.25, H 5.44, N 9.75; found: C 62.51, H 5.55, N 9.60.

[FeL1(bipy)] (5): A solution of [FeL1(MeOH)₂] (0.49 g, 0.97 mmol) and 4,4'-bipyridine (1.51 g, 9.68 mmol) in methanol (35 mL) was heated to reflux for 1 h. After cooling down to room temperature, a violet precipitate had formed which was filtered off, washed with methanol (2 × 5 mL) and dried *in vacuo* (yield: 0.37 g, 64%). Elemental analysis calcd (%) for $C_{29}H_{29}FeN_4O_6$ (598.43): C 60.21, H 5.05, N 9.36; found: C 60.12, H 5.05, N 9.62.

[FeL1(bipy)]·MeOH (5·MeOH): Crystals of 5·MeOH were obtained from a slow diffusion process by using methanol solutions of [FeL1[MeOH]₂] (0.10 g, 0.19 mmol) and of bipy (0.15 g, 0.94 mmol). After one week, violet acicular crystals had formed. Elemental analysis calcd (%) for $C_{31}H_{34}FeN_4O_7$ (630.47): C 59.06, H 5.44, N 8.89; found: C 59.04, H 5.12, N 9.11.

Supplementary material: An overview of the magnetic properties of the compounds, the intermolecular hydrogen bonds and nonclassical hydrogen bonds, the short intermolecular contacts and the thermogravimetric analysis of 5·MeOH are presented on the WWW under <http://dx.doi.org/10.1002/ejic201001363>.

Acknowledgements

This work has been supported financially by the Deutsche Forschungsgemeinschaft (SPP 1137 and SPP 1178), the Fonds der Chemischen Industrie and the Center for Integrated Protein Science Munich (CIPSM). The main part of the experiments were done at the University of Munich.

4.6 References

- [1] a) H.A. Goodwin, *Coord. Chem. Rev.* **1976**, *18*, 293; b) P. Gütlich, *Struct. Bonding (Berlin)* **1981**, *44*, 83; c) E. König, *Prog. Inorg. Chem.* **1987**, *35*, 527; d) P. Gütlich, A. Hauser, *Coord. Chem. Rev.* **1990**, *97*, 1; e) E. König, *Struct. Bonding (Berlin)* **1991**, *76*, 51; f) P. Gütlich, A. Hauser, H. Spiering, *Angew. Chem. Int. Ed. Engl.* **1994**, *33*, 2024, and references therein; g) P. Gütlich, J. Jung, H.A. Goodwin, *Molecular Magnetism: From Molecular Assemblies to the Devices* (Eds.: Coronado *et al.*), NATO ASI Series E: *Applied Sciences*, Vol. 321, Kluwer, Dordrecht, **1996**, 327; h) P. Gütlich, H.A. Goodwin (Eds.), *Spin Crossover in Transition Metal Compounds I–III, Topics in Current Chemistry*, Springer, Berlin, Heidelberg, New York, **2004**; i) J.A. Real, A.B. Gaspar, M.C. Munoz, *Dalton Trans.* **2005**, 2062; j) O. Sato, J. Tao, Y.-Z. Zhang, *Angew. Chem.* **2007**, *119*, 2200; *Angew. Chem. Int. Ed.* **2007**, *46*, 2152.
- [2] a) O. Kahn, C. Jay Martinez, *Science* **1998**, *279*, 44; b) O. Kahn, C. Jay, J. Kröber, R. Claude, F. Grolière, *Patent EP0666561* **1995**; c) J.-F. Létard, O. Nguyen, N. Daro, *Patent FR0512476* **2005**; d) J.-F. Létard, P. Guionneau, L. Goux-Capes, *Topics in Current Chemistry*, Vol. 235 (Eds.: P. Gütlich, H.A. Goodwin), Springer, Wien, New York, **2004**, 221; e) A. Galet, A.B. Gaspar, M.C. Munoz, G.V. Bukin, G. Levchenko, J.A. Real, *Adv. Mater.* **2005**, *17*, 2949.
- [3] J.A. Real, A.B. Gaspar, V. Niel, M.C. Munoz, *Coord. Chem. Rev.* **2003**, *236*, 121.
- [4] a) B. Weber, *Coord. Chem. Rev.* **2009**, *253*, 2432; b) B. Weber, E.-G. Jäger, *Eur. J. Inorg. Chem.* **2009**, 465.
- [5] B. Weber, W. Bauer, J. Obel, *Angew. Chem.* **2008**, *120*, 10252; *Angew. Chem. Int. Ed.* **2009**, *47*, 10098.
- [6] a) J.A. Real, A.B. Gaspar, M.C. Munoz, P. Gütlich, V. Ksenofontov, H. Spiering, *Topics in Current Chemistry*, Vol. 233 (Eds.: P. Gütlich, H.A. Goodwin), Springer, Wien, New York, **2004**, 167; b) A.B. Gaspar, M.C. Munoz, J.A. Real, *J. Mater. Chem.* **2006**, 2522; c) A. Bousseksou, G. Molnar, J.A. Real, K. Tanaka, *Coord. Chem. Rev.* **2007**, *251*, 1822.

- [7] S. Zein, S.A. Borshch, *J. Am. Chem. Soc.* **2005**, *127*, 16197.
- [8] a) Y. Garcia, O. Kahn, L. Rabardel, B. Chansou, L. Salmon, J.-P. Tuchagues, *Inorg. Chem.* **1999**, *38*, 4663; b) G.S. Matouzenko, J.-F. Létard, S. Lecocq, A. Bousseksou, L. Capes, L. Salmon, M. Perrin, O. Kahn, A. Collet, *Eur. J. Inorg. Chem.* **2001**, 2935; c) W. Hibbs, P.J. van Koningsbruggen, A.M. Arif, W.W. Shum, J.S. Miller, *Inorg. Chem.* **2003**, *42*, 5645; d) P. Poganiuch, S. Decurtins, P. Gütllich, *J. Am. Chem. Soc.* **1990**, *112*, 3270; e) L. Wiehl, *Acta Crystallogr., Sect. B* **1993**, *49*, 289; f) R. Hinek, H. Spiering, D. Schollmeyer, P. Gütllich, A. Hauser, *Chem. Eur. J.* **1996**, *2*, 1427; g) B. Weber, C. Carbonera, C. Desplanches, J.-F. Létard, *Eur. J. Inorg. Chem.* **2008**, 1589.
- [9] a) M. Mikami, M. Konno, Y. Saito, *Chem. Phys. Lett.* **1979**, *63*, 566; b) N. Sasaki, T. Kambara, *Phys. Rev. B* **1989**, *40*, 2442; c) A. Bousseksou, J. Nasser, J. Linares, K. Boukheddaden, F. Varret, *J. Phys. I* **1992**, *2*, 1381; d) H. Spiering, T. Kohlhaas, H. Romstedt, A. Hauser, C. Bruns-Yilmaz, P. Gütllich, *Coord. Chem. Rev.* **1999**, *190*, 629.
- [10] a) V. Petrouleas, J.-P. Tuchagues, *Chem. Phys. Lett.* **1987**, *137*, 21; b) D. Boinnard, A. Bousseksou, A. Dworkin, J.-M. Savariault, F. Varret, J.-P. Tuchaugues, *Inorg. Chem.* **1994**, *33*, 271; c) K. Boukheddaden, J. Linares, H. Spiering, F. Varret, *Eur. Phys. J. B.* **2000**, *15*, 317; d) D. Chernyshov, M. Hostettler, K.W. Törnroos, H.B. Bürgi, *Angew. Chem.* **2003**, *115*, 3955; *Angew. Chem. Int. Ed.* **2003**, *42*, 3825.
- [11] J.J. M. Amooore, C.J. Kepert, J.D. Cashion, B. Moubaraki, S.M. Neville, K.S. Murray, *Chem. Eur. J.* **2006**, *12*, 8220.
- [12] S.M. Neville, B.A. Leita, G.J. Halder, C. Kepert, B. Moubaraki, J.-F. Létard, K.S. Murray, *Chem. Eur. J.* **2008**, *14*, 10123.
- [13] a) B. Weber, E. Kaps, J. Weigand, C. Carbonera, J.-F. Létard, K. Achterhold, F.G. Parak, *Inorg. Chem.* **2008**, *47*, 487; b) B. Weber, C. Carbonera, C. Desplanches, J.-F. Létard, *Eur. J. Inorg. Chem.* **2008**, 1589; c) B. Weber, E.S. Kaps, C. Desplanches, J.-F. Létard, K. Achterhold, F.G. Parak, *Eur. J. Inorg. Chem.* **2008**, 4891.
- [14] a) B. Weber, R. Tandon, D. Himsl, *Z. Anorg. Allg. Chem.* **2007**, *633*, 1159; b) B. Weber, E.S. Kaps, C. Desplanches, J.-F. Létard, *Eur. J. Inorg. Chem.* **2008**, 2963.

- [15] a) B. Weber, E. Kaps, *Heteroatom Chem.* **2005**, *16*, 391; b) B. Weber, F.-A. Walker, *Inorg. Chem.* **2007**, *46*, 6794; c) B. Weber, E.S. Kaps, J. Obel, K. Achterhold, F.G. Parak, *Inorg. Chem.* **2008**, *47*, 10779
- [16] W. Bauer, B. Weber, *Inorg. Chim. Acta* **2009**, *362*, 2341.
- [17] P.J. van Koningsbruggen, Y. Garcia, O. Kahn, L. Fournès, H. Kooijman, A.L. Spek, J.G. Haasnoot, J. Moscovici, K. Provost, A. Michalowicz, F. Renz, P. Gütllich, *Inorg. Chem.* **2000**, *39*, 1891.
- [18] G.S. Matouzenko, M. Perrin, B. le Guennic, C. Genre, G. Molnar, A. Bousseksou, S.A. Borshch, *Dalton Trans.* **2007**, *9*, 934.
- [19] a) G.S. Matouzenko, G. Molnar, N. Brefuel, M. Perrin, A. Bousseksou, S.A. Borshch, *Chem. Mater.* **2003**, *15*, 550. b) C. Genre, G.S. Matouzenko, E. Jeanneau, D. Luneau, *New J. Chem.* **2006**, *30*, 1669.
- [20] C. Genre, E. Jeanneau, A. Bousseksou, D. Luneau, S.A. Borshch, G.S. Matouzenko, *Chem. Eur. J.* **2008**, *14*, 697.
- [21] J. Linares, H. Spiering, F. Varret, *Eur. Phys. J. B.* **1999**, *10*, 271.
- [22] a) A.B. Koudriavtsev, A.F. Strassen, J.G. Haasnoot, M. Grunert, P. Weinberger, W. Linert, *Phys. Chem. Chem. Phys.* **2003**, *5*, 3676; b) A.B. Koudriavtsev, A.F. Strassen, J.G. Haasnoot, M. Grunert, P. Weinberger, W. Linert, *Phys. Chem. Chem. Phys.* **2003**, *5*, 3666.
- [23] A. Altomare, M.C. Burla, G.M. Camalli, G. Cascarano, C. Giacovazzo, A. Guagliardi, A.G.G. Moliterni, G. Polidori, R. Spagna, SIR-97, University of Bari, Bari (Italy), **1997**; *J. Appl. Crystallogr.* **1999**, *32*, 115.
- [24] G.M. Sheldrick, SHELXL-97, University of Göttingen, Göttingen (Germany), **1993**.
- [25] C.K. Johnson, M.N. Burnett, ORTEP-III, Oak-Ridge National Laboratory, Oak-Ridge TN (USA) **1996**; L.J. Farrugia, *J. Appl. Crystallogr.* **1997**, *30*, 565.
- [26] E. Keller, SCHAKAL-99, University of Freiburg, Freiburg (Germany), **1999**.
- [27] Team of authors: *Organikum*, Johann Ambrosius Barth, Leipzig, Berlin, Heidelberg, **1993**.

[28] E.-G. Jäger, E. Häussler, M. Rudolph, M. Rost, *Z. Anorg. Allg. Chem.* **1985**, 525, 67.

4.7 Supporting Information

Table S1.1. Single-crystal diffraction data and parameters of the compounds discussed in this work.

compound	1 ^{HS}	1 ^{HS-LS}	2 ^{HS} ·MeOH	2 ^{HS-LS} ·MeOH
formula	C ₃₃ H ₃₆ FeN ₄ O ₆	C ₆₆ H ₇₂ Fe ₂ N ₈ O ₁₂	C ₃₂ H ₃₆ FeN ₄ O ₅	C ₆₄ H ₇₂ Fe ₂ N ₈ O ₁₀
$M_r / \text{g mol}^{-1}$	640.51	1281.02	612.50	1225.00
crystal system	monoclinic	monoclinic	monoclinic	monoclinic
space group	$P2_1/c$	$P2_1/c$	$C2/c$	$P2_1/c$
$a / \text{Å}$	12.292(6)	19.714(5)	17.861(4)	17.857(5)
$b / \text{Å}$	18.983(8)	18.697(5)	15.197(3)	15.105(5)
$c / \text{Å}$	16.256(5)	16.196(5)	22.713(5)	22.214(6)
$\alpha / ^\circ$	90.00	90.00	90.00	90.00
$\beta / ^\circ$	126.59(2)	95.047(5)	97.918(1)	98.077(2)
$\gamma / ^\circ$	90.00	90.00	90.00	90.00
$V / \text{Å}^3$	3046(2)	5947(3)	6106.3(2)	5932.3(3)
Z	4	4	8	4
$\rho / \text{g cm}^{-3}$	1.397	1.431	1.332	1.372
μ / mm^{-1}	0.547	0.560	0.540	0.556
crystal size	0.24 × 0.22 × 0.08	0.25 × 0.16 × 0.10	0.10 × 0.09 × 0.03	0.10 × 0.09 × 0.02
T / K	200(2)	100(2)	225(2)	125(2)
diffractometer	Oxford XCalibur	Oxford XCalibur	KappaCCD	KappaCCD
$\lambda (\text{MoK}\alpha) / \text{Å}$	0.71073	0.71073	0.71073	0.71073
θ -range / $^\circ$	3.78–25.31	3.80–25.37	3.24–27.48	3.15–25.32
reflns. collected	56020	62758	23796	36238
indep. reflns. (R_{int})	5544 (0.0629)	10855 (0.0793)	6996 (0.0471)	10807 (0.0779)
mean $\sigma(I) / I$	0.0602	0.0981	0.0522	0.0872
reflns. with $I \geq 2\sigma(I)$	3360	5852	4601	6611
x, y (weighting scheme)	0.0484, 0	0.0361, 0	0.0549, 2.2532	0.0712
parameters	401	801	386	768
restraints	0	0	0	0
$R(F)$ (all data) ^[a]	0.0345 (0.0720)	0.0389 (0.0992)	0.0443 (0.0791)	0.0564 (0.1058)
$wR(F^2)$ ^[b]	0.1011	0.0998	0.1206	0.1544
$GooF$	1.058	0.999	1.026	1.023
shift/error _{max}	0.001	0.000	0.002	0.001
max., min. resd. dens. / e Å^{-3}	0.451, -0.262	0.511, -0.466	0.335, -0.352	0.857, -0.590

[a] $R(F) = \sum ||F_o| - |F_c|| / \sum |F_o|$. [b] $wR(F^2) = [\sum [w(F_o^2 - F_c^2)^2] / \sum w(F_o^2)^2]^{1/2}$, $w = 1 / [\sigma^2(F_o^2) + (aP)^2 + bP]$, where $P = [F_o^2 + 2(F_c^2)]/3$.

4. Two-Step versus One-Step Spin Transition in Iron(II) 1D Chain Compounds

Table S1.2. Single-crystal diffraction data and parameters of the compounds discussed in this work. For the structure motif of $3^{\text{HS-LS}}$.1.5 tol only the crystal data are given.

compound	3^{HS} .MeOH	3^{HS} .1.5 tol	$3^{\text{HS-LS}}$.1.5 tol
formula	$\text{C}_{33}\text{H}_{38}\text{FeN}_4\text{O}_7$	$\text{C}_{85}\text{H}_{92}\text{Fe}_2\text{N}_8\text{O}_{12}$	$\text{C}_{163}\text{H}_{176}\text{Fe}_4\text{N}_{16}\text{O}_{24}$
$M_r / \text{g mol}^{-1}$	658.52	1529.37	2966.60
crystal system	triclinic	triclinic	triclinic
space group	$P\bar{1}$	$P\bar{1}$	$P\bar{1}$
$a / \text{\AA}$	11.7025(3)	12.7120(13)	12.7815(6)
$b / \text{\AA}$	12.2137(4)	13.0428(13)	16.7360(6)
$c / \text{\AA}$	12.4828(2)	13.8537(15)	18.4934(8)
$\alpha / ^\circ$	72.9593(15)	68.631(10)	94.294(3)
$\beta / ^\circ$	80.6512(16)	75.539(9)	101.732(3)
$\gamma / ^\circ$	70.5753(11)	68.030(10)	90.514(3)
$V / \text{\AA}^3$	1604.6(7)	1966.5(4)	3861.2(3)
Z	2	1	1
$\rho / \text{g cm}^{-3}$	1.363	1.291	1.281
μ / mm^{-1}	0.523	0.435	0.422
crystal size	$0.22 \times 0.17 \times 0.06$	$0.32 \times 0.20 \times 0.09$	$0.32 \times 0.20 \times 0.09$
T / K	200(2)	200(2)	130(3)
diffractometer	KappaCCD	Oxford XCalibur	Oxford XCalibur
$\lambda (\text{MoK}\alpha) / \text{\AA}$	0.71073	0.71073	0.71073
θ -range / $^\circ$	3.44–27.44	3.82–24.74	
reflns. collected	13747	13020	
indep. reflns. (R_{int})	7275 (0.0310)	6707 (0.0320)	
mean $\sigma(I) / I$	0.0497	0.0985	
reflns. with $I \geq 2\sigma(I)$	5605	3668	
x, y (weighting scheme)	0.0325, 1.2232	0.0784	
parameters	412	507	
restraints	0	93	
$R(F)$ (all data) ^[a]	0.0429 (0.0639)	0.0557 (0.1038)	
$wR(F^2)$ ^[b]	0.1053	0.1469	
$Goof$	1.059	0.894	
shift/error _{max}	0.002	0.000	
max., min. resd. dens. / e \AA^{-3}	0.295, -0.425	0.587, -0.399	

[a] $R(F) = \sum ||F_o| - |F_c|| / \sum |F_o|$. [b] $wR(F^2) = [\sum [w(F_o^2 - F_c^2)^2] / \sum w(F_o^2)^2]^{1/2}$, $w = 1 / [\sigma^2(F_o^2) + (aP)^2 + bP]$, where $P = [F_o^2 + 2(F_c^2)] / 3$.

4. Two-Step versus One-Step Spin Transition in Iron(II) 1D Chain Compounds

Table S1.3. Single-crystal diffraction data and parameters of the compounds discussed in this work.

compound	4 ^{HS} .0.25 MeOH	4 ^{LS} .0.25 MeOH	5 ^{LS/LS} .MeOH
formula	C _{30.27} H _{31.06} FeN ₄ O _{4.27}	C _{30.25} H ₃₁ FeN ₄ O _{4.25}	C ₃₁ H ₃₄ FeN ₄ O ₇
$M_r / \text{g mol}^{-1}$	574.95	574.31	630.47
crystal system	triclinic	triclinic	triclinic
space group	$P\bar{1}$	$P\bar{1}$	$P\bar{1}$
$a / \text{\AA}$	11.559(2)	11.037(2)	11.0987(15)
$b / \text{\AA}$	11.818(3)	11.633(6)	14.6555(13)
$c / \text{\AA}$	11.951(2)	12.196(2)	19.575(4)
$\alpha / ^\circ$	76.206(19)	72.949(36)	75.432(11)
$\beta / ^\circ$	67.861(16)	65.328(16)	75.985(14)
$\gamma / ^\circ$	72.519(17)	71.960(23)	74.820(10)
$V / \text{\AA}^3$	1427.8(5)	1328.4(8)	2920.7(7)
Z	2	2	4
$\rho / \text{g cm}^{-3}$	1.337	1.436	1.434
μ / mm^{-1}	0.571	0.613	0.572
crystal size	0.20 × 0.20 × 0.12	0.20 × 0.20 × 0.12	0.34 × 0.13 × 0.11
T / K	293	7	175(2)
diffractometer	Huber 4-circle	Huber 4-circle	Oxford XCalibur
$\lambda (\text{MoK}\alpha) / \text{\AA}$	0.71073	0.71073	0.71073
θ -range / $^\circ$	1.82–25.35	1.87–25.35	3.80–25.32
reflns. collected	7335	6316	50123
indep. reflns. (R_{int})	4714 (0.0185)	4063 (0.0274)	10642 (0.0808)
mean $\sigma(I) / I$			0.0710
reflns. with $I \geq 2\sigma(I)$			6431
x, y (weighting scheme)	0.0376, 0.8415	0.0261, 14043	0.0628, 3.6444
parameters	368	483	788
restraints	0	0	0
$R(F)$ (all data) ^[a]	0.0384 (0.0420)	0.0517 (0.0733)	0.0564 (0.1140)
$wR(F^2)$ ^[b]	0.0996	0.0941	0.1521
$Goof$	1.146	1.177	1.030
shift/error _{max}			0.001
max., min. resd. dens. / e \AA^{-3}	0.300, -0.303	0.433, -0.519	0.734, -0.642

[a] $R(F) = \sum ||F_o| - |F_c|| / \sum |F_o|$. [b] $wR(F^2) = [\sum [w(F_o^2 - F_c^2)^2] / \sum w(F_o^2)^2]^{1/2}$, $w = 1 / [\sigma^2(F_o^2) + (aP)^2 + bP]$, where $P = [F_o^2 + 2(F_c^2)] / 3$.

5 X-Ray Structure and Magnetic Properties of Dinuclear and Polymer Iron(II) Complexes

Wolfgang Bauer^[a] and Birgit Weber^{*[a]}

[a] Ludwig-Maximilians-Universität München, Department Chemie und Biochemie, Butenandtstr. 5–13 (Haus F), 81377 München, Germany

Keywords: Iron, N,O ligands, X-Ray Structure, Magnetic properties

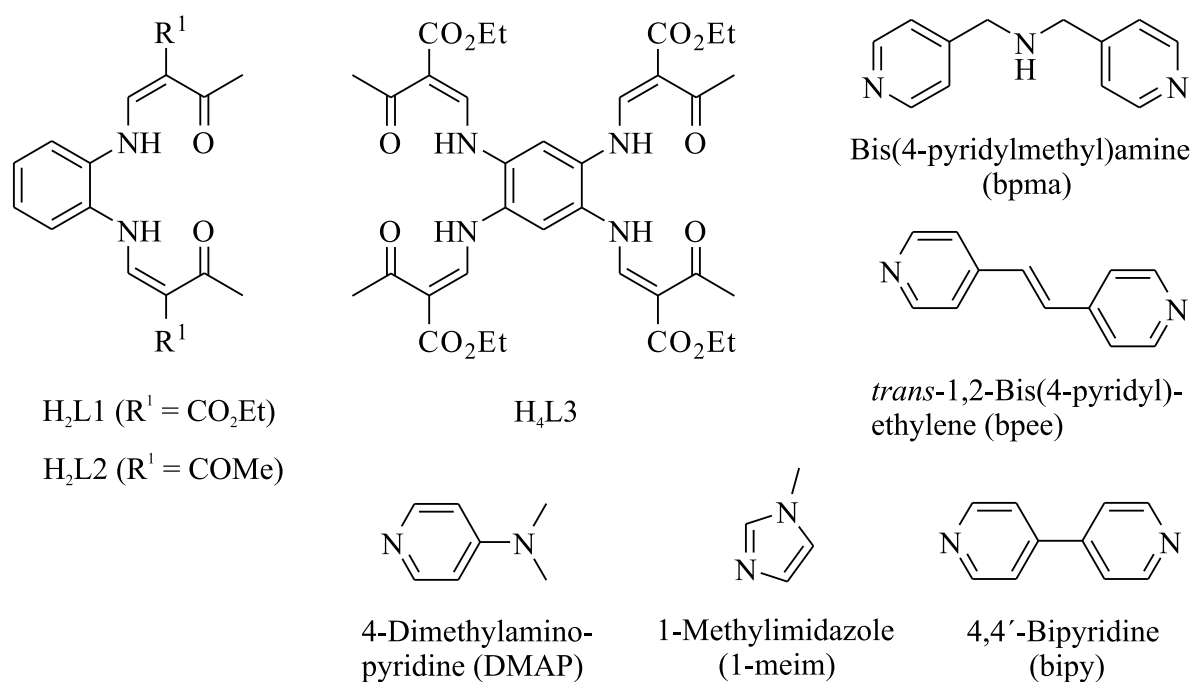
Published in: *Inorg. Chim. Acta* **2009**, *362*, 2341–2346.

Abstract: Five new octahedral iron(II) complexes [FeL2(bpma)]·EtOH (**1**), [FeL2(bipy)]·DMF (**2**), [FeL1(bpee)] (**3**), [Fe₂L3(1-meim)₄]·4 1-meim (**4**) and [FeL1(DMAP)₂] (**5**), with L1 and L2 being tetradentate N₂O₂²⁻ coordinating Schiff base-like ligands (L1 = {diethyl (*E,E*)-2,2'-[1,2-phenyl-bis(iminomethylidene)]bis[3-oxobutanoate] (2-)-*N,N',O³,O^{3'}*}, L2 = {3,3'-[1,2-phenyl-bis(iminomethylidene)]bis[pentane-2,4-dione] (2-)-*N,N',O²,O^{2'}*}) and L3 being an octadentate dinucleating N₂O₂²⁻ coordinating Schiff base-like ligand ({tetraethyl (*E,E,E,E*)-2,2',2'',2''-[1,2,4,5-phenyl-tetra(iminomethylidene)]tetra[3-oxobutanoate] (2-)-*N,N',N'',N''',O³, O^{3'},O^{3''},O^{3'''}*}); bpma = bis(4-pyridylmethyl)amine, bipy = 4,4'-bipyridine, bpee = *trans*-1,2-bis(4-pyridyl)ethylene, 1-meim = 1-methylimidazole and DMAP = 4-dimethylaminopyridine, have been synthesised and characterised by using X-ray structure analysis and *T*-dependent susceptibility measurements. Both methods indicate that all iron(II) centres are in the paramagnetic high-spin state over the whole temperature range investigated. The O-Fe-O angle, the so-called bite of the equatorial ligand, is with an average of 111° in the region typical for high-spin iron(II) complexes of this ligand type. In the case of compound **1** an infinite two-dimensional hydrogen bond network can be found, for the compounds **2–4** no hydrogen bond interactions are observed between the complex molecules. A comparison of the curve progression obtained from the magnetic measurements of the mononuclear complex **5** and the polymeric complexes **1–3** leads to the conclusion that no magnetic interactions are mediated over the bridging axial ligands. For the dinuclear complex **4** weak antiferromagnetic interactions between the two iron centres are found.

5.1 Introduction

Octahedral iron(II) complexes are an interesting class of complexes because of the possible occurrence of the spin crossover phenomenon. This switching behaviour on the molecular level between two or more states by the change of temperature, pressure or light is of potential interest for future applications as for example in molecular switches or memory devices.^[1,2] If technical applications are envisioned, spin crossover (SCO) complexes with wide thermal hysteresis loops are necessary. The occurrence of such a cooperative behaviour is strongly connected with the efficiency by which the volume changes associated with the spin transition can be transmitted through the crystal. Covalent linkers between the single metal centres are a promising possibility as the spreading of those contacts can be easily controlled by a preparative chemist. This did establish a lively interest in polymer SCO compounds, but also in dinuclear systems. The latter are the simplest system of spin-coupled polymers and provide fundamental information about intramolecular magnetic interactions and a possible synergy between those interactions and the SCO properties. It seems, that weak intramolecular interactions are responsible for the direct HS-HS \leftrightarrow LS-LS transformation,^[3] while a plateau in the $\chi_{\text{HS}} \approx 0.5$ (χ_{HS} = HS molar fraction) region might be either due to the intramolecular energetic stabilisation of an HS-LS species^[4,5] or due to intermolecular interactions.^[6] The intramolecular energetic stabilisation is often associated with antiferromagnetic exchange interactions and the investigation of the magnetic properties of pure high-spin (HS) complexes is of great importance in order to understand the corresponding dinuclear or polymer SCO systems.

In this paper we present the synthesis, magnetic properties and results from X-ray structure analysis of five new octahedral iron(II) complexes, one monomer $[\text{FeL1}(\text{DMAP})_2]$ (**5**), one dimer $[\text{Fe}_2\text{L3}(\text{1-meim})_4] \cdot 4 \text{ 1-meim}$ (**4**) and three polymer compounds $[\text{FeL2}(\text{bpma})] \cdot \text{EtOH}$ (**1**), $[\text{FeL2}(\text{bipy})] \cdot \text{DMF}$ (**2**) and $[\text{FeL1}(\text{bpee})]$ (**3**). Complexes of this type of tetradentate $\text{N}_2\text{O}_2^{2-}$ coordinating Schiff base-like ligands are known to be suitable for the synthesis of spin crossover compounds if *N*-heterocycles are used as axial ligands.^[7,8,9] This paper will concentrate on the influence of the covalent bridges on magnetic exchange interactions in those compounds. The understanding of those properties is essential for the understanding of the SCO properties in related di- and polynuclear complexes.



Scheme 1. General schema of the ligands discussed in this work and the used abbreviations.

5.2 Results and Discussion

Synthesis of the complexes: Scheme 1 shows the general structure of the complexes discussed in this work together with the used equatorial and axial ligands and their abbreviations. The complexes can be obtained in a one-pot reaction by conversion of the equatorial ligand with a slight excess of iron(II) acetate in the presence of the desired axial ligand. Methanol is the most frequently used solvent so far, but for the synthesis of polymeric chains ethanol and dimethylformamide was also used. Alternatively, an iron complex of the tetradentate equatorial ligand with methanol as axial ligands ($[\text{FeL}1/2(\text{MeOH})_2]$ or $[\text{Fe}_2\text{L}3(\text{MeOH})_4]$) can be prepared in a first step that is then converted with the desired axial ligand in a second step. To ensure the formation of octahedral complexes with both axial coordination sites occupied, a 30–50 molar excess of the axial ligand is used for the synthesis of the mono- and dinuclear complexes **5** and **4**. However, to obtain polymeric chains instead of mononuclear complexes the molar excess mustn't be this high on the one side but not too low on the other side to prevent the formation of *penta*-coordinated species. Accordingly, a ratio of 1:10 of iron complex to axial ligand is used. Additionally the reaction time is extended to several hours to ensure the formation of the thermodynamically stable chain compound

X-Ray structure analysis: Crystals suitable for X-ray structure analysis were obtained for all complexes. The crystallographic data are summarised in Supporting Information Table S1.1–2. Due to the low quality of the crystals of **3**, only the motive of the structure could be obtained and therefore we will only discuss the conformation of this polymeric chain. Figures 1, 2 and 3 display the monomer units of the polymer chains and the molecule structure of the mono- and dinuclear complex, respectively. Selected bond lengths and angles are summarised in Table 1. The bond lengths and angles within the first coordination sphere of the iron centres are within the region reported for octahedral HS iron(II) complexes of the same ligand type.^[7–9] The average bond lengths are 2.10 Å (Fe- N_{eq}), 2.03 Å (Fe- O_{eq}) and 2.26 Å (Fe- N_{ax}). A characteristic tool for the determination of the spin state of this type of iron(II) complexes is the O-Fe-O angle, which changes from about 110° in the HS state to about 90° in the LS state. Obviously all complexes reported here are in the HS state, because the angle is in the region between 108° to 113°. The $N_{\text{ax}}\text{-Fe-}N_{\text{ax}}$ angle is not ideally linear but in the region between 170° to 180°, which is also in the region reported so far for this type of complexes.^{[7–}

⁹¹ Due to the octahedral coordination sphere for all complexes the iron centre is situated in the plane of the equatorial ligand.

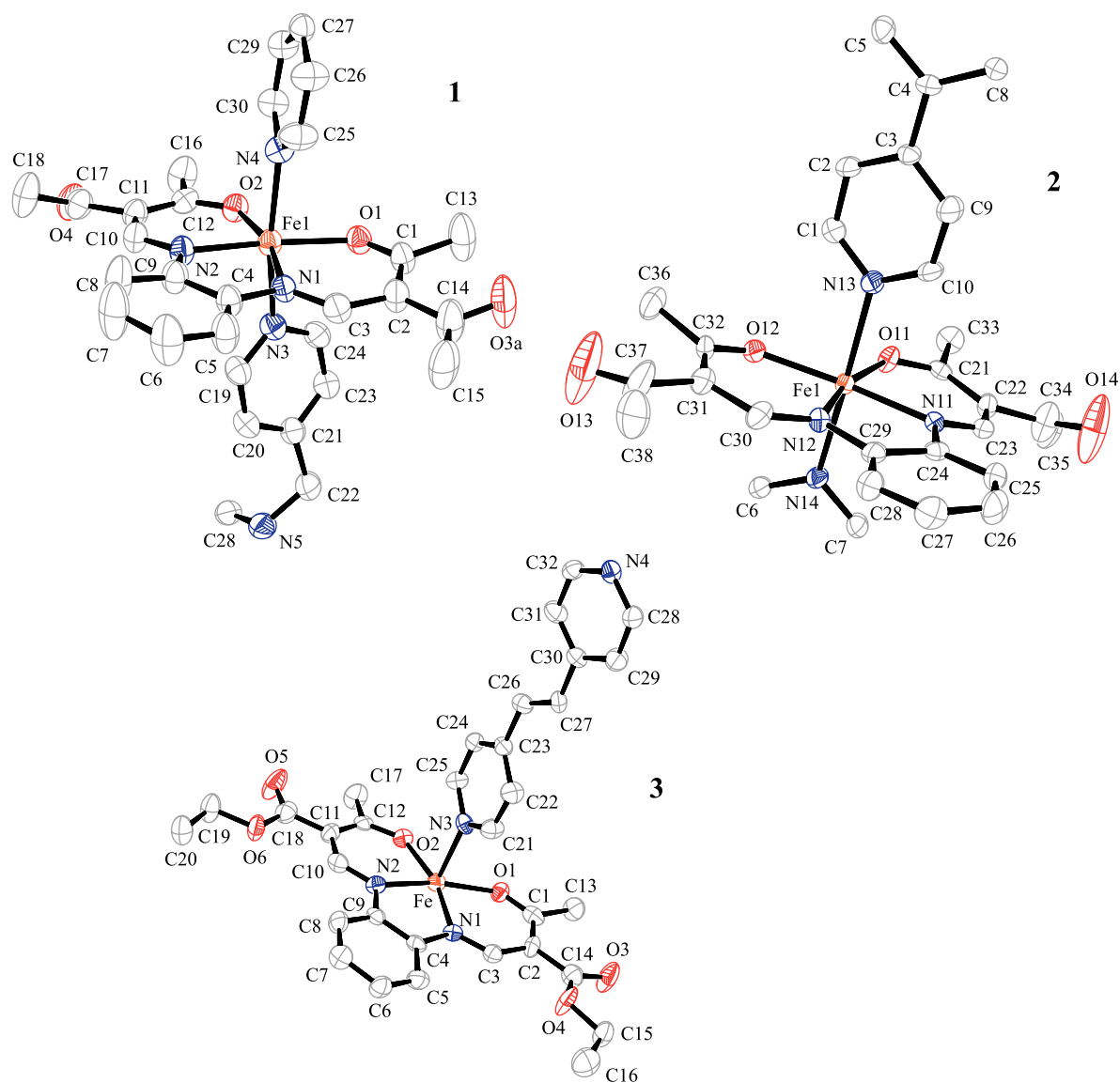
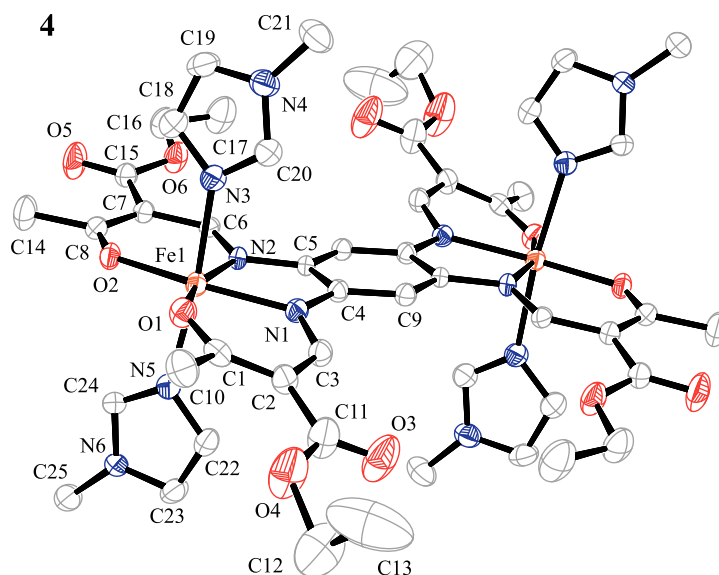


Figure 1. ORTEP drawing of the monomer unit of the three polymer chain compounds **1**, **2** and **3**. Hydrogen atoms and additional solvent molecules were omitted for clarity. Thermal ellipsoids are shown with a 50% probability.

Table 1: Selected bond lengths [\AA] and angles [degree] within the first coordination sphere of the iron complexes [FeL2(bpma)]·EtOH (**1**), [FeL2(bipy)]·DMF (**2**), [FeL1(bpee)] (**3**), [Fe₂L3(1-meim)₄]·4 1-meim (**4**), [FeL1(DMAP)₂] (**5**).

compound	Fe-N _{eq}	Fe-O _{eq}	Fe-N _{ax}	O _{eq} -Fe-O _{eq}	N _{ax} -Fe-N _{ax}
1	2.102(2)	2.033(2)	2.250(3)	110.37(8)	169.45(9)
	2.095(2)	2.028(2)	2.252(3)		
2	2.090(3)	2.016(3)	2.301(3)	108.13(12)	176.99(13)
	2.087(4)	2.010(3)	2.274(3)		
3	2.101(5)	2.044(4)	2.262(4)	112.71(17)	169.76(17) ^[a]
	2.092(5)	2.017(4)	2.280(4) ^[a]		
4	2.094(2)	2.052(2)	2.217(2)	111.10(9)	173.94(9)
	2.112(2)	2.023(2)	2.248(2)		
5	2.082(4)	2.017(3)	2.220(4)	111.22(14)	169.09(17)
	2.097(4)	2.018(3)	2.304(4)		

Symmetry code: [a] $-1 + x, y, -1 + z$.**Figure 2.** ORTEP drawing of the molecule structure of the dinuclear complex **4**. Hydrogen atoms and solvent molecules were omitted for clarity. Thermal ellipsoids are shown with a 50% probability.

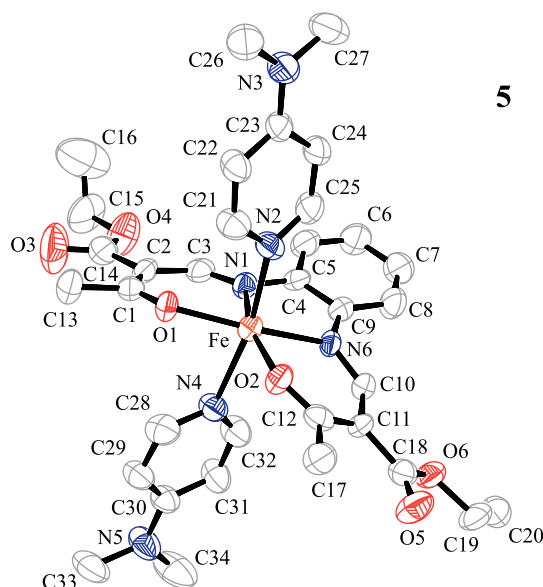


Figure 3. ORTEP drawing of the molecule structure of the mononuclear complex **5**. Hydrogen atoms and solvent molecules were omitted for clarity. Thermal ellipsoids are shown with a 50% probability.

For the characterisation of potential spin crossover complexes it is very important to investigate the intermolecular interactions, because there is a close relation between the type of intermolecular contacts and the cooperative interactions between the single metal centres during the spin transition. The term cooperativity describes the efficiency of the crystal lattice to transmit the geometry changes and electronic features that occur during a spin transition from one molecule to another. Besides π -stacking and van der Waals interactions, particularly hydrogen bonds are thought to play a central role as information transmitter.^[10] They are stronger than the first two possibilities and the volume changes during the spin transition can be transmitted more efficiently through the crystal. Analysing the complexes presented in this paper, only **1**, with its bridging axial ligand containing a NH group, is able to form strong hydrogen bonds as classified by Jeffrey *et al.*^[11] The other examples have no suitable donor groups. This is in agreement with the obtained results: complex **1** forms an infinite two-dimensional hydrogen bond network in the plane (0 0 1) as illustrated in Figure 4. The amine nitrogen N5 acts as donor *via* H51 and the carbonyl oxygen O4 of the substituent at the equatorial ligand serves as hydrogen bond acceptor, linking the polymer chains along [1 0 0] and [0 1 0]. No classical hydrogen bonds can be found for complexes **2–5**. Here only weak interactions are observed, mainly between aromatic CH protons of the axial ligands and carbonyl or carboxylate oxygen of the substituents at the equatorial ligands. The packing of

the molecules in the crystals are illustrated in the Supplementary material. In compounds **1**, **2** and **4** solvate molecules were found to be incorporated in the crystal lattice, which can have a noticeable influence on the spin transition behaviour in SCO complexes as we recently reported for three examples.^[7b,8b,c] For the magnetic exchange interactions communicated over the covalent linker they are of no importance, hence this is not considered any further.

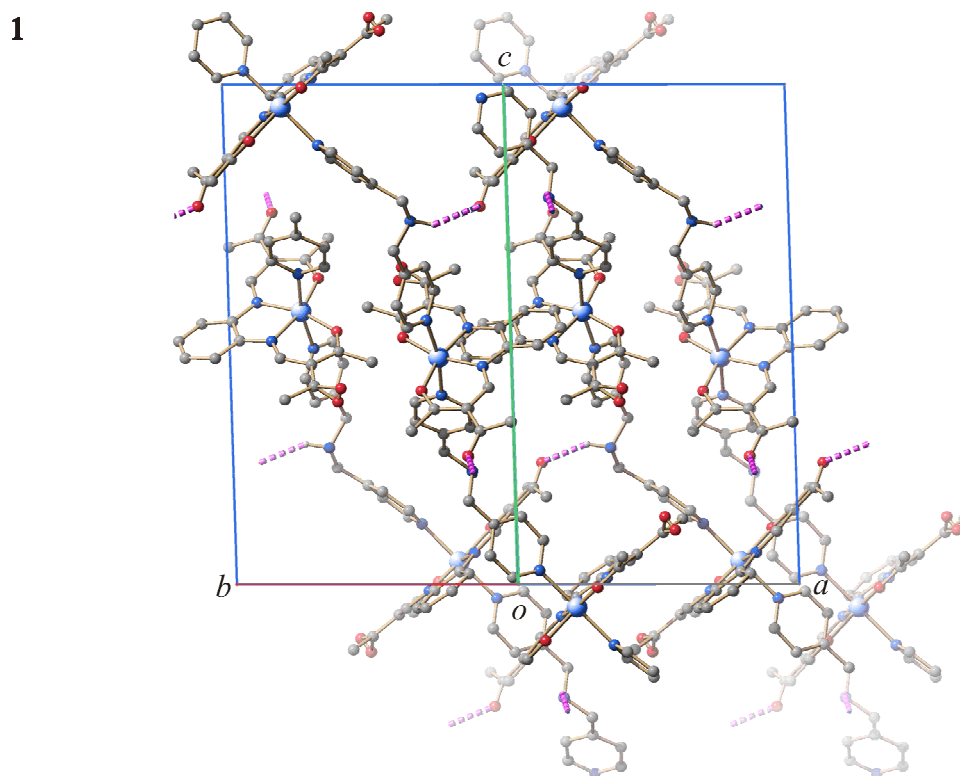


Figure 4. Packing of the polymer chains of **1** in the crystal projected in the plane (110). An infinite 2D hydrogen bond network in the plane (001) is observed (dashed lines).

Magnetic susceptibility data: The magnetic properties of the complexes were investigated by using a Quantum Design MPMSR-XL SQUID magnetometer in the temperature range from 295–5 K. The measurements indicate that all compounds are HS over the entire temperature range with the magnetic moment remaining constant down to approximately 50 K for all the complexes. Figure 5 gives a plot of the $\chi_M T$ product vs. temperature (with χ_M being the molar susceptibility) for the mononuclear complex **5**, the dinuclear complex **4** and the polymer chain compound **3** as typical representative. The plots of compounds **1** and **2** are illustrated in the Supplementary material.

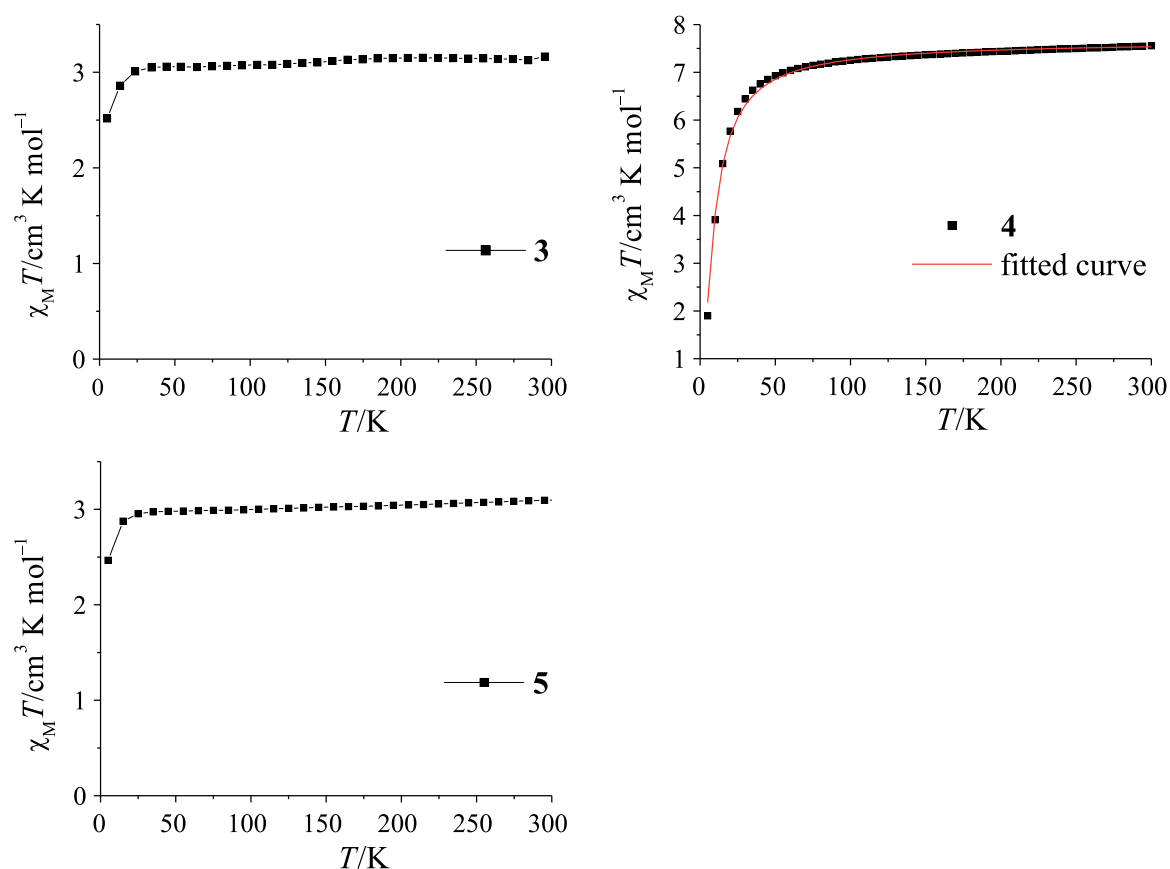


Figure 5. Plot of the $\chi_M T$ product vs. T for the compounds **3** to **5**. For the dinuclear complex **4**, the results from the fit with the equation and parameters given in the text are included as solid line.

At room temperature the magnetic moment of the polymer chain compounds **1–3** and complex **5** is in the region of $\chi_M T = 3.1\text{--}3.2 \text{ cm}^3 \text{ K mol}^{-1}$, typical for HS iron(II). For the dinuclear complex the calculated spin only value is equal to $6.0 \text{ cm}^3 \text{ K mol}^{-1}$. With $\chi_M T = 7.55 \text{ cm}^3 \text{ K mol}^{-1}$ the experimental value is in good agreement with theory, as the additional orbital moment contribution has to be considered. Upon cooling, the moment remains almost constant for all compounds. The decrease of the $\chi_M T$ product below 20 K for the monomer complex and the polymer chain compounds can be explained with zero-field splitting. A comparison of the curve progressing between the mononuclear complex **5** and the polymeric chains **1–3** indicates that there are no magnetic interactions mediated over the bridging axial ligands independent of the used bridge. For the dinuclear complex **4** the $\chi_M T$ product starts to decrease below 75 K, an indication for magnetic exchange interactions. Assuming the formula for the magnetic interactions in a $S_1 = 2$ and $S_2 = 2$ spin system with $H = -J S_1 \cdot S_2$,^[12] a weak antiferromagnetic interaction can be estimated to be $J = -1.84 \text{ cm}^{-1}$ ($g = 2.26$) by fitting the observed data given in Figure 5. This weak coupling corresponds to the results obtained for another dinuclear complex of the same ligand type but with different substituents at the equatorial ligand ($J = -1.08 \text{ cm}^{-1}$, $g = 1.96$).^[9a] It is a little bit surprising that complex **1** shows no spin transition as complexes of the ligand L2 with pyridine derivatives did so far always lead to SCO compounds and the ligand field strength should be in the right region. A possible explanation could be that the hydrogen bond network quenches the spin transition by pulling the equatorial and axial ligands away from the iron centre and by this increasing the iron-ligand distances. According to the formula

$$10Dq(r) \sim \mu/r^6 \quad (1)$$

for uncharged ligands,^[1f] with $10Dq$ being the ligand field strength, μ the dipole moment of the ligand and r the metal-to-ligand distance, there is a strong relation between the ligand field strength and the metal-to-ligand distance. A similar reason, maybe steric hindrance, could account for the absence of a spin transition of compound **3**. In the case of compound **2** the included dimethylformamide molecule is clearly responsible for the absence of spin transition behaviour as observed in a solvent-free powder sample of the same complex.^[7a] A similar observation was made for the inclusion of methanol.^[7b]

5.3 Conclusion

In this work the synthesis and characterisation of five new octahedral iron(II) complexes with N_4O_2 coordination sphere is presented. Results from X-ray structure analysis show that only the polymeric chain compound **1** forms an infinite two-dimensional hydrogen bond network, whereas for the compounds **2** to **4** only weak van der Waals-like interactions are observed with no significance for magnetic exchange interactions. Magnetic susceptibility measurements indicate that all compounds stay in the HS state over the whole temperature range investigated. In the case of complex **1** the hydrogen bond network seems to quench the spin transition, whereas for compound **2** the included solvent molecule in the crystal is responsible for the absence of a spin transition. A comparison of the progressing of the $\chi_M T$ vs. T curves for the polymeric chains **1–3** and the mononuclear complex **5** leads to the result that no magnetic interactions are mediated over the bridging axial ligands, independent of the used bridge. For the dinuclear compound **4**, a weak antiferromagnetic interaction of $J = -1.84 \text{ cm}^{-1}$ between the two iron(II) centres could be estimated from the experimental data.

5.4 Experimental Section

Magnetic measurements: Magnetic measurements of the samples were performed on a Quantum-Design-MPMSR-XL-SQUID-Magnetometer in a temperature range from 5 to 295 K. The measurements were carried out at two field strengths (0.02 and 0.05 T) in the settle mode. The data were corrected for the magnetisation of the sample holder, and diamagnetic corrections were made by using estimated values according to $\chi_{\text{dia}} \approx -0.5 M_{\text{complex}} \times 10^{-6}$.

X-Ray crystallography: The intensity data of **1** to **5** were collected on a Nonius KappaCCD diffractometer by using graphite-monochromated MoK α radiation. Data were corrected for Lorentz and polarisation effects. The structures were solved by direct methods (SIR-97)^[13] and refined by full-matrix least-square techniques against F_0^2 (SHELXL-97).^[14] The hydrogen atoms were included at calculated positions with fixed thermal displacement parameters. ORTEP-III was used for structure representation^[15] and SCHAKAL-99 was used for the presentation of the packing of the molecules in the crystal.^[16] Selected distances and angles are presented in Table 1. Crystallographic data for all complexes are summarised in Supporting Information Table S1.1–2.

Further details on the crystal structures of compounds **1** (CCDC 691145), **2** (691146), **4** (691147) and **5** (691144) can be obtained free of charge on application to Cambridge Crystallographic Data Centre, 12 Union Road, Cambridge CB2 1EZ, UK (Fax: int.code+(1223)336-033; e-mail fileserv@ccdc.cam.ac.uk).

Synthesis: All syntheses were carried out under argon by using Schlenk tube techniques. All solvents were purified as described in the literature^[17] and distilled under argon. The synthesis of the ligands H₂L1,^[18] H₂L2,^[18] H₄L3,^[9a] [FeL1(MeOH)₂],^[19] [FeL2(MeOH)₂]^[19] and iron(II)acetate^[20] is described in literature. Bis(4-pyridylmethyl)amine was synthesised by using the same procedure as reported for Bis(2-pyridylmethyl)amine but with the educts functionalised at *para*-position.^[21] Anhydrous 4,4'-bipyridine and 1-methylimidazole were purchased from ACROS, *trans*-1,2-bis(4-pyridyl)ethylene was purchased from Aldrich and 4-dimethylaminopyridine was purchased from Fluka. 1-Methylimidazole was distilled under argon; the others were used as received.

[FeL2(4-dpa)]·EtOH (1): [FeL2(MeOH)₂] (0.46 g, 1.20 mmol) and an ethanol solution of bis(4-pyridylmethyl)amine (1 M, 6.0 mL, 6.0 mmol) were dissolved in ethanol (50 mL) and heated to reflux for 4 h. After cooling down to room temperature, a black precipitate was filtered off, washed with ethanol (10 mL) and dried *in vacuo* (yield: 0.51 g, 73%). MS (DEI-+), 70 eV): *m/z* (%): 382 (100) [FeL2⁺]; elemental analysis calcd (%) for C₃₂H₃₇FeN₅O₅ (627.21): C 61.25, H 5.94, N 11.16; found C 61.57, H 5.55, N 11.57.

[FeL2(bipy)]·DMF (2): [FeL2(MeOH)₂] (0.40 g, 0.90 mmol) and 4,4'-bipyridine (1.40 g, 8.96 mmol) were dissolved in dimethylformamide (40 mL) and heated to reflux for 1 h. After cooling down to room temperature, a black precipitate was filtered off that was washed with methanol (10 mL) and dried *in vacuo* (yield: 0.28 g, 58%). Elemental analysis calcd (%) for C₃₁H₃₃FeN₅O₅ (611.18): C 60.89, H 5.44, N 11.45; found: C 61.10, H 5.24, N 11.05.

[FeL1(bpee)] (3): A suspension of [FeL1(MeOH)₂] (0.31 g, 0.61 mmol) and *trans*-1,2-bis(4-pyridyl)ethylene (1.12 g, 6.12 mmol) in methanol (35 mL) was heated to reflux for 1 h. After cooling down to room temperature the black precipitate was filtered off, washed with methanol (10 mL) and dried *in vacuo* (yield: 0.21 g, 55%). MS (FAB-+): *m/z* (%): 442 (31) [FeL1⁺]; elemental analysis calcd (%) for C₃₂H₃₂FeN₄O₆ (624.17): C 61.55, H 5.17, N 8.97; found: C 61.17, H 5.22, N 8.92.

[Fe₂L3(1-meim)₄]·4 1-meim (4): A solution of H₄L3 (0.60 g, 0.85 mmol), iron(II)acetate (0.38 g, 2.18 mmol) and 1-methylimidazole (1.24 g, 15.2 mmol) in methanol (20 mL) was heated to reflux for 1 h. After cooling down to room temperature the brown precipitate was filtered off, washed with methanol (10 mL) and dried *in vacuo* (yield: 0.15 g, 18%). MS (FAB-+): *m/z* (%): 805 (85) [Fe₂L3⁺]; elemental analysis calcd (%) for C₆₆H₈₆Fe₂N₂₀O₁₂ (1462.54): C 54.18, H 5.92, N 19.15; found: C 53.54, H 5.81, N 19.42.

[FeL1(DMAP)₂] (5): [FeL1(MeOH)₂] (0.85 g, 1.68 mmol) and 4-dimethylaminopyridine (10.5 g, 0.086 mol) were dissolved in methanol (30 mL) and heated to reflux for 0.5 h. After cooling, the solution was left in the refrigerator (4 °C) to form black crystals that were collected, washed with a little methanol and dried *in vacuo* (yield: 0.8 g, 69%). IR (KBr): $\tilde{\nu} = 1683(\text{s}) \text{ cm}^{-1}$ (CO); MS (DEI-+), 70 eV): *m/z* (%): 442 (10) [FeL1⁺], 121 (100) [DMAP⁺]; elemental analysis calcd (%) for C₃₄H₄₂FeN₆O₆Fe (686.25): C 59.47, H 6.17, N 12.24; found: C 59.64, H 6.12, N 12.44; DTG: up to 270°C: -39.5% = loss of 2 DMAP (theory: 35%); at 280°C: decomposition

Supplementary material: Supplementary data associated with this article can be found in the online version at doi: 10.1016/j.ica.2008.10.018.

Acknowledgements

This work has been supported financially by the Deutsche Forschungsgemeinschaft (SPP 1137) the Fonds der Chemischen Industrie and the Center for Integrated Protein Science Munich (CIPSM). The Authors would like to thank E. Kaps and A. Glas for the preparation of some of the complexes and P. Mayer, S. Albrecht and M. Reichvilser for the acquisition of the crystallographic data.

5.5 References

- [1] a) H.A. Goodwin, *Coord. Chem. Rev.* **1976**, *18*, 293; b) P. Gütlich, *Struct. Bonding (Berlin)* **1981**, *44*, 83; c) E. König, *Prog. Inorg. Chem.* **1987**, *35*, 527; d) P. Gütlich, A. Hauser, *Coord. Chem. Rev.* **1990**, *97*, 1; e) E. König, *Struct. Bonding (Berlin)* **1991**, *76*, 51; f) P. Gütlich, A. Hauser, H. Spiering, *Angew. Chem. Int. Ed. Engl.* **1994**, *33*, 2024, and references therein; *Angew. Chem.* **1994**, *106*, 2109; g) P. Gütlich, J. Jung, H.A. Goodwin, *Molecular Magnetism: From Molecular Assemblies to the Devices* (Eds.: E. Coronado *et al.*), NATO ASI Series E: *Applied Sciences*, Vol. 321, Kluwer, Dordrecht, **1996**, 327; h) P. Gütlich, H.A. Goodwin (Eds.), *Spin Crossover in Transition Metal Compounds I–III, Topics in Current Chemistry*, Springer, Berlin, Heidelberg, New York **2004**; i) J.A. Real, A.B. Gaspar, M.C. Munoz, *Dalton Trans.* **2005**, 2062, j) O. Sato, J. Tao, Y.-Z. Zhang, *Angew. Chem.* **2007**, *119*, 2200; *Angew. Chem. Int. Ed.* **2007**, *46*, 2152.
- [2] a) O. Kahn, C. Jay Martinez, *Science* **1998**, *279*, 44; b) O. Kahn, C. Jay, J. Kröber, R. Claude, F. Grolière, *Patent EP0666561* **1995**; c) J.-F. Létard, O. Nguyen, N. Daro, *Patent FR0512476* **2005**; d) J.-F. Létard, P. Guionneau, L. Goux-Capes, *Topics in Current Chemistry*, Vol. 235 (Eds.: P. Gütlich, H.A. Goodwin), Springer, Wien, New York, **2004**, 221; e) A. Galet, A.B. Gaspar, M.C. Munoz, G.V. Bukin, G. Levchenko, J.A. Real, *Adv. Mater.* **2005**, *17*, 2949.
- [3] A.B. Gaspar, V. Ksenofontov, J.A. Real, P. Gütlich, *Chem. Phys. Lett.* **2003**, *373*, 385.
- [4] V. Ksenofontov, A.B. Gaspar, V. Niel, S. Reiman, J.A. Real, P. Gütlich, *Chem. Eur. J.* **2004**, *10*, 1291.
- [5] a) S. Zein, S.A. Borshch, *J. Am. Chem. Soc.* **2005**, *127*, 16197; b) K. Nakano, S. Kawata, K. Yoneda, A. Fuyuhiko, T. Yagi, S. Nasu, S. Morimoto, S. Kaizaki, *Chem. Commun.* **2004**, 2892.
- [6] N. Ortega-Villar, A.L. Thompson, M.C. Munoz, V.M. Ugalde-Sadivar, A.E. Goeta, R. Moreno-Esparza, J.A. Real, *Chem. Eur. J.* **2005**, *11*, 5721.

- [7] a) B. Weber, R. Tandon, D. Himsl, *Z. Anorg. Allg. Chem.* **2007**, *633*, 1159; b) B. Weber, E.S. Kaps, C. Desplanches, J.-F. Létard, *Eur. J. Inorg. Chem.* **2008**, 1589.
- [8] a) B. Weber, E. Kaps, J. Weigand, C. Carbonera, J.-F. Létard, K. Achterhold, F.-G. Parak, *Inorg. Chem.* **2008**, *47*, 487; b) B. Weber, E.S. Kaps, J. Obel, W. Bauer, *Z. Anorg. Allg. Chem.* **2008**, 1421; c) B. Weber, C. Carbonera, C. Desplanches, J.-F. Létard, *Eur. J. Inorg. Chem.* **2008**, 1589.
- [9] a) B. Weber, E. Kaps, *Heteroatom Chem.* **2005**, *16*, 391; b) B. Weber, F.-A. Walker, *Inorg. Chem.* **2007**, *46*, 6794.
- [10] B. Weber, W. Bauer, J. Obel, *Angew. Chem.* **2008**, *120*, 10252; *Angew. Chem., Int. Ed.* **2008**, *47*, 10098;
- [11] G.A. Jeffrey, H. Maluszynska, J. Mitra, *Int. J. Biol. Macromol.* **1985**, *7*, 336.
- [12] A. Real, J. Zarembowitch, O. Kahn, X. Solans, *Inorg. Chem.* **1987**, *26*, 2939.
- [13] A. Altomare, M.C. Burla, G.M. Camalli, G. Cascarano, C. Giacovazzo, A. Guagliardi, A.G.G. Moliterni, G. Polidori, R. Spagna, SIR-97, University of Bari, Bari (Italy), **1997**; *J. Appl. Crystallogr.* **1999**, *32*, 115.
- [14] G.M. Sheldrick, SHELXL-97, University of Göttingen, Göttingen (Germany), **1997**.
- [15] C.K. Johnson, M.N. Burnett, ORTEP-III, Oak-Ridge National Laboratory, Oak-Ridge TN (USA) **1996**; L.J. Farrugia, *J. Appl. Crystallogr.* **1997**, *30*, 565.
- [16] E. Keller, SCHAKAL-99, University of Freiburg, Freiburg (Germany), **1999**.
- [17] Team of authors: *Organikum*, Johann Ambrosius Barth Leipzig, Berlin, Heidelberg, **1993**.
- [18] L. Wolf, E.-G. Jäger, *Z. anorg. allg. Chem.* **1966**, *346*, 76.
- [19] E.-G. Jäger, E. Häussler, M. Rudolph, M. Rost, *Z. Anorg. Allg. Chem.* **1985**, *525*, 67.
- [20] B. Heyn, B. Hipler, G. Kreisel, H. Schreer, D. Walter, *Anorganische Synthesechemie*, 2. edition, Springer, Heidelberg, **1986**.
- [21] C.K. Sams, F. Somoza, I. Bernal, H. Toftlund, *Inorg. Chim. Acta* **2001**, *318*, 45.

5.6 Supporting Information

Table S1.1. Crystallographic data of the iron complexes discussed in this work.

compound	1	2	3
formula	C ₆₂ H ₆₈ Fe ₂ N ₁₀ O ₉	C ₅₉ H ₅₉ Fe ₂ N ₉ O ₉	C ₃₃ H ₃₅ FeN ₄ O ₇
$M_r / \text{g mol}^{-1}$	1208.955	1149.845	655.50
crystal system	monoclinic	triclinic	monoclinic
space group	$C2/c$	$P\bar{1}$	$P2_1/a$
$a / \text{\AA}$	15.9203(4)	11.6970(5)	11.5169(7)
$b / \text{\AA}$	17.9247(6)	11.9128(7)	23.7546(16)
$c / \text{\AA}$	21.1890(6)	19.5728(10)	12.3096(6)
$\alpha / ^\circ$	90.00	82.525(2)	90.00
$\beta / ^\circ$	92.2218(18)	86.110(3)	108.522(3)
$\gamma / ^\circ$	90.00	89.772(3)	90.00
$V / \text{\AA}^3$	6042.1(3)	2697.9(2)	3193.2(3)
Z	4	2	4
$\rho / \text{g cm}^{-3}$	1.329	1.415	1.364
μ / mm^{-1}	0.544	0.605	0.526
crystal size	0.17 × 0.12 × 0.02	0.19 × 0.04 × 0.02	0.10 × 0.04 × 0.03
T / K	200(2)	200(2)	293(2)
diffractometer	KappaCCD	KappaCCD	KappaCCD
$\lambda (\text{MoK}\alpha) / \text{\AA}$	0.71073	0.71073	0.71073
θ -range / $^\circ$	3.14–25.37	3.16–25.00	3.18–24.99
reflns. collected	19117	17231	45102
indep. reflns. (R_{int})	5539 (0.0521)	9468 (0.0724)	5612(0.4071)
mean $\sigma(I) / I$	0.0530	0.1185	0.2256
reflns. with $I \geq 2\sigma(I)$	3902	4944	2231
x, y (weighting scheme)	0.0944, 2.4737	0.0707, 0	0.0574, 0
parameters	388	721	412
restraints	0	0	0
$R(F)$ (all data) ^[a]	0.0526 (0.0801)	0.0633 (0.1422)	0.0794 (0.2394)
$wR(F^2)$ ^[b]	0.1617	0.1645	0.1634
$Goof$	1.041	0.971	0.909
shift/error _{max}	0.992	0.000	0.000
max., min. resd. dens. / e \AA^{-3}	0.818, -0.409	0.854, -0.641	0.443, -0.377

[a] $R(F) = \sum ||F_o| - |F_c|| / \sum |F_o|$. [b] $wR(F^2) = [\sum [w(F_o^2 - F_c^2)^2] / \sum w(F_o^2)^2]^{1/2}$, $w = 1 / [\sigma^2(F_o^2) + (aP)^2 + bP]$, where $P = [F_o^2 + 2(F_c^2)]/3$.

Table S1.2. Crystallographic data of the iron complexes discussed in this work.

compound	4	5
formula	C ₆₆ H ₈₆ Fe ₂ N ₂₀ O ₁₂	C ₃₄ H ₄₂ Fe N ₆ O ₆
$M_r / \text{g mol}^{-1}$	1463.207	686.579
crystal system	triclinic	monoclinic
space group	$P\bar{1}$	$P2_1/c$
$a / \text{Å}$	9.7651(3)	15.2180(18)
$b / \text{Å}$	14.0455(3)	14.4680(11)
$c / \text{Å}$	15.3282(5)	17.1380(15)
$\alpha / ^\circ$	114.2247(10)	90.00
$\beta / ^\circ$	97.1187(9)	114.396(12)
$\gamma / ^\circ$	105.232(2)	90.00
$V / \text{Å}^3$	1784.57(9)	3436.4(6)
Z	1	4
$\rho / \text{g cm}^{-3}$	1.3615	1.3271
μ / mm^{-1}	0.480	0.491
crystal size	$0.30 \times 0.08 \times 0.04$	$0.27 \times 0.12 \times 0.07$
T / K	200(2)	293(2)
diffractometer	KappaCCD	Stoe IPDS
$\lambda (\text{MoK}\alpha) / \text{Å}$	0.71073	0.71073
θ -range / $^\circ$	3.25–25.50	1.47–22.39
reflns. collected	16338	16079
indep. reflns. (R_{int})	6515 (0.0547)	4288 (0.1215)
mean $\sigma(I) / I$	0.0837	0.1680
reflns. with $I \geq 2\sigma(I)$	4448	1930
x, y (weighting scheme)	0.0598, 0.1693	0.0131, 0
parameters	460	433
restraints	0	0
$R(F)$ (all data) ^[a]	0.0569 (0.0957)	0.0421 (0.1148)
$wR(F^2)$ ^[b]	0.1400	0.0778
$Goof$	1.090	0.690
shift/error _{max}	0.000	0.000
max., min. resd. dens. / e Å^{-3}	0.618, -0.535	0.196, -0.309

[a] $R(F) = \sum ||F_o| - |F_c|| / \sum |F_o|$. [b] $wR(F^2) = [\sum [w(F_o^2 - F_c^2)^2] / \sum w(F_o^2)^2]^{1/2}$, $w = 1 / [\sigma^2(F_o^2) + (aP)^2 + bP]$, where $P = [F_o^2 + 2(F_c^2)]/3$.

6 X-Ray Structure and Magnetic Properties of Two New Iron(II) 1D Coordination Polymers with Bis(imidazolyle)-methane as Bridging Ligand

Toni Pfaffeneder,^[a] Wolfgang Bauer^[a] and Birgit Weber*^[a]

[a] Center for Integrated Protein Science Munich at the Department Chemie und Biochemie, Ludwig-Maximilians-Universität München, Butenandtstr. 5–13 (Haus F), 81377 München, Germany

Keywords: Iron; Magnetic properties, Schiff bases; Spin Crossover

Published in: *Z. Anorg. Allg. Chem.* **2010**, 636, 183–187.

Abstract: The reaction of iron(II) acetate with the tetradentate Schiff base-like ligands H₂L1 and H₂L2 (L1²⁻ = {diethyl (*E,E*)-2,2'-[1,2-phenyl-bis(iminomethylidene)]bis[3-oxobutanoate]}, L2²⁻ = 3,3'-[1,2-phenyl-bis(iminomethylidene)]bis[pentane-2,4-dione]) leads to the formation of the octahedral N₂O₄ coordinated iron complexes [FeL1(MeOH)₂] and [FeL2(MeOH)₂], respectively. Conversion of both with bimm (bis(1-imidazolyle)methane) leads to the 1D coordination polymers [FeL1(bimm)]·0.5 MeOH (**1**) and [FeL2(bimm)] (**2**). Compound **1** is a pure high-spin (HS) complex, which was characterised by using magnetic measurements and X-ray structure analysis. Compound **2** undergoes an irregular and incomplete thermal spin transition.

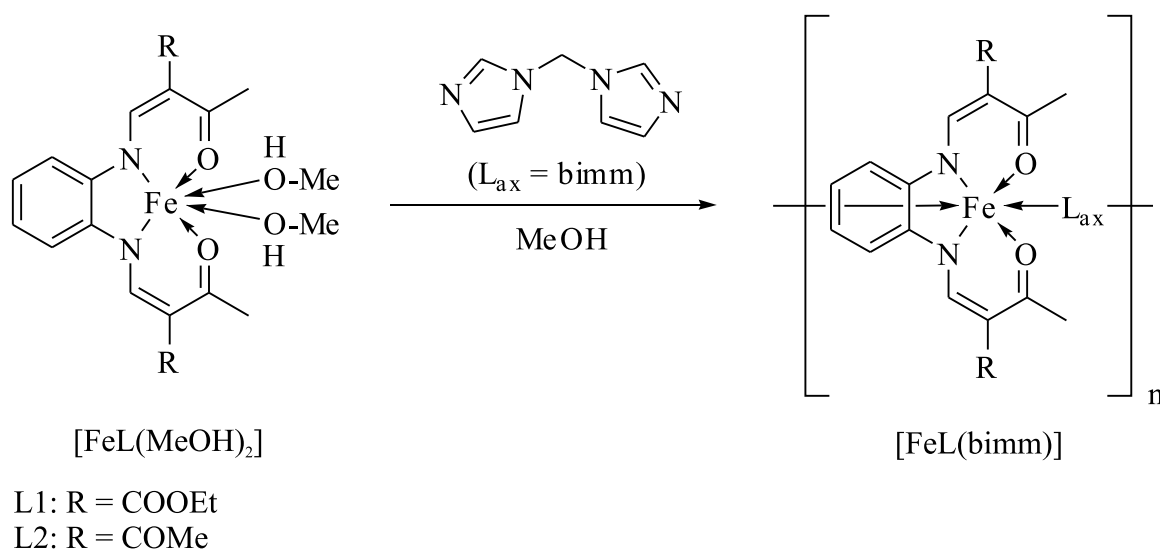
6.1 Introduction

Spin transition complexes (spin crossover, SCO) are an interesting class of compounds that can be switched between two or more states by physical perturbations such as temperature, pressure or light.^[1] Several applications in the field of information technology can be envisioned for this class of substance, especially for complexes that exhibit a wide hysteresis around room temperature (memory effect).^[2] The occurrence of hysteresis and other types of

SCO such as stepwise or abrupt spin transitions depends on the cooperative effects between the metal centres during the spin-transition. Different intermolecular interactions such as π -stacking, hydrogen bonds or van der Waals interactions are suitable transmitters for these effects. The application of covalent linkers as suggested by Kahn *et al.*^[2a] did attract special attention over the last years as the spreading of those interactions can be more easily controlled. This resulted in the synthesis and characterisation of several iron(II) spin crossover coordination polymers.^[3] We have shown in a recent review,^[4] that covalent linkers, most likely, have not the ability to transmit the geometric changes associated with the spin transition through the crystal lattice and, by this, increase the cooperative interactions. We have clearly demonstrated that the increase of cooperative effects during the spin transition is mainly due to an increased number of intermolecular contacts. Furthermore our results have shown that covalent linkers can be used to optimise the packing of the molecules in the crystal in a crystal-engineering like approach.^[4] Next to spin transitions with wide thermal hysteresis loops stepwise transitions are also of interest because of the possibility of addressing more than two different states. The factor, which determines the presence or absence of steps in the transition curve of coordination polymers is the packing of the molecules in the crystals. For the previously reported complex [FeL2(bppa)]·MeOH (bppa = 1,3-bis(4-pyridyl)propane),^[4] a stepwise spin crossover was observed, due to a zigzag-like structure of the 1D chain with alternating HS and LS iron(II) centres on the step. Due to the zigzag-structure the interchain Fe··Fe distances cannot follow the Fe-L distance changes upon spin transition as easily as compared to linear structures because of restraining interactions (steric hindrances) between the neighbouring chains. Very likely this is the reason for the stabilisation of the wide step. Similar structures and magnetic properties could be obtained by the usage of the axial ligand bis(1-imidazolyle)methane (bimm) instead of bppa. So far only few coordination polymers were reported for this ligand that were obtained through the self-assembly with different metal centres.^[5] Those structures indicate that the bimm ligand is well suited for the generation of zigzag chain structures. In this paper we present the synthesis and characterisation of two polymer iron(II) complexes [FeL1(bimm)]·0.5 MeOH and [FeL2(bimm)].

6.2 Results and Discussion

Synthesis of the complexes: The general route for the synthesis of the 1D octahedral iron(II) coordination polymers is depicted in Scheme 1. The complexes could be obtained in a two-pot reaction. In a first step an iron complex of the tetradentate equatorial ligand (H₂L1/2) with methanol as axial ligands was prepared.^[6] In a second step [FeL1/2(MeOH)₂] was converted with the axial ligand bimm. To obtain [FeL1(bimm)]·0.5 MeOH (**1**) and [FeL2(bimm)] (**2**), a 5-fold molar excess of the axial ligand was used. Both complexes were characterised by elemental analysis, IR and mass spectroscopy as well as *T*-dependent magnetic susceptibility measurements.



Scheme 1. General procedure for the synthesis of the 1D octahedral iron(II) coordination polymers.

6. X-Ray Structure and Magnetic Properties of Two New Iron(II) 1D Coordination Polymers with Bis(imidazole)-methane as Bridging Ligand

X-Ray structure analysis: Crystals suitable for X-ray structure analysis were obtained only for **1**. The crystallographic data are summarised in Supporting Information Table S1. Figure 1 displays the asymmetric unit of the octahedral complex. Selected bond lengths and angles within the first coordination sphere are summarised in Table 1.

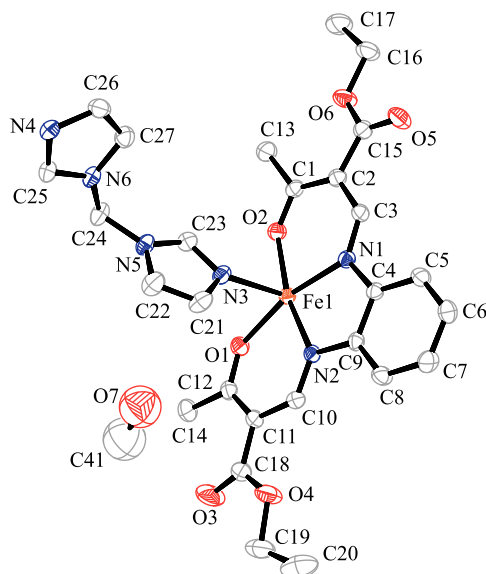


Figure 1. ORTEP drawing of the asymmetric unit of **1**. Hydrogen atoms were omitted for clarity. Thermal ellipsoids are shown with a 50% probability.

Table 1. Selected bond lengths [\AA] and angles [degree] within the first coordination sphere of **1** at 200 K.

Fe-N _{eq}	Fe-O _{eq}	Fe-N _{ax}	O _{eq} -Fe-O _{eq}	N _{ax} -Fe-N _{ax}
2.098(2)	2.048(1)	2.230(1)	108.59(5)	167.52(6) ^[a]
2.083(1)	2.019(1)	2.262(1) ^[a]		

Symmetry code: [a] $1 + x, y, z$.

The bond lengths and angles within the first coordination sphere of **1** are within the region reported for HS iron(II) complexes of the same ligand type.^[7] The average bond lengths are 2.09 Å (Fe-N_{eq}), 2.03 Å (Fe-O_{eq}) and 2.25 Å (Fe-N_{ax}). A characteristic tool for the determination of the spin state of this type of iron(II) complexes is the O-Fe-O angle that changes from about 110° in the HS state to about 90° in the LS state.^[7] For the complex reported here, the angle is with 109° clearly in the region typical for the HS state. The N_{ax}-Fe-N_{ax} angle differs, with 168°, significantly from the expected 180° for an ideal octahedron. A possible explanation for the strong distortion is the intermolecular network of non-classical hydrogen bonds between the axial and the equatorial ligand (C27-H27···O5, C24-H24···O1). Selected intermolecular distances shorter than the sum of the van der Waals radii are summarised in Table 2. In Figure 2 the packing of the complex in the crystal is displayed. For a better understanding of the magnetic properties it is in general necessary to investigate short contacts in the crystal packing. Besides the two contacts, which have been already mentioned, there is a further non-classical hydrogen bond (C6-H6···O3), which contributes to a 3D network of intermolecular interactions between the polymer chains. Furthermore a hydrogen bond (O7-H7···O3) between the hydroxy group of the additional solvent molecule methanol in the crystal and a carbonyl group of the equatorial ligand is formed (Table 2). The methanol molecules occupy a special position (inversion centre) and therefore a disorder model was applied. The equatorial ligands within a 1D chain are ordered in a parallel manner, because of the distortion of the imidazolyle rings of the axial ligand.

6. X-Ray Structure and Magnetic Properties of Two New Iron(II) 1D Coordination Polymers with Bis(imidazolyle)-methane as Bridging Ligand

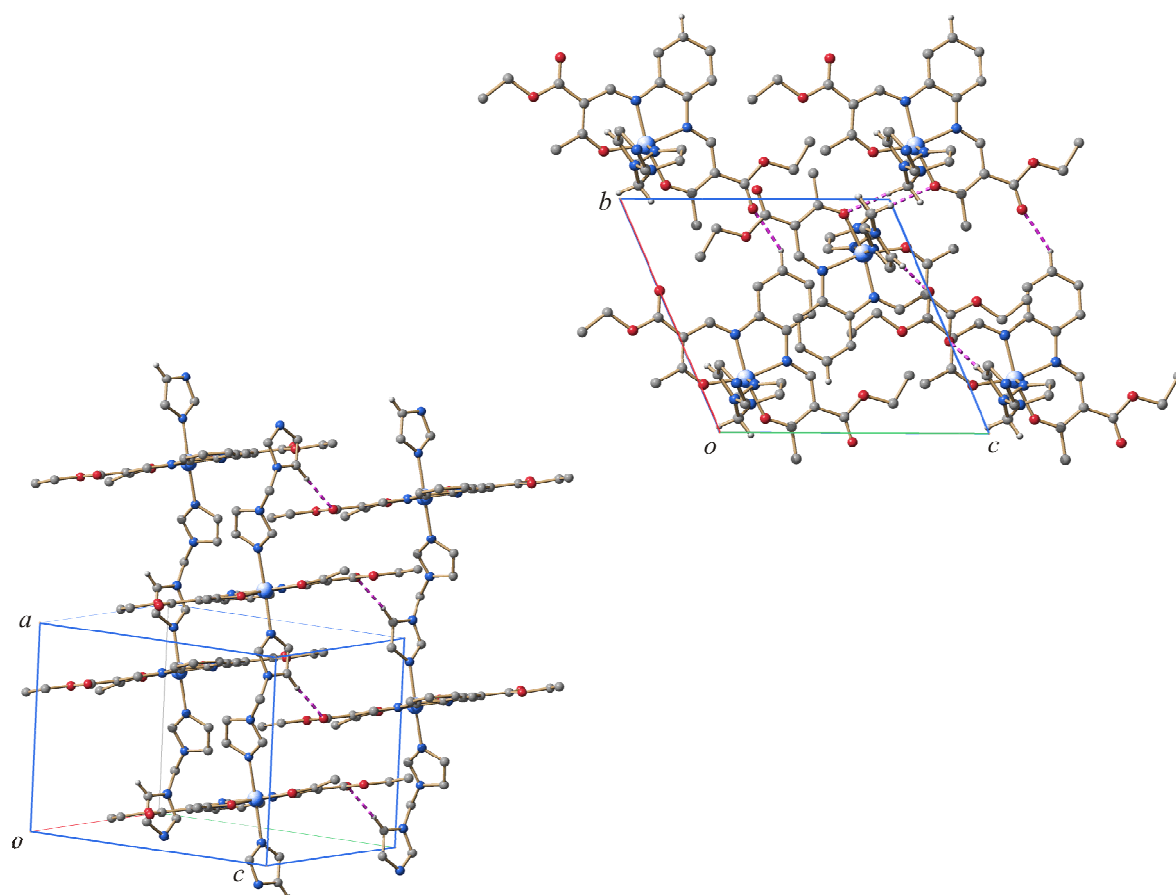


Figure 2. Top: Packing of compound **1** in the crystal at 200 K; view along [1 0 0], bottom: excerpt of a 2D layer of parallel polymer chains. The network of intermolecular contacts is highlighted (dashed lines). Solvent molecules and hydrogen atoms, which do not participate in hydrogen bonding, have been omitted for clarity.

Table 2. Selected intermolecular distances [\AA] and angles [degree] of **1** at 200 K.

D	H	A	D-H	H \cdots A	A \cdots D	D-H \cdots A
O7	H7	O3 ^[a]	0.84	2.32	2.956(6)	133
C6	H6	O3 ^[b]	0.95	2.38	3.185(3)	143
C24	H24	O1 ^[c]	0.95	2.27	3.258(2)	174
C27	H27	O5 ^[d]	0.95	2.36	3.302(3)	173

Symmetry codes: [a] $1 - x, -y, 1 - z$; [b] $x, 1 + y, z$; [c] $1 - x, -y, -z$; [d] $1 - x, 1 - y, -z$.

Magnetic susceptibility data: Magnetic susceptibility measurements for both compounds were investigated in the temperature range from 295 to 10 K at 0.05 T by using a Quantum Design MPMSR-XL SQUID magnetometer. Figure 3 displays the thermal dependence of the $\chi_M T$ product for both compounds.

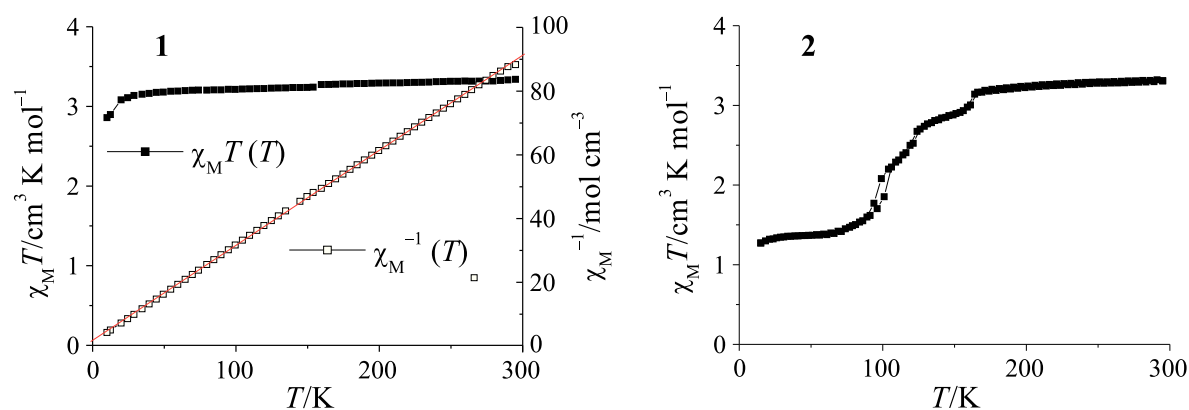


Figure 3. Plots of $\chi_M T$ product (filled squares) vs. T for the compounds **1** and **2**. Reciprocal molar susceptibility χ_M^{-1} (open squares) as function of temperature T and the fits according to the Curie-Weiss law, $\chi_M = C/(T - \Theta)$, with the parameters $\Theta = -2.71$ K, $C = 3.34$ cm³ K mol⁻¹ for compound **1**.

For compound **1** (top of Figure 3) nearly ideal Curie behaviour is observed. Upon cooling, the $\chi_M T$ product decreases from a value of 3.34 cm³ K mol⁻¹ at 295 K to a value of 3.08 cm³ K mol⁻¹ at 20 K. The susceptibility data above 20 K can be fitted very well with the Curie-Weiss law ($\chi_M = C/(T - \Theta)$) with the parameters $\Theta = -2.71$ K and $C = 3.34$ cm³ K mol⁻¹. The Curie constant C is in a region expected for iron(II) HS complexes and the negative Weiss constant Θ in combination with the temperature-dependent decrease of the $\chi_M T$ product is an indication for weak antiferromagnetic interactions between the spin centres. Compound **1** is a typical iron(II) HS complex. For compound **2** (bottom of Figure 3) the situation is more complex. Upon cooling, the $\chi_M T$ product decreases from a value of 3.31 cm³ K mol⁻¹ at 295 K to a value of 1.37 cm³ K mol⁻¹ at 50 K. The room temperature value is in the region typical for an iron(II) HS complex. The curve progressing is very irregular with three steps, a remaining HS molar fraction and a small hysteresis for the last step. Crystals suitable for X-ray analysis were not obtained until now to elucidate the structural reasons for this behaviour. Likely the structure is similar to the observed structure

of compound **1**, because the equatorial ligands vary only in a small residue (methyl instead of ethyl group), which do not participate in intermolecular interactions. A similar network of short contacts like the observed 3D network of non-classical hydrogen bonds in **1** could be the reason for the cooperative effects (hysteresis) during the spin transition of compound **2**. However, the multitude of different steps indicates that there are probably more than two different iron centres. One reason could be that two or more modifications of the polymer chain with different orientations of the rather flexible bimm ligand co-precipitate at the same time. The different plateaus in the transition curve of **2** are less pronounced compared to the complex $[\text{FeL}_2(\text{bppa})]\cdot\text{MeOH}^{[4]}$ in agreement with the almost linear chain structure observed for **1**.

6.3 Conclusion

We have expected similar structures and magnetic properties for the newly synthesised iron(II) coordination polymers with the axial ligand bimm as we have observed for the analogous complex $[\text{FeL}_2(\text{bppa})]\cdot\text{MeOH}^{[4]}$. The latter undergoes a stepwise thermal spin transition with a wide plateau due to a zigzag-like structure, which stabilises the step according to restraining interchain interactions. In the case of the HS compound **1** the formation of a zigzag-like chain is prevented by a distortion of the imidazolyle rings of bimm. For compound **2** an irregular and incomplete spin transition was observed, which indicates several steps and a small hysteresis. Since we have not obtained suitable crystals, we could not elucidate the reason for the magnetic behaviour of this complex. Due to the high flexibility of the bimm ligand the co-precipitation of two or more modifications of the complex with different orientations of the bimm ligand cannot be excluded. For a better understanding and predictability of SCO properties less flexible bridging ligands are necessary.

6.4 Experimental Section

Magnetic measurements: Magnetic measurements of the fine crystalline samples were performed on a Quantum-Design-MPMSR2-SQUID magnetometer in a temperature range from 10 to 295 K. The measurements were carried out at 0.05 T in the settle mode. The data were corrected for the magnetisation of the sample holder and diamagnetic corrections were made by using tabulated Pascals constants.

X-Ray crystallography: The intensity data of **1** were collected on an Oxford XCalibur diffractometer by using graphite-monochromated MoK α radiation. Data were corrected for Lorentz and polarisation effects. The structure was solved by direct methods (SIR-97)^[8] and refined by full-matrix least-square techniques against F_0^2 (SHELXL-97).^[9] The hydrogen atoms were included at calculated positions with fixed thermal parameters. ORTEP-III^[10] was used for structure representation. Selected distances and angles are presented in Table 1. Crystallographic data are summarised in Supporting Information Table S1.

Further details on the crystal structures (CCDC-734192 for **1**) can be obtained free of charge on application to Cambridge Crystallographic Data Centre, 12 Union Road, Cambridge CB2 1EZ, UK (Fax: int.code+(1223)336-033; e-mail fileserv@ccdc.cam.ac.uk).

Synthesis: All syntheses were carried out under argon by using Schlenk tube techniques. Methanol was purified as described in literature^[11] and distilled under argon. The synthesis of the ligands H₂L1^[12] and H₂L2^[12] and [FeL1/2(MeOH)₂]^[13] is already described in literature.

Bis(1-imidazolyle)methane (bimm): The ligand bimm, whose synthesis has already been reported^[14], has been prepared according to the procedure for the synthesis of bis(1-pyrazolyle)methane^[15] and recrystallised from chloroform. ¹H NMR (400 MHz, [D₆]DMSO, 22°C, TMS): δ = 7.9 (s, 2H; CH), 7.4 (s, 2H; CH), 6.9 (s, 2H; CH), 6.2 ppm (s, 2H; CH₂); MS (DEI(+), 70 eV): m/z (%): 148 (53) [M^+], 81 (100) [$M^+ - C_3H_3N_2$]; elemental analysis calcd (%) for C₇H₈N₄ (148.07): C 56.74, H 5.44, N 37.81; found: 56.26, H 5.30, N 37.48.

[FeL1(bimm)]·0.5 MeOH (1): A suspension of [FeL1(MeOH)₂] (0.50 g, 0.99 mmol) and bimm (0.74 g, 4.99 mmol) were refluxed in methanol (20 mL) for 1 h. After cooling down to room temperature the dark brown precipitate was filtered off, washed with methanol (5 mL) and dried *in vacuo* (yield: 0.50 g, 83%). IR (KBr): $\tilde{\nu}$ = 1688(m) (COO), 1663(m),

6. X-Ray Structure and Magnetic Properties of Two New Iron(II) 1D Coordination Polymers with Bis(imidazolyle)-methane as Bridging Ligand

1571(s) cm^{-1} (CO); MS (DEI-(+), 70 eV): m/z (%): 443 (26) [$\text{FeL1}^+ + \text{H}$], 442 (100) [FeL1^+], 397 (22) [$\text{FeL1}^+ - \text{OC}_2\text{H}_5$], 148 (43) [bimm^+], 81 (60) [$\text{bimm}^+ - \text{C}_3\text{H}_3\text{N}_2$]; elemental analysis calcd (%) for $\text{C}_{27.5}\text{H}_{32}\text{FeN}_6\text{O}_{6.5}$ (606.42): C 54.47, H 5.32, N 13.86; found: C 54.39, H 5.04, N 14.04.

Single crystals of **1** were slowly formed by diffusion techniques in methanol solution after several weeks.

[FeL2(bimm)] (2): A suspension of [$\text{FeL2}(\text{MeOH})_2$] (0.24 g, 0.54 mmol) and bimm (0.40 g, 2.69 mmol) were refluxed in methanol (15 mL) for 1 h. After cooling down to room temperature the dark brown precipitate was filtered off, washed with methanol (5 mL) and dried *in vacuo* (yield 0.24 g, 84%). IR (KBr): $\tilde{\nu} = 1558(\text{s}) \text{cm}^{-1}$ (CO); MS (DEI-(+), 70 eV): m/z (%): 383 (22) [$\text{FeL2}^+ + \text{H}$], 382 (96) [FeL2^+], 367 (27) [$\text{FeL2}^+ - \text{CH}_3$], 148 (72) [bimm^+], 81 (100) [$\text{bimm}^+ - \text{C}_3\text{H}_3\text{N}_2$]; elemental analysis calcd (%) for $\text{C}_{25}\text{H}_{26}\text{FeN}_6\text{O}_4$ (530.36): C 56.62, H 4.94, N 15.85; found: C 56.05, H 4.95, N 15.55.

Acknowledgments

This work has been supported financially by the Deutsche Forschungsgemeinschaft (SPP 1137) the Fonds der Chemischen Industrie, the Center for Integrated Protein Science Munich (CIPSM) and the University of Munich.

6.5 References

- [1] a) H.A. Goodwin, *Coord. Chem. Rev.* **1976**, *18*, 293; b) P. Gülich, *Struct. Bonding (Berlin)* **1981**, *44*, 83; c) E. König, *Prog. Inorg. Chem.* **1987**, *35*, 527; d) P. Gülich, A. Hauser, *Coord. Chem. Rev.* **1990**, *97*, 1; e) E. König, *Struct. Bonding (Berlin)* **1991**, *76*, 51; f) P. Gülich, A. Hauser, H. Spiering, *Angew. Chem. Int. Ed. Engl.* **1994**, *33*, 2024, and references therein; g) P. Gülich, J. Jung, H.A. Goodwin, *Molecular Magnetism: From Molecular Assemblies to the Devices* (Eds.: Coronado *et al.*), NATO ASI Series E: *Applied Sciences, Vol 321*, Kluwer, Dordrecht, **1996**, 327; h) P. Gülich, H.A. Goodwin (Eds.), *Spin Crossover in Transition Metal Compounds I–III, Topics in Current Chemistry*, Springer, Berlin, Heidelberg, New York **2004**; i) J.A. Real, A.B. Gaspar, M.C. Munoz, *Dalton Trans.* **2005**, 2062 j) O. Sato, J. Tao, Y.-Z. Zhang, *Angew. Chem.* **2007**, *119*, 2200; *Angew. Chem. Int. Ed.* **2007**, *46*, 2152.
- [2] a) O. Kahn, C. Jay Martinez, *Science* **1998**, *279*, 44; b) O. Kahn, C. Jay, J. Kröber, R. Claude, F. Grolière, *Patent EP0666561* 1995; c) J.-F. Létard, O. Nguyen, N. Daro, *Patent FR0512476* **2005**; d) J.-F. Létard, P. Guionneau, L. Goux-Capes, *Topics in Current Chemistry, Vol. 235* (Eds. P. Gülich, H.A. Goodwin), Springer, Wien, New York, **2004**, 221; e) A. Galet, A.B. Gaspar, M.C. Munoz, G.V. Bukin, G. Levchenko, J.A. Real, *Adv. Mater.* **2005**, *17*, 2949.
- [3] a) C. Genre, G.S. Matouzenko, E. Jeanneau, D. Luneau, *New J. Chem.* **2008**, *30*, 1669; b) P.J. van Koningsbruggen, Y. Garcia, O. Kahn, L. Fournés, H. Kooijman, A.L. Spek, J.G. Haasnoot, J. Moscovici, K. Provost, A. Michalowicz, F. Renz, P. Gülich, *Inorg. Chem.* **2009**, *39*, 1891; c) N. Moliner, M.C. Munoz, S. Létard, L. Salmon, J.-P. Tuchagues, A. Bousseksou, J.A. Real, *Inorg. Chem.* **2002**, *41*, 6997; d) J.A. Real, E. Andrés, M.C. Munoz, M. Julve, T. Granier, A. Bousseksou, F. Varret, *Science* **1995**, *268*, 265; e) N. Moliner, M.C. Munoz, S. Létard, X. Solans, N. Menéndez, A. Goujon, F. Varret, J.A. Real, *Inorg. Chem.* **2000**, *39*, 5390; f) G.S. Matouzenko, G. Molnár, N. Bréfuel, M. Perrin, A. Bousseksou, S.A. Borshch, *Chem. Mater.* **2003**, *15*, 550. g) Y. Garcia, V. Niel, M.C. Munoz, J.A. Real, *Topics in Current Chemistry, Vol. 233* (Eds. P.

- Gütlich, H.A. Goodwin), Springer, Wien, New York, **2004**, 229; h) G.S. Matouzenko, M. Perrin, B. Le Guennic, C. Genre, G. Molnár, A. Bousseksou, S.A. Borshch, *Dalton Trans.* **2007**, 934; i) J.A. Real, A.B. Gaspar, V. Niel, M.C. Munoz, *Coord. Chem. Rev.* **2003**, 236, 121; j) S.M. Neville, B.A. Leita, D.A. Offermann, M.B. Duriska, B. Moubaraki, K.W. Chapman, G.J. Halder, K.S. Murray, *Eur. J. Inorg. Chem.* **2007**, 1073; k) K.S. Murray, C.J. Kepert, *Topics in Current Chemistry, Vol. 233* (Eds. P. Gütlich, H.A. Goodwin), Springer, Wien, New York, **2004**, 195.
- [4] B. Weber, *Coord. Chem. Rev.* **2009**, 253, 2432.
- [5] a) G.H. Cui, J.R. Li, J.L. Tian, X.H. Bu, S.R. Batten, *Cryst. Growth Des.* **2005**, 5, 1775; b) S.W. Jin, W.Z. Chen, *Polyhedron* **2007**, 26, 3074; c) N. Masciocchi, C. Pettinari, E. Alberti, R. Pettinari, C.D. Nicola, A.F. Albisetti, A. Sironi, *Inorg. Chem.* **2007**, 46, 10501; d) C.M. Jin, Z.F. Chen, T.Q. Sun, Y.J. Hu, S.L. Hu, *J. Mol. Struct.* **2008**, 889, 186; e) C.-M. Jin, Z.-F. Chen, H.-F. Mei, X.-K. Shi, *J. Mol. Struct.* **2009**, 921, 58.
- [6] B. Weber, PhD thesis, University of Jena (Germany), **2002**; Der Andere Verlag, Osnabrück, **2003**.
- [7] a) B. Weber, E. Kaps, J. Weigand, C Carbonera, J.-F. Létard, K. Achterhold, F.G. Parak, *Inorg. Chem.* **2008**, 47, 487; b) B. Weber, E. Kaps, J. Obel, W. Bauer, *Z. Anorg. Allg. Chem.* **2008**, 1421; c) B. Weber, C. Carbonera, C. Desplanches, J.-F. Létard, *Eur. J. Inorg. Chem.* **2008**, 1589; d) B. Weber, E. Kaps, C. Desplanches, J.-F. Létard, K. Achterhold, F.G. Parak, *Eur. J. Inorg. Chem.* **2008**, 4891; e) W. Bauer, B. Weber, *Inorg. Chim. Acta* **2009**, 362, 2341; f) B. Weber, E. Kaps, *Heteroatom Chem.* **2005**, 16, 391; g) B. Weber, F.-A. Walker, *Inorg. Chem.* **2007**, 46, 6794; h) B. Weber, E. Kaps, J. Obel, K. Achterhold, F.G. Parak, *Inorg. Chem.* **2008**, 47, 10779; i) B. Weber, R. Tandon, D. Himsl, *Z. Anorg. Allg. Chem.* **2007**, 633, 1159; j) B. Weber, E. Kaps, C. Desplanches, J.-F. Létard, *Eur. J. Inorg. Chem.* **2008**, 2963.
- [8] A. Altomare, M.C. Burla, G.M. Camalli, G. Cascarano, C. Giacovazzo, A. Guagliardi, A.G.G. Moliterni, G. Polidori, R. Spagna, SIR-97, University of Bari, Bari (Italy), **1997**; *J. Appl. Crystallogr.* **1999**, 32, 115.
- [9] G.M. Sheldrick, SHELXL-97, University of Göttingen, Göttingen (Germany), **1997**.

6. X-Ray Structure and Magnetic Properties of Two New Iron(II) 1D Coordination Polymers with Bis(imidazolyle)-methane as Bridging Ligand

- [10] C.K. Johnson, M.N. Burnett, ORTEP-III, Oak-Ridge National Laboratory, Oak-Ridge, TN (USA) **1996**; L.J. Farrugia, *J. Appl. Crystallogr.* **1997**, *30*, 565.
- [11] Team of authors: *Organikum*, Johann Ambrosius Barth Leipzig, Berlin, Heidelberg, **1993**.
- [12] L. Wolf, E.-G. Jäger, *Z. Anorg. Allg. Chem.* **1966**, *346*, 76.
- [13] E.-G. Jäger, E. Häussler, M. Rudolph, M. Rost, *Z. Anorg. Allg. Chem.* **1985**, *525*, 67.
- [14] E. Díez-Barra, A. de la Hoz, A. Sánchez-Migallón, J. Tejada, *Hetreocycles* **1992**, *34*, 1365.
- [15] L.D. Field, B.A. Messerle, M. Rehr, L.P. Soler, T.W. Hambley, *Organometallics* **2003**, *22*, 2387.

6. X-Ray Structure and Magnetic Properties of Two New Iron(II) 1D Coordination Polymers with Bis(imidazolyle)-methane as Bridging Ligand

6.6 Supporting Information

Table S1. Crystallographic data of the complex [FeL1(bimm)]·0.5 MeOH (**1**).

compound	1
formula	C _{27.5} H ₃₂ FeN ₆ O _{6.5}
$M_r / \text{g mol}^{-1}$	606.42
crystal system	triclinic
space group	$P\bar{1}$
$a / \text{Å}$	10.7629(3)
$b / \text{Å}$	11.6648(3)
$c / \text{Å}$	12.3748(3)
$\alpha / ^\circ$	112.978(3)
$\beta / ^\circ$	94.543(2)
$\gamma / ^\circ$	91.001(2)
$V / \text{Å}^3$	1423.87(6)
Z	1
$\rho / \text{g cm}^{-3}$	1.414
μ / mm^{-1}	0.584
crystal size	0.38 × 0.34 × 0.32
T / K	200(2)
diffractometer	Oxford XCalibur
$\lambda (\text{MoK}\alpha) / \text{Å}$	0.71069
θ -range / $^\circ$	3.8–26.1
reflns. collected	26315
indep. reflns. (R_{int})	5632 (0.0343)
mean $\sigma(I) / I$	0.0341
reflns. with $I \geq 2\sigma(I)$	4413
x, y (weighting scheme)	0.0532, 0
parameters	372
restraints	0
$R(F)$ (all data) ^[a]	0.0338 (0.0477)
$wR(F^2)$ ^[b]	0.0910
$GooF$	1.065
shift/error _{max}	0.001
max., min. resd. dens. / e Å^{-3}	0.619, -0.387

[a] $R(F) = \sum ||F_o| - |F_c|| / \sum |F_o|$. [b] $wR(F^2) = [\sum [w(F_o^2 - F_c^2)^2] / \sum w(F_o^2)^2]^{1/2}$, $w = 1 / [\sigma^2(F_o^2) + (aP)^2 + bP]$, where $P = [F_o^2 + 2(F_c^2)] / 3$.

7 Complete and Incomplete Spin Transitions in 1D Chain Iron(II) Compounds

Toni M. Pfaffeneder,^[a] Sebastian Thallmair,^[a] Wolfgang Bauer^[a] and Birgit Weber*^[a,b]

[a] Center for Integrated Protein Science Munich at the Department Chemie und Biochemie, Ludwig-Maximilians-Universität München, Butenandtstr. 5–13 (Haus F), D-81377 München, Germany

[b] Inorganic Chemistry II, Universität Bayreuth, Universitätsstraße 30, NW I, 95440 Bayreuth, Germany. Fax: +49-92155-2157, E-mail: weber@uni-bayreuth.de

Published in: *New J. Chem.* **2011**, 35, 691–700.

Abstract: The syntheses and characterisation of two new octahedral iron(II) SCO coordination polymers [FeL1(bimm)] (**1**) and [FeL2(bppa)]·0.5 MeOH (**2**) (L1 = {2,2'-[1,2-phenyl-bis(iminomethylidene)]bis[1-phenylbutane-1,3-dione] (2-)-*N,N',O³,O^{3'}*}, L2 = {diethyl (*E,E*)-2,2'-[1,2-phenyl-bis(iminomethylidene)]bis[3-oxo-3-phenylpropanoate] (2-)-*N,N',O³,O^{3'}*}, bimm = bis(1-imidazolyle)methane and bppa = 1,3-bis(4-pyridyl)propane) is presented. Results from X-ray structure analysis at different temperatures revealed in case of **1** that the transition from a gradual to a cooperative SCO with a 5 K wide hysteresis is due to an increase of the short intermolecular contacts, which exceed a certain threshold for the cooperative effect. In case of compound **2** an incomplete spin transition with a 4 K wide hysteresis was observed. The low temperature χ_{MT} product remains constant at a value typical for a mixed HS/LS state in stepwise spin transitions. A quantitative correlation between the cooperative effects of 12 monomer and polymer iron(II) SCO complexes and their structural properties derived from X-ray structure analysis, the so-called crystal contact index (CCI) is introduced.

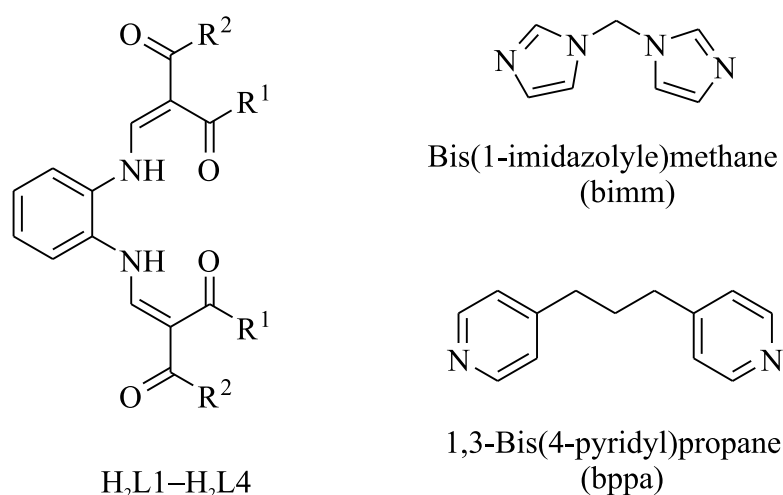
7.1 Introduction

There is an ongoing interest in the bistability of spin crossover (SCO) compounds,^[1] as the thermochromism associated with the spin transition (ST) makes them potentially useful for various applications such as display and memory device units,^[2] sensors^[3] and cold channel control units in food and medical storages.^[4]

The origin of hysteresis loops in ST materials and their thermal width as well as the reason for stepwise or incomplete spin transitions are not yet fully understood. In the case of 1D chain SCO compounds, bridges with flexible linkers (triply bis-tetrazole bridges with flexible spacers^[5] or flexible single bridges as 1,2-bis(4-pyridyl)ethane^[6]) so far resulted in gradual ST. In the case of rigid linkers the ST behaviour depends on the intermolecular interactions (hydrogen bonds, π -stacking, van der Waals interactions) that are discussed to be suitable for transmitting cooperative interactions. This was recently demonstrated for 4,4'-bipyridine linked SCO complexes, where either gradual^[7] or abrupt ST with 18 K wide thermal hysteresis loops^[8] were obtained. A similar observation was made for triply 1,2,4-triazole bridged iron(II) complexes.^[9] Stepwise spin transitions are often associated with two or more nonequivalent iron centres. This was observed for the first 1D polymeric material undergoing a two-step spin transition recently presented by Neville, Murray and co-workers.^[10] Of the two compounds presented performing a stepwise spin transition, results from X-ray structure analysis revealed, that one ($[\text{Fe}(\text{NCS})_2(\text{bdpp})]$, with $\text{bdpp} = 4,6\text{-bis}(2',2''\text{-pyridyl})\text{pyrazine}$) has two distinct iron(II) centres at each temperature with ordered, alternating HS and LS sites at the intermediate plateau (IP) temperatures. In contrast to this the second complex ($[\text{Fe}(\text{NCSe})_2(\text{bdpp})]$) has one unique iron(II) centre at each temperature with an averaged HS/LS character at the IP temperature. Great efforts were made by the authors to explain the two-step spin transition in this compound.

In this paper we present two examples for 1D chain iron (II) SCO complexes with flexible bridges, but a cooperative spin transition with small thermal hysteresis loops. The complexes are obtained by the combination of Schiff base-like equatorial tetradentate ligands $\text{H}_2\text{L1}$ and $\text{H}_2\text{L2}$ with the bridging axial ligands bimm (bis(1-imidazolyle)methane) and bppa (1,3-bis(4-pyridyl)propane) (Scheme 1). The two equatorial ligands were so far not used for the synthesis of SCO complexes. They can be derived from the ligands $\text{H}_2\text{L3}$ and $\text{H}_2\text{L4}$, which were demonstrated to be highly suitable for the synthesis of SCO complexes,^[11,12] by

replacement of two of the methyl groups by phenyl groups. Bimm^[13] and bppa^[14] were already demonstrated to be suitable for the synthesis of SCO complexes of this ligand type. In the last section of the manuscript a quantitative model is introduced to correlate the strength of the cooperative interactions with the number and intensity of the intermolecular interactions.



Scheme 1. Ligands used in this work. H₂L1: R¹ = Me, R² = Ph; H₂L2: R¹ = Ph, R² = OEt; H₂L3: R¹ = Me, R² = OEt; H₂L4: R¹ = Me, R² = Me.

7.2 Results and Discussion

Synthesis: Scheme 1 displays the ligands used in this work. H₂L1 and H₂L2 were synthesised as previously described in literature.^[15,16] The 1D octahedral iron(II) coordination polymers could be obtained in a two-pot reaction. In a first step, iron complexes of the tetradentate equatorial ligands H₂L1 and H₂L2 with methanol as axial ligands were prepared starting from iron(II)acetate.^[17] In a subsequent ligand substitution reaction [FeL1(MeOH)₂] and [FeL2(MeOH)₂] were converted with the axial-bridging ligands bimm and bppa, respectively, to give [FeL1(bimm)] (**1**), [FeL2(bppa)]·0.5 MeOH (**2**) and [FeL2(bimm)]·0.5 MeOH (**3**) in good yields. The complexes were fully characterised by elemental analysis, IR and mass spectroscopy. X-Ray diffraction data could be obtained for **1** and **2**. The magnetic properties were determined by *T*-dependent susceptibility measurements using a SQUID magnetometer.

Magnetic properties: Magnetic susceptibility measurements for all compounds were performed in the temperature range from 5 to 300 K. The thermal dependence of the product $\chi_M T$ (χ_M is the molar susceptibility and T the temperature) for **1** is displayed at the left of Figure 1. The room temperature value, $\chi_M T = 3.67 \text{ cm}^3 \text{ K mol}^{-1}$, is within the range expected for an iron(II) complex in the HS state. Upon cooling, the $\chi_M T$ product decreases first slowly, until at 180 K about 30% of the iron centres are in the LS state. Below this point, the remaining HS iron centres perform an abrupt transition into the LS state with $\chi_M T = 0.14 \text{ cm}^3 \text{ K mol}^{-1}$ at 5 K. The critical temperatures are 171 K in the cooling and 176 K in the heating mode, corresponding to a 5 K wide thermal hysteresis loop.

The plot of $\chi_M T$ vs. the temperature for complex **2** is given at the top right of Figure 1. The room temperature value of $\chi_M T = 3.27 \text{ cm}^3 \text{ K mol}^{-1}$ is typical for iron(II) in the HS state. Upon cooling the moment remains constant until about 160 K where a very abrupt ST takes place. A 4 K wide thermal hysteresis loop is observed with critical temperatures of 136 K upon cooling and 140 K upon heating. In the low temperature region a mixed HS/LS state is obtained with $\chi_M T = 1.58 \text{ cm}^3 \text{ K mol}^{-1}$. For compound **3** (bottom of Figure 1), nearly ideal Curie behaviour is observed. Upon cooling the $\chi_M T$ product decreases from a value of $3.56 \text{ cm}^3 \text{ K mol}^{-1}$ at 295 K to a value of $3.08 \text{ cm}^3 \text{ K mol}^{-1}$ at 20 K. The susceptibility data above 20 K can be fitted very well with the Curie-Weiss law ($\chi_M = C/(T - \Theta)$) with the parameters $\Theta = -5.44 \text{ K}$ and $C = 3.57 \text{ cm}^3 \text{ K mol}^{-1}$. The Curie constant C is in a region expected for iron(II) HS complexes and the negative Weiss constant Θ in combination with the temperature dependent decrease of the $\chi_M T$ product could be an indication for weak antiferromagnetic interactions between the chains, but other reasons are also possible. This is a typical behaviour for an iron(II) HS complex of this ligand type.^[18]

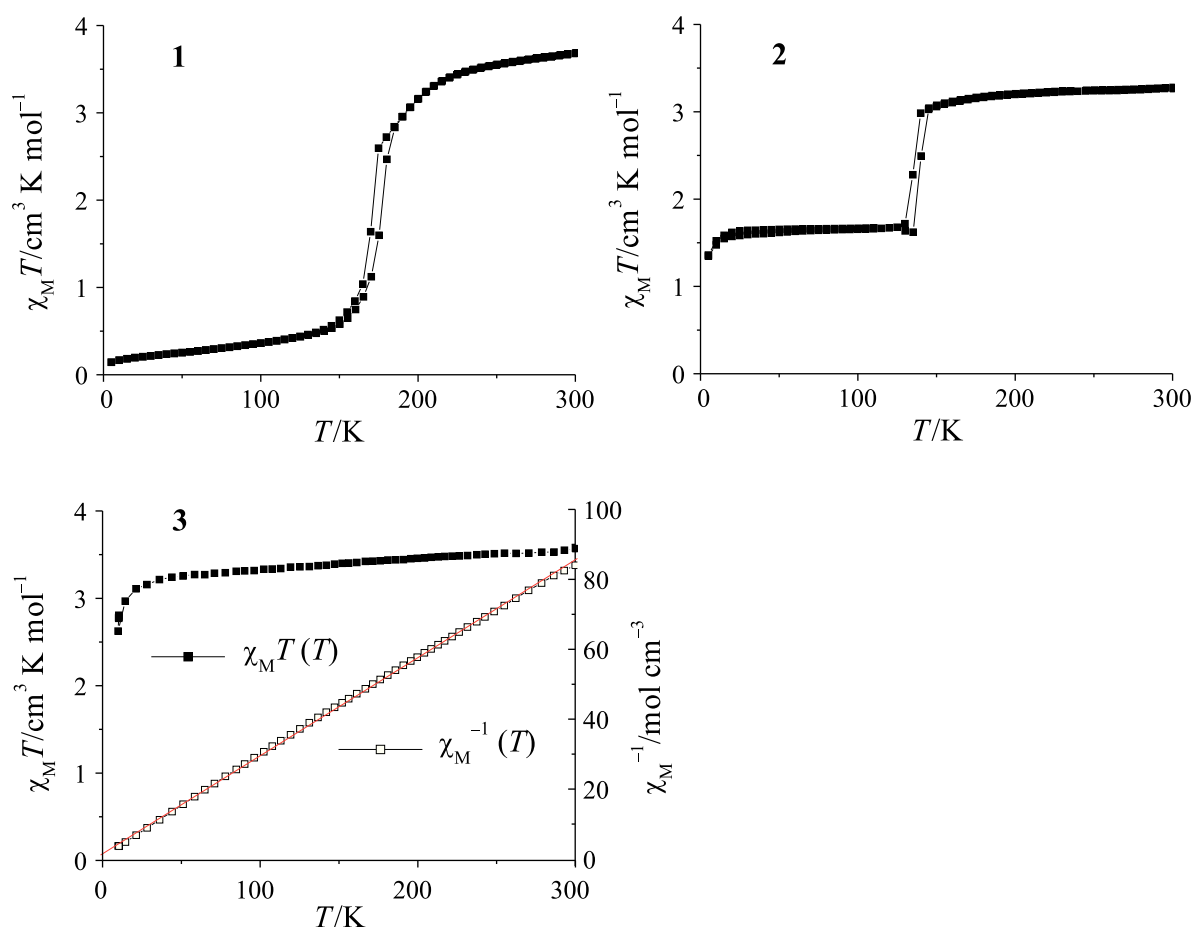


Figure 1. Plots of the $\chi_M T$ product (filled squares) vs. T for the compounds **1**, **2** and **3**. Reciprocal molar susceptibility χ_M^{-1} (open squares) as a function of T and the fit according to the Curie-Weiss law, $\chi_M = C/(T - \Theta)$, with the parameters $\Theta = -5.44$ K, $C = 3.57$ cm³ K mol⁻¹ for compound **3**.

Structural descriptions: Crystals suitable for X-ray structure analysis were obtained for both spin crossover complexes **1** and **2**. The crystallographic data are summarised in Supporting Information Table S1. Selected bond lengths and angles within the first coordination sphere are summarised in Table 1. ORTEP representations of the HS forms of **1** and **2** are given in Figure 2 and Figure 3, respectively. In the case of **1**, the X-ray structure was measured at three temperatures before (250 K), during (180 K) and after the spin transition (125 K). In the case of **2** a determination of the X-ray structure was only possible for the HS state as the crystals crumble while cooling down.

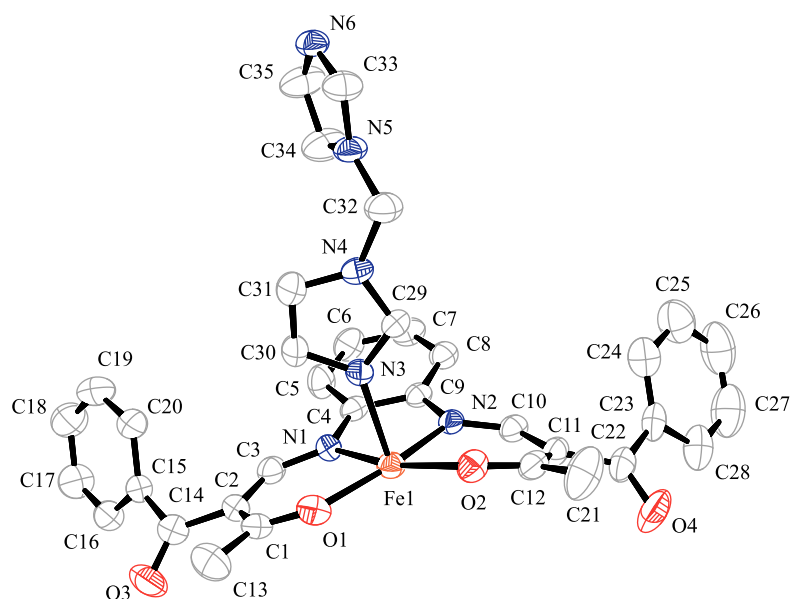


Figure 2. ORTEP drawing of the asymmetric unit of **1** at 250 K. Hydrogen atoms were omitted for clarity. Thermal ellipsoids are shown with a 50% probability.

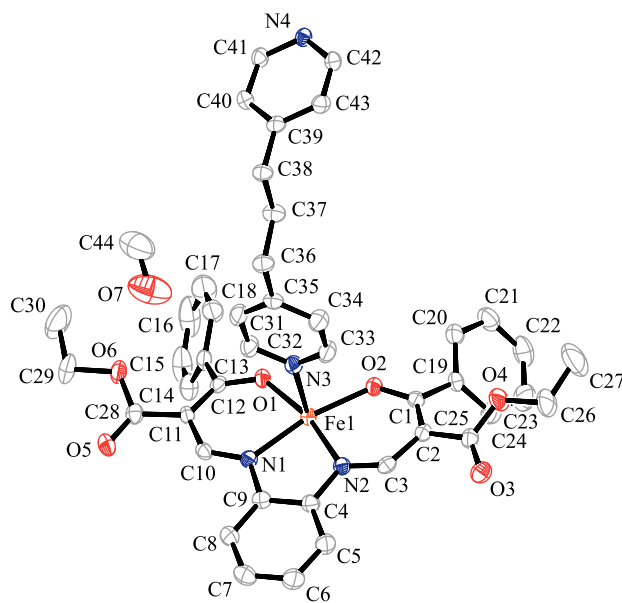


Figure 3. ORTEP drawing of the asymmetric unit of **2** at 173 K. Hydrogen atoms were omitted for clarity. Thermal ellipsoids are shown with a 50% probability.

7. Complete and Incomplete Spin Transitions in 1D Chain Iron(II) Compounds

Table 1. Selected bond lengths [\AA] and angles [$^\circ$] within the first coordination sphere of **1** at 125 K, 180 K and 250 K and of **2** at 173 K.

compound	<i>T</i> /K	<i>S</i>	Fe-N _{eq}	Fe-O _{eq}	Fe-N _{ax}	O _{eq} -Fe-O _{eq}	N _{ax} -Fe-N _{ax}
1	250	2	2.090(3)	2.028(3)	2.205(3)	109.47(10)	171.44(11)
			2.099(3)	2.027(2)	2.225(3)		
1	180	2/0	2.049(3)	2.014(3)	2.159(3)	106.69(11)	172.00(12)
			2.070(3)	2.005(3)	2.177(3)		
1	125	0	1.910(4)	1.931(3)	2.017(3)	91.43(13)	175.21(13)
			1.919(4)	1.936(3)	2.017(3)		
2	173	2	2.093(1)	2.004(1)	2.231(1)	106.56(5)	177.26(5)
			2.083(1)	2.013(1)	2.249(1)		

Intramolecular changes upon spin transition of 1: In the HS state the average bond lengths within the first coordination sphere of **1** are 2.09 \AA (Fe-N_{eq}), 2.03 \AA (Fe-O_{eq}) and 2.22 \AA (Fe-N_{ax}). The values are within the region reported for HS iron(II) complexes of the same ligand type.^[11–14] Upon spin transition a shortening of the bond lengths of about 10% is observed, as discussed for other iron(II) spin crossover complexes in literature.^[1] This shortening is more pronounced for the axial ligands, which connect the iron centres in the 1D chain, than for the equatorial ones in agreement with previous findings on mononuclear analogues.^[11–14] The average bond lengths in the LS state are 1.91 \AA (Fe-N_{eq}), 1.93 \AA (Fe-O_{eq}) and 2.02 \AA (Fe-N_{ax}). A characteristic tool for the determination of the spin state of this type of iron(II) complexes is the O-Fe-O angle that changes from 109° in the HS state to 91° in the LS state.^[11,14] The 1D chain of compound **1** is linear, with the equatorial ligands being parallel to each other within one chain. (Figure 4, at the top).

Intermolecular interactions of 1: Selected intermolecular distances for the 250 K, 180 K and 125 K structure of **1** are shown in Table 2. Selected views of the molecule packing of **1** in the crystal at 250 K and 125 K are given in Figure 5. Between 200 K and 180 K compound **1** undergoes a gradual spin transition with no indications for cooperative interactions. Then upon further cooling an abrupt transition with a 5 K wide hysteresis occurs. The initial gradual transition is explained by the presence of only a few short intermolecular contacts in the high temperature structure (see Figure 5, 250 K). Upon cooling the number of short contacts increases. The 180 K-structure has one additional contact beside the other more shortened contacts in comparison to the 250 K-structure. This increases the total communication of elastic interactions and accounts for a certain threshold value for the occurrence of the observed cooperative effect. The additional contact (C7 · · C8) in the 180 K-structure facilitates the π -stacking of the 1,2-disubstituted benzene ring of the equatorial ligand between adjacent chains and makes the interaction network three-dimensional. The low temperature structure (125 K) is characterised by many additional short intermolecular contacts which satisfactorily explain the small hysteresis observed in the magnetic measurements.

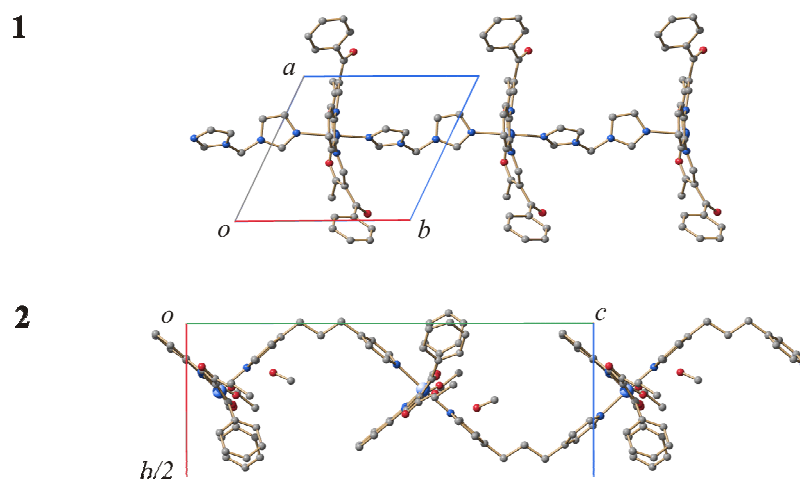


Figure 4. Top: excerpt of the 1D polymeric chain of compound **1** in the crystal at 250 K, view along [0 0 1]; bottom, zigzag motif of the 1D polymeric chain of compound **2** in the crystal at 173 K, view along [1 0 0]. Hydrogen atoms have been omitted for clarity.

Discontinuous spin transitions were recently associated with order/disorder transitions of counter ions^[19] or additional ligand molecules^[20] in the crystal packing. The order/disorder transition at a certain temperature facilitated a significant increase in the number of intermolecular contacts below this temperature that exceed a threshold and therefore mediates the cooperative effect. Compound **1** does not exhibit an additional disordered counter ion, solvent or ligand molecule or any other disordered parts. Thus only the number and the nature (or strength) of the intermolecular interactions are important for the discussion of cooperative interactions.

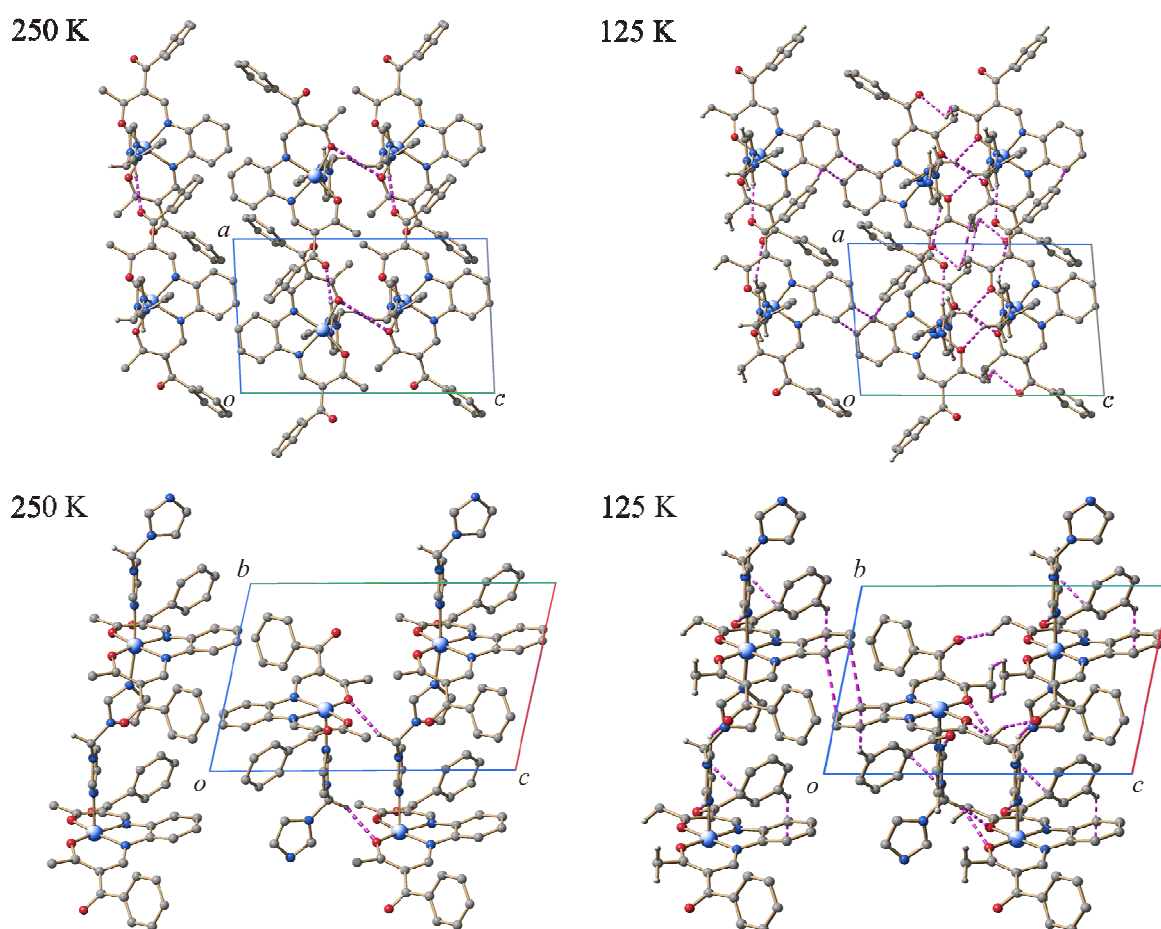


Figure 5. Left: packing of compound **1** in the crystal at 250 K; right: packing at 125 K; top: view along $[0\ 1\ 0]$, bottom: view along $[1\ 0\ 0]$. Hydrogen atoms, which do not participate in short intermolecular interactions, have been omitted for clarity. Crystal contacts shorter than the sum of the van der Waals radii minus 0.1 Å are depicted in dashed bond.

Table 2. Selected intermolecular distances $d(D \cdots A)$ [Å] and differences between atomic distances and the sum of the van der Waals radii (vdW) [Å] of **1** at 250 K, 180 K and 125 K.

D	H	A	T/K	$d(D \cdots A)$	$d - \text{vdW}$
C29	H29	O3 ^[a]	250	2.26	-0.46
			180	2.24	-0.48
			125	2.42	-0.30
C32	H32B	O2 ^[b]	250	2.48	-0.24
			180	2.43	-0.29
			125	2.51	-0.21
C7		C8 ^[c]	180	3.28	-0.12
C7		C8 ^[c]	125	3.19	-0.21
C31	H31	O4 ^[d]	125	2.46	-0.26
C32	H32B	O1 ^[b]	125	2.49	-0.23
C13	H13A	O4 ^[e]	125	2.57	-0.15
H13A		H21B ^[e]	125	2.27	-0.13
C32	H32A	C15 ^[f]	125	2.78	-0.12
C34		C18 ^[a]	125	3.29	-0.11
C17	H17	C8 ^[a]	125	2.79	-0.11
H21A		H21B ^[g]	125	2.30	-0.10

Symmetry codes: [a] $-1 + x, y, z$; [b] $1 - x, -y, 1 - z$; [c] $1 - x, 1 - y, -z$; [d] $-1 + x, 1 + y, z$; [e] $1 - x, 1 - y, 1 - z$; [f] $1 + x, y, z$; [g] $-x, 1 - y, 1 - z$.

A zigzag motif in the crystal structure of **2:** The average bond lengths within the first coordination sphere of **2** are 2.09 Å (Fe-N_{eq}), 2.01 Å (Fe-O_{eq}) and 2.24 Å (Fe-N_{ax}). The values are within the region reported for HS iron(II) complexes as discussed above (see Table 1).^[11-14] The O-Fe-O angle is 107° and thus clearly in the range typical for a HS complex. Selected intermolecular distances of **2** are summarised in Table 3. In Figure 4 the 1D polymeric chain of octahedral iron(II) centres (at the bottom) and in Figure 6 the packing of the chains in the crystal are displayed. The 1D chain of **2** exhibits a zigzag motif with an angle between two adjacent equatorial ligands of 99°. Such motifs were previously found in the crystal structure of the closely related [FeL3(bppa)]^[14] and [FeL4(bppa)]·MeOH^[21] (see Scheme 2). The first compound undergoes an incomplete spin transition that stops at an intermediate plateau (IP)

while the latter compound undergoes a stepwise thermal spin transition with a very wide step. It could be deduced from the structures and the structures of related 1D chain SCO complexes that the zigzag motif of the 1D chain as well as a dense packing (intermolecular contacts shorter than the sum of the van der Waals radii) are responsible for restraining interactions between these chains and hence stabilise the mixed HS/LS state of the step. In general, a HS \rightarrow LS transition in 1D chain compounds involves a relocation of the ligands towards the smaller LS molecule. If the Fe...Fe distances cannot follow the changes in Fe-L bonds due to restraining interactions, a stabilisation of a mixed HS/LS state can be observed.^[14,22] For zigzag chains restraining intermolecular interactions can be more easily imagined compared to linear structures and therefore wider steps can be expected.^[14] The spin transition behaviour of **1** and **2** is in agreement with this idea. In the case of the linear chain compound **1** a one-step ST is observed while for **2** the ST stops at the IP (see Figure 1 and 4). Compound **2** differs only in one homotopic residues from the previously published [FeL3(bppa)] and in two homotopic residues from the previously published [FeL4(bppa)]·MeOH. Instead of two methyl groups in L3 and L4 it contains two sterically more demanding phenyl groups in the equatorial ligand, which are distorted out of the plane. The second difference between L2 and L4 are two ethoxycarbonyl groups instead of two acetyl groups. In contrast to [FeL3(bppa)] (abrupt incomplete one-step spin transition)^[14] and [FeL4(bppa)]·MeOH (gradual two-step spin transition),^[21] compound **2** shows a very abrupt but incomplete spin transition with a small hysteresis. The distorted phenyl groups may increase the extent of restraining interactions within the zigzag structure and by this prevent the ST of the second half of the iron centres. Furthermore, the two ethoxycarbonyl groups of the equatorial ligand provide an intertwining of adjacent chains (see Figure 6, left), which are closely connected by several short contacts. Moreover, π -stacking of the 1,2-disubstituted benzene rings of the equatorial ligand of two adjacent chains (Figure 6, right) may become the most restraining interaction for the ligand relocation along [0 0 1] due to the usually pronounced shortening of the axial bond lengths. Very likely, all these interactions explain the remaining in the mixed HS/LS state through the whole low temperature range as well as the small hysteresis loop.

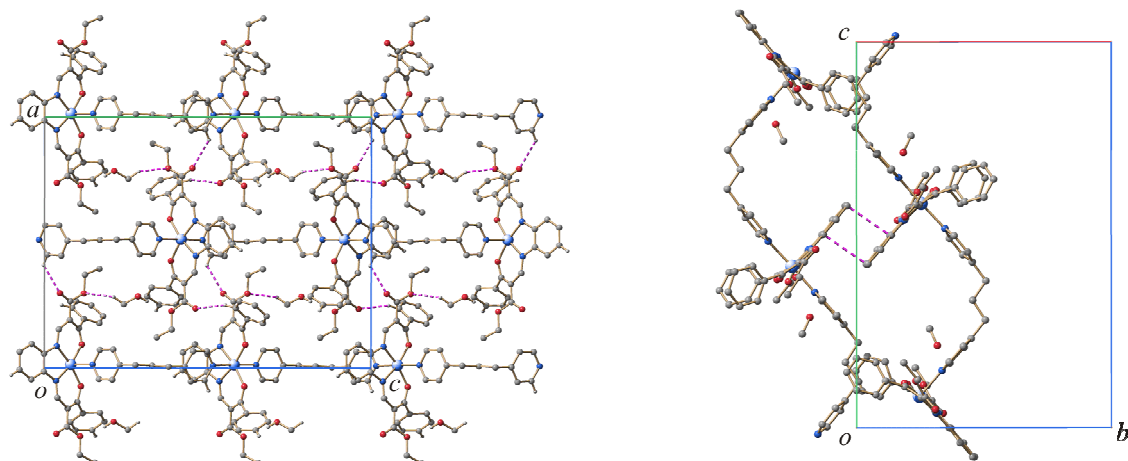


Figure 6. Left: excerpt of a 2D layer of parallel chains of **2** in the crystal packing, view along [0 1 0]; right: π -stacking of the equatorial ligands of two adjacent chains of **2**, view along [1 0 0]. Hydrogen atoms, which do not participate in short intermolecular interactions, have been omitted for clarity. Crystal contacts shorter than the sum of the van der Waals radii minus 0.1 Å are depicted in dashed bonds.

Table 3. Selected intermolecular distances $d(D \cdots A)$ [Å] and differences between atomic distances and the sum of the van der Waals radii (vdW) [Å] of **2** at 173 K.

D	H	A	$d(D \cdots A)$	$d - \text{vdW}$
O7	H7	O6	2.12	-0.60
C24	H24	O5 ^[a]	2.50	-0.22
C44	H44B	O4 ^[b]	2.53	-0.19
C41	H41	O3 ^[b]	2.56	-0.16
C38	H38A	O1 ^[c]	2.59	-0.13
C16	H16	O7 ^[d]	2.59	-0.13
C7		C9 ^[e]	3.43	+0.03

Symmetry codes: [a] $\frac{1}{2} + x, \frac{1}{2} - y, 1 - z$; [b] $-\frac{1}{2} + x, y, \frac{1}{2} - z$; [c] $1 - x, \frac{1}{2} + y, \frac{1}{2} - z$; [d] $\frac{3}{2} - x, \frac{1}{2} + y, z$; [e] $1 - x, -y, 1 - z$.

Crystal contacts mediate cooperative effects beyond a threshold: There are several examples that demonstrate that the number and intensity of contacts shorter than the sum of the van der Waals radii correlate with the cooperative nature of the spin transition.^[14,23] The idea of a threshold for elastic interactions mediating cooperative effects in a spin crossover compound led us to the question, if there is a quantitative way to describe structural features. We discovered a simple approach to correlate the sum of short contacts of selected structures with the strength of the cooperative effect (gradual, abrupt or accompanied by hysteresis). Thereby we assume that every short contact (shorter than the sum of the van der Waals radii) contributes to the elastic interactions mediating the cooperative effect. Those which are very short (non-classical and classical hydrogen bonds) contribute more to the cooperative effect than those which are longer (π -stacking, van der Waals contacts). Equation (1) combines all these assumptions. The crystal contact index (CCI) is the sum of all short and weighted contacts. The differences between the sum of the van der Waals radii (vdW) and the atomic distances of the contacts (d) were obtained by using the programme MERCURY 2.2^[24] and were weighted by an exponential function, in which very short contacts are more pronounced. Table 4 gives an overview of the selected compounds, which were analysed by this method. The further ligands which are mentioned therein and in the following are displayed in Scheme 2.

$$\text{CCI} = \sum_{x>0} (e^{x_n^{\frac{1}{2}}} - 1) \quad (1)$$

$$x = \frac{\text{vdW} - d}{[\text{\AA}]} > 0$$

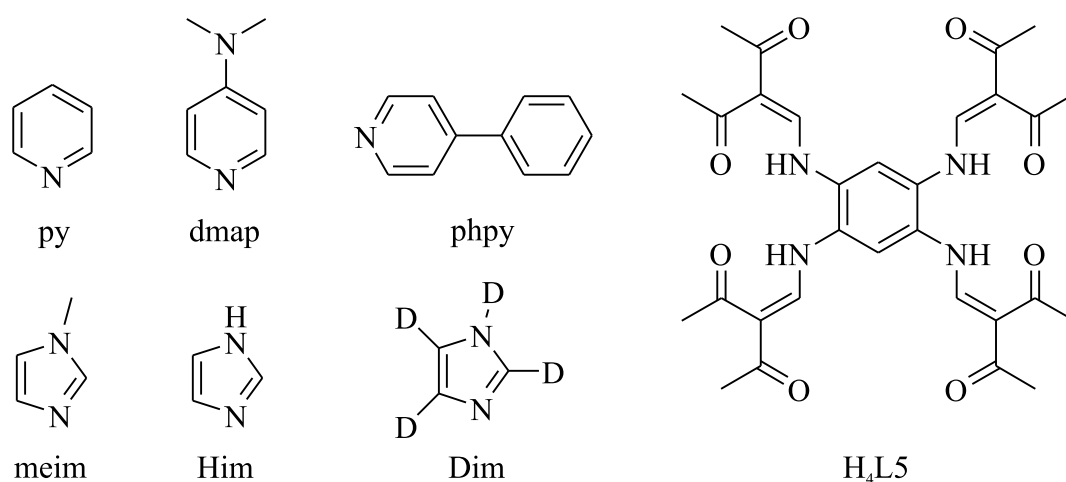
For compound **1** the CCI values represent the results made in the preceding section by analysis of the crystal packing. Upon cooling, the CCI value increases from 1.2 (250 K) to 1.5 (180 K) and finally to 2.2 (125 K) indicating that the strength and the number of short contacts increases. Below 180 K the threshold value for the elastic interactions seems to be reached and the remaining HS centres perform now a cooperative spin transition. The CCI thus helps to explain the observed spin transition. A similar behaviour as for **1** was observed for compound **5** ([FeL3(phpy)₂], HS: 1.2, LS: 2.0)^[12d] with a similar curve progression while an opposite trend was observed for the previously published compound **8** ([FeL4(meim)₂·meim]).^[20] Here the CCI value for the HS structure (1.8) is higher than the value for the LS structure (1.4). Although the number of short contacts increases upon cooling, the intensity of

7. Complete and Incomplete Spin Transitions in 1D Chain Iron(II) Compounds

the contacts decreases. This is in good agreement with the results from the magnetic measurements where a 2 K wide thermal hysteresis loop is observed in the beginning and a more gradual character is observed in the second part of the transition curve.^[20]

Table 4. Correlation between cooperative effects and structural analysis of selected spin crossover compounds of the Jäger-ligand system. Type: m = monomeric, d = dimeric, p = 1D polymeric coordination compound; $S = 2$: high-spin structure, $S = 0$: low-spin structure; h.w. = hysteresis width [K]; CCI = crystal contact index; Δa , Δb , Δc = percentaged difference in cell parameter change upon spin transition; AP = anisotropy parameter; CI = crystal index.

No.	compound	ref.	type	S	feature	h.w.	CCI	Δa	Δb	Δc	AP	CI
1	[FeL1(bimm)]	this work	p	2	gradual,	5	1.2	0.6	-3.8	-2.3	3.3	7.3
				2/0	then hys.							
				0								
2	[FeL2(bppa)]· 0.5 MeOH	this work	p	2	hys.,	4	2.0					
					incompl.							
4	[FeL3(py) ₂]	[25]	m	2	gradual		0.7	-1.1	-0.9	-1.5	0.1	0.1
				0								
5	[FeL3(phpy) ₂]	[12d]	m	2	gradual,	4	1.2	0.6	0.6	-2.6	2.3	4.6
				0	then hys.							
6	[FeL4(py) ₂]	[12a]	m	2	hys.	2	0.9	0.0	-1.0	-3.8	2.6	2.6
				0								
7	[FeL4(phpy) ₂] phpy	[12d]	m	0	gradual		1.5					
8	[FeL4(meim) ₂] meim	[20]	m	2	hys., then	2	1.8	-0.9	-1.2	-1.1	0.0	0.0
				0	gradual							
9	[FeL4(dmap) ₂]	[12a]	m	2	hys	9	0.6					
10	[Fe ₂ (L5)(meim) ₄] 2 meim	[20]	d	0	gradual,	21	2.5	-3.1	-3.8	-2.4	0.3	0.75
					then hys.							
11	[FeL3(Him) ₂]	[26]	m	2	hys.	70	4.1					
12	[FeL3(Dim) ₂]	[27]	m	2	hys.	66	4.0					
13	[FeL3(Him) ₂], 2nd modification	[28]	m	0	hys.	4	4.2					



Scheme 2. Further ligands discussed in this work.

On the basis of the data in Table 4, it can be concluded that low cooperativity can be expected for CCI values between 0 and 1.5, medium cooperativity between 1.0 and 2.0 and high cooperativity for values higher than 2.0. This general trend is visualised on top of Figure 7.

The CCI value is not only useful to explain the curve progression of spin transition curves, it can also be used to estimate if solvent molecules included in the crystal packing contribute to the cooperative effects or have a dilution effect. Such dilution effects are well known in spin crossover research and have been for example demonstrated for a series of mixed crystals with the general composition $[M_{1-x}Fe_x(pic)_3]X_2 \cdot solv$ (solv = MeOH, EtOH; X = Cl, Br; M = Co, Zn, Mn) with decreasing x .^[29] The relative high LS-CCI-value for compound **7** ($[FeL4(phpy)_2] \cdot phpy$, 1.5)^[12d] with an additional non-coordinated ligand molecule phpy can clearly be explained with a dilution effect of the additional phenylpyridine, as given in Table 5. In the case of compound **8**^[20] or compound **2** the CCI values corrected by the solvent distribution (Table 5) are too low—here the molecules clearly contribute to the cooperative effects. For compound **2** the additional methanol molecules cross-link three different zigzag chains in the structure and contribute with three short contacts, containing a strong hydrogen bond (O7-H7 ··· O6), to the cooperative effect without a doubt (see Table 3).

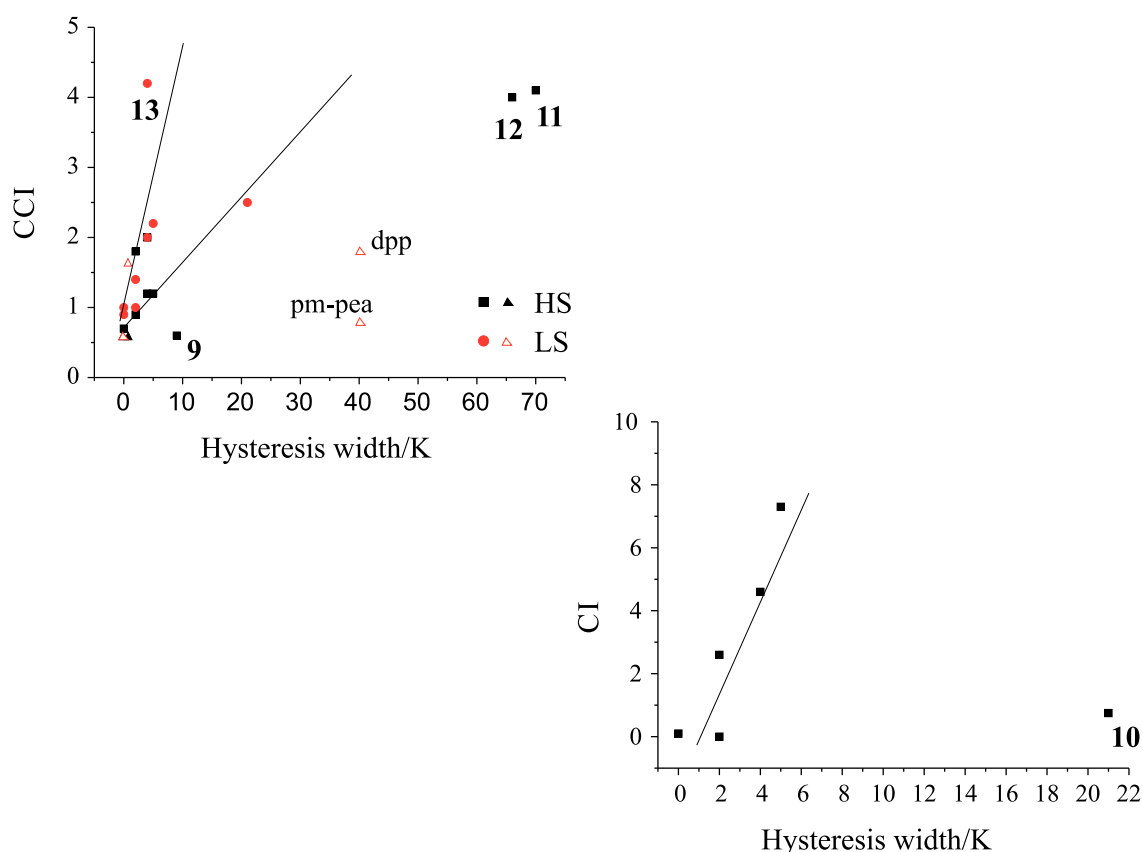


Figure 7. Plots of the crystal contact index (CCI) (top) and the crystal index (CI, at the bottom) against the hysteresis width. Values are taken from Table 4 (circles and squares) and from the text (triangles, literature examples).

Of course these values can only be seen as rough guidelines with exceptions due to many factors which cannot easily be quantified. Examples for such exceptions are compounds **9**^[12a] and **11–13**,^[27–30] see Figure 7, top. In the case of **9** the CCI value leads to a clear underestimation of the hysteresis width, whereas for the compounds **11–13** the CCI value is in the same order of magnitude but very different hysteresis widths are obtained.^[28] In the case of **13** an agreement with the steeper branch of the correlation could be discussed, for **11** and **12** again the hysteresis width is underestimated. Obviously additional factors contribute to the cooperative interactions in the case of **9**, **11** and **12**. Interestingly, for all four complexes hydrogen bonds are observed that involve an oxygen atom directly coordinated to the metal centre, as illustrated in Figure 8 for **9** and **11**. Further going investigations are in progress to more clearly analyse the influence of hydrogen bonds on cooperative interactions in spin crossover systems.

Table 5. Selected CCI values corrected by disregarding of the short contacts provided by additional solvent or ligand molecules in the crystal structure (compare with Table 4).

No.	add. mol.	<i>S</i>	SCO	CCI (eqn (1))	CCI (corr.)	comment on correction
7	phpy	LS	grad.	1.5	0.9	better value; dilution effect.
8	meim	HS	2 K hys.	1.8	1.0	value too low; meim contributes to the cooperative effect.
		LS		1.4	0.8	
2	0.5 MeOH	HS	4 K hys.	2.0	0.5	value too low; MeOH contributes to the cooperative effect.

Guionneau *et al.* reported that very large and anisotropic unit cell modifications and the SCO phenomenon are probably indissociable. The unit cell temperature dependence evidences the amplitude of the strong structural rearrangement that accompanies the SCO as well as the hysteresis width.^[30] Therefore we applied equation (2) on the percentaged change in the cell parameters *a*, *b* and *c* of compounds whose HS and LS structures are known (Table 4). Equation (2) simply calculates the variance of the cell parameter change giving the value of the anisotropy parameter (AP).

$$AP = \text{Var}(\Delta a, \Delta b, \Delta c) \times 10^4 = \frac{\sum (x - \bar{x})^2}{n} \times 10^4 \quad (2)$$

$$\Delta a = 1 - \frac{a_{\text{HS}}}{a_{\text{LS}}}; \Delta b = 1 - \frac{b_{\text{HS}}}{b_{\text{LS}}}; \Delta c = 1 - \frac{c_{\text{HS}}}{c_{\text{LS}}}$$

$$CI = CCI \cdot AP \quad (3)$$

As the variance is a measure of the amount of variation within the values of a variable it could be seen as a measure of the anisotropy of the parameter change in this particular case. This approach provides also a good correlation between the observed cooperative effect and the AP value. If the value is very low, the anisotropy in the cell parameter change is low as well as the cooperative effect (*e.g.* the value is 0.1 for the gradual SCO complex **4** in comparison to 3.3 for compound **1**).

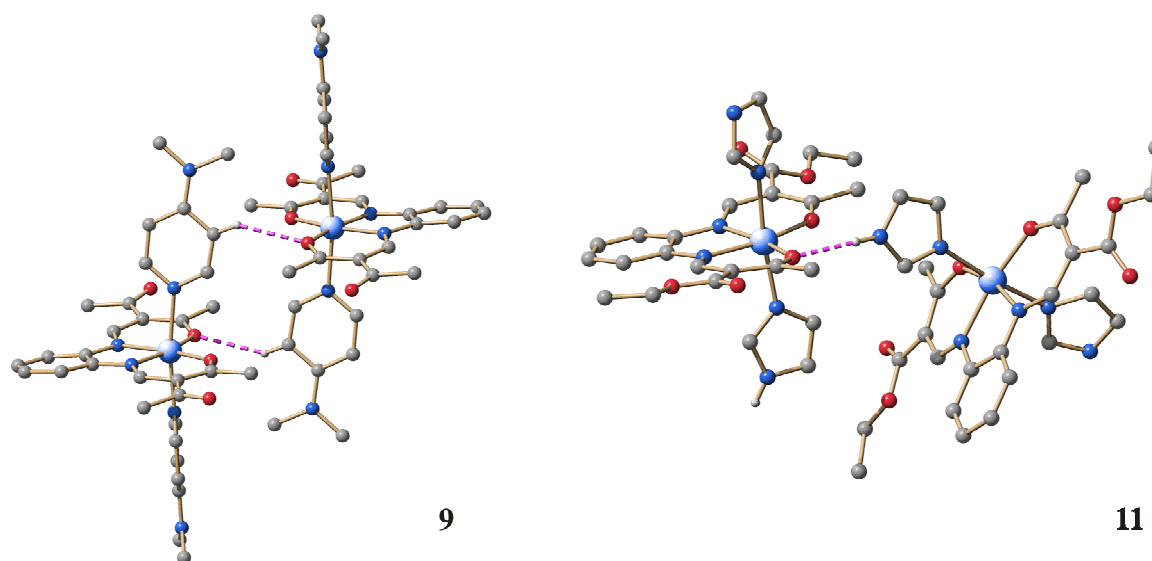


Figure 8. Excerpt of the crystal packing of **9** (left) and **11** (right). Hydrogen bonds indicated as dashed lines. Hydrogen atoms omitted for clarity.

Since there are some deviations, equations (1) and (2) are combined by equation (3) to give the crystal index (CI), which is the product of both parameters CCI and AP. Equation (3) provides an improved correlation as can be seen in Table 4 and at the bottom of Figure 7. A nearly linear dependency is observed for the compounds with smaller hysteresis loops, while the complex **10** ($[\text{Fe}_2(\text{L5})(\text{meim})_4] \cdot 2 \text{ meim}$, 21 K wide hysteresis loop)^[20] no longer fits into the correlation, probably because of its dinuclear nature. At this point it should be noted that no difference is observed between the mononuclear complexes and the polymer chain compounds with flexible linkers. A disadvantage in using AP and CI values is the limited availability of high- and low-spin structures of a particular complex due to crystal damages during the spin transition. In contrast, the CCI scale could be used for each structure. The concept of the CCI was tested on four SCO complexes that belong to the series $[\text{FeL}_2(\text{NCS})_2]$ with $\text{L} = \text{btz}$ ^[31] (2,2'-bi-4,5-dihydrothiazin, gradual spin transition), phen ^[32] (1,10-phenanthroline, abrupt spin transition), dpp (dipyrido[3,2-*a*:2'3'-*c*]phenazine, hysteresis 40 K) and pm-pea ^[30] (*N*-2'-pyridylmethylene-4-phenylethynyl, hysteresis 40 K). For this series the increasing cooperative interactions are correlated with an increasing number of intermolecular contacts.^[23] Indeed, the CCI of the first three complexes rises from 0.6 (btz) over 1.6 (phen) to 1.8 (dpp). The values of the first two compounds (btz and phen) fit nicely into the correlation given at the top of Figure 7, while the value for the system $[\text{Fe}(\text{dpp})_2(\text{NCS})_2]$ is too low,

indicating that π -stacking probably cannot be expressed solemnly by the number of intermolecular contacts. This suggestion is reinforced by the last example (pm-pea) where a significantly lower CCI of 0.8 is obtained although the hysteresis with is similar to those of the dpp complex (see Figure 7).

7.3 Conclusion

In this work we have presented the synthesis and characterisation of two new octahedral iron(II) SCO coordination polymers. Results from X-ray structure analysis at different temperatures revealed in case of **1** that the transition from a gradual to a cooperative SCO with a 5 K wide hysteresis is due to an increase of the short intermolecular contacts, which exceed a certain threshold for the cooperative effect. In case of compound **2** an incomplete spin transition with a 4 K wide hysteresis was observed. The low temperature $\chi_M T$ product remains constant at a value typical for a mixed HS/LS state in stepwise spin transitions. The structure of the 1D polymeric chain of **2** exhibits a further zigzag motif, which was previously found in a related compounds with a stepwise or incomplete spin transition.^[14,29] Restraining interactions provided by the zigzag motif as well as additional restraining interactions of the equatorial ligand may stabilise the mixed HS/LS state and make a further progression of the spin transition impossible.

Furthermore we established a correlation between the cooperative effects of 12 iron(II) SCO complexes and their structural properties derived from X-ray structure analysis, the so-called crystal contact index, CCI. For small hysteresis loops this correlation is in agreement with the model of elastic interactions mediating the structural rearrangements during the cooperative spin transition in the solid phase. It provides a good estimation to accompany the structural interpretation of spin transition properties and can to some extent also be applied to other SCO systems. In the case of spin transition compounds with wider hysteresis loops the correlation fails, indicating that there are additional mechanisms responsible for cooperative interactions. The clarification of the exact nature of those factors will be the topic of subsequent work.

7.4 Experimental Section

Magnetic measurements: Magnetic susceptibility data were collected by using a Quantum Design MPMSR-2 SQUID magnetometer under an applied field of 0.05 T over the temperature range 5 to 300 K. All samples were placed in gelatine capsules held within a plastic straw. The data were corrected for the magnetisation of the sample holder and the ligands by using tabulated Pascal's constants.

X-Ray crystallography: The intensity data of **1** and **2** were collected on an Oxford XCalibur diffractometer by using graphite-monochromated MoK α radiation. The data were corrected for Lorentz and polarisation effects. The structure was solved by direct methods (SIR-97)^[33] and refined by full-matrix least-square techniques against F_0^2 (SHELXL-97).^[34] The hydrogen atoms were included at calculated positions with fixed displacement parameters. All non-hydrogen atoms were refined anisotropically. ORTEP-III was used for the structure representation.^[35] Graphical representations of the molecular packing were done with SCHAKAL-99.^[36] The crystallographic data are summarised in Supporting Information Table S1.

Further details on the crystal structures (CCDC-794657, -58 and -59 for **1** at 250 K, 180 K and 125 K, CCDC-794656 for **2**) can be obtained free of charge on application to Cambridge Crystallographic Data Centre, 12 Union Road, Cambridge CB2 1EZ, UK (Fax: int.code +(1223)336-033; e-mail fileserv@ccdc.cam.ac.uk).

Synthesis: All syntheses were carried out under argon by using Schlenk techniques. Methanol was purified as described in literature and distilled under argon.^[37] The synthesis of H₂L1,^[15] H₂L2,^[16] [FeL2(MeOH)₂]^[17] and iron(II)acetate^[38] is described in literature. The axial ligand bimm was prepared according to the literature,^[13] bppa was purchased from Aldrich Chemical Co. and used as received.

[FeL1(MeOH)₂]: A mixture of anhydrous iron(II)acetate (2.04 g, 11.7 mmol) and H₂L1 (3.12 g, 6.90 mmol) in methanol (150 mL) was heated at reflux for 1 h. After cooling down to room temperature the dark purple precipitate was filtered off, washed with methanol (2 × 5 mL) and dried *in vacuo* (yield: 2.85 g, 72%). IR (KBr): $\tilde{\nu} = 1556(\text{s}) \text{ cm}^{-1}$ (CO); MS (DEI(+), 70 eV): m/z (%): 507 (33) [FeL1⁺ + H], 506 (100) [FeL1⁺], 464 (6) [FeL1⁺ –

COCH₃], 429 (4) [FeL1⁺ – C₆H₅], 105 (25) [COC₆H₅⁺], 77 (19) [C₆H₅⁺]; elemental analysis calcd (%) for C₃₀H₃₀FeN₂O₆ (602.46): C 63.2, H 5.3, N 4.9; found: C 63.1, H 5.2, N 4.9.

[FeL1(bimm)] (1): A mixture of [FeL1(MeOH)₂] (0.12 g, 0.21 mmol) and bimm (0.25 g, 1.66 mmol) in methanol (10 mL) was heated at reflux for 1 h. After cooling down to room temperature the dark brown precipitate was filtered off, washed with methanol (1 × 3 mL) and dried *in vacuo* (yield: 0.09 g, 65%). IR (KBr): $\tilde{\nu}$ = 1557(s) cm⁻¹ (CO); MS (DEI-+, 70 eV): *m/z* (%): 506 (45) [FeL1⁺], 148 (66) [bimm⁺], 81 (100) [bimm⁺ – C₃H₃N₂]; elemental analysis calcd (%) for C₃₅H₃₀FeN₆O₄ (654.50): C 64.2, H 4.6, N 12.8; found: C 63.7, H 4.6, N 12.5.

Single crystals of **1** were slowly formed by diffusion techniques in methanol solution after several weeks.

[FeL2(bppa)]·0.5 MeOH (2): A mixture of [FeL2(MeOH)₂] (0.29 g, 0.45 mmol) and bppa (0.25 g, 1.66 mmol) in methanol (20 mL) was heated at reflux for 1 h. After cooling down to room temperature the black precipitate was filtered off, washed with methanol (2 × 5 mL) and dried *in vacuo* (yield: 0.23 g, 67%). IR (KBr): $\tilde{\nu}$ = 1679(s) (COO), 1552(s) cm⁻¹ (CO); MS (DEI-+, 70 eV): *m/z* (%): 567 (43) [FeL2⁺ + H], 566 (100) [FeL2⁺], 521 (13) [FeL2⁺ – O₂CH₃], 198 (23) [bppa⁺]; elemental analysis calcd (%) for C_{43.5}H₄₂FeN₄O_{6.5} (780.67): C 66.9, H 5.4, N 7.2; found: C 67.2, H 5.2, N 7.3.

Single crystals of **2** were slowly formed by diffusion techniques in methanol solution after several weeks.

[FeL2(bimm)]·0.5 MeOH (3): A mixture of [FeL2(MeOH)₂] (0.10 g, 0.16 mmol) and bimm (0.12 g, 0.79 mmol) in methanol (10 mL) was heated at reflux for 1 h. After cooling down to room temperature the green precipitate was filtered off, washed with methanol (1 × 3 mL) and dried *in vacuo* (yield: 0.08 g, 68%). IR (KBr): $\tilde{\nu}$ = 1668(m), 1660(m) (COO), 1557(s) cm⁻¹ (CO); MS (FAB-+, 70 eV): *m/z* (%): 714 (1) [M⁺], 566 (4) [M⁺ – bimm], 307 (30), 154 (100); elemental analysis calcd (%) for C_{37.5}H₃₆FeN₆O_{6.5} (730.57): C 61.6, H 5.0, N 11.5; found: C 61.4, H 4.7, N 11.6.

7.5 References

- [1] a) H.A. Goodwin, *Coord. Chem. Rev.*, **1976**, *18*, 293; b) E. König, *Struct. Bonding (Berlin)* **1991**, *76*, 51; c) P. Gülich, A. Hauser, H. Spiering, *Angew. Chem. Int. Ed. Engl.* **1994**, *33*, 2024, and references therein; d) P. Gülich, H.A. Goodwin (Eds.), *Spin Crossover in Transition Metal Compounds I–III, Topics in Current Chemistry*, Springer, Berlin, Heidelberg, New York, **2004**; e) J.A. Real, A.B. Gaspar, M.C. Munoz, *Dalton Trans.* **2005**, 2062; f) K. Nakano, N. Suemura, K. Yoneda, S. Kawata, S. Kaizaki, *Dalton Trans.* **2005**, 740; g) O. Sato, J. Tao, Y.-Z. Zhang, *Angew. Chem.* **2007**, *119*, 2200; *Angew. Chem. Int. Ed.* **2007**, *46*, 2152; h) J.A. Kitchen, S. Brooker, *Coord. Chem. Rev.* **2008**, *252*, 2072; i) K.S. Murray, *Eur. J. Inorg. Chem.* **2008**, 3101; k) M.A. Halcrow, *Coord. Chem. Rev.* **2009**, 2059; l) S. Brooker, J.A. Kitchen, *Dalton Trans.* **2009**, 7331; m) C.J. Kepert, *Aust. J. Chem.* **2009**, *62*, 1079; n) K.S. Murray, *Aust. J. Chem.* **2009**, *62*, 1081; o) A.B. Koudriavtsev, W. Linert, *J. Struct. Chem.* **2010**, *51*, 335.
- [2] a) O. Kahn, C. Jay Martinez, *Science* **1998**, *279*, 44; b) O. Kahn, C. Jay, J. Kröber, R. Claude, F. Grolière, *Patent EP0666561* **1995**; c) J.-F. Létard, O. Nguyen, N. Daro, *Patent FR0512476* **2005**; d) J.-F. Létard, P. Guionneau, L. Goux-Capes, *Topics in Current Chemistry, Vol. 235* (Eds.: P. Gülich, H.A. Goodwin), Springer, Wien, New York, **2004**, 221; e) A. Galet, A.B. Gaspar, M.C. Munoz, G.V. Bukin, G. Levchenko, J.A. Real, *Adv. Mater.* **2005**, *17*, 2949.
- [3] Y. Garcia, V. Kseofontov, P. Gülich, *Hyperfine Interact.* **2002**, *139/140*, 543.
- [4] Y. Garcia, V. Kseofontov, S. Mentior, M.M. Dîrtu, C. Gieck, A. Bhatthacharjee, P. Gülich, *Chem. Eur. J.* **2008**, *14*, 3745.
- [5] P.J. van Koningsbruggen, Y. Garcia, O. Kahn, L. Fournès, H. Kooijman, A.L. Spek, J.G. Haasnoot, J. Moscovici, K. Provost, A. Michalowicz, F. Renz, P. Gülich, *Inorg. Chem.* **2000**, *39*, 1891.
- [6] G.S. Matouzenko, M. Perrin, B. le Guennic, C. Genre, G. Molnar, A. Bousseksou, S.A. Borshch, *Dalton Trans.* **2007**, *9*, 934.

- [7] a) G.S. Matouzenko, G. Molnar, N. Brefuel, M. Perrin, A. Bousseksou, S.A. Borshch, *Chem. Mater.* **2003**, *15*, 550. b) C. Genre, G.S. Matouzenko, E. Jeanneau, D. Luneau, *New J. Chem.* **2006**, *30*, 1669.
- [8] a) B. Weber, R. Tandon, D. Himsl, *Z. Anorg. Allg. Chem.* **2007**, *633*, 1159; b) B. Weber, E.S. Kaps, C. Desplanches, J.-F. Létard, *Eur. J. Inorg. Chem.* **2008**, 2963.
- [9] M.M. Dîrtu, C. Neuhausen, A.D. Naik, A. Rotaru, L. Spinu, Y. Garcia, *Inorg. Chem.* **2010**, *49*, 5723.
- [10] S.M. Neville, B.A. Leita, G.J. Halder, C. Kepert, B. Moubaraki, J.-F. Létard, K.S. Murray, *Chem. Eur. J.* **2008**, *14*, 10123.
- [11] B. Weber, E.-G. Jäger, *Eur. J. Inorg. Chem.* **2009**, 465.
- [12] a) B. Weber, E.S. Kaps, J. Weigand, C. Carbonera, J.-F. Létard, K. Achterhold, F.G. Parak, *Inorg. Chem.* **2008**, *47*, 487; b) B. Weber, E.S. Kaps, J. Obel, W. Bauer, *Z. Anorg. Allg. Chem.* **2008**, 1421; c) B. Weber, C. Carbonera, C. Desplanches, J.-F. Létard, *Eur. J. Inorg. Chem.* **2008**, 1589; d) B. Weber, E.S. Kaps, C. Desplanches, J.-F. Létard, K. Achterhold, F.G. Parak, *Eur. J. Inorg. Chem.* **2008**, 4891.
- [13] T. Pfaffeneder, W. Bauer, B. Weber, *Z. Anorg. Allg. Chem.* **2010**, *636*, 183.
- [14] B. Weber, *Coord. Chem. Rev.* **2009**, *253*, 2432.
- [15] L. Wolf, E.-G. Jäger, *Z. Anorg. Allg. Chem.* **1966**, *346*, 76.
- [16] E.-G. Jäger, E. Häussler, M. Rudolph, M. Rost, *Z. Anorg. Allg. Chem.* **1985**, *525*, 67.
- [17] a) B. Weber, H. Görls, M. Rudolf, E.-G. Jäger, *Inorg. Chim. Acta* **2002**, *337*, 247; b) B. Weber, PhD thesis, University of Jena (Germany), **2002**; Der Andere Verlag, Osnabrück, **2003**.
- [18] W. Bauer, B. Weber, *Inorg. Chim. Acta* **2009**, *362*, 2341.
- [19] V.A. Money, J. Elhaik, I.R. Evans, M.A. Halcrow, J.A.K. Howard, *Dalton Trans.* **2004**, 65.
- [20] B. Weber, E.S. Kaps, J. Obel, K. Achterhold, F.G. Parak, *Inorg. Chem.* **2008**, *47*, 10779.
- [21] W. Bauer, W. Scherer, S. Altmannshofer, B. Weber, *Eur. J. Inorg. Chem.* **2011**, 2803.

- [22] a) A.B. Koudriavtsev, A.F. Strassen, J.G. Haasnoot, M. Grunert, P. Weinberger, W. Linert, *Phys. Chem.* **5** **2003**, 3676; b) A.B. Koudriavtsev, A.F. Strassen, J.G. Haasnoot, M. Grunert, P. Weinberger, W. Linert, *Chem. Phys.* **5** **2003**, 3666.
- [23] J.A. Real, A.B. Gaspar, V. Niel, M.C. Munoz, *Coord. Chem. Rev.* **2003**.
- [24] C.F. Macrae, I.J. Bruno, J.A. Chisholm, P.R. Edgington, P. McCabe, E. Pidcock, L. Rodriguez-Monge, R. Taylor, J. van de Streek, P.A. Wood, *J. Appl. Cryst.* **2008**, *41*, 466.
- [25] G. Leibelng, PhD thesis, University of Jena (Germany), **2003**.
- [26] B. Weber, W. Bauer, J. Obel, *Angew. Chem.* **2008**, *120*, 10252; *Angew. Chem., Int. Ed.* **2008**, *47*, 10098;
- [27] B. Weber, W. Bauer, T. Pfaffeneder, M.M. Dîrtu, A.D. Naik, A. Rotaru, Y. Garcia, *Eur. J. Inorg. Chem.* **2011**, DOI: 10.1002/ejic.201100394.
- [28] B.R. Müller, G. Leibelng, E.-G. Jäger, *Chem. Phys. Lett.* **2000**, *319*, 368.
- [29] H. Spiering, E. Meissner, H. Köppen, E.W. Müller, P. Gütlich, *Chem. Phys.* **1982**, *68*, 65.
- [30] P. Guionneau, F. Le Gac, S. Lakhoufi, A. Kaiba, D. Chasseau, J.-F. Létard, P. Négrier, D. Mondieig, J.A.K. Howard, J.-M. Léger, *J. Phys.: Condens. Matter* **2007**, *19*, 326211.
- [31] J.-A. Real, B. Gallois, T. Granier, F. Suez-Panamá, J. Zarembowitch, *Inorg. Chem.* **1992**, *31*, 4972.
- [32] B. Gallois, J.-A. Real, C. Hauw, J. Zarembowitch, *Inorg. Chem.* **1990**, *29*, 1152.
- [33] A. Altomare, M.C. Burla, G.M. Camalli, G. Cascarano, C. Giacovazzo, A. Guagliardi, A.G.G. Moliterni, G. Polidori, R. Spagna, SIR-97, University of Bari, Bari (Italy), **1997**; *J. Appl. Crystallogr.* **1999**, *32*, 115.
- [34] G.M. Sheldrick, SHELXL-97, University of Göttingen, Göttingen (Germany), **1997**.
- [35] C.K. Johnson, M.N. Burnett, ORTEP-III, Oak-Ridge National Laboratory, Oak-Ridge, TN (USA), **1996**; L.J. Farrugia, *J. Appl. Crystallogr.* **1997**, *30*, 565.
- [36] E. Keller, SCHAKAL-99, University of Freiburg, Freiburg (Germany), **1999**.

- [37] Team of authors: *Organikum*, Johann Ambrosius Barth Leipzig, Berlin, Heidelberg, **1993**.
- [38] B. Heyn, B. Hipler, G. Kreisel, H. Schreer, D. Walter, *Anorganische Synthesechemie*, 2. edition, Springer, Heidelberg, **1986**.

7.6 Supporting Information

Table S1. Crystallographic data of the complexes [FeL1(bimm)] (**1**) and [FeL2(bppa)]·0.5 MeOH (**2**).

compound	1 (125 K)	1 (180 K)	1 (250 K)	2
formula	C ₃₅ H ₃₀ FeN ₆ O ₄	C ₃₅ H ₃₀ FeN ₆ O ₄	C ₃₅ H ₃₀ FeN ₆ O ₄	C _{43.5} H _{42.2} FeN ₄ O _{6.5}
$M_r / \text{g mol}^{-1}$	654.50	654.50	654.50	782.01
crystal system	triclinic	triclinic	triclinic	orthorhombic
space group	$P\bar{1}$	$P\bar{1}$	$P\bar{1}$	$Pbca$
$a / \text{\AA}$	10.4117(14)	10.3326(16)	10.3530(16)	19.3122(4)
$b / \text{\AA}$	10.5247(12)	10.8298(17)	10.928(2)	16.5116(3)
$c / \text{\AA}$	15.4338(18)	15.672(3)	15.794(4)	25.1186(5)
$\alpha / ^\circ$	74.913(10)	74.763(14)	75.074(19)	90
$\beta / ^\circ$	79.006(11)	80.991(14)	81.233(17)	90
$\gamma / ^\circ$	64.091(13)	64.329(15)	64.423(18)	90
$V / \text{\AA}^3$	1463.0(3)	1523.2(4)	1555.7(5)	8009.7(3)
Z	2	2	2	8
$\rho / \text{g cm}^{-3}$	1.486	1.427	1.397	1.297
μ / mm^{-1}	0.569	0.546	0.535	0.430
crystal size	0.27 × 0.11 × 0.05	0.26 × 0.11 × 0.05	0.26 × 0.11 × 0.05	0.41 × 0.34 × 0.22
T / K	125(2)	180(2)	250(2)	173(2)
diffractometer	Oxford XCalibur	Oxford XCalibur	Oxford XCalibur	Oxford XCalibur
$\lambda (\text{MoK}\alpha) / \text{\AA}$	0.71073	0.71073	0.71073	0.71073
θ -range / $^\circ$	3.83–25.35	3.74–25.35	3.76–25.35	4.20–26.28
reflns. collected	17191	17037	17523	33558
indep. reflns. (R_{int})	5339 (0.0819)	5537 (0.0631)	5624 (0.0634)	8121 (0.0379)
mean $\sigma(I) / I$	0.1154	0.1010	0.0976	0.0604
reflns. with $I \geq 2\sigma(I)$	3226	3470	3350	4814
x, y (weighting scheme)	0.0683, 0	0.0560, 0	0.0527, 0	0.0380, 0
parameters	417	417	417	509
restraints	0	0	0	0
$R(F)$ (all data) ^[a]	0.0635 (0.1183)	0.0567 (0.1025)	0.0484 (0.0946)	0.0325 (0.0664)
$wR(F^2)$ ^[b]	0.1494	0.1243	0.1179	0.0744
$Goof$	1.025	1.002	0.960	0.841
shift/error _{max}	0.000	0.000	0.000	0.001
max., min. resd. dens. / e \AA^{-3}	0.557, -0.344	0.333, -0.299	0.254, -0.238	0.283, -0.346

[a] $R(F) = \sum ||F_o| - |F_c|| / \sum |F_o|$. [b] $wR(F^2) = [\sum [w(F_o^2 - F_c^2)^2] / \sum w(F_o^2)^2]^{1/2}$, $w = 1 / [\sigma^2(F_o^2) + (aP)^2 + bP]$, where $P = [F_o^2 + 2(F_c^2)]/3$.

8 A Promising New Schiff Base-like Ligand for the Synthesis of Octahedral Iron(II) Spin Crossover Complexes

Wolfgang Bauer,^[a] Tanja Ossiander^[a] and Birgit Weber*^[a]

[a] Center for Integrated Protein Science Munich at the Department Chemie und Biochemie, Ludwig-Maximilians-Universität München, Butenandtstraße 5–13 (Haus F), D-81377 München, Germany

Dedicated to Professor Rolf W. Saalfrank on the occasion of his 70th birthday

Keywords: Schiff base-like Ligand, Iron Complexes, Magnetic Properties

Published in: *Z. Naturforsch. B* **2010**, *65*, 323–328.

Abstract: A new tetradentate Schiff base-like ligand H₂L (**1**) (dimethyl (*E,E*)-2,2'-[1,2-phenyl-bis(aminomethylidene)]bis[3-oxobutanoate]) was synthesised and structurally characterised. Its reaction with iron(II) acetate leads to the formation of the octahedral N₂O₄ coordinated complex [FeL(MeOH)₂] (**2**). The complex is a pure high spin (HS) compound as is evident from magnetic measurements and X-ray crystallography.

8.1 Introduction

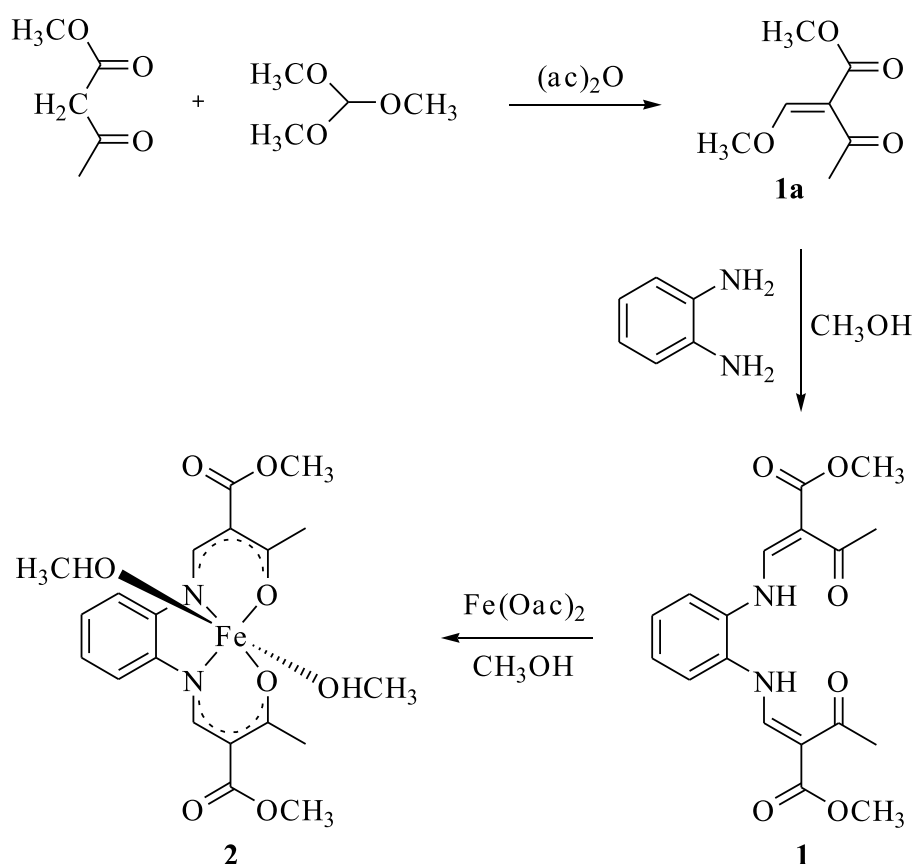
The bistability of spin transition complexes (spin crossover, SCO) is one of the most promising possibilities for new electronic devices in molecular memories and switches as it may be controlled by different physical perturbations such as temperature, pressure or light.^[1,2] Of the possible types of spin transition (gradual, abrupt, with hysteresis, stepwise, incomplete), much of the interest is focused on the bistability in highly cooperative systems (hysteresis or memory effect) as such compounds can exist in two different electronic states, depending on the history of the system. With regard to this we recently characterised an iron(II) spin crossover complex with a 70 K wide thermal hysteresis loop around room

temperature based on a 2D network of hydrogen bonds between the complex molecules.^[3] In order to more deeply understand the role of hydrogen bonds for cooperative effects in spin crossover systems we designed a new ligand with two ethyl groups substituted by methyl groups—a comparatively small modification that can, however, significantly influence the magnetic properties. In Scheme 1 the general procedure for the synthesis of the new ligand and its iron(II) complexes is given. In this paper we present the synthesis and characterisation of the free ligand H₂L and its octahedral iron(II) complex with two methanol molecules as axial ligands. This is the first example of this type of complexes, where we were able to analyse the X-ray structure of both, the free ligand and its iron complex.

8.2 Results and Discussion

Synthesis: Scheme 1 gives the general synthetic route of the tetradentate Schiff base-like ligand H₂L (**1**) and the octahedral iron(II) complex [FeL(MeOH)₂] (**2**). The synthesis of the ligand is an adaptation of Claisen,^[4] who first described the preparation of oxymethylene derivatives and their reaction with amines in the late 19th century and of Jäger and Wolf,^[5] who first described the preparation of this type of ligand in the 1960s. The synthesis of H₂L is carried out in two independent steps. At first the methoxymethylene derivative **1a** is directly synthesised by oxymethylation of methyl acetoacetate using trimethyl orthoformate in acetic anhydride. Contrary to literature it is essential to use trimethyl orthoformate instead of triethyl orthoformate, in order to prevent the substitution of the methoxy ester group by an ethoxy ester group. The second step is the condensation of **1a** with 1,2-*ortho*-phenylenediamine (stoichiometric ratio 2:1) in methanol as solvent, which gives **1** (H₂L) as a yellow precipitate. The synthesis of the octahedral complex **2** ([FeL(MeOH)₂]), where L²⁻, the deprotonated form of H₂L, acts as equatorial ligand and the methanol molecules as axial ligands, is carried out in a one-pot reaction by treatment of **1** with a slight excess of anhydrous iron(II) acetate in methanol.

8. A Promising New Schiff Base-like Ligand for the Synthesis of Octahedral Iron(II) Spin Crossover Complexes

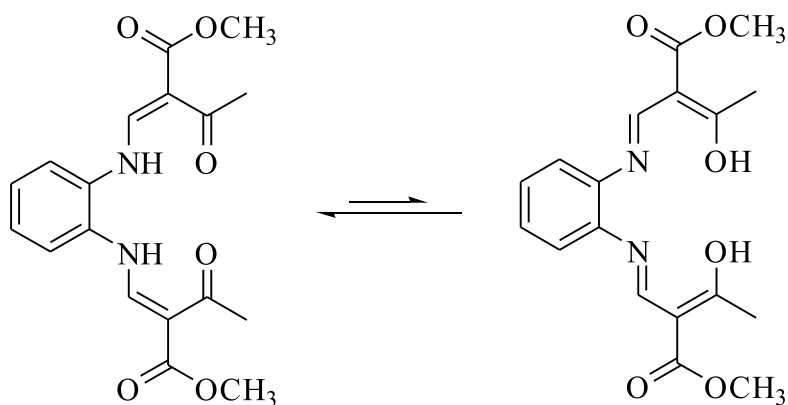


Scheme 1. General route for the synthesis of the Schiff base-like ligand **1** (H_2L) and its octahedral iron(II) complex **2** ($[FeL(MeOH)_2]$).

X-Ray structure analysis: Crystals suitable for X-ray analysis of the free equatorial ligand **1** and its iron(II) complex **2** were obtained by slow crystallisation out of the mother liquor. The crystallographic data are summarised in Supporting Information Table S1. Figure 2 displays the asymmetric units of **1** and **2**, respectively. Selected bond lengths and angles are summarised in Table 1. Compound **1** crystallises with the orthorhombic space group $Pbca$. The unit cell contains 8 formula units. The molecular structure of **1** is non-planar and thus the N_2O_2 coordination sites are not in a common plane. This is indicated by the two dihedral angles, which are defined by atoms C3-N1-C4-C5 and C10-N2-C9-C8 and display the torsion of the conjugated aminomethylidyne chains, which build up the chelate ring, relative to the phenylene ring. Their values are $7.6(3)^\circ$ and $34.3(2)^\circ$. The average bond lengths within the conjugated π -system of the chelate ring [1.34 \AA (C-N), 1.38 \AA (C-C), 1.46 \AA (C-C) and 1.24 \AA (C-O), see Figure 2] are in line with literature values for similar single and double bonds. This leads to the result that the equilibrium between the two possible tautomeric

8. A Promising New Schiff Base-like Ligand for the Synthesis of Octahedral Iron(II) Spin Crossover Complexes

structures “enol-imine” and “keto-enamine” (see Scheme 2) is shifted to the keto-enamine form, in contrast to classic Schiff base ligands (*e.g.* salen). The ^1H NMR spectrum, pictured in Figure 1, in which a CH-NH coupling constant in the range of 12 Hz is observed, supports this finding. Between the carbonyl oxygen atoms O1 and O2 of the acetyl groups and the amino groups N1-H1 and N2-H2 intramolecular hydrogen bonds are formed.



Scheme 2. Possible tautomeric structures of **1**, keto-enamine (left) and enol-imine (right). The equilibrium is shifted to the keto-enamine form.

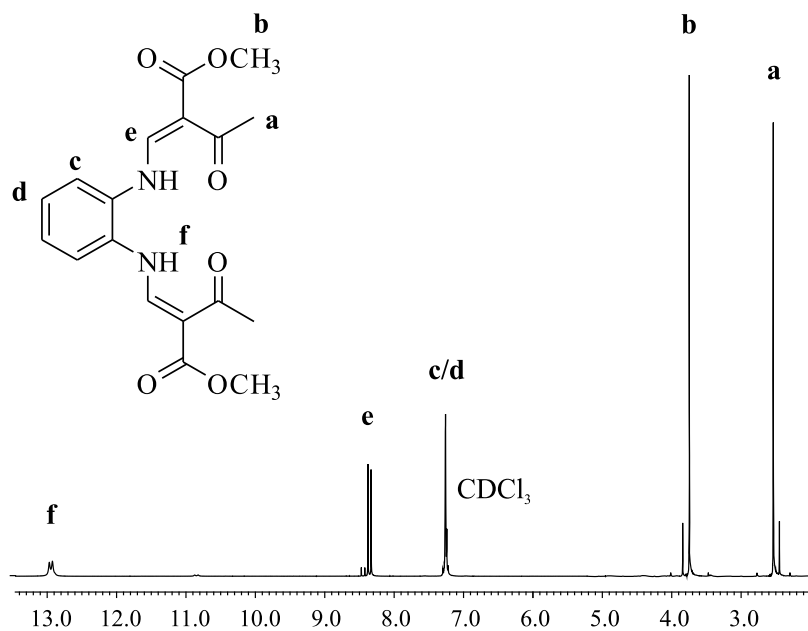


Figure 1. ^1H NMR spectrum of **1** (in CDCl_3) with the signal assignment given at the left.

8. A Promising New Schiff Base-like Ligand for the Synthesis of Octahedral Iron(II) Spin Crossover Complexes

Compound **2** crystallises in the monoclinic space group $P2_1$, with 2 formula units per cell. The bond lengths and angles around the iron atom are within the range reported for octahedral HS iron(II) complexes of the same ligand type with two axial ligands.^[6,7] The average values are 2.08 Å (Fe-N_{eq}), 2.00 Å (Fe-O_{eq}) and 2.23 Å (Fe-O_{ax}). The exact values are listed in Table 1. A characteristic tool for the determination of the spin state of this type of iron(II) complexes is the O-Fe-O angle, which changes from about 110° in the HS state to about 90° in the LS state.^[6,7] With 105.6° compound **2** is clearly in the HS state.

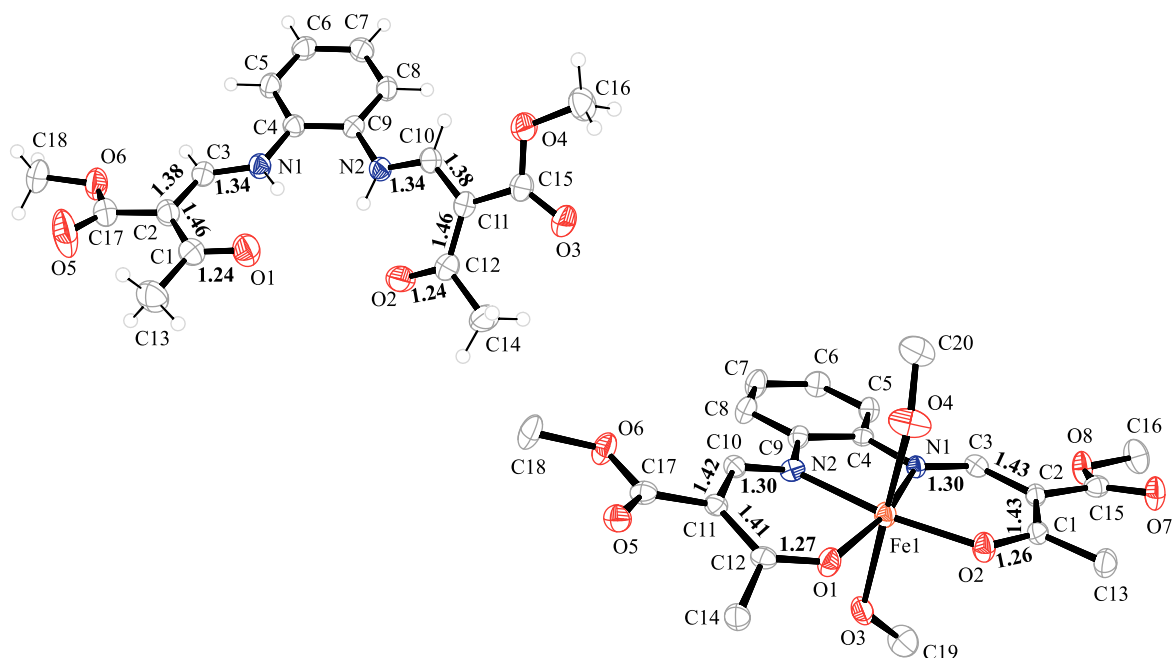


Figure 2. ORTEP drawing of the asymmetric units of ligand **1** (top) and complex **2** (bottom) with selected bond lengths [Å] for comparison. For clarity reasons the hydrogen atoms of **2** have been omitted. Displacement ellipsoids are shown with a 50% probability.

Table 1. Selected bond lengths [Å] and angles [°] of complex **2** with estimated standard deviations in parentheses.

Fe-N _{eq}	Fe-O _{eq}	Fe-O _{ax}	O _{eq} -Fe-O _{eq}	O _{ax} -Fe-O _{ax}
2.075(2)	2.011(2)	2.264(2)	105.62(8)	174.77(8)
2.0810(19)	1.990(2)	2.189(2)		

8. A Promising New Schiff Base-like Ligand for the Synthesis of Octahedral Iron(II) Spin Crossover Complexes

The average values of the bond lengths within the conjugated π -system of the chelate ring [1.30 Å (C-N), 1.43 Å (C-C), 1.42 Å (C-C) and 1.26 Å (C-O), see Figure 2] reveal that the negative charge of the deprotonated form of the Schiff base-like ligand L^{2-} is delocalised over the chelate six-membered ring. For the discussion of cooperative interactions or spontaneous magnetic ordering, intermolecular interactions such as hydrogen bonding or π -stacking are thought to play a central role as such contacts are necessary for long range ordering effects. In complex **2** two different intermolecular hydrogen bonds can be found, which are listed in Table 2, leading to an infinite one-dimensional chain with the base vector [0 1 0], as can be seen in Figure 3. The hydroxy oxygen atoms of both axial methanol ligands act as hydrogen bond donors. In both cases, an ester carbonyl oxygen atom O5 of the respective neighbouring complex is the acceptor.

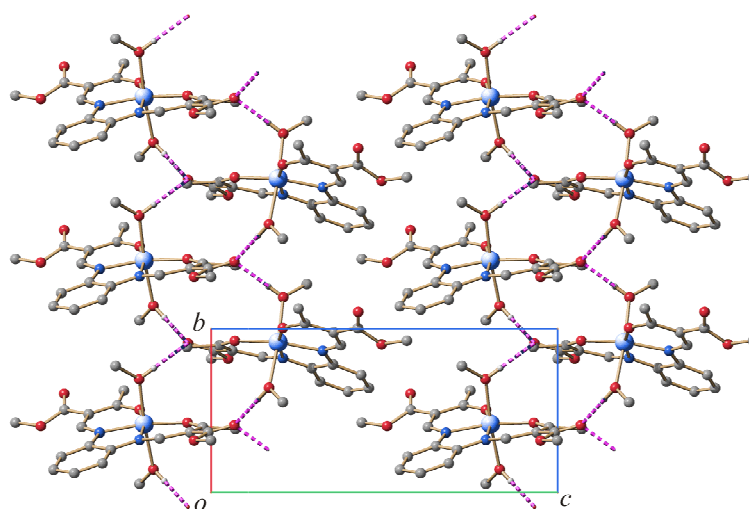


Figure 3. Molecule packing of the hydrogen bonded (dashed lines) molecules of complex **2** projected along [1 0 0].

Table 2. Bond lengths (Å) and angles (deg) of intermolecular hydrogen bonds of complex **2** with $d(D\cdots A) < R(D) + R(A) + 0.50$, $d(H\cdots A) < R(H) + R(A) - 0.12$ Å, $D-H\cdots A > 100.0^\circ$.

D	H	A	D-H	H \cdots A	A \cdots D	D-H \cdots A
O3	H31	O5 ^[a]	0.84	1.93	2.763(3)	175
O4	H41	O5 ^[b]	0.84	1.92	2.758(3)	173

Symmetry codes: [a] $2 - x, -\frac{1}{2} + y, -z$; [b] $2 - x, \frac{1}{2} + y, -z$.

Magnetic susceptibility data: The magnetic susceptibility of the iron(II) complex **2** was measured in the temperature range from 300 to 2 K. The plots of $\chi_M T$ and χ_M^{-1} vs. T (χ_M being the molar susceptibility) are given in Figure 4 (left). Over the whole temperature range investigated, **2** remains in the paramagnetic high-spin state, with typical $\chi_M T$ values, considering four unpaired electrons ($S = 2$).

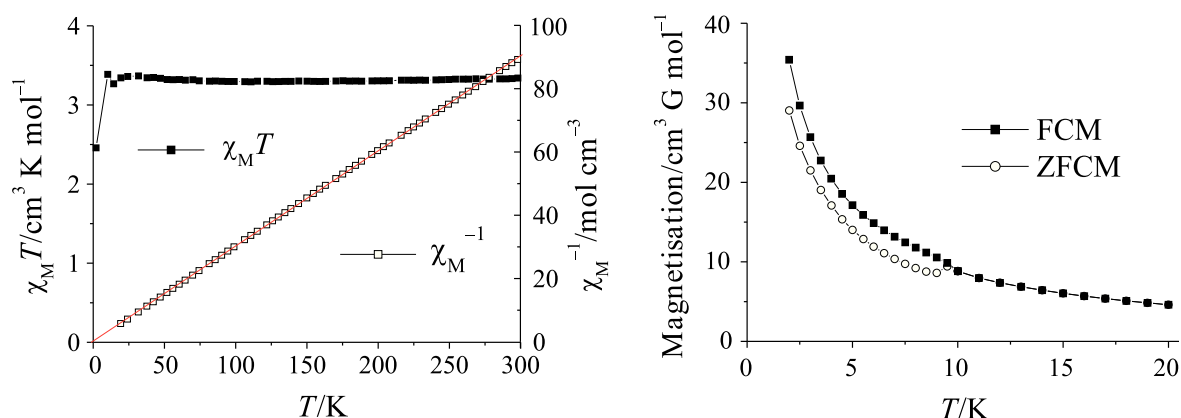


Figure 4. Plot of the $\chi_M T$ product and χ_M^{-1} vs. T for complex **2** between 5 and 300 K (left) and the fits according to the Curie-Weiss law, $\chi_M = C/(T - \theta)$, with the parameters $\theta = -0.65$ K and $C = 3.33$ cm³ K mol⁻¹ for complex **2**. Right: (zero) field-cooled magnetisation ((Z)FCM) plots measured under a weak magnetic field of $H < 30$ G.

The $\chi_M T$ product slightly decreases from a value of 3.34 cm³ K mol⁻¹ at 300 K to 3.29 cm³ K mol⁻¹ at 110 K, and then again rises to 3.34 cm³ K mol⁻¹ at 20 K. The decrease of $\chi_M T$ below 20 K is due to zero field splitting. The susceptibility data above 20 K can be fitted with the Curie-Weiss law ($\chi_M = C/(T - \theta)$), with the parameters $\theta = -0.65$ K and $C = 3.33$ cm³ K mol⁻¹. The Curie constant C of the complex is in a region expected for iron(II) complexes in the high-spin state, and the negative Weiss constant θ together with the temperature-dependent decrease of the $\chi_M T$ product above 110 K are indications of weak antiferromagnetic interactions between the spin centres. The increase of the magnetic moment below 110 K is probably due to spin canting as observed previously for similar complexes of this ligand system.^[8] A zero field-cooled (ZFCM) and a field-cooled magnetisation (FCM) measurement with $H = 30$ G was performed for compound **2** and the result is shown in Figure 4 (right). As expected from results of the magnetic susceptibility measurement only very weak indications for long-range magnetic ordering can be found. The FCM measurement

exhibits no abrupt increase in the magnetisation (typical for spontaneous magnetic ordering) but only a small slope in the magnetisation curve at about 10 K. This is in line with the ZFCM measurement. However, the spontaneous magnetic ordering is significantly less pronounced compared to other iron(II) complexes of this type with methanol molecules as axial ligands and a Schiff base-like equatorial ligand.^[8]

8.3 Conclusion

Compound **1** is the first example of this ligand type where the determination of the X-ray structure was possible. This enabled us to provide a further proof for the suggested keto-enol isomeric structure for this type of Schiff base-like ligands. Upon coordination to a metal centre the two amino nitrogens are deprotonated and the negative charge is delocalised over the chelate six-membered ring. The magnetic properties of **2** demonstrate how small changes in the ligand structure influence the magnetic properties of the related complexes. While for other methanol diadducts of this complex type a spontaneous magnetisation due to canted antiferromagnetism is observed, for complex **2** the observed effects in the FCM/ZFCM measurements are too small to be seriously discussed any further.

8.4 Experimental Section

Magnetic measurements: Magnetic susceptibility data were collected by using a Quantum Design MPMSR-2 SQUID magnetometer under an applied field of 0.5 T over the temperature range 2 to 300 K. The sample of **2** was placed in gelatine capsules held within a plastic straw. The data were corrected for the diamagnetic magnetisation of the ligands by using tabulated Pascal's constants and of the sample holder.

X-Ray structure determination: The intensity data of **1** were collected on a Nonius Kappa CCD diffractometer by using graphite-monochromated MoK α radiation. The intensity data of **2** were collected on an Oxford XCalibur diffractometer by using graphite-monochromated MoK α radiation. The data were corrected for Lorentz and polarisation effects. The structure was solved by direct methods (SIR-97)^[9] and refined by full-matrix least-square techniques against F_0^2 (SHELXL-97).^[10] The hydrogen atoms were included at calculated positions with fixed displacement parameters. ORTEP-III was used for structure representation,^[11] SCHAKAL-99 to illustrate molecule packings.^[12] The crystallographic data are summarised in Supporting Information Table S1.

CCDC 753713 (**1**) and CCDC 753714 (**2**) contain the supplementary crystallographic data for this paper. These data can be obtained free of charge from The Cambridge Crystallographic Data Centre *via* www.ccdc.cam.ac.uk/data_request/cif.

Synthesis: The synthesis of the iron(II) complex was carried out under argon by using Schlenk tube techniques. The solvent methanol was purified as described in literature^[13] and distilled under argon. The synthesis of iron(II) acetate is described in the literature.^[14]

(E)-Methyl 2-(methoxymethylidene)-3-oxobutanoate (1a): A mixture of methyl acetoacetate (58.1 g, 0.5 mol), trimethyl orthoformate (53.1 g, 0.5 mol) and acetic anhydride (102.1 g, 1.0 mol) was heated to reflux for 75 min, while the colour of the reaction mixture turned into dark red. At first, under normal pressure the low-boiling side products were distilled off. At second, by fractionated vacuum distillation **1a** was isolated as slightly yellow oil at about 90 °C (1.7 mbar) and used immediately for further synthesis (yield: 39.5 g, 50%). ¹H NMR (270 MHz, CDCl₃, 25°C, TMS): δ = 7.52 (s, 1H; CH) 3.95 (s, 3H; CO₂CH₃), 3.72 (s, 3H; OCH₃), 2.30 ppm (s, 3H; COCH₃).

H₂L (1): To a solution of *ortho*-phenylenediamine (4.56 g, 42.4 mmol) in methanol (60 mL) was added drop-wise a solution of **1a** (14.7 g, 93.4 mmol) in of methanol (20 mL). The reaction mixture was heated to reflux for 30 min. After cooling to room temperature light-yellow crystals formed which were recrystallised from methanol. Crystals suitable for X-ray analysis formed in the mother liquor at 4 °C within one day (yield: 14.0 g, 92%). M.p. 132–133 °C; ¹H NMR (270 MHz, CDCl₃, 25°C, TMS): δ = 12.95 (d, ³J(H,H) = 12.0 Hz, 2H; NH), 8.36 (d, ³J(H,H) = 12.0 Hz, 2H; CH), 7.23–7.30 (m, 4H; Ar-H), 3.75 (s, 6H; OCH₃), 2.54 ppm (s, 6H; CH₃); MS (DEI-(+), 70 eV): *m/z* (%): 360 (17) [*M*⁺], 285 (84) [C₁₅H₁₃N₂O₄⁺], 253 (100) [C₁₄H₉N₂O₄⁺], 232 (83) [C₁₂H₁₂N₂O₃⁺]; elemental analysis calcd (%) for C₁₈FeH₂₀N₂O₆ (360.36): C 59.99, H 5.59, N 7.77; found: C 60.07, H 5.51, N 7.73.

[FeL(MeOH)₂] (2): Anhydrous iron(II)acetate (2.95 g, 17.0 mmol) and H₂L (3.60 g, 10.0 mmol) were dissolved in methanol (100 mL) and heated to reflux for 1 h. After two days a black fine-crystalline precipitate has formed that was filtered off, washed with methanol (2 × 5 mL) and dried *in vacuo*. Crystals suitable for X-ray analysis formed in the mother liquor within further two days (yield: 4.26 g, 71%). IR (KBr): $\tilde{\nu}$ = 3398(w) (OH), 1702(s) (COO), 1572(s) cm⁻¹ (CO); MS (DEI-(+), 70 eV): *m/z* (%): 414 (100) [FeL⁺]; elemental analysis calcd (%) for C₂₀FeH₂₆N₂O₈ (478.3): C 50.23, H 5.48, N 5.86; found: C 49.80, H 4.43, N 5.85.

Acknowledgement

This work has been supported financially by the Deutsche Forschungsgemeinschaft (SPP 1137), the Fonds der Chemischen Industrie, the Center for Integrated Protein Science Munich (CIPSM), and the University of Munich. The authors thank M. Reichvilser and P. Mayer for the acquisition of the crystallographic data.

8.5 References

- [1] a) H.A. Goodwin, *Coord. Chem. Rev.* **1976**, *18*, 293; b) P. Gülich, *Struct. Bonding (Berlin)* **1981**, *44*, 83; c) E. König, *Prog. Inorg. Chem.* **1987**, *35*, 527; d) P. Gülich, A. Hauser, *Coord. Chem. Rev.* **1990**, *97*, 1; e) E. König, *Struct. Bonding (Berlin)* **1991**, *76*, 51; f) P. Gülich, A. Hauser, H. Spiering, *Angew. Chem., Int. Ed. Engl.* **1994**, *33*, 2024, and references therein; *Angew. Chem.* **1994**, *106*, 2109 g) P. Gülich, J. Jung, H.A. Goodwin, *Molecular Magnetism: From Molecular Assemblies to the Devices* (Eds.: Coronado *et al.*), NATO ASI Series E: *Applied Sciences*, Vol. 321, Kluwer, Dordrecht, **1996**, 327; h) P. Gülich, H.A. Goodwin (Eds.), *Spin Crossover in Transition Metal Compounds I–III, Topics in Current Chemistry*, Springer, Berlin, Heidelberg, New York, **2004**; i) J.A. Real, A.B. Gaspar, M.C. Munoz, *Dalton Trans.* **2005**, 2062, j) O. Sato, J. Tao, Y.-Z. Zhang, *Angew. Chem.* **2007**, *119*, 2200; *Angew. Chem., Int. Ed.* **2007**, *46*, 2152.
- [2] a) O. Kahn, C. Jay Martinez, *Science* **1998**, *279*, 44; b) O. Kahn, C. Jay, J. Kröber, R. Claude, F. Grolière, *Patent EP0666561* **1995**; c) J.-F. Létard, O. Nguyen, N. Daro, *Patent FR0512476* **2005**; d) J.-F. Létard, P. Guionneau, L. Goux-Capes, *Topics in Current Chemistry*, Vol. 235 (Eds.: P. Gülich, H.A. Goodwin), Springer, Wien, New York **2004**, 221; e) A. Galet, A.B. Gaspar, M.C. Munoz, G.V. Bukin, G. Levchenko, J.A. Real, *Adv. Mater.* **2005**, *17*, 2949.
- [3] B. Weber, W. Bauer, J. Obel, *Angew. Chem.* **2008**, *120*, 10252; *Angew. Chem., Int. Ed.* **2008**, *47*, 10098.
- [4] L. Claisen, *Liebigs Ann. Chem.* **1897**, *297*, 1.
- [5] L. Wolf, E.-G. Jäger, *Z. Anorg. Allg. Chem.* **1966**, *346*, 76.
- [6] a) B. Weber, E.S. Kaps, J. Obel, W. Bauer, *Z. Anorg. Allg. Chem.* **2008**, 1421; b) B. Weber, C. Carbonera, C. Desplanches, J.-F. Létard, *Eur. J. Inorg. Chem.* **2008**, 1589; c) B. Weber, E.S. Kaps, C. Desplanches, J.-F. Létard, K. Achterhold, F.G. Parak, *Eur. J. Inorg. Chem.* **2008**, 4891; d) W. Bauer, B. Weber, *Inorg. Chim. Acta* **2009**, *362*, 2341;

- e) B. Weber, E. Kaps, *Heteroatom Chem.* **2005**, *16*, 391; f) B. Weber, E.S. Kaps, J. Obel, K. Achterhold, F.G. Parak, *Inorg. Chem.* **2008**, *47*, 10779; g) B. Weber, R. Tandon, D. Himsl, *Z. Anorg. Allg. Chem.* **2007**, *633*, 1159; h) B. Weber, E.S. Kaps, C. Desplanches, J.-F. Létard, *Eur. J. Inorg. Chem.* **2008**, 2963.
- [7] a) B. Weber, *Coord. Chem. Rev.* **2009**, *253*, 2432; b) B. Weber, E.-G. Jäger, *Eur. J. Inorg. Chem.* **2009**, 465.
- [8] a) B.R. Müller, G. Leibelng, E.-G. Jäger, *Chem. Phys. Lett.* **2000**, *319*, 368; b) B. Weber, E.-G. Jäger, *Z. Anorg. Allg. Chem.* **2009**, *635*, 130.
- [9] A. Altomare, M.C. Burla, G.M. Camalli, G. Cascarano, C. Giacovazzo, A. Guagliardi, A.G.G. Moliterni, G. Polidori, R. Spagna, SIR-97, University of Bari, Bari (Italy), **1997**; *J. Appl. Crystallogr.* **1999**, *32*, 115.
- [10] G.M. Sheldrick, SHELXL-97, University of Göttingen, Göttingen (Germany), **1997**.
- [11] C.K. Johnson, M.N. Burnett, ORTEP-III, Oak-Ridge National Laboratory, Oak-Ridge, TN (USA), **1996**; L.J. Farrugia, *J. Appl. Crystallogr.* **1997**, *30*, 565.
- [12] E. Keller, SCHAKAL-99, University of Freiburg, Freiburg (Germany), **1999**.
- [13] Team of authors: *Organikum*, Johann Ambrosius Barth Leipzig, Berlin, Heidelberg, **1993**.
- [14] B. Heyn, B. Hipler, G. Kreisler, D. Schreer, D. Walter, *Anorganische Synthesechemie*, 2. edition, Springer, Heidelberg, **1986**.

8. A Promising New Schiff Base-like Ligand for the Synthesis of Octahedral Iron(II) Spin Crossover Complexes

8.6 Supporting Information

Table S1. Crystallographic data for H₂L (**1**) and [FeL(MeOH)₂] (**2**).

compound	1	2
formula	C ₁₈ H ₂₀ N ₂ O ₆	C ₂₀ H ₂₆ N ₂ O ₈ Fe
M_r / g mol ⁻¹	360.36	478.28
crystal system	orthorhombic	monoclinic
space group	<i>Pbca</i>	<i>P2</i> ₁
a / Å	15.0360(2)	8.9590(6)
b / Å	8.60200(10)	7.4730(5)
c / Å	27.3832(4)	15.840(3)
α / °	90	90
β / °	90	92.955(10)
γ / °	90	90
V / Å ³	3541.73(8)	1059.1(2)
Z	8	2
ρ / g cm ⁻³	1.35	1.50
μ / mm ⁻¹	0.102	0.762
crystal size	0.35 × 0.25 × 0.20	0.36 × 0.20 × 0.15
T / K	200(2)	173(2)
diffractometer	KappaCCD	Oxford XCalibur
λ (MoK α) / Å	0.71073	0.71069
θ -range / °	3.27–25.03	4.32–26.36
reflns. collected	18940	4371
indep. reflns. (R_{int})	3124 (0.0297)	3094 (0.0247)
mean $\sigma(I)$ / I	0.0184	0.0556
reflns. with $I \geq 2\sigma(I)$	2660	2659
x, y (weighting scheme)	0.0486, 2.4133	0.0231, 0
parameters	239	286
restraints	0	1
$R(F)$ (all data) ^[a]	(0.0476)	(0.0392)
$wR(F^2)$ ^[b]	0.1199	0.0603
$Goof$	1.072	0.942
shift/error _{max}	0.000	0.001
max., min. resd. dens. / e Å ⁻³	0.281, -0.274	0.220, -0.293

[a] $R(F) = \sum ||F_o| - |F_c|| / \sum |F_o|$. [b] $wR(F^2) = [\sum [w(F_o^2 - F_c^2)^2] / \sum w(F_o^2)^2]^{1/2}$, $w = 1 / [\sigma^2(F_o^2) + (aP)^2 + bP]$, where $P = [F_o^2 + 2(F_c^2)]/3$.

9 Complete Two-Step Spin-Transition in a 1D Chain Iron(II) Complex with 110 K Wide Intermediate Plateau

Wolfgang Bauer^[a,b], Toni Pfaffeneder^[b], Klaus Achterhold^[c] and Birgit Weber^{*[a]}

[a] Inorganic Chemistry II, Universität Bayreuth, Universitätsstraße 30, NW I, 95440 Bayreuth, Germany. Fax: +49-92155-2157, E-mail: weber@uni-bayreuth.de

[b] Center for Integrated Protein Science Munich at the Department Chemie und Biochemie, Ludwig-Maximilians-Universität München, Butenandtstr. 5–13 (Haus F), D-81377 München, Germany

[c] Technische Universität München, Physik-Department E17, James-Franck Straße 1, 85747 Garching, Germany

Keywords: Spin Crossover, Coordination polymer, Magnetism, Mössbauer spectroscopy

Published in: *Eur. J. Inorg. Chem.* **2011**, DOI: 10.1002/ejic.201100224.

Abstract: Three new spin crossover compounds [FeL1(azpy)] (**1**), [FeL1(azpy)]·toluene (**1(tol)**) and [FeL2(azpy)] (**2**), (L1 and L2 are the tetradentate N₂O₂²⁻ coordinating Schiff base-like ligands {diethyl (*E,E*)-2,2'-[1,2-phenyl-bis(iminomethylidene)]bis[3-oxobutan-oate] (2-)-*N,N',O³,O^{3'}*} and {dimethyl (*E,E*)-2,2'-[1,2-phenyl-bis(iminomethylidene)]bis[3-oxo-utanoate] (2-)-*N,N',O³,O^{3'}*}, respectively, and azpy = 4,4'-azopyridine) are presented. All compounds have been investigated by using *T*-dependent susceptibility measurements, and different types of spin transitions are observed. In the case of **1** and **2**, intermediate plateaus ($\chi_{\text{HS}} \approx 0.5$) with widths of 110 and 75 K, respectively, were observed, while for **1(tol)** a gradual spin transition is obtained. Upon heating of **1(tol)** above 390 K, a loss of the included solvent molecule toluene is observed, which results in a two-step spin transition of the tempered sample similar to that of **1**. Mössbauer spectra of **1**, **1(tol)** and the tempered sample **1(temp)** reveal two different iron(II) sites in the low-spin (LS) state for all three samples. *T*-dependent Mössbauer spectra indicate that the nonequivalent iron centres are one but not the only reason for the wide plateau of **1**. Results from X-ray structure analysis of **1** in the region

of the plateau show the presence of two nonequivalent iron centres, of which one is in the high-spin (HS) state and one in the low-spin state. The 1D chains with alternating HS and LS iron centres are arranged in a parallel manner within one layer; between the different layers, the direction of the chains rotates by 90° relative to the previous one. This cross-linked arrangement with an interlocking of the layers is most likely the reason for the appearance of the wide plateau.

9.1 Introduction

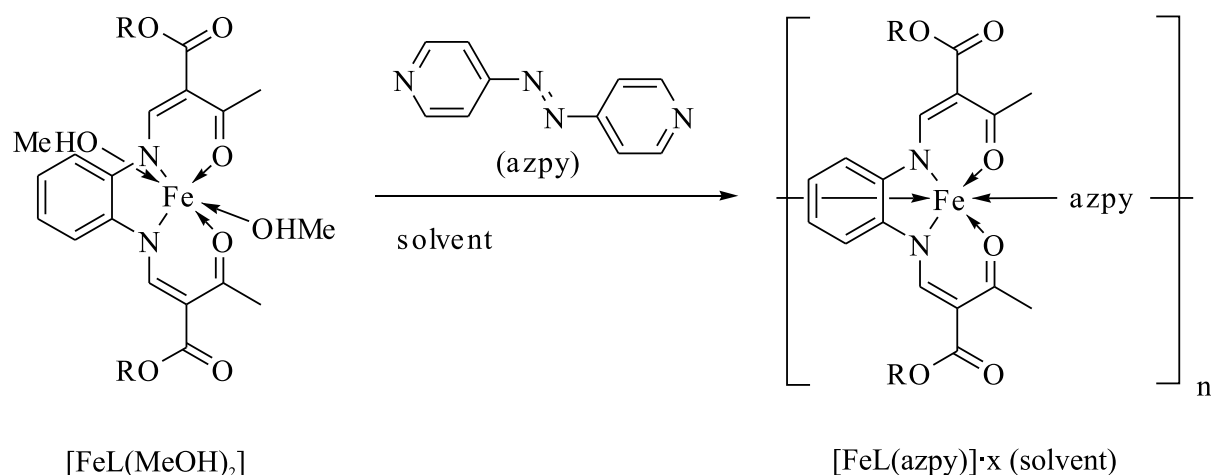
Spin transition complexes (spin crossover, SCO) are an interesting class of compounds that can be switched on the molecular level between two different states by the use of external perturbations such as temperature, pressure or electromagnetic radiation. The SCO bistability is one of the most promising aspects for new electronic devices in molecular memories and switches, as the switching progress is associated with a change in the magnetic and physical properties, which can be easily detected by different means.^[1,2] Of the possible types of spin transition, stepwise transitions between three or more states attracted the interest of several research groups, because of versatile switching possibilities.^[3] To date, three different possibilities are discussed for describing stepwise spin transitions. One is related to dinuclear complexes and explained with the formation of [HS-HS], [HS-LS] and [LS-LS] spin pair states (where HS and LS represent the local high-spin and low-spin states of the dinuclear species). These states could directly be monitored, for example, by Mössbauer spectroscopy and switched selectively by different wavelengths.^[3,4] An interplay between intramolecular magnetic exchange interactions and spin transition is made responsible for the step in the transition curve.^[3,5] Another possibility to have a multi-step spin transition is attributed to two (or more) different SCO sites, each undergoing a transition at different temperatures.^[6] We presented a mononuclear system clearly belonging to this category, with a large plateau in the range 225–125 K and at $\chi_{\text{HS}} \approx 0.25$. The reason for this behaviour is four nonequivalent iron(II) sites in the crystal lattice with slightly different chemical surroundings, which result from an additional distorted 4-cyanopyridine molecule, in combination with strong π - π interactions between two neighbouring molecules.^[6g] Finally, there are two examples of mononuclear complexes with a unique crystallographic iron(II) site, at which the effects of ferromagnetic-type long-range and antiferromagnetic-type short-range interactions of an

elastic origin induce a crystallographic phase transition that is responsible for steps in the transition curve.^[7,8] Those crystallographic phase transitions are accompanied or triggered by a symmetry breaking in the crystal, which leads to two^[9] or even more^[10] intermediate phases, each accompanied by a spin-state change in the system. Different theoretical models were developed to describe the HS/LS ordering in such systems.^[11]

Recently, the first two examples for a 1D polymeric material undergoing a two-step spin transition were presented by Neville, Murray and co-workers.^[12] In the case of the first complex, the two-step behaviour can be related to two different iron(II) environments, whereas for the second complex with a slightly broader intermediate plateau (IP), only one distinct iron(II) site is observed at all temperatures. Systematic investigations on a series of 1D chain compounds with the Schiff base like equatorial ligands used in our group, lead to different types of stepwise spin transition.^[13,14] Two different reasons were identified to be responsible for the step in the transition curve: nonequivalent iron sites in the HS state or, if a single iron site is observed in the HS state, a change in symmetry leading to a phase with two iron sites (HS, LS) in the region of the plateau. An analysis of the intermolecular interactions revealed that a pronounced zigzag structure of the 1D chain combined with restraining interactions between the 1D chains (several short contacts) favour such a phase transition and lead to steps in the transition curve.^[13]

In this work we present two iron(II) 1D coordination polymers [FeL1(azpy)] (**1**) and [FeL2(azpy)] (**2**), whose solvent-free samples show a complete two-step spin transition with an > 75-K wide IP around room temperature. The SCO of the solvent-containing sample [FeL1(azpy)]·toluene (**1(tol)**) is gradual but can be transferred to a two-step transition by solvent-loss. The complexes are based on a N₂O₂ coordinating Schiff base-like ligand system that was demonstrated to be highly suitable for the synthesis of iron(II) SCO complexes if combined with *N*-heterocycles as axial ligands.^[15] 4,4'-Azopyridine (azpy) was used as a bridging axial ligand. In Scheme 1 the formula of the used ligands and the general synthesis route is given.

9. Complete Two-Step Spin-Transition in a 1D Chain Iron(II) Complex with 110 K Wide Intermediate Plateau



L1: R = CH₂CH₃

L2: R = CH₃

Scheme 1. General synthesis of the 1D octahedral iron(II) coordination polymers discussed in this work.

9.2 Results

Magnetic measurements: The thermal dependence of the product $\chi_M T$ (χ_M is the molar susceptibility and T the temperature) for [FeL1(azpy)] (**1**) and [FeL1(azpy)]·toluene (**1(tol)**) is displayed in Figure 1. Both compounds reach their maximum $\chi_M T$ values not before 400 K. Compound **1** shows a complete two-step SCO with a wide IP, whereas **1(tol)** shows a complete gradual SCO at first, but after being heated to 400 K, the SCO behaviour changes into a two-step transition similar to that of **1**. The room temperature $\chi_M T$ value of **1** is 1.63 cm³ K mol⁻¹ and therefore in the region expected for an approximately 50:50 mixture of LS and HS iron centres. The maximum $\chi_M T$ value of 2.99 cm³ K mol⁻¹, indicative of iron(II) in the high-spin state, is obtained when **1** is heated to 400 K. Upon cooling, the $\chi_M T$ values decrease gradually in the temperature range 400–295 K to a value of 1.63 cm³ K mol⁻¹, which indicates that half of the iron(II) sites are in the HS state ($\chi_{\text{HS}} = 0.5$). The $T_{1/2}(1)$ value of this step is 326 K. In the whole temperature range 295–185 K, the $\chi_M T$ values slightly decrease by about 0.27 cm³ K mol⁻¹ to a value of 1.36 cm³ K mol⁻¹, which results overall in a 110-K wide IP. Below 185 K, the $\chi_M T$ values decrease rapidly to a minimum value of 0.08 cm³ K mol⁻¹ at 128 K, indicative of iron(II) in its diamagnetic LS state. Upon further cooling, the $\chi_M T$ values remain approximately constant. The $T_{1/2}^{\downarrow}(2)$ value of the second step is 152 K, which means a

9. Complete Two-Step Spin-Transition in a 1D Chain Iron(II) Complex with 110 K Wide Intermediate Plateau

separation distance between both $T_{1/2}$ values of 174 K. Upon heating, the $\chi_M T$ values remain approximately constant up to 150 K, followed by an abrupt increase, with $T_{1/2}^\uparrow(1) = 159$ K. This results in a thermal hysteresis loop with an average width of 7 K. Above 160 K, the curve progression of the heating and cooling mode is identical. The heating and cooling cycle could be repeated several times.

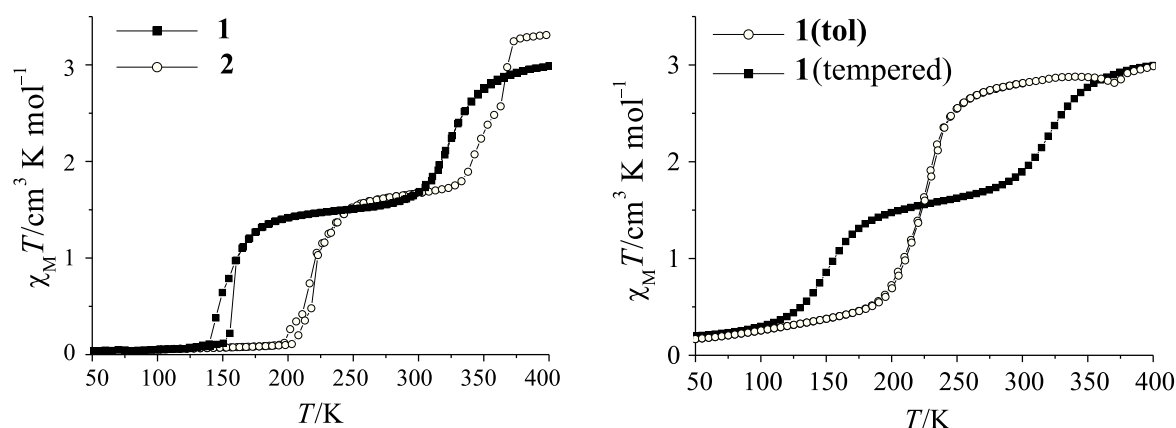


Figure 1. Plot of the $\chi_M T$ product vs. T over the temperature range 50 to 400 K. Left: compound **1** and compound **2**. Right: compound **1(tol)** and **1(tol)** after heating to 400 K (**1(temp)**).

The room temperature $\chi_M T$ value of **1(tol)** is $2.81 \text{ cm}^3 \text{ K mol}^{-1}$, which indicates that almost all iron(II) sites are in the HS state. Upon cooling, the $\chi_M T$ values decrease, gradually then more rapidly then again gradually, to attain a minimum value of $0.16 \text{ cm}^3 \text{ K mol}^{-1}$ at 50 K, indicative of iron(II) in the LS state. A thermal hysteresis is not observed upon heating. Above 300 K, the $\chi_M T$ values slightly increase to attain a maximum of $2.88 \text{ cm}^3 \text{ K mol}^{-1}$ at 340 K. The $T_{1/2}$ value of this SCO is 222 K. Further heating causes a decrease to a local minimum of $2.81 \text{ cm}^3 \text{ K mol}^{-1}$ at 370 K, before the $\chi_M T$ values finally increase up to $2.99 \text{ cm}^3 \text{ K mol}^{-1}$ at 400 K. This irregularity at about 370 K is probably due to the loss of the uncoordinated toluene molecule. This assumption is strengthened when measuring the tempered sample (**1(temp)**) in the cooling mode. The previously obtained gradual SCO behaviour is not observed, but a stepwise spin transition curve very similar to the solvent-free compound **1**. With a maximum $\chi_M T$ value of $2.99 \text{ cm}^3 \text{ K mol}^{-1}$ at 400 K and a minimum value of $0.16 \text{ cm}^3 \text{ K mol}^{-1}$ at 50 K, the two-step SCO of **1(temp)** is complete too. Marginal

differences can be found by looking at the $T_{1/2}$ values of **1**(temp) ($T_{1/2}(1) = 320$ and $T_{1/2}(2) = 150$ K), which are slightly lower than the values of **1** ($T_{1/2}(1) = 326$ and $T_{1/2}(2) = 152$ K). Further, the SCO curve progression of **1**(temp) is more gradual. Thermogravimetric measurements of **1**(tol) confirm the presumption that the loss of toluene has to be responsible for the different spin transition behaviour. At 388 K (boiling point toluene: 384.2 K), **1**(tol) has lost 13.7% of its mass (theory for one toluene molecule: 12.8%), which is consistent with the result from elemental analysis. The differences between the transition curves of **1** and **1**(temp) are most likely because of differences in the particle size (grinding effects).

The thermal dependence of the product $\chi_M T$ for compound [FeL2(azpy)] (**2**) is also plotted in Figure 1. Overall, **2** provides a complete two-step SCO that reaches its maximum $\chi_M T$ value of $3.30 \text{ cm}^3 \text{ K mol}^{-1}$, indicative of HS iron(II), not before 375 K. However, a closer look reveals an irregular curve progression, which could be confirmed by calculation of the first derivation of the curve (Supplementary material). Altogether four maxima at different temperatures were found, which correspond to four inflection points in the $\chi_M T$ vs. T plot. Starting at 400 K, the $\chi_M T$ values remain approximately constant between 400 and 370 K. Between 370 and 325 K, the $\chi_M T$ values rapidly decrease to attain a minimum value of $1.72 \text{ cm}^3 \text{ K mol}^{-1}$, which indicates that half of the iron(II) centres are in the HS state. The $T_{1/2}(1)$ value of this step is 365 K. During this first step, an anomaly is observed with an inflection point at 340 K. In the temperature range 325–250 K, the $\chi_M T$ values slightly decrease by about $0.18 \text{ cm}^3 \text{ K mol}^{-1}$ to a value of $1.54 \text{ cm}^3 \text{ K mol}^{-1}$, which results in a 75-K wide IP. Between 250 and 190 K, the $\chi_M T$ values rapidly decrease to a minimum value of $0.09 \text{ cm}^3 \text{ K mol}^{-1}$, indicative of iron(II) in the LS state. The $T_{1/2}^{\downarrow}(2)$ value of this step is 214 K. During this second step another anomaly, similar to the previous one, is observed with an inflection point at 199 K. Below 190 K, the $\chi_M T$ values remain approximately constant. Comparison with the heating mode reveals a 4-K wide hysteresis loop for the second step, with a $T_{1/2}^{\uparrow}(2)$ value of 218 K.

Mössbauer spectroscopy: The two-step SCO of **1** was followed by Mössbauer spectroscopy in the temperature range 80 to 300 K in the heating and cooling mode. For comparison, the Mössbauer spectra of **1(tol)** and **1(temp)** were recorded at selected temperatures. Selected spectra at different temperatures of the three compounds are given in Figure 2, and the corresponding values of the Mössbauer parameters obtained by least-squares fitting are given in Table 1. A complete list of all T -dependent Mössbauer parameters and a detailed description of the interpretation of the Mössbauer spectra is given in the Supplementary material.

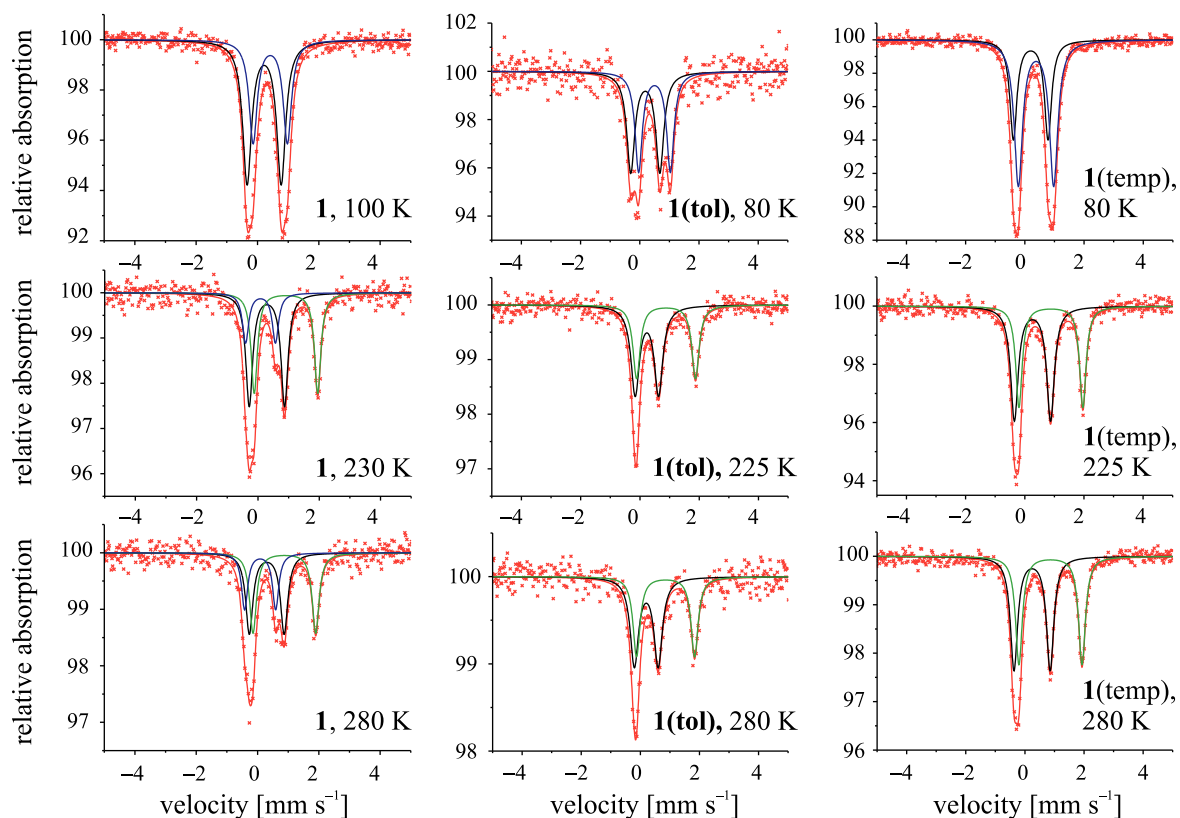


Figure 2. Mössbauer spectra of **1**, **1(tol)** and **1(temp)** at different temperatures; black and blue: LS and green: HS

9. Complete Two-Step Spin-Transition in a 1D Chain Iron(II) Complex with 110 K Wide Intermediate Plateau

At 80 K (**1**: until 150 K), the Mössbauer parameters of the three compounds are typical for octahedral iron(II) complexes of this ligand type in the LS state ($\Delta E_Q \approx 1.1 \text{ cm}^{-1}$, $\delta = 0.3\text{--}0.6 \text{ cm}^{-1}$)^[16,17] with no indication of a remaining HS fraction. The Mössbauer spectra of **1** and **1(temp)** are very similar, both consisting of a quadrupole split doublet with a wide line width, which suggests two (or more) nonequivalent iron centres. In the case of **1(tol)**, two quadrupole split doublets of two nonequivalent iron centres are clearly visible. Upon heating, a new quadrupole split doublet appears with parameters ($\Delta E_Q \approx 2.0 \text{ cm}^{-1}$, $\delta \approx 1.0 \text{ cm}^{-1}$) typical for iron(II) complexes in the HS state.^[16,17]

Table 1. Representative least-squares-fitted Mössbauer data for **1**, **1(tol)** and **1(temp)**.

compound	low-spin 1		low-spin 2		high-spin	
	$\delta^{[a]}$	$\Delta E_Q^{[a]}$	$\delta^{[a]}$	$\Delta E_Q^{[a]}$	$\delta^{[a]}$	$\Delta E_Q^{[a]}$
<u>80 K</u>						
1 (100 K)	0.33(1)	1.11(1)	0.53(1)	1.12(1)		
1(tol)	0.30(1)	0.98(1)	0.61(2)	1.07(2)		
1(temp)	0.31(1)	1.17(1)	0.49(1)	1.19(1)		
<u>225 K</u>						
1 (230 K)	0.19(1)	0.98(2)	0.40(1)	1.15(1)	1.03(1)	2.07(1)
1(tol)	0.34(1)	0.79(2)			0.99(1)	1.99(2)
1(temp)	0.37(1)	1.22(1)			0.99(1)	2.16(1)
<u>280 K</u>						
1	0.20(1)	1.01(2)	0.41(1)	1.14(2)	0.99(1)	2.05(1)
1(tol)	0.31(1)	0.81(2)			0.96(1)	1.96(2)
1(temp)	0.35(1)	1.22(1)			0.98(1)	2.14(1)

[a] Isomer shifts (δ , mm s^{-1}) refer to α iron; ΔE_Q = quadrupole splitting (mm s^{-1}). Statistical standard deviations are given in parentheses.

At 280 K, the spin transition is not complete for all three compounds, in agreement with the outcomes from the susceptibility measurements. However, in the case of **1(tol)** a nearly complete spin transition would be expected that is not reflected in the spectrum at 280 K. Probably, during the long measurement time (one month at 280 K), a partial loss of the

included toluene occurs. For **1(tol)** and **1(temp)** two quadrupole split doublets are observed, one is assigned to the HS and one to the LS state. This behaviour is expected for a stepwise SCO because of nonequivalent iron centres. Despite this observation, in the case of **1(tol)** a one-step spin transition is observed. In the case of **1**, three quadrupole split doublets are clearly visible—two belong to the LS and one to the HS state. This is unexpected, as, in this case, a stepwise spin transition is observed. If nonequivalent iron centres are responsible for the step, one would assume that first one and then the second iron centre undergo spin transition. Thus, at the IP, one doublet for the HS state and one doublet for the LS state should be observed as described for **1(tol)**. For the 1D chain compounds investigated here the situation is more complex. Although the area of one of the LS doublets ($\Delta E_Q = 1.11 \text{ cm}^{-1}$, $\delta = 0.33 \text{ cm}^{-1}$) decreases at the beginning of the spin transition, it does not completely vanish, but instead the area of the second LS doublet ($\Delta E_Q = 1.12 \text{ cm}^{-1}$, $\delta = 0.53 \text{ cm}^{-1}$) starts to decrease, while the area of the HS doublet continuously increases. A good agreement between the transition curve obtained by Mössbauer spectroscopy and SQUID measurements is obtained as given in Figure 3. However, the nonequivalent iron centres detected by Mössbauer spectroscopy in the LS state clearly cannot be the only reason for the wide IP in the transition curve of **1**, as they are also observed for **1(tol)** with the gradual spin transition.

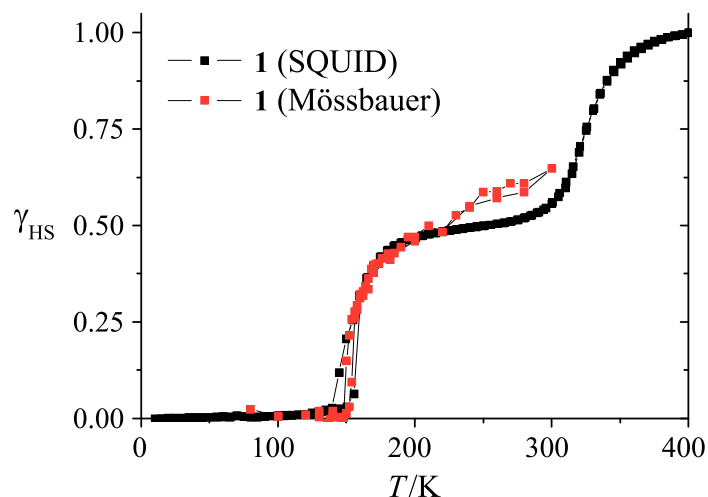


Figure 3. Thermal dependence of γ_{HS} of **1** obtained from Mössbauer spectroscopy and SQUID measurements.

X-Ray structure analysis: Crystals suitable for X-ray structure analysis were obtained for compound **1**. Additionally, a few single crystals were obtained from a diluted toluene solution of **1(tol)** with the composition $[\text{FeL1}(\text{azpy})] \cdot 2 \text{ toluene}$ (**1(2 tol)**). The crystal structure of **1** was determined on the IP at 200 K and in the LS state at 130 K. Unfortunately, the crystallographic data of the LS structure were inferior, as twinning occurred upon phase transition while cooling down. As a result of technical limitations, a lower temperature was not accessible and therefore only the structure motif is presented here. The crystal structure of **1(2 tol)** was determined at 173 K. The crystallographic data of the complexes are summarised in Supporting Information Table S1. Selected bond lengths and angles within the inner coordination sphere of the iron(II) ion are summarised in Table 2. ORTEP drawings of the asymmetric units of **1** (200 K) and **1(2 tol)** are given in Figure 4, the atom numbering scheme is indicated. In Figure 5, the asymmetric unit of **1** in the LS state is shown. For both materials, structure analysis reveals an octahedral iron(II) N_4O_2 environment consisting of one equatorially coordinated Schiff base-like ligand with N_2O_2 binding sites and two axially coordinated azpy ligands bound through terminal pyridyl groups. Each azpy ligand bridges two iron(II) centres to form infinite 1D chains.

Compound **1** crystallises at room temperature in the region of the IP with the orthorhombic space group $P2_12_12_1$. The asymmetric unit contains two crystallographically distinct iron(II) centres, one can be assigned to iron(II) in the HS state (Fe1) and one to iron(II) in the LS-state (Fe2). The averaged metal-ligand distances around the inner coordination sphere of Fe1 (Fe1- N_{eq} : 2.09 Å, Fe1- O_{eq} : 2.01 Å, Fe1- N_{ax} : 2.25 Å) indicate a distorted, axially elongated octahedral environment, typically for HS iron(II) of this ligand type.^[15,16,17] The averaged metal-ligand distances in the $[\text{FeN}_4\text{O}_2]$ coordination core of Fe2 (Fe2- N_{eq} : 1.90 Å, Fe2- O_{eq} : 1.93 Å, Fe2- N_{ax} : 1.99 Å) are about 10% shorter than those for the HS state, as discussed in the literature for iron(II) SCO complexes.^[1] Especially, the pronounced reduction of the Fe- N_{ax} distance (0.26 Å) in the direction of a more regular octahedral environment is indicative of LS iron(II). The O-Fe-O angle, the so-called bite of the ligand, is another characteristic tool to determine the spin state of the central iron(II) ion for this type of complex, as it changes from about 110° in the HS state to about 90° in the LS state.^[16] The bite angle for Fe1 (112°) suggests that it is clearly in the HS state and that for Fe2 (88°) indicates that it is clearly in the LS state.

9. Complete Two-Step Spin-Transition in a 1D Chain Iron(II) Complex with 110 K Wide Intermediate Plateau

Analysis of the polymeric structure shows the formation of infinite one-dimensional chains with the base vector [1 0 1]. Along the chains, an alternating arrangement of HS and LS iron(II) centres is observed, which results in a mixed spin state with $\chi_{\text{HS}} \approx 0.5$, in agreement with the magnetic measurements. The intrachain Fe1...Fe2 separation distances alternate between 13.2 and 13.3 Å. The azpy bridging ligand is strongly distorted, as the planes, which are spanned by the pyridyl rings are twisted by about 37° and 53°, respectively, to each other. This leads overall to a straight-lined progression of the chains. In contrast to compound **1**, coordination polymers with the closely related bridging ligands bpee and bpea (bpee = bis(4-pyridyl)ethylene, bpea = bis(4-pyridyl)ethane) do not show distortions of the linker molecules, and, therefore, a stepped chain progression is observed.^[13,16f] Upon cooling to 130 K, the symmetry of the system is reduced to the monoclinic space group $P2_1$. This structural phase transition is one explanation for the observed hysteresis at the second step of the spin transition curve. It is also responsible for the decrease in quality of the data as the formation of domains is highly likely. The asymmetric unit contains four crystallographic distinct iron(II) centres (Figure 5). As can be seen from Table 3, the bite of the ligand of these iron(II) centres is in the range 85.5–92.8°, and, therefore, all iron(II) centres are definitively in the LS state.

Table 2. Selected bond lengths [Å] and angles [degree] within the inner coordination sphere of HS ($S = 2$) and LS ($S = 0$) iron centres of **1** (200 K) and **1(2 tol)** (173 K).

compound	S	Fe-N _{eq}	Fe-O _{eq}	Fe-N _{ax}	O _{eq} -Fe-O _{eq}	N _{ax} -Fe-N _{ax}
1	2	2.090(3)	2.016(3)	2.214(3)	112.4(1)	176.1(1)
	(Fe1)	2.083(3)	2.006(3)	2.283(3)		
	0	1.891(3)	1.933(3)	1.976(3)	87.6(1)	179.0(1) ^[a]
	(Fe2)	1.903(3)	1.934(3)	2.001(3) ^[a]		
1(2 tol)	2	2.046(5)	1.991(4)	2.209(5) ^[b]	105.2(2)	177.1(2) ^[b]
		2.051(5)	1.989(4)	2.217(5)		

Symmetry codes: [a] $-1 + x, y, -1 + z$; [b] $1 + x, y, 1 + z$.

9. Complete Two-Step Spin-Transition in a 1D Chain Iron(II) Complex with 110 K Wide Intermediate Plateau

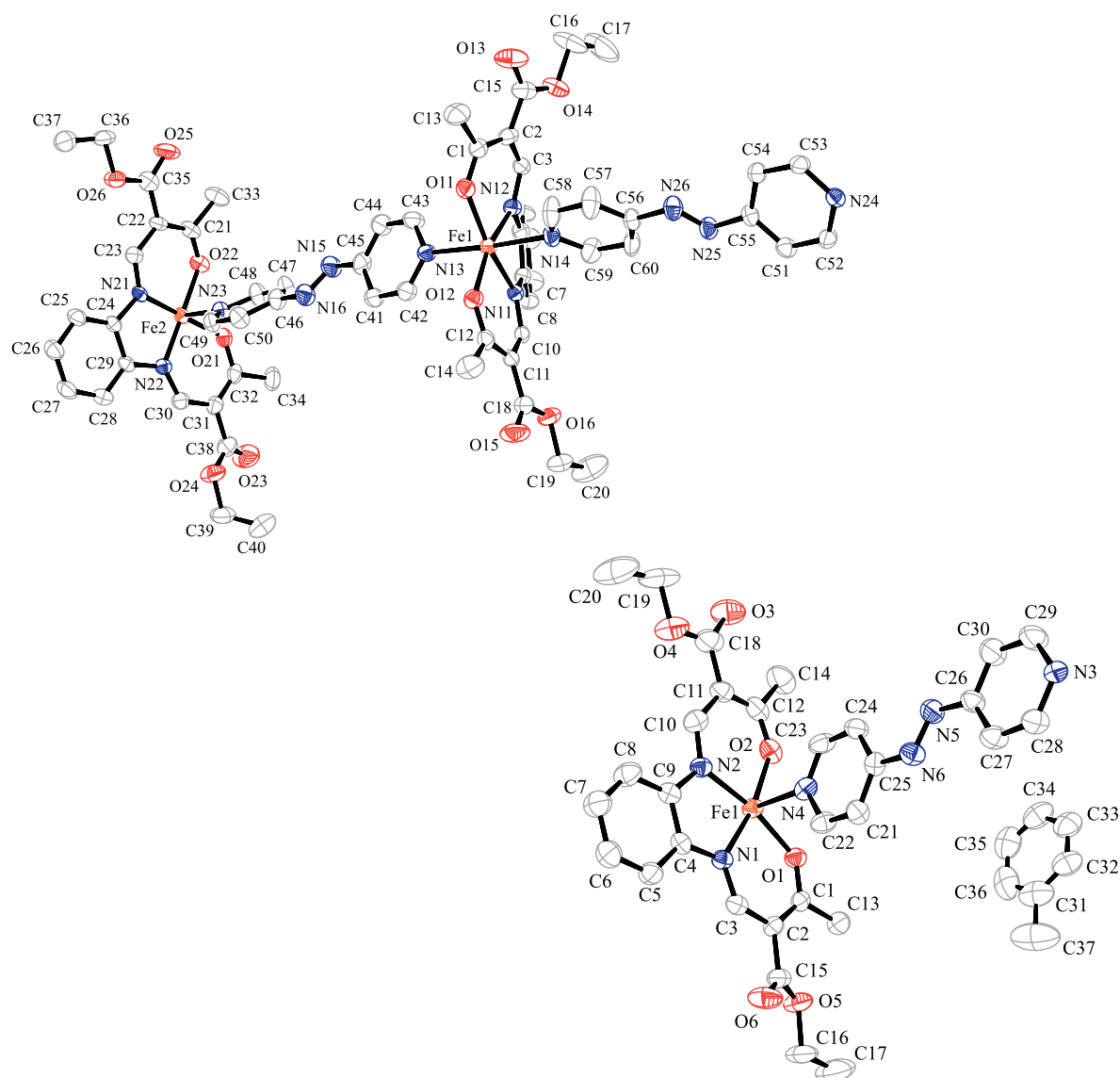


Figure 4. ORTEP drawings of the asymmetric units; top: **1** (200 K), bottom: **1(2 tol)** (173 K). Hydrogen atoms as well as both disordered half occupied toluene molecules of **1(2 tol)** have been omitted for clarity. Displacement ellipsoids are shown with a 50% probability.

Compound **1(2 tol)** crystallises with the monoclinic space group $P2_1/c$. The asymmetric unit contains one crystallographic distinct iron(II) centre that is clearly in the HS state (Fe-N_{ax} : 2.21 Å, $\text{O}_{\text{eq}}\text{-Fe-O}_{\text{eq}}$: 105°). Together with the complex, uncoordinated solvent toluene was found to be intercalated within the asymmetric unit; one regular toluene molecule in addition to two disordered half occupied molecules. The composition of the crystals of **1(2 tol)** significantly differs from the powder sample of **1(tol)** used for the SQUID and Mössbauer measurements. For those studies, only one toluene molecule is observed according to

9. Complete Two-Step Spin-Transition in a 1D Chain Iron(II) Complex with 110 K Wide Intermediate Plateau

elemental analysis and DTG measurements. At 173 K, **1(tol)** is in the LS state according to SQUID and Mössbauer measurements, while the results from X-ray structure analysis of **1(2 tol)** clearly indicate that the crystals are in the HS state at 173 K. Thus, the powder sample **1(tol)** and the crystals **1(2 tol)** are clearly two different samples. An analysis of the polymeric structure of **1(2 tol)** indicates the formation of infinite one-dimensional chains that propagate along the [1 0 1] direction. In contrast to that for compound **1**, the azpy ligand is not distorted and a stepped chain progression is observed. The intrachain Fe···Fe separation distance is 13.4 Å and is similar to that of **1**.

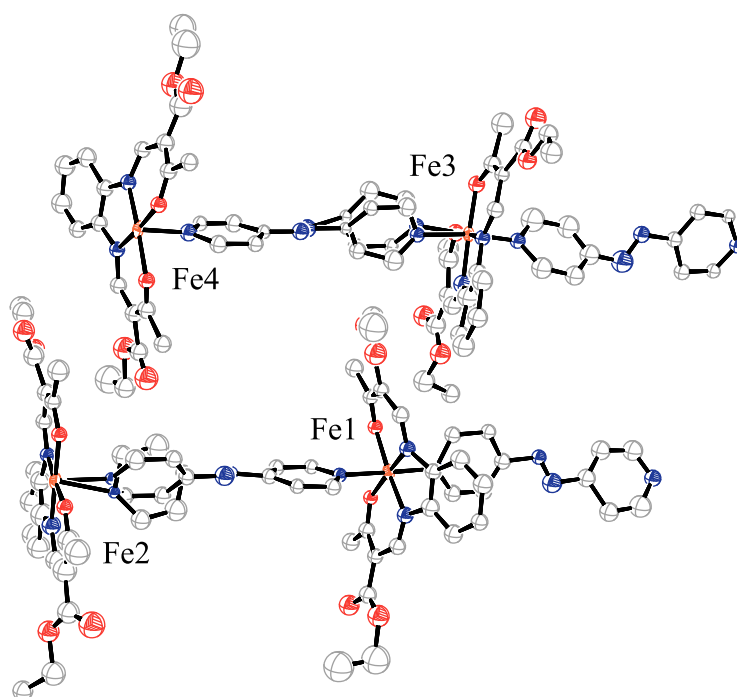


Figure 5. Asymmetric unit of the LS structure motif of **1** (130 K) with the nonequivalent iron(II) centres numbered. Hydrogen atoms have been omitted for clarity. Displacement ellipsoids are shown with a 50% probability.

Table 3. Bite of the ligand [°] of the 4 nonequivalent iron(II) LS centres of the low-temperature structure of **1**.

	Fe1	Fe2	Fe3	Fe4
O _{eq} -Fe-O _{eq}	91.9	85.8	88.5	92.8

Intermolecular investigations: In order to find possible reasons for the wide step in the transition curve of **1**, a detailed investigation of the intermolecular interactions and the molecule packing is necessary. As can be seen in Figure 6, compound **1** exhibits a layered structure. Within each layer, the chains are arranged in a parallel manner (Figure 6A). The shortest Fe··Fe separation distance between adjacent chains is 12.5 Å (Fe1··Fe2*) and no short contacts (contacts shorter than the sum of the van der Waals-radii minus 0.19 Å) can be found. From symmetry reasons it follows that altogether four layers A, B, C and D, can be observed in which the direction of the chains rotates by 90° relative to the previous layer (i.e. A: 0°; B: 90°; C: 180°; D: 270°) (Figure 4B, C), which results overall in a rectangular arrangement of the chains. As a consequence, the chains in layer A and C run perpendicular to the chains in layers B and D, whereas the chains of A and C, respectively B and D, proceed in an (anti-)parallel fashion. The shortest separation distance of two iron centres between layers of perpendicular chains is 8.51 Å (Fe1··Fe2*). This is smaller than the shortest Fe··Fe separation distance between (anti-)parallel chains (9.26 Å, Fe1··Fe2*) and even much smaller than the shortest intrachain distance. This is, to the best of our knowledge, the first example of a 1D chain iron(II) SCO complex with a rectangular arrangement of the single chains. This allows a very dense molecule packing and an interlocking of the layers, what could be one reason for the broadness of the IP.

In general, a HS to LS transition in 1D chain compounds involves a relocation of the ligands towards the smaller LS molecule. If the Fe··Fe distances within the chain cannot follow the changes in Fe-L bonds because of restraining interactions, a stabilisation of a mixed HS/LS state can be observed.^[13,18] We recently showed for 1D chain SCO complexes that a pronounced zigzag chain motif as well as a dense packing (intermolecular contacts shorter than the sum of the van der Waals radii) is responsible for restraining interactions between the chains and hence stabilise the mixed HS/LS state of a step.^[13] In the case of compound **1**, the rigid packing and cross-linking of the chains probably counteracts the structural changes expected for a SCO system in a way similar to that observed for the zigzag 1D chains. During the HS to LS transition, a shortening of the bond lengths of one iron centre results in an elongation of the bond length of the neighbouring iron centre. The latter is involved in the stabilisation of the HS state at this iron centre and thus has a lower transition temperature. In fact, a number of intermolecular non-classical hydrogen bonds of the type C-H··O, which are listed in Table 4, can be found between the layers, which support this theory, as stabilised

9. Complete Two-Step Spin-Transition in a 1D Chain Iron(II) Complex with 110 K Wide Intermediate Plateau

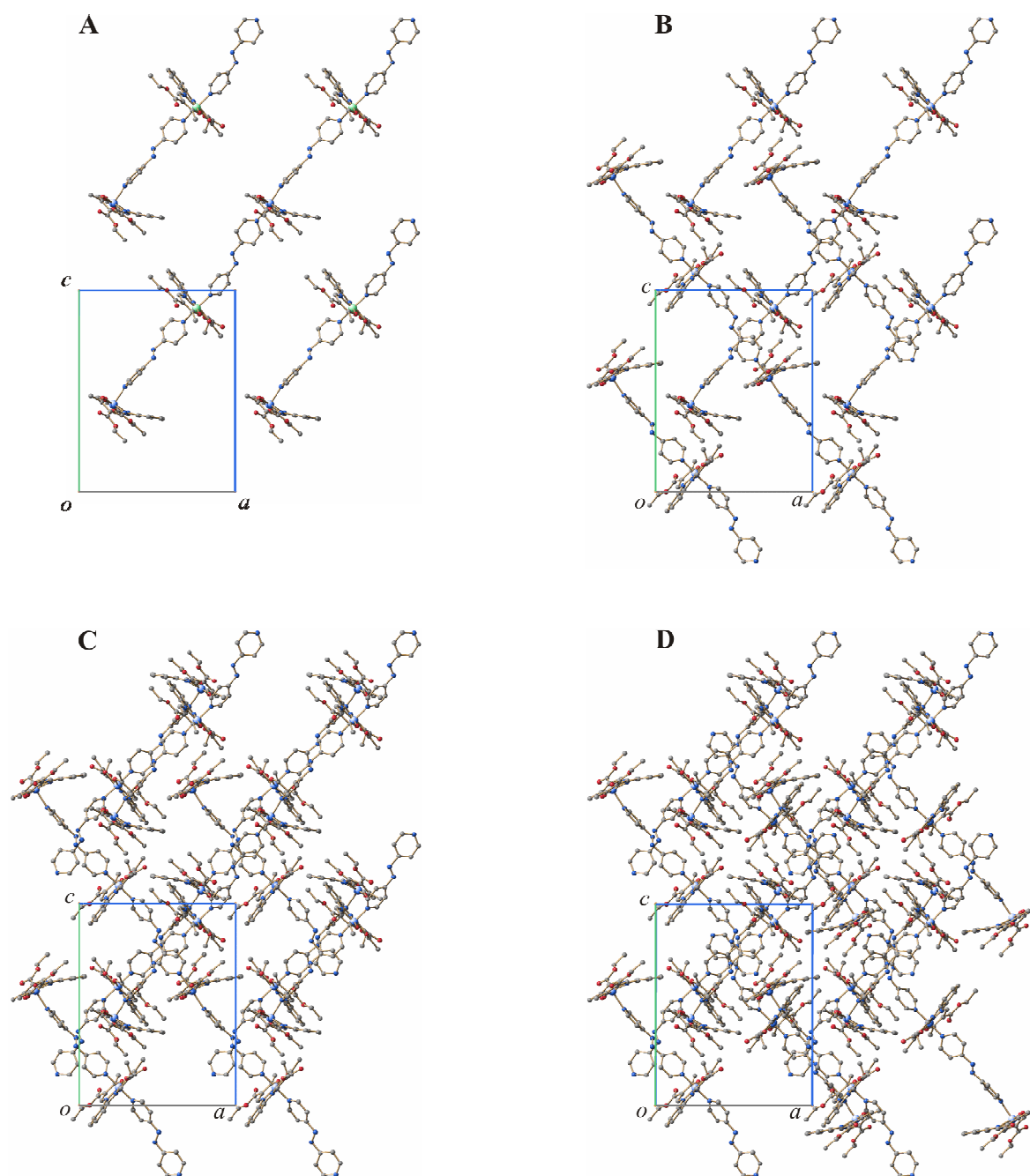


Figure 6. Packing of the polymer chains of **1** in the crystal projected in the ac -plane. For a better illustration of the layered, planar structure and the rectangular arrangement of the chains, the unit cell content along the b axis is displayed layer-by-layer: 20% (A), 50% (B) and 70% (C) and 100% (D).

9. Complete Two-Step Spin-Transition in a 1D Chain Iron(II) Complex with 110 K Wide Intermediate Plateau

[HS···LS] pairs are built between adjacent chains. The hydrogen bond involving oxygen atom O13 (Fe1, HS) and hydrogen atom H50 (Fe2, LS), directly links a HS and a LS centre of adjacent perpendicular chains. In the same way, intermolecular [HS···LS] pairs are built between (anti-)parallel chains through the hydrogen bonds involving O25 (Fe2)/H41 (Fe1) and O15 (Fe1)/H53/54 (Fe2), respectively.

Table 4. Bond lengths [Å] and angles [degree] of intermolecular interactions with $d(\text{D} \cdots \text{A}) < R(\text{D}) + R(\text{A}) + 0.50$, $d(\text{H} \cdots \text{A}) < R(\text{H}) + R(\text{A}) - 0.12$ Å, $\text{D}-\text{H} \cdots \text{A} > 100.0^\circ$ of compound **1**.

compound	D	H	A	D-H	H···A	D···A	D-H···A
1	C41	H41	O25 ^[a]	0.95	2.49	3.119(5)	123
	C50	H50	O13 ^[b]	0.95	2.49	3.262(5)	139
	C53	H53	O15 ^[c]	0.95	2.36	3.015(5)	126
	C54	H54	O15 ^[c]	0.95	2.52	3.085(5)	118
1(2 tol)	C29	H29	O3 ^[d]	0.95	2.56	3.204(8)	126

Symmetry codes: [a] $-x, \frac{1}{2} + y, \frac{1}{2} - z$; [b] $\frac{1}{2} - x, 1 - y, -\frac{1}{2} + z$; [c] $1 - x, -\frac{1}{2} + y, \frac{3}{2} - z$; [d] $-x, -y, 1 - z$.

To quantitatively describe the structural properties derived from X-ray structure analysis, we recently established the crystal contact index (CCI), which correlates the sum of intermolecular contacts with the strength of the cooperative effect.^[14] The CCI scale proved to provide a good estimation to accompany the structural interpretation of spin transition properties.^[11] All short intermolecular contacts (shorter than sum of van der Waals radii) are listed in Supplementary material. The corresponding CCI value of 2.0 for compound **1** indicates a relatively high cooperativity (gradual SCO: < 1.5), which is in line with the strong restraining interactions observed as a result of the cross-linking of the chains and thus satisfactorily explains the wide IP. Because of the inferior structural data of the low-temperature structure of **1**, no far-reaching conclusions can be drawn with regard to the intermolecular short contacts. However, the structure motif of the molecule packing displayed in Figure 7 reveals a cross-linked arrangement of the chains as well.

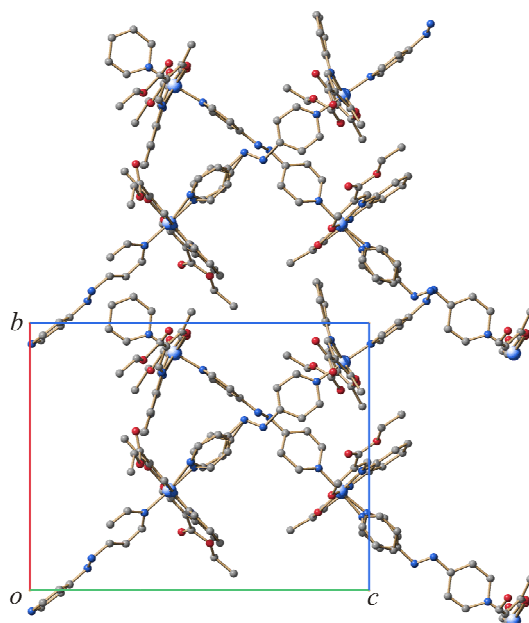


Figure 7. Packing of the polymer chains of the low-temperature structure motif of **1**, projected in the *bc*-plane. For clarity reasons only 50% of the unit cell content along the *a* axis is displayed.

An excerpt of the molecule packing of **1(2 tol)** is shown in Figure 8. In contrast to the packing of compound **1**, all chains run in a parallel fashion. The chains are arranged such that, between the bulky equatorial ligands and the smaller axial ligand, tube-like solvent accessible void volumes, reminiscent of molecule organic frameworks (MOFs), occur along the *a* and *c* axis, in which the toluene molecules are intercalated (Figure 8). The shortest Fe···Fe separation distance between adjacent chains is 9.36 Å, and therefore shorter than within the chain, but longer than that in **1**. As consequence, the total number of short contacts between adjacent chains is smaller (Supplementary material) and only one non-classical hydrogen bond is observed, which involves the carbonyl oxygen atom O3 of the equatorial ligand and H29 at the pyridyl ring of the axial ligand. As expected, the CCI of compound **1(2 tol)** is relatively low (0.4), indicative of very weak cooperativity.^[11] Unfortunately, we were not able to get enough crystals of **1(2 tol)** to do any magnetic measurements

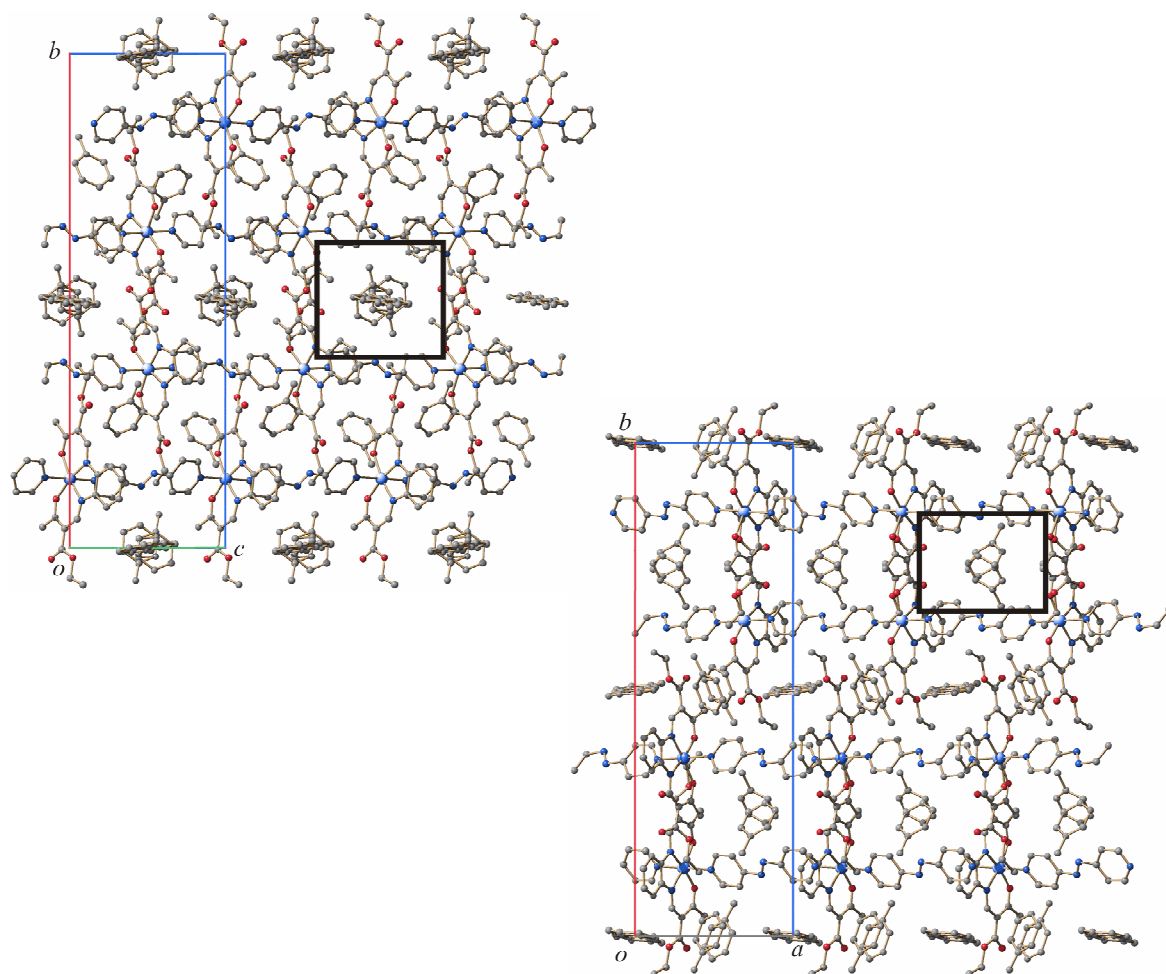


Figure 8. Packing of the polymer chains of **1(2 tol)** in the crystal projected in the *bc*-plane (left) and the *ab*-plane (right). The tube-like void volumes with intercalated toluene are highlighted for clarification.

9.3 Discussion

In order to reach an application for SCO compounds, a purposeful synthesis of such materials with defined properties is essential. Consequently, the question needs to be answered, why in the case of **1** and **2** such wide IPs are observed. The first suggestion from the X-ray structure analysis of **1** and the Mössbauer spectra would be that nonequivalent iron centres are responsible for the different transition temperatures. However, the Mössbauer parameters of **1(tol)** are very similar to that of **1**, and here two nonequivalent iron centres are clearly visible, although, in the magnetic measurements, only a gradual one-step spin transition is observed. The fact that the magnetic behaviour of **1(tol)** changes from gradual to steplike with the loss of toluene, similar to that seen in the $\chi_M T$ curve of **1**, leads to the assumption that the structure

of **1(tol)** has to be more related to **1** than to **1(2 tol)**. Thus, it is highly probable that the special cross-linked arrangement of the 1D chains of **1** is responsible for the 110-K wide IP. As a very similar SCO is observed for **2**, a similar structure can be assumed that is probably related to the azpy ligand.

Next to the reasons for steps in the transition curve, it is important to investigate and understand the influence of solvent-inclusions on the magnetic behaviour of SCO materials, as future applications as solvent-sensors are foreseeable. It is well known that solvent molecules intercalated into the crystal structure can either enhance or diminish cooperative effects and spin transition.^[1] Networks of the stoichiometry $[\text{Fe}(\text{bpee})_2(\text{NCS})_2]$ ^[19] and $[\text{Fe}(\text{azpy})_2(\text{NCS})_2]$ ^[20] represented the first porous 2D grid metal-organic frameworks that exhibit a spin-state change triggered by host-guest chemistry, several further examples followed.^[21] A similar dependence can be observed for the system described here: at room temperature, the solvent-free compound **1** is at the IP; if one toluene molecule is included, the complex is switched to the HS state (**1(tol)**). Similar effects were observed for related 1D chain SCO compounds of these Schiff base-like equatorial ligands.^[13] It appears that solvent effects are much more pronounced for 1D chain materials than for mononuclear complexes of the same ligand type. Further going investigations with regard to the reversibility of those effects are in progress.

9.4 Conclusion

In this work, we presented the synthesis and characterisation of new SCO coordination polymers with up to a 110-K wide IP. The complexes were investigated by using *T*-dependent susceptibility measurements, Mössbauer spectroscopy and X-ray diffraction. The results show that a clear assignment of the reasons for such a wide intermediate plateau is difficult. Although in-equivalent iron centres are observed in the Mössbauer spectra and X-ray structures, their *T*-dependent behaviour indicates that this is not the only factor responsible for the plateau. The special cross-linked arrangement of the 1D chains of **1** also contributes to the spin transition behaviour. The results provide a unique insight into the formation of a two-step spin transition and nicely show the influence of solvent molecules on a SCO.

9.5 Experimental Section

Magnetic measurements: Magnetic susceptibility data were collected with a Quantum Design MPMSR2 SQUID magnetometer under an applied field of 0.5 T over the temperature range 50 to 400 K in the settle mode. All samples were placed in gelatine capsules held within plastic straws. The data were corrected for the diamagnetic magnetisation of the ligands, which were estimated by using tabulated Pascal's constants, and of the sample holder.

Mössbauer spectroscopy: Mössbauer spectra have been recorded by using a conventional Mössbauer spectrometer operating in a sinusoidal velocity profile. The sample was placed in a bath cryostat (Cryo Industries of America Inc., Model 11CC).

Differential thermogravimetry: The thermal behaviour was studied by using a Setaram TG-92 equipped with a protected DTA-TG rod. The measurement was conducted under streaming Helium atmosphere at a scanning rate of 10 K min⁻¹ by using 100 mL alumina crucibles.

X-Ray crystallography: The intensity data of **1** and **1(tol)** were collected on a Nonius Kappa CCD diffractometer by using graphite-monochromated MoK_α radiation. The data were corrected for Lorentz and polarisation effects. The structure was solved by direct methods (SIR-97)^[22] and refined by full-matrix least-square techniques against F_0^2 (SHELXL-97).^[23] The hydrogen atoms were included at calculated positions with fixed displacement parameters. All non-hydrogen atoms were refined anisotropically. ORTEP-III^[24] was used for the structure representation, SCHAKAL-99^[25] for the representation of the molecule packing. Cell parameters and refinement results are summarised in Supporting Information Table S1.

Synthesis: If not described differently, all syntheses of the iron(II) complexes were carried out under argon by using Schlenk tube techniques. All solvents were purified as described in the literature^[26] and distilled under argon. The syntheses of anhydrous iron(II) acetate,^[27] ligand H₂L1,^[28] ligand H₂L2^[29] and the precursors [FeL1(MeOH)₂]^[30] and [FeL2(MeOH)₂]^[26] were published before. 4-Aminopyridine was purchased from Aldrich Chemical Co. and used as received. All complex syntheses were reproduced at least once.

4,4'-Azopyridine (azpy): 4,4'-Azopyridine was prepared by oxidative coupling of 4-aminopyridine and hypochlorite by using an adaption of Launay *et al.*^[31] A cold solution of 4-aminopyridine (5.05 g, 53.7 mmol) in water (100 mL) was added dropwise to a 6.5% NaOCl

9. Complete Two-Step Spin-Transition in a 1D Chain Iron(II) Complex with 110 K Wide Intermediate Plateau

solution (300 mL). The mixture was stirred at 5 °C as an orange precipitate formed. After completion of the addition, the reaction mixture was stirred for another 15 min. The precipitate was filtered off and washed with cold water. The aqueous phase was extracted three times with diethyl ether. The combined organic phases were dried on MgSO₄, and the solvent evaporated. The crude products were recrystallised from water to yield 4,4'-azopyridine as orange needles (yield: 1.70 g, 34%). ¹H NMR (270 MHz, CDCl₃, 25 °C, TMS): δ = 8.9 (m, 4H, Ar-H), 7.7 ppm (m, 4H, Ar-H); MS (DEI(+), 70 eV): *m/z* (%): 184 (55) [*M*⁺], 78 (100) [C₅H₄N⁺]; elemental analysis calcd (%) for C₁₀H₈N₄ (184.20): C 65.21, H 4.38, N 30.42; found: C 64.67, H 4.20, N 30.18.

[FeL1(azpy)] (1): [FeL1(MeOH)₂] (0.26 g, 0.51 mmol) and azpy (0.47 g, 2.57 mmol) were dissolved in ethanol (40 mL) and heated to reflux for 4 h. Compound **1** precipitated from the reaction mixture after 4 d at room temperature in the form of black crystals, which were filtered off, washed with ethanol and dried *in vacuo* (yield: 0.25 g, 78%). IR (KBr): $\tilde{\nu}$ = 1686 (COO), 1566 (CO) cm⁻¹; MS (DEI(+), 70 eV): *m/z* (%): 442 (20) [FeL1⁺], 184 (48) [azpy⁺]; elemental analysis calcd (%) for C₃₀H₃₀FeN₆O₆ (626.44): C 57.52, H 4.83, N 13.42; found: C 57.16, H 4.70, N 12.91.

[FeL1(azpy)]·toluene (1(tol)): [FeL1(MeOH)₂] (1.11 g, 2.19 mmol) and azpy (2.02 g, 11.0 mmol) were dissolved in toluene (60 mL) and warmed to 80°C for 1 h. Compound **1(tol)** was obtained after 1 d at room temperature in the form of a black microcrystalline precipitate, which was filtered off from the reaction mixture, washed with toluene and dried *in vacuo*. (yield: 1.41 g, 90%). IR (KBr): $\tilde{\nu}$ = 1685 (COO), 1566 (CO) cm⁻¹; MS (DEI(+), 70 eV): *m/z* (%): 442 (100) [FeL1⁺], 184 (25) [azpy⁺]; elemental analysis calcd (%) for C₃₀H₃₀FeN₆O₆·C₇H₈ (718.58): C 61.84, H 5.33, N 11.70; found: C 62.79, H 5.41, N 11.32.

The mother liquor of **1(tol)** was allowed to stand at 4 °C. After two months, black crystals with the composition **1(2 tol)** had formed, which were of sufficient quality for crystal structure analysis.

[FeL2(azpy)] (2): [FeL2(MeOH)₂] (0.30 g, 0.63 mmol) and azpy (0.59 g, 3.20 mmol) were dissolved in methanol (20 mL) and heated to reflux for 1 h. After 16 h at 4 °C, **2** precipitated from the reaction mixture in the form of a black, microcrystalline solid, which was filtered off, washed with methanol and dried *in vacuo* (yield: 0.14 g, 37%). IR (KBr): $\tilde{\nu}$ = 1692 (COO), 1567 (CO) cm⁻¹; MS (DEI(+), 70 eV): *m/z* (%): 414 (100) [FeL2⁺], 184 (35) [azpy⁺];

9. Complete Two-Step Spin-Transition in a 1D Chain Iron(II) Complex with 110 K Wide Intermediate Plateau

elemental analysis calcd (%) for $C_{28}H_{26}FeN_6O_6$ (598.39): C 56.20, H 4.38, N 14.04; found: C 55.81, H 4.41, N 13.99.

Supplementary material: The details for the analysis of the Mössbauer spectra and the least-squares-fitted Mössbauer data, the analysis of short inter-molecular contacts of **1** and **1(2 tol)**, the first derivative of the $\chi_M T$ vs. T plot of **1(tol)** and **2** and the crystallographic information files (CIF) of **1** and **1(2 tol)** are available on the WWW under <http://www.eurjic.org/> or from the author.

Acknowledgments

This work has been supported financially by the Deutsche Forschungsgemeinschaft (SPP 1137), the Fonds der Chemischen Industrie and the Center for Integrated Protein Science Munich (CIPSM).

9.6 References

- [1] a) H.A. Goodwin, *Coord. Chem. Rev.*, **1976**, *18*, 293; b) E. König, *Struct. Bonding (Berlin)* **1991**, *76*, 51; c) P. Gülich, A. Hauser, H. Spiering, *Angew. Chem. Int. Ed. Engl.* **1994**, *33*, 2024, and references therein; d) P. Gülich, H.A. Goodwin (Eds.), *Spin Crossover in Transition Metal Compounds I–III, Topics in Current Chemistry*, Springer, Berlin, Heidelberg, New York **2004**; e) J.A. Real, A.B. Gaspar, M.C. Munoz, *Dalton Trans.* **2005**, 2062; f) K. Nakano, N. Suemura, K. Yoneda, S. Kawata, S. Kaizaki, *Dalton Trans.* **2005**, 740; g) O. Sato, J. Tao, Y.-Z. Zhang, *Angew. Chem.* **2007**, *119*, 2200; *Angew. Chem. Int. Ed.* **2007**, *46*, 2152; h) J.A. Kitchen, S. Brooker, *Coord. Chem. Rev.* **2008**, *252*, 2072; i) K.S. Murray, *Eur. J. Inorg. Chem.* **2008**, 3101; k) M.A. Halcrow, *Coord. Chem. Rev.* **2009**, 2059; l) S. Brooker, J.A. Kitchen, *Dalton Trans.* **2009**, 7331; m) C.J. Kepert, *Aust. J. Chem.* **2009**, *62*, 1079; n) K.S. Murray, *Aust. J. Chem.* **2009**, *62*, 1081; o) A.B. Koudriavtsev, W. Linert, *J. Struct. Chem.* **2010**, *51*, 335.
- [2] a) O. Kahn, C.J. Martinez, *Science* **1998**, *279*, 44; b) O. Kahn, C. Jay, J. Kröber, R. Claude, F. Grolière, *Patent* EP0666561 **1995**; c) J.-F. Létard, O. Nguyen, N. Daro, *Patent* FR0512476 **2005**; d) J.-F. Létard, P. Guionneau, L. Goux-Capes, *Topics in Current Chemistry, Vol. 235* (Eds.: P. Gülich, H.A. Goodwin), Springer, Wien, New York, **2004**, 221; e) A. Galet, A.B. Gaspar, M.C. Munoz, G.V. Bukin, G. Levchenko, J.A. Real, *Adv. Mater.* **2005**, *17*, 2949.
- [3] a) J.A. Real, A.B. Gaspar, M.C. Munoz, P. Gülich, V. Ksenofontov, H. Spiering, *Topics in Current Chemistry, Vol. 233* (Eds.: P. Gülich, H.A. Goodwin), Springer, Wien, New York, **2004**, 167; b) A.B. Gaspar, M.C. Munoz, J.A. Real, *J. Mater. Chem.* **2006**, 2522; c) A. Bousseksou, G. Molnar, J.A. Real, K. Tanaka, *Coord. Chem. Rev.* **2007**, *251*, 1822.
- [4] S. Zein, S.A. Borshch, *J. Am. Chem. Soc.* **2005**, *127*, 16197.
- [5] A.B. Gaspar, M. Seredyuk, P. Gülich, *J. Mol. Struct.* **2009**, 924–926, 9.
- [6] a) Y. Garcia, O. Kahn, L. Rabardel, B. Chansou, L. Salmon, J.-T. Tuchagues, *Inorg. Chem.* **1999**, *38*, 4663; b) G.S. Matouzenko, J.-F. Létard, S. Lecocq, A. Bousseksou, L.

- Capes, L. Salmon, M. Perrin, O. Kahn, A. Collet, *Eur. J. Inorg. Chem.* **2001**, 2935; c) W. Hibbs, P.J. van Koningsbruggen, A.M. Arif, W.W. Shum, J.S. Miller, *Inorg. Chem.* **2003**, *42*, 5645; d) P. Poganiuch, S. Decurtins, P. Gütllich, *J. Am. Chem. Soc.* **1990**, *112*, 3270; e) L. Wiehl, *Acta Crystallogr., Sect. B* **1993**, *49*, 289; f) R. Hinek, H. Spiering, D. Schollmeyer, P. Gütllich, A. Hauser, *Chem. Eur. J.* **1996**, *2*, 1427; g) B. Weber, C. Carbonera, C. Desplanches, J.-F. Létard, *Eur. J. Inorg. Chem.* **2008**, 1589.
- [7] a) M. Mikami, M. Konno, Y. Saito, *Chem. Phys. Lett.* **1979**, *63*, 566; b) N. Sasaki, T. Kambara, *Phys. Rev. B* **1989**, *40*, 2442; c) A. Bousseksou, J. Nasser, J. Linares, K. Boukheddaden, F. Varret, *J. Phys. I* **1992**, *2*, 1381; d) H. Spiering, T. Kohlhaas, H. Romstedt, A. Hauser, C. Bruns-Yilmaz, P. Gütllich, *Coord. Chem. Rev.* **1999**, *190–192*, 629.
- [8] a) V. Petrouleas, J.-P. Tuchagues, *Chem. Phys. Lett.* **1987**, *137*, 21; b) D. Boinnard, A. Bousseksou, A. Dworkin, J.-M. Savariault, F. Varret, J.-P. Tuchaugues, *Inorg. Chem.* **1994**, *33*, 271.
- [9] a) D. Chernyshov, M. Hostettler, K.W. Törnroos, H.-B. Bürgi, *Angew. Chem.* **2003**, *115*, 3955; *Angew. Chem. Int. Ed.* **2003**, *42*, 3825; b) N. Huby, L. Guérin, E. Collet, L. Toupet, J.-C. Ameline, H. Cailleau, T. Roisnel, T. Tayagaki, K. Tanaka, *Phys. Rev. B* **2004**, *69*, 2; c) M. Yamada, H. Hagiwara, H. Torigoe, N. Matsumoto, M. Kojima, F. Dahan, J.-P. Tuchagues, N. Re, S. Iijima, *Chem. Eur. J.* **2006**, *12*, 4536; d) S. Bonnet, M.A. Siegler, J.S. Costa, G. Molnar, A. Bousseksou, A.L. Spek, P. Gamez, J. Reedijk, *Chem. Commun.* **2008**, 5619; e) M. Griffin, S. Shakespeare, H.J. Shepherd, C.J. Harding, J.-F. Létard, C. Desplanches, A.E. Goeta, J.A.K. Howard, A.K. Powell, V. Mereacre, Y. Garcia, A.D. Naik, H. Müller-Bunz, G.G. Morgan, *Angew. Chem. Int. Ed.* **2011**, *50*, 896.
- [10] N. Bréfuel, H. Watanabe, L. Toupet, J. Come, N. Matsumoto, E. Collet, K. Tanaka, J.-P. Tuchagues, *Angew. Chem.* **2009**, *121*, 9468; *Angew. Chem. Int. Ed.* **2009**, *48*, 9304.
- [11] a) A. Bousseksou, J. Nasser, J. Linares, K. Boukheddaden, F. Varret, *J. Phys. I France* **1992**, *2*, 1381; b) D. Chernyshov, H.-B. Bürgi, M. Hostettler, K. Törnroos, *Phys. Rev. B*

- 2004**, 70, 9; c) M. Nishino, K. Boukheddaden, S. Miyashita, F. Varret, *Polyhedron* **2005**, 24, 2852.
- [12] S.M. Neville, B.A. Leita, G.J. Halder, C. Kepert, B. Moubaraki, J.-F. Létard, K.S. Murray, *Chem. Eur. J.* **2008**, 14, 10123.
- [13] W. Bauer, W. Scherer, S. Altmannshofer, B. Weber, *Eur. J. Inorg. Chem.* **2011**, 2803.
- [14] T.M. Pfaffeneder, S. Thallmair, W. Bauer, B. Weber, *New J. Chem.* **2011**, 35, 691.
- [15] a) B. Weber, *Coord. Chem. Rev.* **2009**, 253, 2432; b) B. Weber, E.-G. Jäger, *Eur. J. Inorg. Chem.* **2009**, 465.
- [16] a) B. Weber, E. Kaps, J. Weigand, C. Carbonera, J.-F. Létard, K. Achterhold, F.G. Parak, *Inorg. Chem.* **2008**, 47, 487; b) B. Weber, E. Kaps, J. Obel, W. Bauer, *Z. Anorg. Allg. Chem.* **2008**, 1421; c) B. Weber, E. Kaps, C. Desplanches, J.-F. Létard, K. Achterhold, F.G. Parak, *Eur. J. Inorg. Chem.* **2008**, 4891; d) B. Weber, W. Bauer, J. Obel, *Angew. Chem.* **2008**, 120, 10252; *Angew. Chem., Int. Ed.* **2008**, 47, 10098; e) W. Bauer, B. Weber, B. *Inorg. Chim. Acta* **2009**, 362, 2341; f) B. Weber, J. Obel, D. Henner-Vásquez, W. Bauer, *Eur. J. Inorg. Chem.* **2009**, 5527.
- [17] a) B. Weber, E. Kaps, *Heteroatom Chem.* **2005**, 16, 391; b) B. Weber, F.-A. Walker, *Inorg. Chem.* **2007**, 46, 6794; c) B. Weber, E. Kaps, J. Obel, K. Achterhold, F.G. Parak, *Inorg. Chem.* **2008**, 47, 10779.
- [18] a) A.B. Koudriavtsev, A.F. Strassen, J.G. Haasnoot, M. Grunert, P. Weinberger, W. Linert, *Phys. Chem. 5* **2003**, 3676; b) A.B. Koudriavtsev, A.F. Strassen, J.G. Haasnoot, M. Grunert, P. Weinberger, W. Linert, *Chem. Phys. 5* **2003**, 3666.
- [19] J.A. Real, E. Andrés, M.C. Munoz, M. Julve, T. Granier, A. Bousseksou, F. Varret, *Science* **1995**, 268, 265.
- [20] a) G.J. Halder, C.J. Kepert, *Aust. J. Chem.* **2005**, 58, 311; b) G.J. Halder, C.J. Kepert, B. Moubaraki, K.S. Murray, J.D. Cashion, *Science* **2002**, 298, 1762.
- [21] a) V. Niel, A.L. Thompson, M.C. Muñoz, A. Galet, A.E. Goeta, J.A. Real, *Angew. Chem.* **2003**, 115, 3890; *Angew. Chem. Int. Ed.* **2003**, 42, 3760; b) S.M. Neville, G.J.

- Halder, K.W. Chapman, M.B. Duriska, P.D. Southon, J.D. Cashion, J.-F. Létard, B. Moubaraki, K.S. Murray, C.J. Kepert, *J. Am. Chem. Soc.* **2008**, *130*, 2869.
- [22] A. Altomare, M.C. Burla, G.M. Camalli, G. Cascarano, C. Giacovazzo, A. Guagliardi, A.G.G. Moliterni, G. Polidori, R. Spagna, SIR-97, University of Bari, Bari (Italy), **1997**; *J. Appl. Crystallogr.* **1999**, *32*, 115.
- [23] G.M. Sheldrick, SHELXL-97; University of Göttingen, Göttingen (Germany), **1993**.
- [24] a) C.K. Johnson, M.N. Burnett, ORTEP-III, Oak-Ridge National Laboratory, Oak-Ridge, TN (US), **1996**; b) L.J. Farrugia, *J. Appl. Cryst.* **1997**, *30*, 565.
- [25] E. Keller, SCHAKAL-99, University of Freiburg, Freiburg (Germany), **1999**.
- [26] Team of authors: *Organikum*; Johann Ambrosius Barth, Berlin, Heidelberg, **1993**.
- [27] B. Weber, R. Betz, W. Bauer, S. Schlamp, *Z. Anorg. Allg. Chem.* **2011**, *673*, 102.
- [28] L. Wolf, E.-G. Jäger, *Z. anorg. allg. Chem.* **1966**, *346*, 76.
- [29] W. Bauer, T. Ossiander, B. Weber, *Z. Naturforsch. B* **2010**, *65*, 323.
- [30] E.-G. Jäger, E. Häussler, M. Rudolph, A. Schneider, *Z. Anorg. Allg. Chem.* **1985**, *525*, 67.
- [31] J.-P. Launay, M. Turrel-Pagis, J.-F. Lipskier, V. Marvaud, C. Joachim, *Inorg. Chem.* **1991**, *30*, 1033.

9. Complete Two-Step Spin-Transition in a 1D Chain Iron(II) Complex with 110 K Wide Intermediate Plateau

9.7 Supporting Information

Table S1. Crystallographic data of iron(II) coordination polymers **1** and **1(2 tol)**. For the structure motif of **1^{LS}** only the crystal data are given.

compound	1^{HS-LS}	1^{LS}	1(2 tol)
formula	C ₆₀ Fe ₂ H ₆₀ N ₁₂ O ₁₂	C ₁₂₀ H ₁₂₁ Fe ₄ N ₂₄ O ₂₄	C ₄₄ H ₄₆ FeN ₆ O ₆
$M_r / \text{g mol}^{-1}$	1252.90	2506.81	810.72
crystal system	orthorhombic	monoclinic	monoclinic
space group	$P2_12_12_1$	$P2_1$	$P2_1/c$
$a / \text{Å}$	16.2024(4)	17.8442(7)	11.2681(4)
$b / \text{Å}$	17.8809(4)	16.1027(7)	33.9573(11)
$c / \text{Å}$	20.8774(5)	20.3955(8)	11.1503(4)
$\alpha / ^\circ$	90.00	90.00	90.00
$\beta / ^\circ$	90.00	90.614(2)	106.2810(10)
$\gamma / ^\circ$	90.00	90.00	90.00
$V / \text{Å}^3$	6048.5(2)	5860.1(4)	4095.4(2)
Z	4	2	4
$\rho / \text{g cm}^{-3}$	1.376	1.421	1.315
μ / mm^{-1}	0.551	0.569	0.424
crystal size	0.35 × 0.25 × 0.20	0.23 × 0.13 × 0.07	0.19 × 0.07 × 0.05
T / K	200(2)	130(2)	173(2)
diffractometer	KappaCCD	KappaCCD	KappaCCD
$\lambda (\text{MoK}\alpha) / \text{Å}$	0.71073	0.71073	0.71073
θ -range / $^\circ$	3.18–25.34		3.26–23.50
reflns. collected	38753		17933
indep. reflns. (R_{int})	11033 (0.0906)		5979 (0.1011)
mean $\sigma(I) / I$	0.0800		0.1021
reflns. with $I \geq 2\sigma(I)$	8142		3509
x, y (weighting scheme)	0.0368, 0.3874		0.1014, 3.3410
parameters	783		481
restraints	0		14
$R(F)$ (all data) ^[a]	0.0443 (0.0788)		0.0784 (0.1516)
$wR(F^2)$ ^[b]	0.0948		0.2085
$GooF$	1.022		1.059
shift/error _{max}	0.001		0.000
max., min. resd. dens. / e Å^{-3}	0.309, -0.292		0.827, -0.491

[a] $R(F) = \sum ||F_o| - |F_c|| / \sum |F_o|$. [b] $wR(F^2) = [\sum [w(F_o^2 - F_c^2)^2] / \sum w(F_o^2)^2]^{1/2}$, $w = 1 / [\sigma^2(F_o^2) + (aP)^2 + bP]$, where $P = [F_o^2 + 2(F_c^2)]/3$.

10 Influence of Hydrogen Bonding on the Hysteresis Width in Iron(II) Spin Crossover Complexes

Birgit Weber,^{*,[a,b]} Wolfgang Bauer,^[b] Toni Pfaffeneder,^[b] Marinela M. Dîrtu,^[c] Anil D. Naik,^[c] Aurelian Rotaru^[d] and Yann Garcia^{*,[c]}

[a] Inorganic Chemistry II, Universität Bayreuth, Universitätsstraße 30, NW I, 95440 Bayreuth, Germany. Fax: +49-92155-2157, E-mail: weber@uni-bayreuth.de

[b] Center for Integrated Protein Science Munich at the Department Chemie und Biochemie, Ludwig-Maximilians-Universität München, Butenandtstr. 5–13 (Haus F), D-81377 München, Germany

[c] Institute of Condensed Matter and Nanosciences, Université Catholique de Louvain, Place L. Pasteur, 1, 1348 Louvain-la-Neuve Belgium

[d] Department of Electrical Engineering and Computer Science, "Stefan cel Mare" University, University Street, No. 13, Suceava 720229, Romania

Keywords: Molecular Bistability, Spin Crossover, Memory Effect, Hydrogen Bonding, Crystal Engineering

Published in: *Eur. J. Inorg Chem.* **2011**, DOI: 10.1002/ejic.201100394.

Abstract: A detailed investigation on the properties of the high-temperature and low-temperature modifications of the iron(II) spin crossover complex [FeL1(Him)₂] (**1**) and its isotopic deuterium-labelled analogue [FeL1(Dim)₂] (**1D**), and the pair [FeL2(azpy)]·MeOH/[FeL2(azpy)]·CD₃OD/[FeL2(azpy)] (**2·MeOH/2·CD₃OD/2**), in which L1 and L2 are tetradentate N₂O₂²⁻-coordinating Schiff base-like ligands, L1 = {diethyl (*E,E*)-2,2'-[1,2-phenyl-bis(iminomethylidene)]bis[3-oxobutanoate] (2-)-*N,N',O³,O^{3'}*}, L2 = {2,2'-[1,2-phenyl-bis(iminomethylidene)]bis[1-phenylbutane-1,3-dione] (2-)-*N,N',O³,O^{3'}*}, Him = imidazole, and azpy = 4,4'-azopyridine, is presented. All complexes except **2** show a cooperative spin transition with hysteresis widths between approximately 5 K (**1^{LT}** and **1^{LT}D**), 70 K (**1^{HT}**^[9] and **1^{HT}D**, both around room temperature) and 80 K (**2·MeOH** and **2·CD₃OD**). In all cases, an

influence of the H/D-exchange on the transition temperature and the hysteresis width is observed. For **1^{HT}**, first-order reversal curves (FORCs) have been recorded, and a statistical analysis gives the interaction parameter $J = 560$ K, indicating strong intermolecular interactions. X-Ray structure analysis of the different samples (**1^{HT}**^[9] and **1^{HT}D**: HS; **1^{LT}** and **1^{LT}D**: LS; and **2·MeOH** and **2·CD₃OD**: HS) gives a deeper insight into the molecular packing in the crystals and helps explain the increase of cooperative interactions during the spin transition. In all cases, one hydrogen bond involves an oxygen atom of the Schiff base like ligand that serves as a donor for the iron centre. The influence of this hydrogen bond on the ligand field strength of the iron centre is discussed and a new model is developed to explain the observed connection between hydrogen bonds and exceptionally wide hysteresis loops for the complexes presented in this work and other examples from literature.

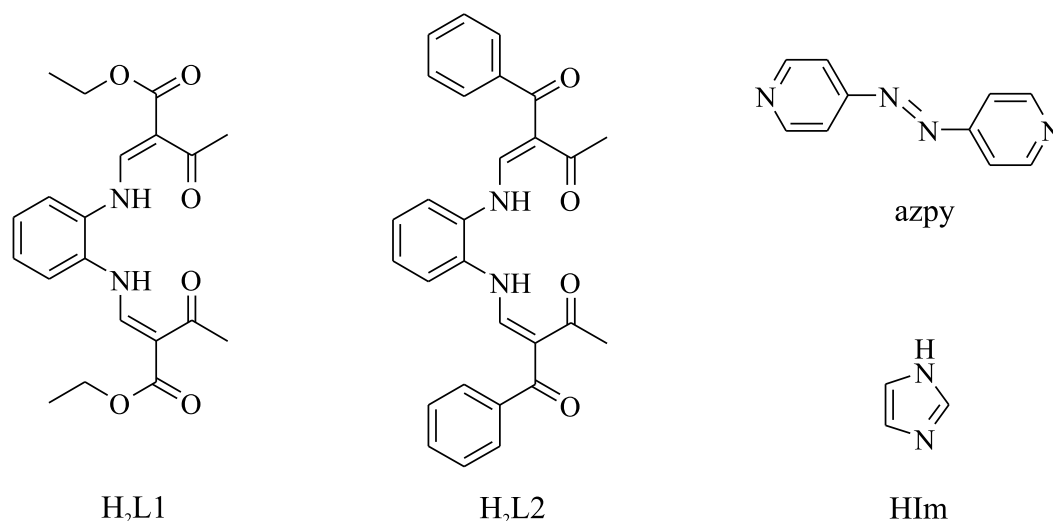
10.1 Introduction

There is an on-going interest in the bistability of spin crossover (SCO) compounds^[1] as the thermochromism associated with the spin transition (ST) makes them potentially useful for various applications, such as display and memory device units,^[2] sensors^[3] and cold channel control units in food and medical storage devices.^[4] Recent research activities in this field explore the possibility of combining the SCO bistability with additional properties (*e.g.*, liquid crystalline properties^[5] and magnetic exchange interactions^[6]) resulting in multi-functional SCO materials,^[7] or are focused on the rational design of nano-structured SCO materials and their chemical and physical properties.^[8] Of the possible types of ST (gradual, abrupt, with hysteresis, stepwise, incomplete), much of the interest is focused on the bistability in highly cooperative systems (hysteresis or memory effect) as such compounds can exist in two different electronic states depending on the history of the system. In this regard, we recently characterised an iron(II) SCO complex with a 70 K wide thermal hysteresis loop around room temperature based on a 2D network of hydrogen bonds between the complex molecules (compound **1**, [FeL1(HIm)₂]).^[9] The possibility to influence the ST behaviour by hydrogen bonds has been already introduced in the literature. Several examples demonstrate an influence of the presence or absence of hydrogen bonds on both, the transition temperature^[10,11,12,13] as well as on cooperative effects.^[9,13,14,15] For some of the examples, an influence of the hydrogen bonds on the electron density of donor atoms and by this on the

ligand field strength is discussed.^[10-13] To date, however, no consistent model for the explanation of the different effects is available. A detailed understanding of the interplay of hydrogen bonds and wide hysteresis loops is essential for a purposeful synthesis of SCO materials for potential applications.

We decided to use two different approaches to more clearly investigate the effect of hydrogen bonds on the cooperative interactions and the transition temperature of our systems. From one side we are searching for more examples of complexes with wide hysteresis loops and hydrogen bonds. Here, we obtained a 1D chain iron(II) SCO complex with an 80-K wide hysteresis loop, probably also due to the presence of hydrogen bonds (compound **2·MeOH**). For this complex, a second modification with a gradual SCO behaviour was obtained (compound **2**). Additionally, we decided to investigate complexes **1** and **2·MeOH** with all hydrogen atoms involved in the hydrogen-bond network substituted by deuterium. This information, together with data detailing a second modification of compound **1** with a 4 K wide hysteresis loop reported by Müller *et al.*^[16] and the variety of other literature examples, build the foundation for a model to explain the different effects, which are presented in this work.

In Scheme 1, the ligands used to modify **1** (H_2L1 and HIm) and **2** (H_2L2 and $azpy$) are given.



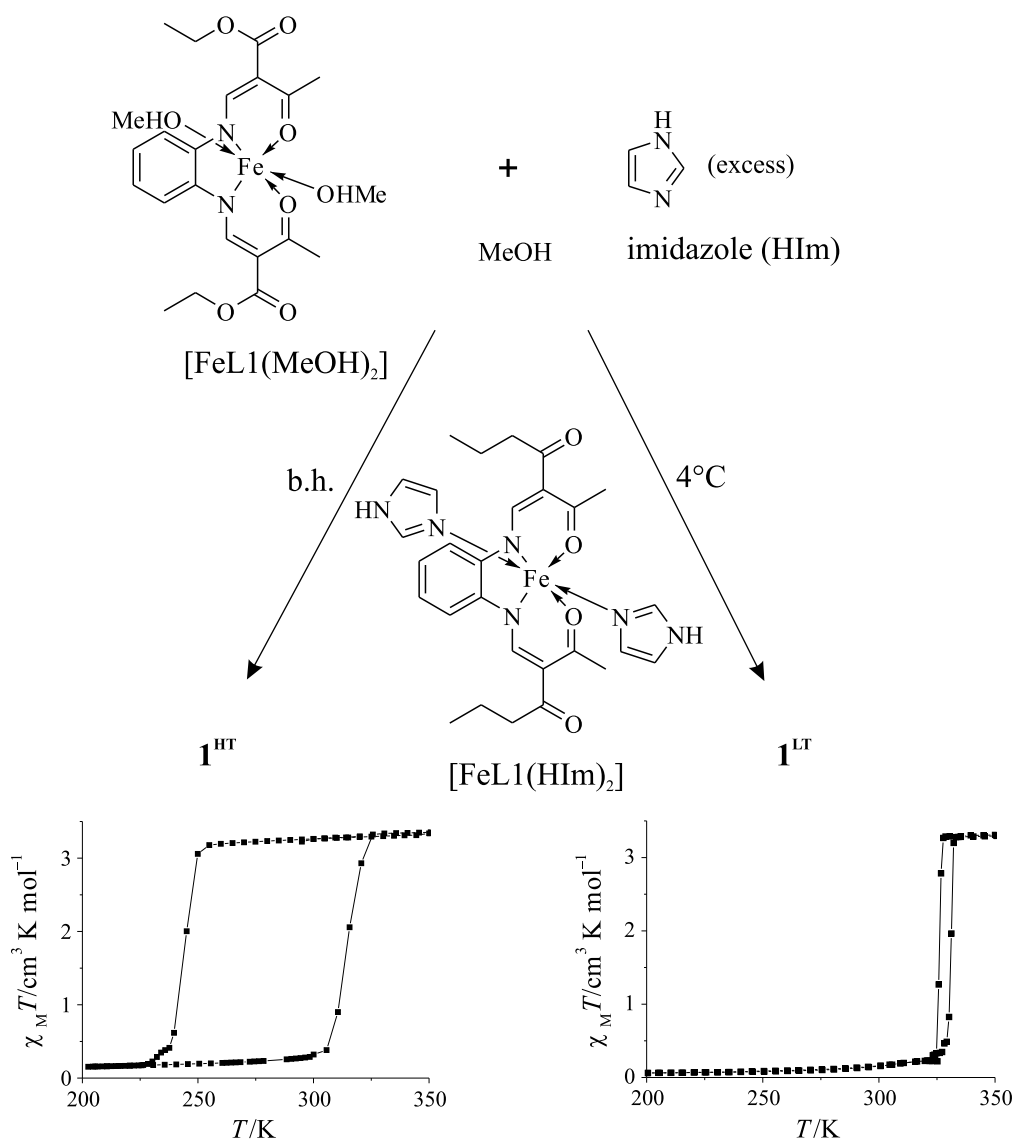
Scheme 1. Schematic representation of the ligands used in this work.

10.2 Results

Synthesis and general characterisation: The reaction of $[\text{FeL1}(\text{MeOH})_2]$ with an excess of imidazole in methanol leads to two different modifications of the corresponding imidazole diadduct $[\text{FeL1}(\text{HIm})_2]$ (**1**) as given in Scheme 2. Whereas for the modification with the 70 K wide thermal hysteresis around room temperature, an exact 1:2 ratio of FeL1/HIm is obtained as confirmed by X-ray structural and elemental analyses, for the second modification the exact composition is unclear. According to literature, the formula is $[\text{FeL1}(\text{HIm})_x]$ with values of x between 1.8 and 2.2.^[16] In both cases, a 4 K wide thermal hysteresis loop above room temperature is observed. Although the loss of cooperative interactions when going from the exact 1:2 ratio to a higher or lower imidazole content can be easily explained by the partial destruction of the hydrogen-bond network responsible for the cooperative interactions, it is puzzling that the same transition curve is obtained irrespective of the FeL1/HIm ratio. We therefore decided to have a deeper look into this matter before starting any experiments with deuterated imidazole.

The results of different synthetic approaches are summarised in Scheme 2. For the modification resulting in the wide thermal hysteresis loop, a higher ratio of FeL1/HIm was necessary (1:50 instead of 1:30) and significantly less solvent was used (18 mL of MeOH instead of 67 mL per mmol iron complex). In contrast to literature results, however, the obtained precipitate of the second modification has exactly the same composition (FeL1/HIm = 1:2) as the modification with wide thermal hysteresis loop. Differences were observed when different times were allowed for the precipitation to occur. The compound with the wide hysteresis loop precipitates from boiling solution (high temperature modification: **1**^{HT}), whereas the solution with the lower concentration is clear and the precipitate is obtained after standing for a period at room temperature (fine needles) or at 4 °C (powder, low temperature modification: **1**^{LT}). The magnetic properties of the powder and the fine crystalline sample of **1**^{LT} are identical. Another possibility to obtain **1**^{LT} is to store the filtrate of the reaction mixture of **1**^{HT} at 4 °C.

10. Influence of Hydrogen Bonding on the Hysteresis Width in Iron(II) Spin Crossover Complexes



Scheme 2. Synthetic approach towards the two different modifications of the complex $[\text{FeL1}(\text{HIm})_2]$.

The powder sample of **2** can be obtained by the direct conversion of $[\text{FeL2}(\text{MeOH})_2]$ and azopyridine in methanol. Single crystals of **2**·MeOH and **2**·CD₃OD were obtained by slow diffusion techniques. A loss of the included methanol/[D₄]-methanol can be observed when warming the crystals above room temperature, and **2** is obtained. To prevent the loss of the solvent, the crystals are stored at 4°C .

Magnetic measurements: In Figure 1, the ST curves of $\mathbf{1}^{\text{HT}}$ and $\mathbf{1}^{\text{LT}}$ are compared with those obtained for the analogous complexes with $[\text{D}_4]$ -imidazole, $\mathbf{1}^{\text{HTD}}$ and $\mathbf{1}^{\text{LTD}}$. For the complex $\mathbf{1}^{\text{LT}}$, slightly different transition temperatures are obtained compared with the results described by Müller *et al.*^[16] At room temperature, the $\chi_{\text{M}}T$ product is with $0.15 \text{ cm}^3 \text{ K mol}^{-1}$ in the region typical for an iron(II) complex in the low-spin (LS) state. Upon heating, the magnetic moment remains constant up to 328 K, after which an abrupt transition in the HS state takes place with a transition temperature (HS molar fraction; $\chi_{\text{HS}} = 0.5$) of $T_{1/2}^{\uparrow} = 331 \text{ K}$. At 345 K, the $\chi_{\text{M}}T$ product is with $3.29 \text{ cm}^3 \text{ K mol}^{-1}$ in the region typical for an iron(II) complex in the HS state. Upon cooling, the magnetic moment remains constant down to 328 K. Below this temperature an abrupt transition in the LS state takes place with $T_{1/2}^{\downarrow} = 326 \text{ K}$. Upon deuteration, the transition temperature in the heating mode is shifted by 1 K to higher temperature, whereas the transition temperature in the cooling mode remains the same ($T_{1/2}^{\uparrow} = 332 \text{ K}$ and $T_{1/2}^{\downarrow} = 326 \text{ K}$ for $\mathbf{1}^{\text{LTD}}$). The width of the thermal hysteresis loop increases from 5 to 6 K. The measurements were reproduced twice (for all samples) to verify the observed trend.

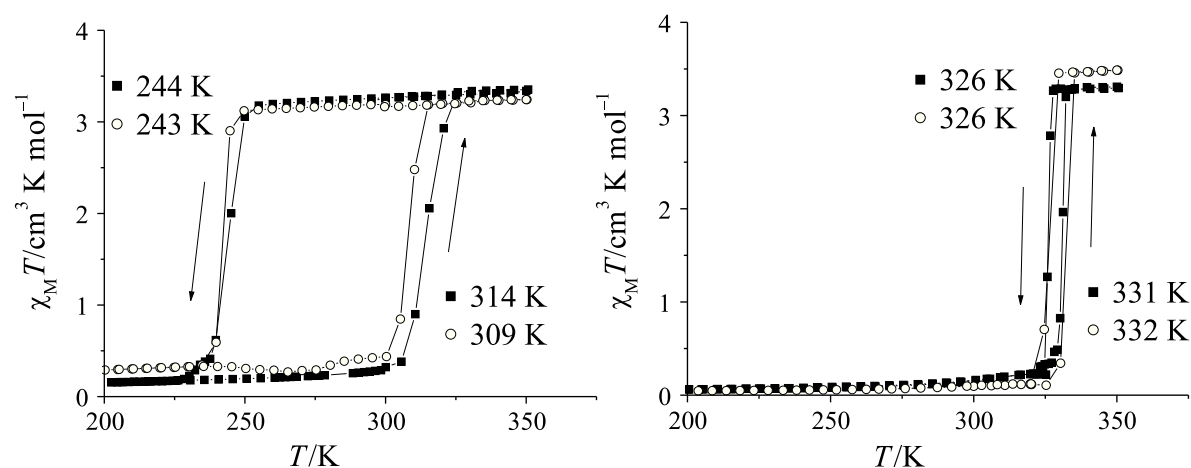


Figure 1. Thermal variation of the $\chi_{\text{M}}T$ product of the different modifications of $\mathbf{1}$ discussed in this work. Left: wide hysteresis of $\mathbf{1}^{\text{HT}}$ (squares) and $\mathbf{1}^{\text{HTD}}$ (open circles) and right: small hysteresis of $\mathbf{1}^{\text{LT}}$ (squares) and $\mathbf{1}^{\text{LTD}}$ (open circles).

The transition curves of $\mathbf{1}^{\text{HT}}$ and $\mathbf{1}^{\text{HTD}}$ are very similar, and a pronounced difference is only obtained for the transition temperature in the heating mode that is with a value of 309 K in the deuteriated compound, 5 K lower than the original complex. In the cooling mode, the transition temperature is also shifted towards lower temperatures, but only by 1 K (243 instead of 244 K). As a consequence, the width of the thermal hysteresis loop is reduced by 4 K (from 70 to 66 K) upon H/D exchange. This significant change in the width of the hysteresis loop upon deuteration for both samples clearly demonstrates that the hydrogen-bond network influences the hysteresis width in this complex.

In Figure 2 the ST curves of $\mathbf{2}\cdot\text{MeOH}$, $\mathbf{2}\cdot\text{CD}_3\text{OD}$ and the solvent-free samples of $\mathbf{2}$ are displayed. The shape of the curve progression is very similar for the two solvated compounds. For the first cycle, the magnetic behaviour was measured in the 50–280 K temperature range. After heating to 300 K, significant changes in the ST behaviour were observed, resulting in a decrease in the hysteresis loop width and the overall completeness of the SCO. Measurements up to 400 K cause a complete loss of the solvent methanol/ $[\text{D}_4]$ -methanol and the ST is shifted to a higher temperature, its curve progression becoming gradual ($\mathbf{2}\cdot\text{MeOH}$: $T_{1/2} = 314$ K; $\mathbf{2}\cdot\text{CD}_3\text{OD}$: $T_{1/2} = 310$ K). The same gradual curve progression is obtained for a separately prepared powder sample of $\mathbf{2}$.

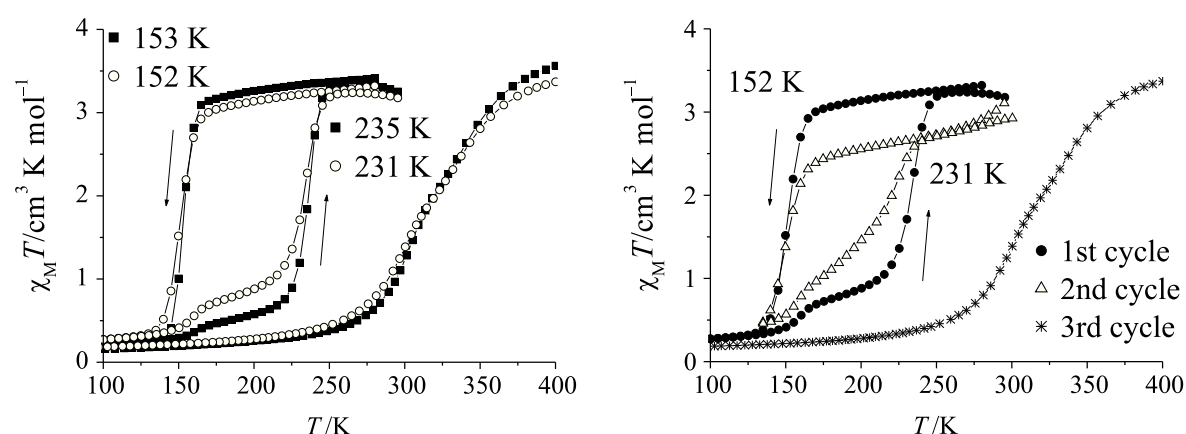


Figure 2. Left: thermal variation of the $\chi_M T$ product of the complexes $\mathbf{2}\cdot\text{MeOH}$ (squares) and $\mathbf{2}\cdot\text{CD}_3\text{OD}$ (open circles). Comparison of the hysteresis loop of $\mathbf{2}\cdot\text{MeOH}$ and $\mathbf{2}\cdot\text{CD}_3\text{OD}$ and the gradual spin transition after tempering to 400 K. Right: thermal variation of the $\chi_M T$ product of the complexes $\mathbf{2}\cdot\text{CD}_3\text{OD}$ at the first cycle (cycles), second cycle (after heating to 300 K, open triangles) and after heating to 400 K (stars).

Thermogravimetric measurements of **2·MeOH** and **2·CD₃OD** confirm the presumption that the loss of one methanol molecule has to be responsible for the different spin transition behaviour. At 280 K, the $\chi_{\text{M}}T$ product of **2·MeOH** is with $3.41 \text{ cm}^3 \text{ K mol}^{-1}$ in the typical range expected for an iron(II) HS centre, as for the $\chi_{\text{M}}T$ value of **2·CD₃OD** with $3.32 \text{ cm}^3 \text{ K mol}^{-1}$. Upon cooling, the $\chi_{\text{M}}T$ values of **2·MeOH** remain approximately constant between 280 and 164 K. Over the range 164 to 130 K an abrupt ST takes place to a minimum value of $0.28 \text{ cm}^3 \text{ K mol}^{-1}$, indicating that all the iron(II) sites are in the LS state. Below 130 K, the $\chi_{\text{M}}T$ values remain approximately constant again. The $T_{1/2}$ value of this SCO is 153 K. The $\chi_{\text{M}}T$ values of **2·CD₃OD** remain approximately constant between 280 and 169 K, then over the range 169 to 125 K the $\chi_{\text{M}}T$ values rapidly decrease to a minimum value of $0.32 \text{ cm}^3 \text{ K mol}^{-1}$. Below 125 K, the $\chi_{\text{M}}T$ values remain approximately constant. The $T_{1/2}$ value of this SCO is 152 K. For both compounds, thermal hysteresis is observed in the $\chi_{\text{M}}T$ values upon heating. Above 144 K, the $\chi_{\text{M}}T$ values of **2·MeOH** increase gradually, then, above 200 K, rapidly, to attain a maximum value of $3.65 \text{ cm}^3 \text{ K mol}^{-1}$ at 265 K, indicative of HS iron(II). The $T_{1/2}$ value of this step is 235 K. The $\chi_{\text{M}}T$ values of **2·CD₃OD** increase, first gradually above 140 K, then rapidly above 200 K, to a maximum value of $3.23 \text{ cm}^3 \text{ K mol}^{-1}$ at 260 K. The $T_{1/2}$ value of this SCO is 231 K. This means a thermal hysteresis loop of 82 K for **2·MeOH** and 79 K for **2·CD₃OD**. The small step in the heating mode is probably an indication for a partial loss of the included methanol molecules.

FORC analysis: To obtain a complete picture of the interaction distribution in **1^{HT}**, a set of first order reversal curves (FORCs) have been recorded (Figure 3). For each reversal temperature, $T_{\text{a}} = [T_{\text{HS}}, T_{\text{LS}}]$ (T_{HS} and T_{LS} are the temperature for which the system is saturated in the HS state and in the LS state, respectively), by steps of 0.5 K, the magnetisation is recorded for decreasing temperatures T_{b} spanning from T_{a} to T_{LS} also in steps of 0.5 K. The full set of FORCs is then transformed into the so-called FORC distribution defined by Equation (1) by using the original algorithm developed by Pike.^[17]

$$\rho(T_{\text{a}}, T_{\text{b}}) = -\frac{\partial^2 n_{\text{HS}}(T_{\text{a}}, T_{\text{b}})}{\partial T_{\text{a}} \partial T_{\text{b}}} \quad (1)$$

Finally, the set of the variables is changed from T_a , T_b to “coercitivity” (c) and ‘bias’ (b), as indicated in Equations (2) and (3).

$$c = \frac{T_a - T_b}{2}, \quad (2)$$

$$b = \frac{T_a + T_b}{2}, \quad (3)$$

The “bias” parameter, which is related to the equilibrium temperature $T_{1/2}$, roughly corresponds to the energy gap Δ between the HS and LS states. The “coercitivity”, which is related to the hysteresis width, reflects the strength of intra-domain interactions, which is characterised by the J parameter.^[18,19] J corresponds to an interaction parameter derived from a two-level Ising-like description of interacting SCO units (Figure 4).

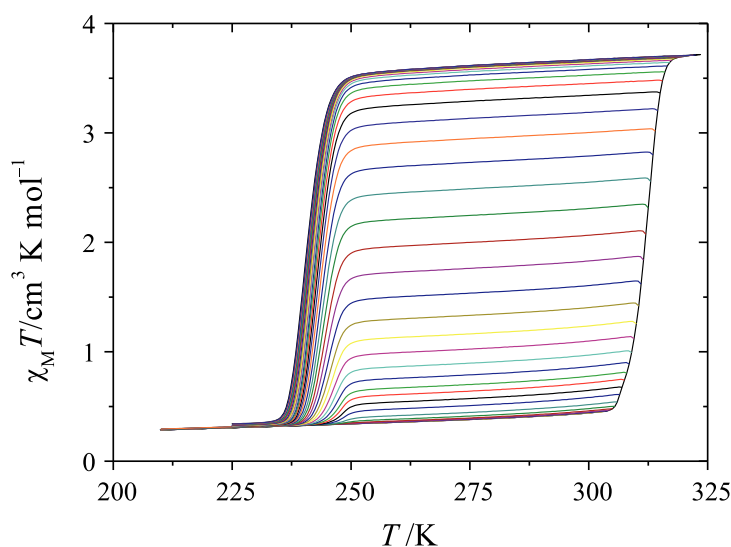


Figure 3. FORCs of the thermal hysteresis loop of $\mathbf{1}^{\text{HT}}$ recorded in the cooling mode.

Further, we discuss the FORC data in terms of the standard deviations σ and of the dimensionless correlation parameter $r_{b,c}$ defined in Equation (4).

$$r_{b,c} = \text{cov}(b, c) / \sigma(b)\sigma(c) \quad (4)$$

10. Influence of Hydrogen Bonding on the Hysteresis Width in Iron(II) Spin Crossover Complexes

The main parameters obtained from statistical analysis of the FORC diagrams are collected in Table 1.

The mean value of the interaction parameter, $J = 560$ K and an energy gap $\Delta = 2439$ K have been determined for $\mathbf{1}^{\text{HT}}$. This interaction parameter is much higher than that of the model 2D ST coordination polymer $[\text{Fe}(\text{btr})_2(\text{NCS})_2] \cdot \text{H}_2\text{O}$ ($J = 235$ K),^[21] which presents a hysteresis width of 25 K,^[20] free of any structural phase transition.^[21] It is also higher than that of the 1D ST chain compound $[\text{Fe}(\text{NH}_2\text{trz})_3](\text{NO}_3)_2$ ($J = 496$ K),^[22] which present an hysteresis width of 33 K and which is also free of structural phase transformation.^[22] A strong correlation between statistical parameters is observed, which suggests that the intra-layer interaction strength within the 2D hydrogen-bond network^[9] is higher than the inter-layer interaction one giving rise to anisotropy in the propagation of the interactions, that is along the 2D layer of $\mathbf{1}^{\text{HT}}$. This result agrees very well with earlier FORCs studies carried out on 1D ST systems that concluded on the nature of the correlation taking its origin from an anisotropy source induced, for instance, by interchain interactions^[22] or by an external pressure.^[23] The composition distribution suggested by Tanasa *et al.*^[19] in a diluted 2D ST system as the origin of the correlation can also be regarded as an anisotropy source. A comprehensive FORC study of $\mathbf{1}^{\text{HT}}$ and $\mathbf{1}^{\text{HTD}}$ will be devoted to a future study.

Table 1. Statistical analysis of the FORC distributions obtained on $\mathbf{1}^{\text{HT}}$.

\bar{b} [a]	\bar{c} [a]	$\sigma(b)$	$\sigma(c)$	$r_{b,c}$	\bar{J} [a]	$\sigma(J)$	$\bar{\Delta}$ [a]	$\sigma(\Delta)$	$r_{J,\Delta}$
(K)	(K)	(K)	(K)	(K)	(K)	(K)	(K)	(K)	(K)
272.2	36.1	1.1	3.4	-0.31	560	20.3	2439	11.3	0.59

[a] $\bar{b}, \bar{c}, \bar{J}, \bar{\Delta}$ represent the mean values of the parameters b, c, Δ and J , respectively.

10. Influence of Hydrogen Bonding on the Hysteresis Width in Iron(II) Spin Crossover Complexes

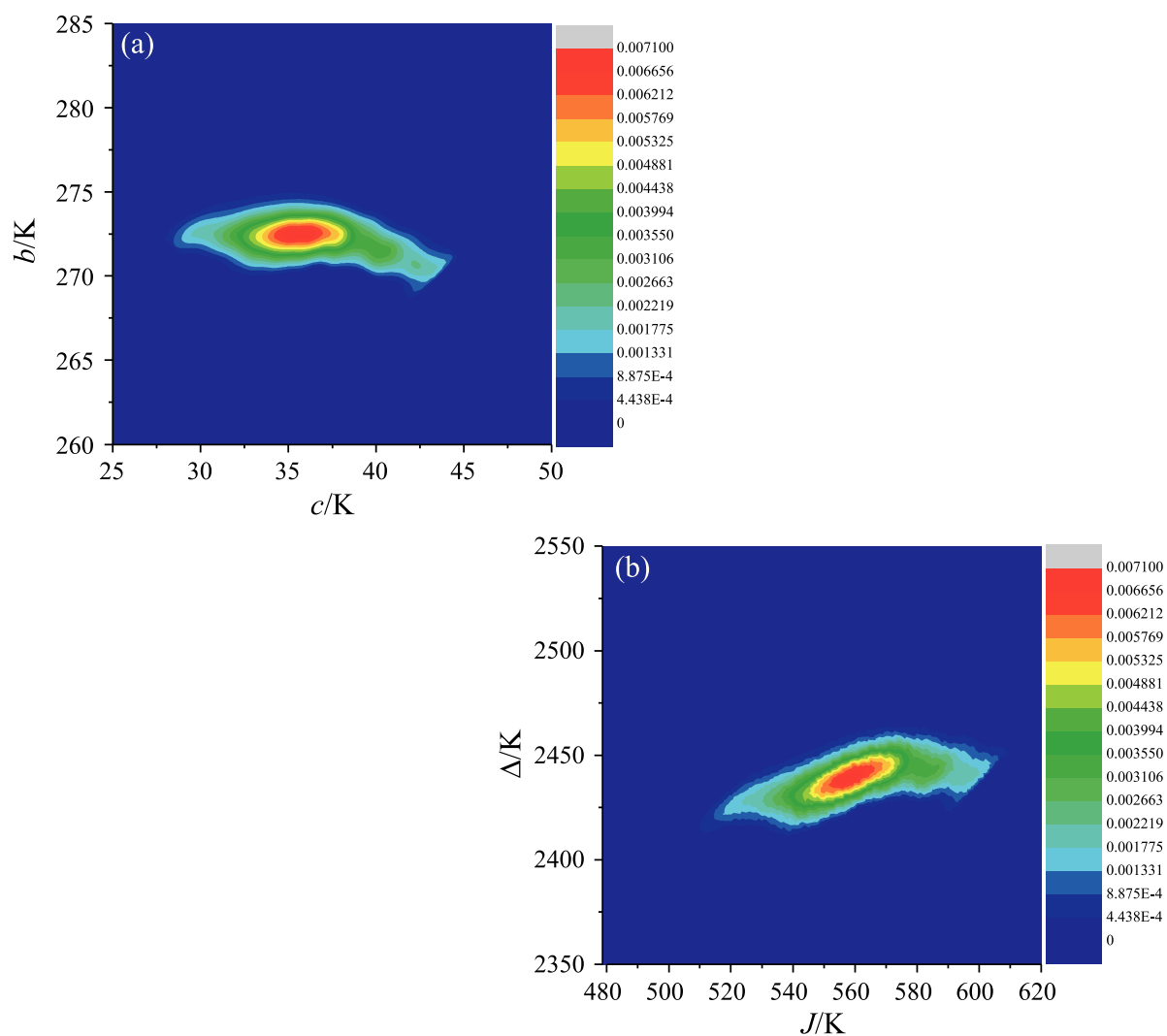


Figure 4. Experimental FORC diagram derived from Figure 3, in: (a) coercivity-bias coordinates and (b) in J - Δ coordinates. Probability that a single domain is characterised by a given value is given by its shade (very low in the blue region and very high in the red region).

DSC measurements: $\mathbf{1}^{\text{HT}}$ and $\mathbf{1}^{\text{HTD}}$ were studied by differential scanning calorimetry (DSC) over the 200–345 K temperature range (Figure 5). The thermal profile of the two complexes is very similar. They both exhibit, on warming, an endothermic peak and on cooling, an exothermic peak, whose shape is characteristic of a first-order phase transition. The peaks are separated by a wide temperature domain, which is indicative for the presence of a hysteresis loop for both compounds, as detected in SQUID measurements (Figure 1). The transition temperatures have been evaluated as $T_{\text{max}}^{\uparrow} = 321(4)$ K and $T_{\text{max}}^{\downarrow} = 247(4)$ K with $\Delta H = 20(1)$ kJ mol⁻¹ and $\Delta S = 72.5(1)$ J mol⁻¹ K⁻¹ for $\mathbf{1}^{\text{HT}}$, and as $T_{\text{max}}^{\uparrow} = 315(1)$ K and $T_{\text{max}}^{\downarrow} = 249(1)$ K for $\mathbf{1}^{\text{HTD}}$ with $\Delta H = 16(1)$ kJ mol⁻¹ and $\Delta S = 64.2(1)$ J mol⁻¹ K⁻¹. These transition temperatures agree rather well with those obtained by SQUID measurements, the hysteresis width being identical for $\mathbf{1}^{\text{HTD}}$ (66 K), whereas for $\mathbf{1}^{\text{HT}}$ a value of 74.4 (K) was obtained, compared with 70 K by SQUID. The vibrational contribution to the entropy variation is evaluated as $\Delta S_{\text{vib}} = 59.2(1)$ J mol⁻¹ K⁻¹ and $\Delta S_{\text{vib}} = 31.9(1)$ J mol⁻¹ K⁻¹, for $\mathbf{1}^{\text{HT}}$ and $\mathbf{1}^{\text{HTD}}$ respectively; the electronic contribution being equal to $R \ln 5 = 13.4$ J mol⁻¹ K⁻¹ for iron(II) SCO compounds.^[1b]

Compounds $\mathbf{1}^{\text{LT}}$ and $\mathbf{1}^{\text{LTD}}$ were also studied by DSC over the range 300–355 K. They both display a reversible first-order phase transition with transition temperatures $T_{\text{max}}^{\uparrow} = 346$ K and $T_{\text{max}}^{\downarrow} = 325$ K with $\Delta H = 23(1)$ kJ mol⁻¹ and $\Delta S = 68.7(1)$ J mol⁻¹ K⁻¹ for $\mathbf{1}^{\text{LT}}$, and $T_{\text{max}}^{\uparrow} = 345$ K and $T_{\text{max}}^{\downarrow} = 322$ K for $\mathbf{1}^{\text{LTD}}$ with $\Delta H = 20(1)$ kJ mol⁻¹ and $\Delta S = 61.2(1)$ J mol⁻¹ K⁻¹.

The unusual ST behaviour of $\mathbf{2}\cdot\text{MeOH}$ and $\mathbf{2}\cdot\text{CD}_3\text{OD}$ was investigated by DSC at a scan rate of 10 K min⁻¹ over the temperature range 120–300 K in warming and cooling modes (Figure 6). For $\mathbf{2}\cdot\text{MeOH}$, a steep endothermic peak was observed on warming at $T_{\text{max}}^{\uparrow} = 239$ K and an exothermic peak was recorded at $T_{\text{max}}^{\downarrow} = 153$ K, on cooling, thus revealing a hysteresis loop with a width of 86 K. This behaviour is characteristic of a first-order phase transition and can be related to the hysteretic ST tracked by SQUID measurements (Figure 2), with an excellent agreement regarding transition temperatures.

10. Influence of Hydrogen Bonding on the Hysteresis Width in Iron(II) Spin Crossover Complexes

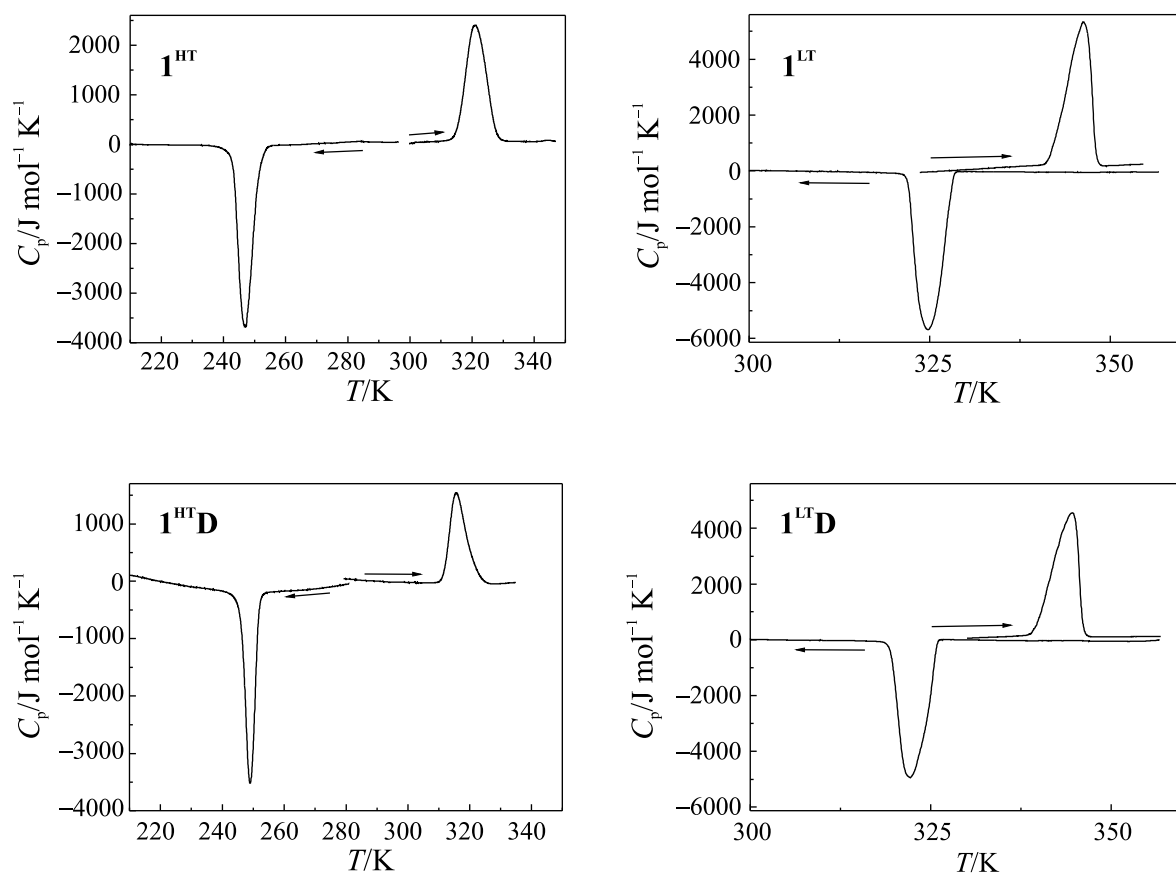


Figure 5. DSC profiles of 1^{HT} , 1^{HTD} , 1^{LT} and 1^{LTD} in the cooling (\leftarrow) and warming (\rightarrow) modes.

The enthalpy and entropy variations of $2\cdot\text{MeOH}$ have been evaluated as $\Delta H = 15(1) \text{ kJ mol}^{-1}$ and $\Delta S = 90.3(1) \text{ J mol}^{-1} \text{ K}^{-1}$. For $2\cdot\text{CD}_3\text{OD}$, the transition temperatures were found as $T_{\text{max}}^{\uparrow} = 237 \text{ K}$ and $T_{\text{max}}^{\downarrow} = 156 \text{ K}$ with $\Delta H = 9(1) \text{ kJ mol}^{-1}$ and $\Delta S = 76.3(1) \text{ J mol}^{-1} \text{ K}^{-1}$. The entropy variation for $2\cdot\text{MeOH}$ is much larger than that of $2\cdot\text{CD}_3\text{OD}$, and, most interestingly, higher than those reported for other 1D iron(II) coordination polymers.^[4,22, 24] This high value calls for the presence of a structural phase transformation. Interestingly, a shoulder is detected on the endothermic peak of $2\cdot\text{MeOH}$ at $T_{\text{max}}^{\uparrow} = 229 \text{ K}$, but absent on the exothermic peak associated with the spin transition. This signal is not an artefact as it was observed in several DSC experiments in cooling and warming modes. Most interestingly, an unusual increase of $\chi_M T$ was detected in the SQUID measurements recorded on warming over the same temperature range (Figure 2, left).

10. Influence of Hydrogen Bonding on the Hysteresis Width in Iron(II) Spin Crossover Complexes

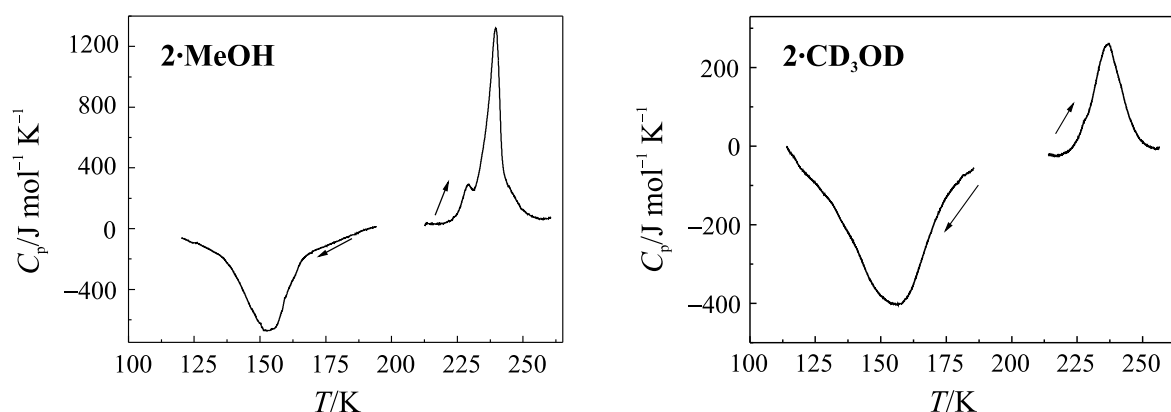


Figure 6. DSC profile of **2·MeOH** and **2·CD₃OD** in the 120–300 K temperature range in the cooling (←) and warming (→) modes.

Compound **2·MeOH** was studied by DSC on warming from 120 to 345 K (Figure 7) enabling us to fully reproduce the two endothermic signals displayed in Figure 6, which thus confirm a step in the warming branch of the ST curve of this material. The sample was then warmed and studied above room temperature, allowing the detection of a steeper endothermic peak, reminiscent of both methanol release and spin-state change as confirmed by both SQUID measurements (Figure 2) and thermogravimetric analyses.

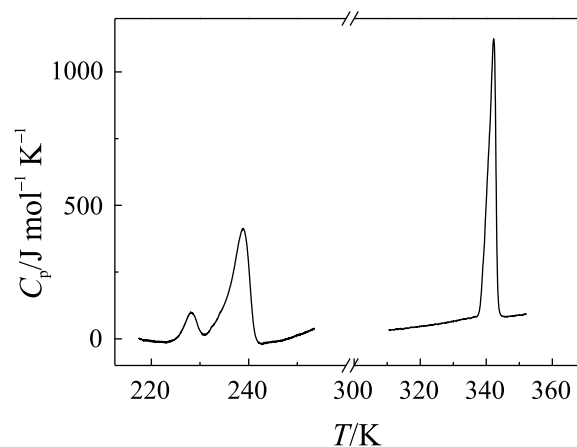


Figure 7. DSC profile of **2·MeOH** on warming over the temperature range 120–360 K.

In Table 2, the transition temperatures obtained by SQUID and DSC measurements and the thermodynamic parameters of the ST complexes are summarised. In general, a very good agreement between the transition temperatures is obtained by the two different methods.

10. Influence of Hydrogen Bonding on the Hysteresis Width in Iron(II) Spin Crossover Complexes

Differences (especially for $\mathbf{1}^{\text{LT}}/\mathbf{1}^{\text{LT}}\mathbf{D}$) can be explained by the difference in scan rates. A comparison of the obtained entropy values reveals, that upon deuteration, a significant decrease of the entropy is observed for all samples. In contrast, the values of the HT and LT modifications of $\mathbf{1}$ are very similar. This indicates that the hydrogen bonds (ref. [9]; see X-ray structures) significantly influence the SCO properties of the compounds presented here. The entropy values are significantly higher than the values determined for two monomeric complexes of this type of Schiff base-like ligands with pyridine (37.8 kJ mol⁻¹, abrupt ST with 2 K wide hysteresis) or *N,N*-dimethylaminopyridine (31.5 kJ mol⁻¹, abrupt ST with 9 K wide hysteresis) as axial ligands in which no hydrogen-bond network is observed.^[25] They are, however, with the exception of $\mathbf{2}\cdot\text{MeOH}$, in the range reported for highly cooperative 1D coordination polymers.^[4,22,24] All these parameters indicate that, for the complexes discussed in this work, the hydrogen bond network plays an important role for the spin transition and that most presumably the ST is associated with a structural phase transition.

Table 2. Transition temperatures recorded by SQUID and DSC measurements.

	$T_{1/2}^{\uparrow}/\text{K}$	$T_{1/2}^{\downarrow}/\text{K}$	$\Delta T/\text{K}$	$\Delta H/\text{kJ mol}^{-1}$	$\Delta S/\text{J mol}^{-1} \text{K}^{-1}$
$\mathbf{1}^{\text{HT}}$ (SQUID)	314	244	70		
$\mathbf{1}^{\text{HT}}$ (DSC)	321	247	74	20(1)	72.5(1)
$\mathbf{1}^{\text{HT}}\mathbf{D}$ (SQUID)	309	243	66		
$\mathbf{1}^{\text{HT}}\mathbf{D}$ (DSC)	315	249	66	16(1)	64.2(1)
$\mathbf{1}^{\text{LT}}$ (SQUID)	331	326	5		
$\mathbf{1}^{\text{LT}}$ (DSC)	346	325	21	23(1)	68.7(1)
$\mathbf{1}^{\text{LT}}\mathbf{D}$ (SQUID)	332	326	6		
$\mathbf{1}^{\text{LT}}\mathbf{D}$ (DSC)	345	322	23	20(1)	61.2(1)
$\mathbf{2}\cdot\text{MeOH}$ (SQUID)	235	153	82		
$\mathbf{2}\cdot\text{MeOH}$ (DSC)	239	153	86	15(1)	90.3(1)
$\mathbf{2}\cdot\text{CD}_3\text{OD}$ (SQUID)	231	152	79		
$\mathbf{2}\cdot\text{CD}_3\text{OD}$ (DSC)	237	156	81	9(1)	76.3(1)

X-Ray structure analysis: Crystals suitable for X-ray structure analysis were obtained for $\mathbf{1}^{\text{LT}}$, $\mathbf{1}^{\text{HTD}}$, $\mathbf{1}^{\text{LTD}}$, $\mathbf{2}\cdot\text{MeOH}$ and $\mathbf{2}\cdot\text{CD}_3\text{OD}$ (the same samples as those used for the magnetic measurements in all cases). In the case of $\mathbf{1}^{\text{LTD}}$, only the cell parameters were determined. Selected bond lengths and angles as well as selected intermolecular distances are reported in Table 3 and Table 4. Full refinement details are given Supporting Information Table S1.1–2. For completeness, the data of $\mathbf{1}^{\text{HT}}^{[9]}$ are also given. ORTEP drawings illustrating the asymmetric units of the different modifications of $\mathbf{1}$ and $\mathbf{2}$ are given in Figure 8 and Figure 9. The molecule structures of $\mathbf{1}^{\text{LT}}$ and $\mathbf{1}^{\text{HTD}}$ were determined at 200 K and 275 K, respectively. The molecule structures of $\mathbf{2}\cdot\text{MeOH}$ and $\mathbf{2}\cdot\text{CD}_3\text{OH}$ could only be determined at 200 K and 173 K, respectively, as the crystals crumbled at higher/lower temperatures due to the spin transition. For each of these materials, structural analysis revealed a distorted octahedral iron(II) environment consisting of the equatorially coordinating tetradentate Schiff base-like ligand and two axially coordinating ligands with a *N*-heterocycle. In the case of $\mathbf{1}$, the two monodentate axial imidazole/[D₄]-imidazole ligands led to mononuclear complexes. In case of $\mathbf{2}$, each bidentate 4,4'-azopyridine ligand bridges two iron(II) centres and thus propagates to form extended 1D chains.

The complexes $\mathbf{1}^{\text{HT}}^{[9]}$ and $\mathbf{1}^{\text{HTD}}$ crystallise with monoclinic symmetry. Both complexes are isostructural with the average bond length and angles of the inner coordination sphere around the iron centre in the region typically reported for HS iron(II) complexes of this ligand type (2.09 Å (Fe-N_{eq}), 2.03 Å (Fe-O_{eq}), 2.22 Å (Fe-N_{ax}) and 108° (O_{eq}-Fe-O_{eq})).^[26,27] The complexes $\mathbf{1}^{\text{LT}}$ and $\mathbf{1}^{\text{LTD}}$ crystallise with orthorhombic symmetry. For $\mathbf{1}^{\text{LT}}$, the average bond lengths and angles of the inner coordination sphere around the iron centre (1.88 Å (Fe-N_{eq}), 1.94 Å (Fe-O_{eq}), 2.00 Å (Fe-N_{ax}) and 88° (O_{eq}-Fe-O_{eq})) are in the region reported previously for similar LS iron(II) complexes—in full agreement with the results of the susceptibility measurements.^[26,27] No values give an indication why such pronounced differences are observed between the ST values of the two modifications. A detailed analysis of the intermolecular interactions can provide an answer to this question.

10. Influence of Hydrogen Bonding on the Hysteresis Width in Iron(II) Spin Crossover Complexes

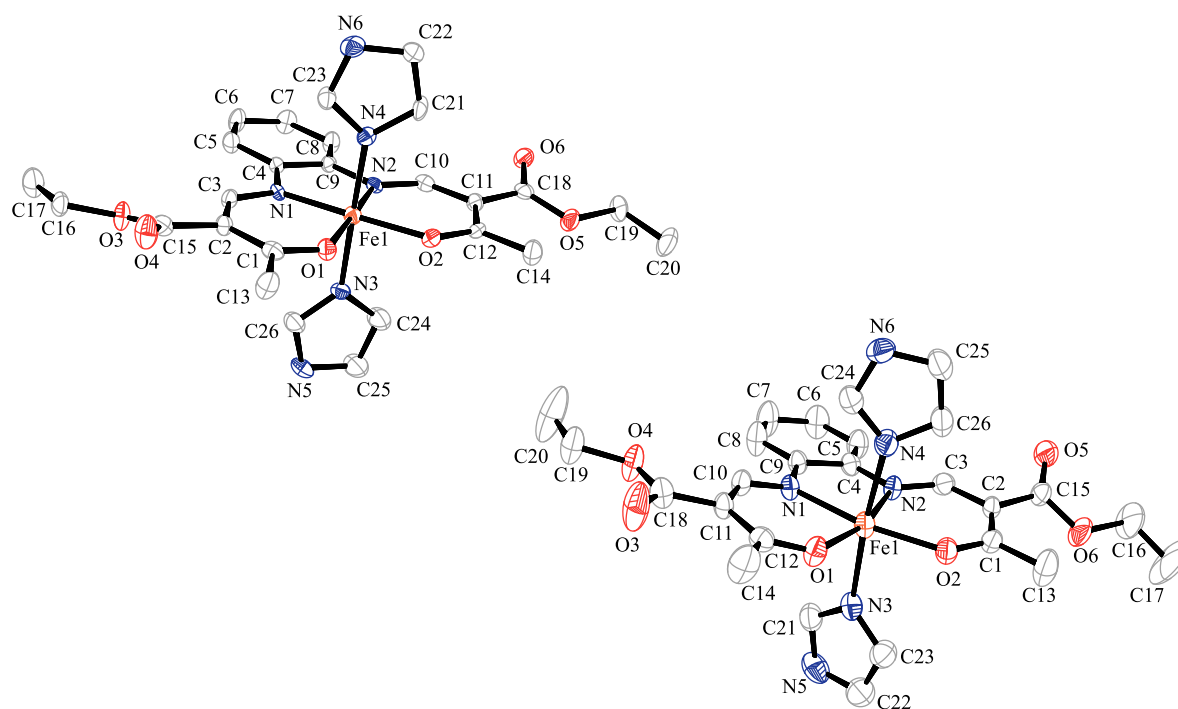


Figure 8. ORTEP drawing of the asymmetric units of compounds 1^{LT} at 200 K (left) and 1^{HTD} at 275 K (right). Hydrogen atoms have been omitted for clarity. Displacement ellipsoids are shown with a 50% probability.

Table 3. Selected bond lengths [\AA] and angles [$^\circ$] of 1^{LT} , $1^{HT [9]}$, 1^{HTD} , $2 \cdot \text{MeOH}$ and $2 \cdot \text{CD}_3\text{OD}$ within the first coordination sphere.

compound	Fe-N _{eq}	Fe-O _{eq}	Fe-N _{ax}	O _{eq} -Fe-O _{eq}	N _{ax} -Fe-N _{ax}
1^{LT}	1.879(2)	1.951(2)	1.989(2)	88.26(8)	178.9(1)
	1.890(2)	1.929(2)	2.011(3)		
$1^{HT [9]}$	2.086(3)	2.048(3)	2.196(4)	108.0(1)	173.8(1)
	2.079(4)	2.010(3)	2.241(3)		
1^{HTD}	2.096(2)	2.052(2)	2.195(3)	108.22(8)	173.5(1)
	2.092(2)	2.013(2)	2.242(2)		
$2 \cdot \text{MeOH}$	2.093(3)	2.011(2)	2.271(3)	109.70(8)	177.05(9)
	2.092(3)	2.020(2)	2.245(3)		
$2 \cdot \text{CD}_3\text{OD}$	2.091(4)	2.014(4)	2.260(5)	109.41(16)	176.99(19)
	2.096(5)	2.017(4)	2.231(5)		

10. Influence of Hydrogen Bonding on the Hysteresis Width in Iron(II) Spin Crossover Complexes

The complexes **2·MeOH** and **2·CD₃OD** crystallise with triclinic symmetry and have one iron(II) centre in the asymmetric unit. The parallel 1D chains of both complexes propagate along the $[1\bar{1}\bar{2}]$ direction and are stacked such that there is a solvent accessible void volume for one methanol/[D₄]-methanol molecule per iron(II) centre. Both complexes are isostructural. The average bond lengths around the iron centre (**2·MeOH**: 2.09 Å (Fe-N_{eq}), 2.02 Å (Fe-O_{eq}), 2.26 Å (Fe-N_{ax}); **2·CD₃OD**: 2.09 Å (Fe-N_{eq}), 2.01 Å (Fe-O_{eq}), 2.25 Å (Fe-N_{ax})) and the O_{eq}-Fe-O_{eq} angles (**2·MeOH**: 110° ; **2·CD₃OD**: 109°) are indicative of iron(II) in the HS state.^[26,27]

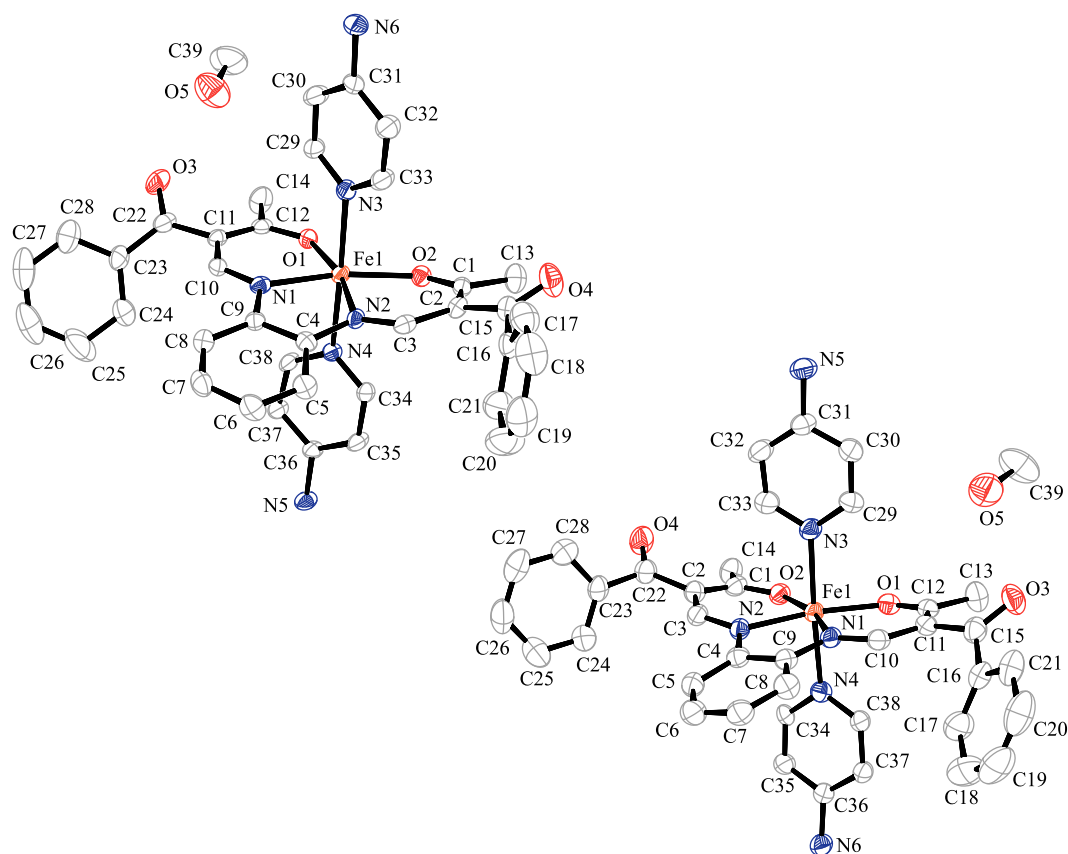


Figure 9. ORTEP drawing of the asymmetric units of compounds **2·MeOH** (left) and **2·CD₃OD** (right). Hydrogen atoms have been omitted for clarity. Displacement ellipsoids are shown with a 50% probability.

Intermolecular investigations: In contrast to $\mathbf{1}^{\text{HT}}$,^[9] the packing of the molecules of $\mathbf{1}^{\text{LT}}$ in the crystal (Figure 10) reveals three different hydrogen bonds between neighbouring molecules. The one involving the NH hydrogen atom (H6A) of the imidazole unit and the OCOEt oxygen atom (O6) of the equatorial ligand is comparable to that observed in the $\mathbf{1}^{\text{HT}}$ structure.^[9] The second one involving the NH hydrogen atom (H5A) and the coordinated carbonyl oxygen atom (O1) of the equatorial ligand is significantly weaker than the second H-bond in $\mathbf{1}^{\text{HT}}$ (A · · D 2.95 Å instead of 2.83 Å in the $\mathbf{1}^{\text{HT}}$ modification).^[9] This is probably due to the third hydrogen bond that also involves the NH hydrogen atom (H5A) and the coordinated carbonyl oxygen atom (O2) of the equatorial ligand. One could argue that those two hydrogen bonds are the reason for the higher transition temperature of $\mathbf{1}^{\text{LT}}$. Upon spin transition the equatorial ligand expands; this is reflected by an increase in the value of the O1-Fe-O2 angle. This angle, however, is to some extent fixed by the bridging hydrogen bond and by this the LS state of the complex is stabilised compared to $\mathbf{1}^{\text{HT}}$. The combination of the three hydrogen bonds leads to an infinite 3D network of linked molecules. Some additional weak contacts between the imidazole CH (H22) and the OCOEt oxygen atom (O4) and the hydrogen atom of the ethoxy group of the equatorial ligand (H16B) and the OCOEt oxygen atom (O6) are also involved in the hydrogen-bonding network. For $\mathbf{1}^{\text{HT}}$, three additional weak contacts were obtained; two of them involving the same donor atom, the total number of short contacts is the same for both modifications of $\mathbf{1}$. The details for all intermolecular contacts are given in Table 4. The first suggestion would be that the 3D hydrogen-bond network of $\mathbf{1}^{\text{LT}}$ should lead to wider hysteresis loops, quite contrary to the experimental results. This discrepancy can be explained by the significantly weaker hydrogen bonds between the N5 hydrogen and O1/O2. Additionally, the stabilisation of the LS state due to this bridging hydrogen bond can account for the small hysteresis loop in $\mathbf{1}^{\text{LT}}$.

The molecule packing of $\mathbf{2}\cdot\text{MeOH}$ and $\mathbf{2}\cdot\text{CD}_3\text{OD}$ (Figure 11) reveals four hydrogen bonds between adjacent chains, which are identical when comparing the two modifications. Most obvious is the hydrogen bond formed between the hydroxy group of the methanol molecule and the carbonyl oxygen atom O3 of the equatorial ligand. Moreover, three non-classical hydrogen bonds of the type C-H · · O are found. Two of which involve the carbonyl oxygen atoms O3 and O4 as H-acceptor and two CH groups of the pyridyl-rings of the axial ligand (C-H32, C-H35) act as H-donors. The third non-classical hydrogen bond involves carbonyl oxygen atom O1, which is also directly coordinated to the iron(II) centre and a proton of the

10. Influence of Hydrogen Bonding on the Hysteresis Width in Iron(II) Spin Crossover Complexes

methyl group of the included methanol molecule. This weak hydrogen bond is similar to the hydrogen bonds observed in the different modifications of **1** that also include the oxygen atom O1 that is coordinated to the iron centre. As for **1**, a H/D exchange leads to differences in the hysteresis width suggesting a similar mechanism in both cases.

Table 4. Selected intermolecular distances [\AA] of the three modifications **1^{HT}** (275 K), **1^{HTD}** (275 K) and **1^{LT}** (200 K) and of the two modifications **2·MeOH** and **2·CD₃OD**. For **1^{HT}** and **1^{HTD}** an infinite 2D hydrogen bond network with the base vectors: [0 1 0] and [0 0 1], along the plane: (1 0 0) with additional weak contacts between the single planes is obtained. For the compound **1^{LT}** an infinite 3D hydrogen bond network with the base vectors: [1 0 0], [0 1 0], [0 0 1] is observed.

compound	D	H	A	D-H	H···A	D···A	D-H···A
1^{HT} ^[9]	N4	H4	O1 ^[a]	0.86	2.00	2.832(5)	161
	N6	H66	O5 ^[b]	0.86	1.98	2.841(4)	176
1^{HTD}	N5	D5	O1 ^[a]	0.86	2.02	2.847(4)	162
	N6	D6	O5 ^[b]	0.86	1.99	2.846(3)	177
1^{LT}	N6	H6A	O6 ^[c]	0.88	2.01	2.832(3)	155
	N5	H5A	O1 ^[d]	0.88	2.10	2.950(3)	162
	N5	H5A	O2 ^[d]	0.88	2.39	2.945(3)	121
	C22	H22	O4 ^[e]	0.95	2.57	3.520(4)	178
	C16	H16B	O6 ^[f]	0.99	2.56	3.508(4)	161
2·MeOH	O5	H5A	O3	0.84	2.03	2.865(4)	174
	C32	H32	O4 ^[b]	0.95	2.57	3.415(5)	148
	C35	H35	O3 ^[g]	0.95	2.42	3.331(49)	161
	C39	H39B	O1 ^[h]	0.98	2.53	3.346(5)	141
2·CD₃OD	O5	D5	O3	0.84	2.03	2.867(8)	171
	C32	H32	O4 ^[j]	0.95	2.57	3.416(9)	148
	C35	H35	O3 ^[i]	0.95	2.42	3.329(8)	161
	C39	D39A	O1 ^[k]	0.98	2.50	3.344(8)	144

Symmetry codes: [a] $-x, \frac{1}{2} + y, -\frac{1}{2} - z$; [b] $-x, -1 - y, -z$; [c] $2 - x, \frac{1}{2} + y, \frac{5}{2} - z$; [d] $\frac{1}{2} + x, \frac{5}{2} - y, 2 - z$; [e] $2 - x, -\frac{1}{2} + y, \frac{5}{2} - z$; [f] $1 + x, 1 + y, z$; [g] $-1 + x, y, z$; [h] $1 - x, -y, -z$; [i] $1 + x, y, z$; [j] $1 - x, 2 - y, 2 - z$; [k] $-x, 1 - y, 2 - z$.

10. Influence of Hydrogen Bonding on the Hysteresis Width in Iron(II) Spin Crossover Complexes

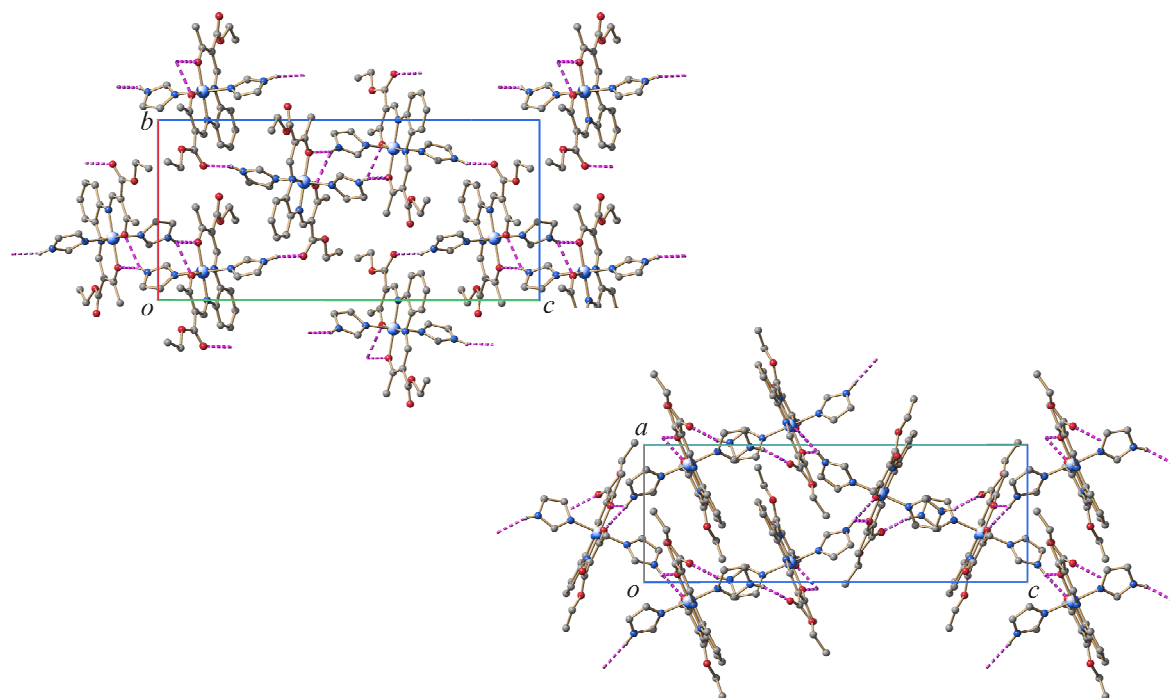


Figure 10. Packing of compound 1^{LT} in the crystal at 200 K. Top: view along $[1\ 0\ 0]$, bottom: view along $[0\ 1\ 0]$. Hydrogen bonds are shown as dashed lines.

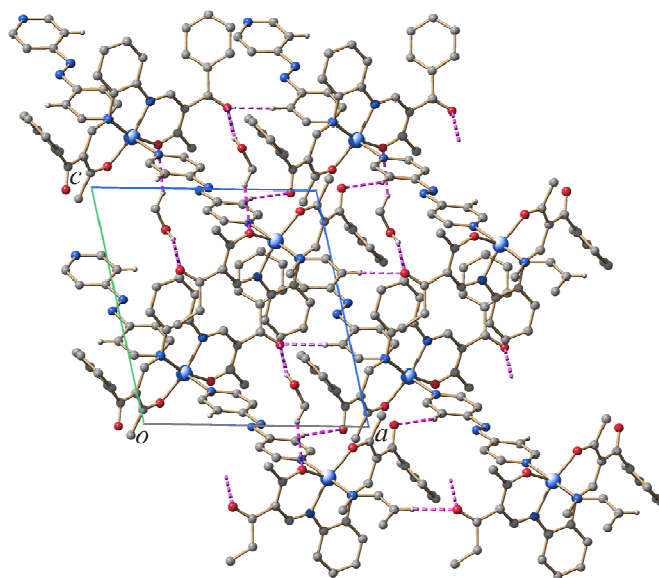


Figure 11. Packing of compound $2\cdot\text{MeOH}$ in the crystal. View along $[0\ 1\ 0]$. Hydrogen bonds are shown as dashed lines.

10.3 Discussion

Labelling experiments: For the different systems investigated in this work ($\mathbf{1}^{\text{HT}}/\mathbf{1}^{\text{HTD}}$, $\mathbf{1}^{\text{LT}}/\mathbf{1}^{\text{LTD}}$ and $\mathbf{2}\cdot\text{MeOH}/\mathbf{2}\cdot\text{CD}_3\text{OD}$) the H/D exchange influences the width of the thermal hysteresis loop, whereas the shape of the transition curve remains unchanged. In the case of $\mathbf{1}^{\text{HT}}/\mathbf{1}^{\text{HTD}}$ and $\mathbf{2}\cdot\text{MeOH}/\mathbf{2}\cdot\text{CD}_3\text{OD}$, the width of the hysteresis loop is reduced upon deuteration and the transition temperatures are shifted to lower temperatures, whereas for $\mathbf{1}^{\text{LT}}/\mathbf{1}^{\text{LTD}}$ the transition temperature is shifted to higher temperatures and the hysteresis width is increased. A H/D isotope effect on $T_{1/2}$ was already observed for the coordination polymer $[\text{Fe}(\text{pyridine})_2][\text{Ni}(\text{CN})_4]$ by Kitazawa, Bousseksou and co-workers^[28] (shift to lower temperatures) or for the mononuclear system $[\text{Fe}(\text{2-pic})_3]\text{Cl}_2\cdot\text{Sol}$ (2-pic = 2-picolyamine, Sol = $\text{C}_2\text{H}_5\text{OD}$ and CH_3OD) (shift to higher temperatures) by Gütllich *et al.*^[29] As different electronic and vibrational factors contribute to the relative energies of the HS and the LS state, the direction of the H/D effect on $T_{1/2}$ is difficult to predict.

A possible explanation for the observed effects concerning the hysteresis loop width can be related to the higher N-D bond strength compared with the N-H bond^[30] and consequently the hydrogen bond strength decreases upon H/D exchange^[31] leading to weaker intermolecular interactions. This is in agreement with a comparison of the cell parameters of $\mathbf{1}^{\text{HT}}$ and $\mathbf{1}^{\text{HTD}}$, which reveals that for the deuteriated sample, all cell parameters are slightly larger; the most pronounced difference is found for the *c* axis with a value of 27.37 Å instead of 27.25 Å. As the 2D hydrogen-bond network runs along the *b/c* axis this agrees well with the weaker hydrogen-bonds in $\mathbf{1}^{\text{HTD}}$. The intermolecular hydrogen bonds in the deuteriated sample are slightly longer than in the previously reported complex. Nevertheless, the effect is negligible for the one involving the NH/D atom (H66/D6) of the imidazole unit and the OCOEt oxygen atom (O5) of the equatorial ligand. In contrast, the difference between the second hydrogen-bond between the NH/D atom (H4/D5) of the imidazole unit and the coordinated carbonyl oxygen atom (O1) of the equatorial ligand is more pronounced (A · · · D 2.85 compared with 2.83 Å in the $\mathbf{1}^{\text{HT}}$ modification). For the second pair $\mathbf{2}\cdot\text{MeOH}/\mathbf{2}\cdot\text{CD}_3\text{OD}$, however, no such pronounced differences were observed, but the effect on the transition curve is similar, whereas for $\mathbf{1}^{\text{LT}}/\mathbf{1}^{\text{LTD}}$ a different trend is observed.

A comparison of $\mathbf{1}^{\text{HT}}$ and $\mathbf{2}\cdot\text{MeOH}$ complicates the situation even more: Here strong differences in the hydrogen-bond network are observed, but the width of the hysteresis loop is

in the same order of magnitude. For $\mathbf{1}^{\text{HT}}$, direct hydrogen bonds between the complex molecules are observed whereas for $\mathbf{2}\cdot\text{MeOH}$ it is highly likely that the interactions mediated over the solvent molecule methanol are responsible for the wide hysteresis loop. The $\text{MeOH}/\text{CD}_3\text{OD}$ exchange influences the width of the hysteresis loop and the loss of the methanol results in a gradual spin transition. In contrast, a comparison of $\mathbf{1}^{\text{HT}}$ and $\mathbf{1}^{\text{LT}}$ reveals a very similar hydrogen-bond network, but strong differences in the width of the hysteresis loop.

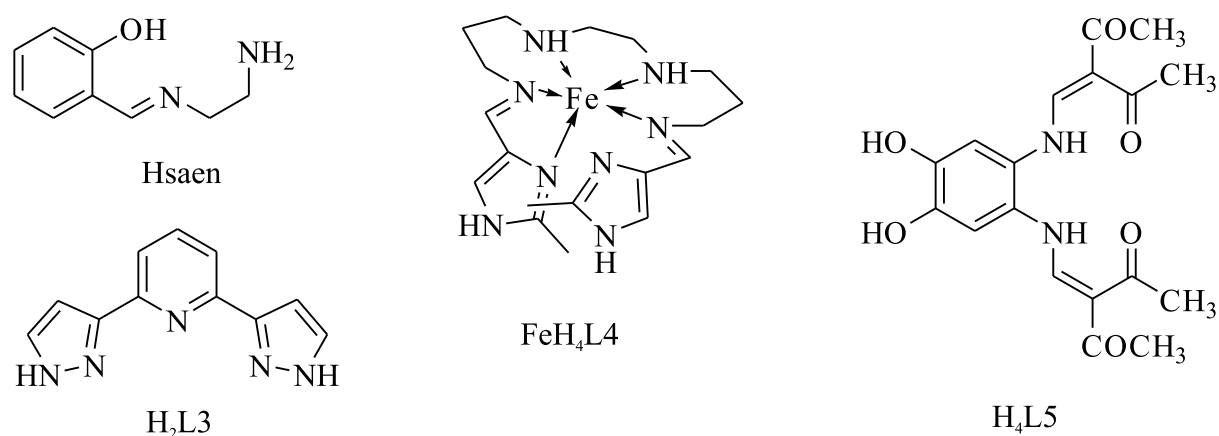
The different degrees of cooperative interactions cannot be directly correlated with the number and strength of hydrogen bonds. Several examples suggested that this is possible for the number of short van der Waals contacts.^[11] For this purpose, we suggested the introduction of a quantitative parameter, the crystal contact index (CCI) that is the sum of all short and weighted contacts.^[32] We assumed that every short contact (shorter than the sum of the van der Waals radii) contributes to the interactions mediating the cooperative effect. Those that are very short contribute more to the cooperative effect than those that are longer. Although this concept works rather nicely for several complexes of the family discussed in this work and also for other ST complexes,^[32] it fails as soon as hydrogen bonds are involved in the intermolecular interactions. The values obtained for $\mathbf{1}^{\text{HT}}$ (4.1), $\mathbf{1}^{\text{HTD}}$ (4.0) and $\mathbf{1}^{\text{LT}}$ (4.2) are of the same order of magnitude, thus the hysteresis width does not correlate with the number of short contacts.^[32] Moreover, the value of $\mathbf{2}\cdot\text{MeOH}$ (1.7) is significantly lower, despite the even larger hysteresis loop. Nevertheless, the importance of the hydrogen bonds in connection with the wide hysteresis loops cannot be put into question as it is underlined by the DSC results in which a significant decrease of the entropy is observed upon deuteration for all complexes. The FORCs analysis of $\mathbf{1}^{\text{HT}}$ also indicates strong interactions within the 2D layer of hydrogen-bond-linked molecules as origin of the wide hysteresis loops.

To obtain a better understanding of the influence of the hydrogen bonds on the hysteresis width, their influence on the ligand field strength was considered.

Influence of H-bonding on the ligand field strength: The general idea that hydrogen bonds to atoms in close vicinity to the metal centre are responsible for variations in the crystal field was already suggested in 1978 for the iron(III) complex $[\text{Fe}(\text{saen})_2]\text{Cl}\cdot\text{H}_2\text{O}$.^[10] The four amine hydrogen atoms of the saen ligand (saen = *N*-(2-aminoethyl)-salicylaldiminato, Scheme 3) are involved in four interactions, three with chloride ions and one with the water molecule. The complex is LS but becomes HS when dehydrated or in solution.^[10] This observation was explained with a slight increase in electron density on the amine nitrogen due to the hydrogen bond, resulting in an enhanced crystal field experienced by the central metal ion.^[10] A similar observation was made for a series of iron complexes of $\text{H}_2\text{L3}$ ($\text{H}_2\text{L3}$ = 2,6-bis(pyrazol-3-yl)pyridine, Scheme 3) with varying counterions and water molecules of the general formula $[\text{Fe}(\text{H}_2\text{L3})_2](\text{X})_2\cdot n\text{H}_2\text{O}$ with $\text{X} = \text{BF}_4^-$,^[33] Γ^- ,^[33c] SCN^- ,^[12] SeCN^- ^[12b] and CF_3SO_3^- .^[13] An increasing amount of water of crystallisation resulted in the stabilisation of the LS state, for example, the crystals of the BF_4^- salt with three water molecules of crystallisation are LS (no magnetic measurements), the powder sample with two water molecules of crystallisation shows a gradual ST with $T_{1/2} \approx 300$ K, whereas the water-free powder sample shows an abrupt ST with $T_{1/2}^\downarrow = 170$ K and $T_{1/2}^\uparrow = 180$ K.^[33] In the X-ray structures analyses, hydrogen bonds were observed between the uncoordinated NH of the pyrazole ring and water, as well as the counterions. The authors assume that the hydrogen-bonded water molecules stabilise the LS state by increasing the electron density at the imine nitrogen.^[33] For two of the complexes $[\text{Fe}(\text{H}_2\text{L3})_2](\text{SCN})_2\cdot 2\text{H}_2\text{O}$ ^[12] and $[\text{Fe}(\text{H}_2\text{L3})_2](\text{CF}_3\text{SO}_3)_2\cdot\text{H}_2\text{O}$,^[13] stepwise spin transitions with hysteresis loop were obtained. In both cases, the step does not occur at $\chi_{\text{HS}} = 0.5$, as for the example **2·MeOH/CD₃OD** in this paper. In the case of the thiocyanate salt, after the first cycling, a second phase with a one-step ST was obtained. A disruption of the hydrogen-bond network associated with a reversible crystallographic change is assumed to be the origin of the unusual ST behaviour.^[12] A structural phase transition and the associated modification of the hydrogen-bond network are discussed as being responsible for the step ST with hysteresis of the compound $\text{FeH}_4\text{L4}$ (Scheme 3).^[15] Significant differences in the transition temperature of $[\text{FeH}_2\text{L5}(\text{py})_2]\cdot\text{py}$ (Scheme 3) in the solid state ($T_{1/2} > 350$ K) and in solution ($T_{1/2} \approx 200$ K, both gradual spin transitions) were also associated with the hydrogen-bond network observed in the X-ray structure.^[11] Such observations are not limited to monomer complexes. For the 1D chain material $[\text{Fe}(\text{NH}_2\text{trz})_3](\text{NO}_3)_2$, the 33 K wide thermal hysteresis loop is associated

10. Influence of Hydrogen Bonding on the Hysteresis Width in Iron(II) Spin Crossover Complexes

with a network of hydrogen bonds,^[22,34] and for the very similar [Fe(Htrz)₂(trz)] (BF₄), an extended network of hydrogen bonds had been singled out to be the origin of the 40 K large hysteresis above room temperature.^[24,35] A detail X-ray structure analysis on the 2D network of [Fe(btr)₂(NCS)₂] \cdot H₂O reveals that the HS \rightarrow LS transition reduces the O-H \cdots N contacts between the water molecules and the free N atoms of the triazole ligand. Those changes and the rigid nature of the bridging ligand are made responsible for the observed highly cooperative SCO behaviour (25 K wide hysteresis).^[20,21]



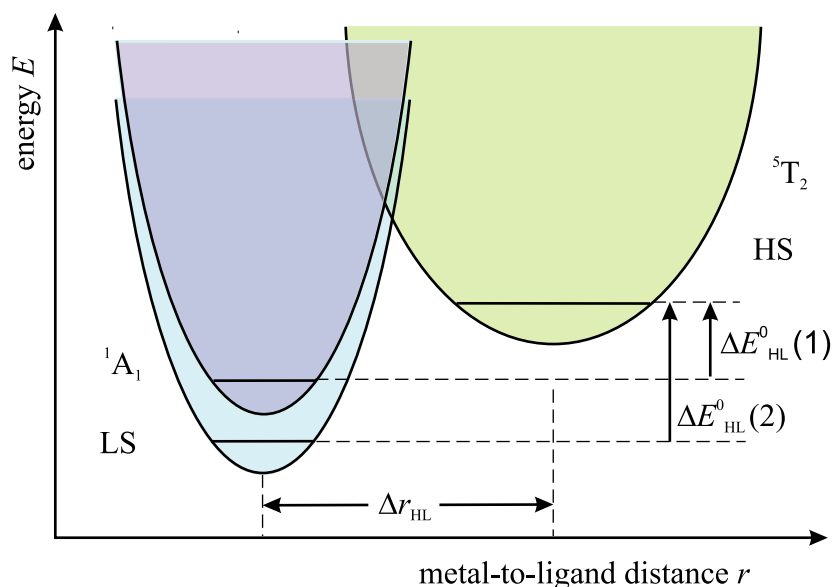
Scheme 3. Schematic representation of ligands and complexes with potential for hydrogen bonding: Hsaen from ref. [10], H₂L3 from ref. [12,13,34], FeH₄L4 from ref. [13] and H₄L5 from ref. [11].

All these examples demonstrate that i) hydrogen bonds significantly influence the ligand field strength if donor atoms or atoms in conjugated systems with donor atoms are involved and ii) changes in the hydrogen-bond network (often, but not necessarily, in line with a structural phase transition) result in changes in the ST behaviour. This information can now be used to suggest a new model for the explanation of the wide thermal hysteresis loops of the high-temperature modification of **1** and **2**·MeOH (as well as the different literature examples with hysteresis loops in which hydrogen bonding is observed):

A ST is associated with changes in the bond length between the iron centre and the donor atoms. These changes most likely influence the strength of the hydrogen bond to the donor atom, *e.g.* in the case of **1**^{HT} between the NH of the imidazole ligand and O1 of the equatorial ligand. This change influences the overall ligand field strength of the complex. In our two

cases, upon cooling, this change results in a stabilisation of the LS state (corresponding to a shift of the LS potential wells to lower energies, see Scheme 4). As a consequence, ΔE_{HL} increases and a higher transition temperature is observed in the heating mode. Wide thermal hysteresis loops should thus be observed if a large enough change in a hydrogen-bond network involving donor atoms or atoms in conjugated systems with donor atoms is observed. Those changes can be associated with reversible structural phase transitions.

The second question to be addressed in this context is that of domain formation as the reason for hysteresis loops (the theory of Sorai and Seki).^[36] The high interaction parameter J of 560 K derived from FORC analysis indicates a pronounced intradomain interaction. A possible explanation to unify both concepts would be that one domain is formed by an assembly of molecules with the same ligand field strength or, if a structural phase transition takes place, of the same structural phase. This implies that both theories not only coexist but also support each other. Further investigations on the compounds presented in this work and on new examples are necessary to verify this concept.



Scheme 4. Schematic representation of the HS and LS potential wells before spin transition (LS dark blue) and after spin transition (LS light blue). Upon spin transition, a change in the H-bond strength results in a different ligand field strength for the LS state and therefore a higher ΔE_{HL} that leads to a higher transition temperature in the heating mode compared to the cooling mode.

10.4 Conclusion

Spin transition molecular materials have a high potential as materials for various applications in display and data processing (memory device units, cold channel control units in food and medical storage devices). These potential applications desire a highly cooperative ST system with an approximate 100-K wide hysteresis loop.^[2a] In this manuscript, we have introduced a new concept to explain the interplay of wide bistability domains and hydrogen bonds between the magnetic centres. This concept brings us one step closer to the application of SCO materials.

10.5 Experimental Section

Magnetic measurements: Were performed on a Quantum-Design-MPMSR-XL-SQUID-Magnetometer in the 50–400 K temperature range at 0.05 T in the settle mode. The data corrections were made by using tabulated Pascal's constants. All measurements were reproduced twice. The FORC distribution is determined at each point by fitting a mixed second-order polynomial of the form $[a_1 + a_2T_a + a_3T_b + a_4T_a^2 + a_5T_b^2 + a_6T_aT_b]$ to a local moving grid. When interpolation is done to obtain the distribution value, we also take into consideration the neighbouring interpolated point. In this case, the value of a_6 provides the mixed second derivative of the fitted surface and it can be assigned to the centre of grid as a representation of the density of the FORC distribution $\rho(T_a, T_b)$ at that point. The value of the magnetisation is interpolated in every measured point with that polynomial of second order.

Differential scanning calorimetric measurements: Were carried out in a He_(g) atmosphere by using a Perkin-Elmer DSC Pyris 1 instrument equipped with a cryostat and operating down to 98 K. An aluminium capsule was loaded with 10 to 30 mg of sample and hermetically sealed. The heating and cooling rates were fixed at 10 K min⁻¹. Temperatures and enthalpies were calibrated over the temperature range of 298 to 400 K by using the solid-liquid transitions of pure Indium (99.99%)^[37] and the crystal-crystal transitions of pure cyclopentane ($\geq 99\%$)^[38] over the range 120 to 298 K. The sample was maintained at room temperature or at the highest temperature for 5 min in order to allow the system to equilibrate, and was further warmed or cooled in the investigated region. The experiments were carried out four times to check the reproducibility.

Crystal structure analysis: The intensity data of **1^{LT}**, **1^{HT}D** and **2·MeOH** were collected on an Oxford XCalibur diffractometer, the intensity data of **2·CD₃OD** were collected on a Nonius Kappa CCD diffractometer, both by using graphite-monochromated MoK_α radiation. The data were corrected for Lorentz and polarisation effects. The structure was solved by direct methods (SIR-97^[39]) and refined by full-matrix least-square techniques against F_0^2 (SHELXL-97^[40]). The hydrogen atoms were included at calculated positions with fixed thermal displacement parameters. Cell parameters and refinement results are summarised in

Supporting Information Table S1.1–2. ORTEP-III was used for structure representation.^[41] SCHAKAL-99 to illustrate molecule packings.^[42]

Crystallographic data for the structures reported in this paper have been deposited with the Cambridge Crystallographic Data Centre as supplementary publication no. CCDC-723037 (**1^{HTD}**), -723038 (**1^{LT}**), -800952 (**2·MeOH**) and -800953 (**2·CD₃OD**). These data can be obtained free of charge via www.ccdc.cam.ac.uk/conts/retrieving.html (or from the Cambridge Crystallographic Data Centre, 12, Union Road, Cambridge CB2 1EZ, UK; fax: (+44) 1223-336-033; or deposit@ccdc.cam.ac.uk).

General synthesis: All syntheses were carried out under argon by using Schlenk tube techniques. Methanol was purified and distilled under argon before use. [FeL1(MeOH)₂] and [FeL2(MeOH)₂] were prepared as described in literature^[43] by using anhydrous iron(II) acetate as starting material.^[44] Imidazole was purchased from Alfa Aesar, [D₄]-imidazole (98 atom %) [D₁]-methanol (CH₃OD, 99.5 atom %) and [D₄]-methanol (HDO + D₂O < 0.03%) were purchased from Aldrich and used as received.

[FeL1(HIm)₂] (1^{LT}): A mixture of [FeL1(MeOH)₂] (0.09 g, 0.18 mmol) and imidazole (0.30 g, 4.41 mmol) was dissolved in methanol (8.0 mL) and refluxed for 5 min. After cooling, the solution was allowed to stand for 3 d until a fine crystalline black precipitate was obtained, which was filtered off, washed with methanol (2 × 5 mL) and dried *in vacuo* (yield: 0.05 g, 48%). IR (KBr): $\tilde{\nu} = 1702(\text{s}), 1575 \text{ cm}^{-1}(\text{s})$; elemental analysis calcd (%) for C₂₆H₃₀N₆O₆Fe: C 53.99, H 5.23, N 14.53; found: C 53.79, H 5.23, N 14.55.

[FeL1(HIm)₂] (1^{HT}): A mixture of [FeL1(MeOH)₂] (0.56 g, 1.11 mmol) and imidazole (3.80 g, 55.5 mmol) was dissolved in methanol (20 mL) and refluxed for 5 min. After cooling, the fine crystalline black precipitate was filtered off immediately, washed with methanol (2 × 5 mL) and dried *in vacuo* (yield: 0.43 g, 67%). IR (KBr): $\tilde{\nu} = 1703, 1672, 1620 \text{ cm}^{-1}(\text{s})$; MS (DEI(+), 70 eV): *m/z* (%): 442 (64) [FeL1⁺], 68 (100) [HIm⁺]. elemental analysis calcd (%) for C₂₆H₃₀N₆O₆Fe: C 53.99, H 5.23, N 14.53; found: C 53.97, H 5.03, N 14.45.

[FeL1([D₄]-imidazole)₂] (1^{HTD}): The synthesis was carried out in a similar manner as described above. A mixture of [FeL1(MeOH)₂] (0.13 g, 0.26 mmol) and [D₄]-imidazole (0.93 g, 12.8 mmol) was dissolved in [D₁]-methanol (6.1 mL) and refluxed for 5 min. After cooling, the fine crystalline black precipitate was immediately filtered off to give **1^{HTD}** (yield: 0.06 g,

38%). IR (KBr): $\tilde{\nu} = 1688(\text{s}), 1671(\text{m}), 1563 \text{ cm}^{-1}$ (vs); MS (DEI(+), 70 eV): m/z (%): 442 (80) $[\text{FeL1}^+]$, 72 (100) $[\text{C}_3\text{D}_4\text{N}_2^+]$; elemental analysis calcd (%) for $\text{C}_{26}\text{H}_{22}\text{D}_8\text{FeN}_6\text{O}_6$: C 53.25, N 14.33; found: C 53.14, N 14.16.

[FeL1([D₄]-imidazole)₂] (1^{LT}D): The mother liquor from the synthesis of **1^{HT}D** was kept refrigerated at 4 °C. After two days **1^{LT}D** precipitated as fine black needles, which were filtered off and dried *in vacuo* (yield: 0.02 g, 13%). Unit cell ($T = 200 \text{ K}$): orthorhombic P , $a = 8.88$, $b = 11.76$, $c = 24.78$, $V = 2587.6$; IR (KBr): $\tilde{\nu} = 1688(\text{w}), 1671(\text{s}), 1562 \text{ cm}^{-1}$ (vs); MS (DEI(+), 70 eV): m/z (%): 442 (49) $[\text{FeL1}^+]$, 72 (100) $[\text{C}_3\text{D}_4\text{N}_2^+]$; elemental analysis calcd (%) for $\text{C}_{26}\text{H}_{22}\text{D}_8\text{FeN}_6\text{O}_6$: C 53.25, N 14.33; found: C 52.97, N 15.34.

4,4'-Azopyridine (azpy): 4,4'-Azopyridine was prepared by the oxidative coupling of 4-aminopyridine and hypochlorite, using an adaptation of Launay *et al.*^[45] A cold solution of 4-aminopyridine (5.05 g, 53.7 mmol) in water (100 mL) was added dropwise to a 6.5% NaOCl solution (300 mL). The mixture was stirred at 5 °C, during which time an orange precipitate formed. After completion of the addition the reaction mixture was stirred for another 15 min. The precipitate was filtered off and washed with cold water. The aqueous phase was extracted three times with diethyl ether. The combined organic phases were dried using MgSO_4 and the solvent evaporated. The crude products were recrystallised in water yielding 4,4'-azopyridine as orange needles (yield: 1.70 g, 34%). ^1H NMR (270 MHz, CDCl_3 , 25 °C, TMS) $\delta = 8.9$ (m, 4H, Ar-H), 7.7 ppm (m, 4H, Ar-H); MS (DEI(+), 70 eV): m/z (%): 184 (55) $[\text{M}^+]$, 78 (100) $[\text{C}_5\text{H}_4\text{N}^+]$; elemental analysis calcd (%) for $\text{C}_{10}\text{H}_8\text{N}_4$: C 65.21, H 4.38, N 30.42; found: C 64.67, H 4.20, N 30.18.

[FeL2(azpy)]·MeOH (2·MeOH): **2·MeOH** was synthesised by a slow diffusion technique by using a Schlenk tube that is, to a certain height, separated into two chambers. Into one chamber $[\text{FeL2}(\text{MeOH})_2]$ (0.09 g, 0.16 mmol) was placed and into the other chamber 4,4'-azopyridine (0.03 g, 0.17 mmol) was placed. Methanol was carefully added to the point to allow slow diffusion at one point of contact. Within a couple of days, **2·MeOH** was obtained as black crystals, which were of sufficient quality for X-ray analysis. After removing the solvent the product was dried *in vacuo* and kept refrigerated at 4 °C (yield: approximately 0.10 g, 85%). IR (KBr): $\tilde{\nu} = 1627(\text{s}), 1554 \text{ cm}^{-1}$ (vs); MS (DEI(+), 70 eV): m/z (%): 506 (24) $[\text{FeL2}^+]$, 184 (73) $[\text{azpy}^+]$, 78 (100) $[\text{C}_5\text{H}_4\text{N}^+]$; DTG: up to 150 °C: -2.12% = loss of 1 methanol (calc.: 4.4%; presumably part of the methanol was lost during the storage of the

sample); elemental analysis calcd (%) for $C_{39}H_{34}FeN_6O_5$: C 64.83, H 4.74, N 11.63; found: C 65.03, H 4.70, N 11.81.

[FeL2(azpy)]·CD₃OD (2·CD₃OD): 2·CD₃OD was synthesised by slow diffusion just as 2·MeOH. [FeL2(MeOH)₂] (0.09 g, 0.16 mmol) and 4,4'-azopyridine (0.03 g, 0.17 mmol) were dissolved in [D₄]-methanol. Within a couple of days, 2·CD₃OD was obtained in form of black crystals, which were of sufficient quality for X-ray analysis. After removing the solvent the product was dried *in vacuo* and kept refrigerated at 4 °C (yield: approximately 0.10 g, 85%). IR (KBr): $\tilde{\nu} = 1627(s), 1555\text{ cm}^{-1}$ (vs); MS (DEI-(+), 70 eV): *m/z* (%): 506 (10) [FeL2⁺], 184 (59) [azpy⁺], 78 (100) [C₅H₄N⁺]; DTG: up to 150 °C: -3.7% = loss of 1 [D₄]-methanol (calc.: 4.9%); elemental analysis calcd (%) for $C_{39}H_{30}D_4FeN_6O_5$: C 64.47, N 11.57; found: C 64.52, N 11.73.

[FeL2(azpy)](2): [FeL2(MeOH)₂] (0.12 g, 0.21 mmol) and 4,4'-azopyridine (0.31 g, 1.66 mmol) were dissolved in methanol (15 mL) and refluxed for 1 h. The product precipitated from the boiling solution as black powder. After cooling to room temperature 2 was filtered off, washed with methanol (5 mL) and dried *in vacuo* (0.09 g, 61%). IR (KBr): $\tilde{\nu} = 1627(m), 1556\text{ cm}^{-1}$ (vs); MS (DEI-(+), 70 eV): *m/z* (%): 506 (9) [FeL2⁺], 184 (43) [azpy⁺], 78 (100) [C₅H₄N⁺]; elemental analysis calcd (%) for $C_{38}H_{30}FeN_6O_4$: C 66.10, H 4.38, N 12.17; found: C 65.34, H 4.73, N 12.12.

Acknowledgements

This work has been supported financially by the Deutsche Forschungsgemeinschaft (SPP 1137), the Fonds der Chemischen Industrie, the Center for Integrated Protein Science Munich (CIPSM) and the University of Munich, the IAP VI (P6/17) INANOMAT, the FNRS-FRFC (No 2.4508308), a Concerted Research Action of the “Communauté Française de Belgique” allotted by the Académie Universitaire Louvain and by the European Social Fund through Sectorial Operational Program Human Resources: PRiDE (No POSDRU/89/1.5/S/57083).

10.6 References

- [1] a) H.A. Goodwin, *Coord. Chem. Rev.*, **1976**, *18*, 293; b) E. König, *Struct. Bonding (Berlin)* **1991**, *76*, 51; c) P. Gütllich, A. Hauser, H. Spiering, *Angew. Chem. Int. Ed. Engl.* **1994**, *33*, 2024, and references therein; d) P. Gütllich, H.A. Goodwin (Eds.), *Spin Crossover in Transition Metal Compounds I–III, Topics in Current Chemistry*, Springer, Berlin, Heidelberg, New York **2004**; e) J.A. Real, A.B. Gaspar, M.C. Munoz, *Dalton Trans.* **2005**, 2062; f) K. Nakano, N. Suemura, K. Yoneda, S. Kawata, S. Kaizaki, *Dalton Trans.* **2005**, 740; g) O. Sato, J. Tao, Y.-Z. Zhang, *Angew. Chem.* **2007**, *119*, 2200; *Angew. Chem. Int. Ed.* **2007**, *46*, 2152; h) J.A. Kitchen, S. Brooker, *Coord. Chem. Rev.* **2008**, *252*, 2072; i) K.S. Murray, *Eur. J. Inorg. Chem.* **2008**, 3101; k) M.A. Halcrow, *Coord. Chem. Rev.* **2009**, 2059; l) S. Brooker, J.A. Kitchen, *Dalton Trans.* **2009**, 7331; m) C.J. Kepert, *Aust. J. Chem.* **2009**, *62*, 1079; n) K.S. Murray, *Aust. J. Chem.* **2009**, *62*, 1081; o) A.B. Koudriavtsev, W. Linert, *J. Struct. Chem.* **2010**, *51*, 335.
- [2] a) O. Kahn, C. Jay Martinez, *Science* **1998**, *279*, 44; b) O. Kahn, C. Jay Martinez, J. Kröber, R. Claude, F. Grolière, *Patent EP0666561* **1995**; c) J.-F. Létard, O. Nguyen, N. Daro, *Patent FR0512476* **2005**; d) J.-F. Létard, P. Guionneau, L. Goux-Capes, *Topics in Current Chemistry, Vol. 235* (Eds.: P. Gütllich, H.A. Goodwin), Springer, Wien, New York, **2004**, 221; e) A. Galet, A.B. Gaspar, M.C. Munoz, G.V. Bukin, G. Levchenko, J.A. Real, *Adv. Mater.* **2005**, *17*, 2949.
- [3] Y. Garcia, V. Ksefontov, P. Gütllich, *Hyperfine Interact.* **2002**, *139/140*, 543.
- [4] Y. Garcia, V. Ksefontov, S. Mentior, M.M. Dîrtu, C. Gieck, A. Bhatthacharjee, P. Gütllich, *Chem. Eur. J.* **2008**, *14*, 3745.
- [5] a) M. Seredyuk, A.B. Gaspar, V. Ksenofontov, Y. Galyametdinov, M. Verdaguer, F. Villain, P. Gütllich, *Inorg. Chem.* **2008**, *47*, 10232; b) M. Seredyuk, A.B. Gaspar, V. Ksenofontov, Y. Galyametdinov, J. Kusz, P. Gütllich, *Adv. Funct. Mater.* **2008**, *18*, 2089; c) M. Seredyuk, A.B. Gaspar, V. Ksenofontov, Y. Galyametdinov, J. Kusz, P. Gütllich, *J. Am. Chem. Soc.* **2008**, *130*, 1431.

10. Influence of Hydrogen Bonding on the Hysteresis Width in Iron(II) Spin Crossover Complexes

- [6] a) J.A. Real, A.B. Gaspar, V. Niel, M.C. Muñoz, *Coord. Chem. Rev.* **2003**, 236, 121; b) A. Bousseksou, G. Molnár, J.A. Real, K. Tanaka, *Coord. Chem. Rev.* **2007**, 251, 1822.
- [7] a) A.B. Gaspar, V. Ksenofontov, M. Seredyuk, P. Gütllich, *Coord. Chem. Rev.* **2005**, 249, 2661; b) A.B. Gaspar, M. Seredyuk, P. Gütllich, *J. Mol. Struct.* **2009**, 924–926, 9.
- [8] a) I. Boldog, A.B. Gaspar, V. Martinez, P. Pardo-Ibanez, V. Ksenofontov, A. Bhattacharjee, P. Gütllich, J.A. Real, *Angew. Chem. Int. Ed. Engl.* **2008**, 47, 6433; b) S. Cobo, G. Molnar, J.A. Real, A. Bousseksou, *Angew. Chem. Int. Ed. Engl.* **2006**, 45, 5786; c) G. Molnár, S. Cobo, J.A. Real, F. Carcenac, E. Daran, C. Vieu, A. Bousseksou, *Adv. Mater.* **2007**, 19, 2163.
- [9] B. Weber, W. Bauer, J. Obel, *Angew. Chem.* **2008**, 120, 10252; *Angew. Chem. Int. Ed.* **2008**, 47, 10098.
- [10] A.P. Summerton, A.A. Diamantis, M.R. Snow, *Inorg. Chim. Acta* **1978**, 27, 123.
- [11] B. Weber, J. Obel, D. Henner-Vásquez, W. Bauer, *Eur. J. Inorg. Chem.* **2009**, 5527.
- [12] a) A. Bhattacharjee, V. Ksenofontov, K.H. Sugiyarto, H.A. Goodwin, P. Gütllich, *Adv. Funct. Mater.* **2003**, 13, 877; b) K.H. Sugiyarto, M.L. Scudder, D.C. Craig, H.A. Goodwin, *Aust. J. Chem.* **2000**, 53, 755; c) A. Bhattacharjee, J. Kusz, M. Zubko, H.A. Goodwin, P. Gütllich, *J. Mol. Struct.* **2008**, 890, 178.
- [13] a) K.H. Sugiyarto, K. Weitzner, D.C. Craig, H.A. Goodwin, *Aust. J. Chem.* **1997**, 50, 869; b) T. Buchen, P. Gütllich, K.H. Sugiyarto, H.A. Goodwin, *Chem. Eur. J.* **1996**, 2, 1134.
- [14] J.A. Real, A.B. Gaspar, V. Niel, M.C. Muñoz, *Coord. Chem. Rev.* **2003**, 236, 121.
- [15] N. Bréfuel, S. Imatomi, H. Torigoe, H. Hagiwara, S. Shova, J.-F. Meunier, S. Bonhommeau, J.-P. Tuchagues, N. Matsumoto, *Inorg. Chem.* **2006**, 45, 8126.
- [16] a) B.R. Müller, G. Leibelng, E.-G. Jäger, *Chem. Phys. Lett.* **2000**, 319, 368; b) G. Leibelng, PhD thesis, University of Jena (Germany), **2003**.
- [17] C. Pike, A. Fernandez, *J. Applied Phys.* **1999**, 85, 6668.

- [18] C. Enachescu, R. Tanasa, A. Stancu, E. Codjovi, J. Linares, F. Varret, *Physica B* **2004**, 343, 15.
- [19] R. Tanasa, C. Enachescu, A. Stancu, J. Linares, E. Codjovi, F. Varret, J.G. Haasnoot, *Phys. Rev. B* **2005**, 71, 014431.
- [20] W. Vreugdenhil, J.H. Vandiemmen, R.A.G. Degraaff, J.G. Haasnoot, J. Reedijk, A.M. Vanderkraan, O. Kahn, J. Zarembowitch, *Polyhedron* **1990**, 9, 2971.
- [21] a) Y. Garcia, V. Niel, M.C. Muñoz, J.A. Real, *Top. Curr. Chem.* **2004**, 233, 229. b) Y. Garcia, C. Gieck, S. Stauf, W. Tremel, P. Gütllich, 4th TMR TOSS-Meeting, Bordeaux (France), **2001** ; c) S. Pillet, J. Hubsch, C. Lecomte, *Eur. Phys. J. B* **2004**, 38, 541.
- [22] M.M. Dîrtu, C. Neuhausen, A.D. Naik, A. Rotaru, L. Spinu, Y. Garcia, *Inorg. Chem.* **2010**, 49, 5723.
- [23] A. Rotaru, PhD thesis, Versailles (France), **2009**.
- [24] Y. Garcia, V. Ksenofontov, S. Mentior, M.M. Dîrtu, C. Gieck, A. Bhatthacharjee, P. Gütllich, *Chem. Eur. J.* **2008**, 14, 3745.
- [25] B. Weber, E. Kaps, J. Weigand, C. Carbonera, J.-F. Létard, K. Achterhold, F.G. Parak, *Inorg. Chem.* **2008**, 47, 487.
- [26] a) B. Weber, *Coord. Chem. Rev.* **2009**, 253, 2432; b) B. Weber, E.-G. Jäger, *Eur. J. Inorg. Chem.* **2009**, 465.
- [27] a) B. Weber, E. Kaps, J. Obel, W. Bauer, *Z. Anorg. Allg. Chem.* **2008**, 1421; b) B. Weber, C. Carbonera, C. Desplanches, J.-F. Létard, *Eur. J. Inorg. Chem.* **2008**, 1589; c) B. Weber, E. Kaps, C. Desplanches, J.-F. Létard, K. Achterhold, F.G. Parak, *Eur. J. Inorg. Chem.* **2008**, 4891; d) W. Bauer, B. Weber, B.; *Inorg. Chim. Acta* **2009**, 362, 2341; e) B. Weber, E. Kaps, *Heteroatom Chem.* **2005**, 16, 391; f) B. Weber, E. Kaps, J. Obel, K. Achterhold, F.G. Parak, *Inorg. Chem.* **2008**, 47, 10779; g) B. Weber, R. Tandon, D. Himsl, *Z. Anorg. Allg. Chem.* **2007**, 633, 1159; h) B. Weber, E.S. Kaps, C. Desplanches, J.-F. Létard, *Eur. J. Inorg. Chem.* **2008**, 2963.

- [28] K. Hosoya, T. Kitazawa, M. Takahashi, M. Takeda, J.-F. Meunier, G. Molnar, A. Bousseksou, *Phys. Chem. Chem. Phys.* **2003**, *5*, 1682.
- [29] P. Gülich, H. Köppen, H.G. Steinhäuser, *Chem. Phys. Letters* **1980**, *74*, 475.
- [30] N. Wiberg, *Holleman Wiberg – Lehrbuch der Anorganischen Chemie*, Walter de Gruyter, Berlin, New York, **2007**.
- [31] see for example: a) Y. Kikuta, T. Ishimoto, U. Nagashima, *Chem. Phys.* **2008**, *354*, 218; b) S. Singh, C.N.R. Rao, *Can. J. Chem.* **1966**, *44*, 2611.
- [32] T. M. Pfaffeneder, S. Thallmair, W. Bauer, B. Weber, *New J. Chem.* **2011**, *35*, 691.
- [33] a) K.H. Sugiyarto, H.A. Goodwin, *Aust. J. Chem.* **1988**, *41*, 1645; b) T. Buchen, P. Gülich, H.A. Goodwin, *Inorg. Chem.* **1994**, *33*, 4573; c) K.H. Sugiyarto, D.C. Craig, A.D. Rae, H.A. Goodwin, *Aust. J. Chem.* **1994**, *47*, 869.
- [34] Y. Garcia, S.J. Campbell, J.S. Lord, Y. Boland, V. Ksenofontov, P. Gülich, *J. Phys. Chem. B* **2007**, *111*, 11111.
- [35] a) J. Krober, J.P. Audiere, R. Clued, E. Codjovi, O. Kahn, J.G. Haasnoot, F. Groliere, C. Jay, A. Bousseksou, J. Linares, F. Varret, A. Gonthiervassal, *Chem. Mater.* **1994**, *6*, 1404; b) K.H. Sugiyarto, H.A. Goodwin, *Aust. J. Chem.* **1994**, *47*, 263.
- [36] a) M. Sorai, S. Seki, *J. Phys. Soc. Jpn.* **1972**, *33*, 575. b) C. Chong, B. Berini, K. Boukheddaden, E. Codjovi, J. Linares, Y. Garcia, A.D. Naik, F. Varret, *Phys. Status Solidi A* **2010**, *207*, 1227.
- [37] W. Eysel, K.H. Breuer, *Thermochim. Acta* **1982**, *57*, 317.
- [38] A. Rotaru, M.M. Dîrtu, C. Enachescu, R. Tanasa, J. Linares, A. Stancu, Y. Garcia, *Polyhedron* **2009**, *28*, 2531.
- [39] A. Altomare, M.C. Burla, G.M. Camalli, G. Cascarano, C. Giacovazzo, A. Guagliardi, A.G.G. Moliterni, G. Polidori, R. Spagna, SIR-97, University of Bari, Bari (Italy), **1997**; *J. Appl. Crystallogr.* **1999**, *32*, 115.
- [40] G.M. Sheldrick, SHELXL-97, University of Göttingen, Göttingen (Germany), **1993**.

- [41] C.K. Johnson, M.N. Burnett, ORTEP-III, Oak-Ridge National Laboratory, Oak-Ridge, TN (US), **1996**; L.J. Farrugia, *J. Appl. Cryst.* **1997**, *30*, 565.
- [42] E. Keller, SCHAKAL-99, University of Freiburg, Freiburg (Germany), **1999**.
- [43] E.-G. Jäger, E. Häussler, M. Rudolph, M. Rost, *Z. Anorg. Allg. Chem.* **1985**, *525*, 67.
- [44] B. Weber, R. Betz, W. Bauer, S. Schlamp, *Z. Anorg. Allg. Chem.* **2011**, *673*, 102.
- [45] J.-P. Launay, M. Tourrel-Pagis, J.-F. Lipskier, V. Marvaud, C. Joachim, *Inorg. Chem.* **1991**, *30*, 1033.

10. Influence of Hydrogen Bonding on the Hysteresis Width in Iron(II) Spin Crossover Complexes

10.7 Supporting Information

Table S1.1. Crystallographic data of compound **1^{LT}** and **1^{HTD}**. For comparison purpose, the data of **1^{HT}** [9] are given as well.

compound	1^{HT} [9], [a]	1^{HTD}	1^{LT}
formula	C ₂₆ H ₃₀ FeN ₆ O ₆	C ₂₆ H ₂₄ D ₆ FeN ₆ O ₆	C ₂₆ H ₃₀ FeN ₆ O ₆
<i>M_r</i> / g mol ⁻¹	578.41	584.45	578.41
crystal system	monoclinic	monoclinic	orthorhombic
space group	<i>P</i> 2 ₁ / <i>c</i>	<i>P</i> 2 ₁ / <i>c</i>	<i>P</i> 2 ₁ 2 ₁ 2 ₁
<i>a</i> / Å	11.6280(12)	11.653(3)	8.8957(8)
<i>b</i> / Å	9.3700(8)	9.375(3)	11.743(2)
<i>c</i> / Å	27.245(2)	27.306(5)	24.832(9)
<i>α</i> / °	90.00	90.00	90.00
<i>β</i> / °	112.037(4)	112.136(15)	90.00
<i>γ</i> / °	90.00	90.00	90.00
<i>V</i> / Å ³	2751.6(4)	2763.2(12)	2594.0(11)
<i>Z</i>	4	4	4
<i>ρ</i> / g cm ⁻³	1.396	1.405	1.481
<i>μ</i> / mm ⁻¹	0.599	0.596	0.635
crystal size	0.14 × 0.03 × 0.03	0.13 × 0.13 × 0.06	0.47 × 0.14 × 0.08
<i>T</i> / K	275(2)	275(2)	200(2)
diffractometer	KappaCCD	Oxford XCalibur	Oxford XCalibur
<i>λ</i> (MoK _α) / Å	0.71073	0.71073	0.71073
<i>θ</i> -range / °	3.18–26.00	3.75–23.54	3.78–24.99
reflns. collected	5295	30838	11093
indep. reflns. (<i>R</i> _{int})	3878 (0.0445)	4102 (0.0920)	4542 (0.0538)
mean <i>σ</i> (<i>I</i>) / <i>I</i>	0.1100	0.1038	0.1061
reflns. with <i>I</i> ≥ 2 <i>σ</i> (<i>I</i>)	2537	2391	3174
<i>x</i> , <i>y</i> (weighting scheme)	0.0444, 0	0.0241, 0	0.0211, 0
parameters	356	356	356
restraints	0	0	0
<i>R</i> (<i>F</i>) (all data) ^[b]	0.0555 (0.0946)	0.0400 (0.0921)	0.0367 (0.0600)
<i>wR</i> (<i>F</i> ²) ^[c]	0.1470	0.0646	0.0632
<i>Goof</i>	1.012	0.848	0.925
shift/error _{max}	0.000	0.000	0.003
max., min. resd. dens. / e Å ⁻³	0.335, -0.435	0.319, -0.249	0.401, -0.348

[a] For a better comparison of the different structures the data of the previously published complex **1^{HT}** (ref. [9]) were translated from *P*2₁/*n* to *P*2₁/*c*. [b] $R(F) = \sum ||F_o| - |F_c|| / \sum |F_o|$. [c] $wR(F^2) = [\sum [w(F_o^2 - F_c^2)^2] / \sum w(F_o^2)^2]^{1/2}$, $w = 1 / [\sigma^2(F_o^2) + (aP)^2 + bP]$, where $P = [F_o^2 + 2(F_c^2)]/3$.

10. Influence of Hydrogen Bonding on the Hysteresis Width in Iron(II) Spin Crossover Complexes

Table S1.2. Crystallographic data of compound **2·MeOH** and **2·CD₃OD**.

compound	2·MeOH	2·CD₃OD
formula	C ₃₉ H ₃₄ FeN ₆ O ₅	C ₃₉ H ₃₀ D ₄ FeN ₆ O ₅
$M_r / \text{g mol}^{-1}$	722.57	726.60
crystal system	triclinic	triclinic
space group	$P\bar{1}$	$P\bar{1}$
$a / \text{Å}$	11.747(7)	11.7410(6)
$b / \text{Å}$	12.103(6)	12.1271(7)
$c / \text{Å}$	13.852(9)	13.8360(8)
$\alpha / ^\circ$	114.173(6)	114.181(3)
$\beta / ^\circ$	101.169(5)	101.169(3)
$\gamma / ^\circ$	92.309(4)	92.240(4)
$V / \text{Å}^3$	1746.9(18)	1747.63(17)
Z	2	2
$\rho / \text{g cm}^{-3}$	1.374	1.381
μ / mm^{-1}	0.485	0.485
crystal size	0.39 × 0.21 × 0.12	0.38 × 0.20 × 0.14
T / K	200(2)	173(2)
diffractometer	Oxford XCalibur	KappaCCD
$\lambda (\text{MoK}_\alpha) / \text{Å}$	0.71073	0.71073
θ -range / $^\circ$	4.13–28.82	3.25–25.30
reflns. collected	20384	10482
indep. reflns. (R_{int})	20384	6269 (0.0379)
mean $\sigma(I) / I$	0.1186	0.0580
reflns. with $I \geq 2\sigma(I)$	11225	4868
x, y (weighting scheme)	0.0694, 0	0.0563, 7.5825
parameters	465	463
restraints	0	0
$R(F)$ (all data) ^[a]	0.0652 (0.1287)	0.0785 (0.1014)
$wR(F^2)$ ^[b]	0.1540	0.2201
$GooF$	0.924	1.173
shift/error _{max}	0.000	0.000
max., min. resd. dens. / e Å^{-3}	0.740, -0.508	0.804, -0.533

[a] $R(F) = \sum ||F_o| - |F_c|| / \sum |F_o|$. [b] $wR(F^2) = [\sum [w(F_o^2 - F_c^2)^2] / \sum w(F_o^2)^2]^{1/2}$, $w = 1 / [\sigma^2(F_o^2) + (aP)^2 + bP]$, where $P = [F_o^2 + 2(F_c^2)] / 3$.

11 Unusual Stepped Spin Transitions at Iron(II) Coordination Polymers with zigzag-Structure

Wolfgang Bauer^[a] and Birgit Weber*^[a]

[a] Inorganic Chemistry II, Universität Bayreuth, Universitätsstraße 30, NW I, 95440 Bayreuth, Germany. Fax: +49-92155-2157, E-mail: weber@uni-bayreuth.de

Keywords: Iron, Magnetism, X-ray structure, Stepwise Spin Crossover

Manuscript in preparation.

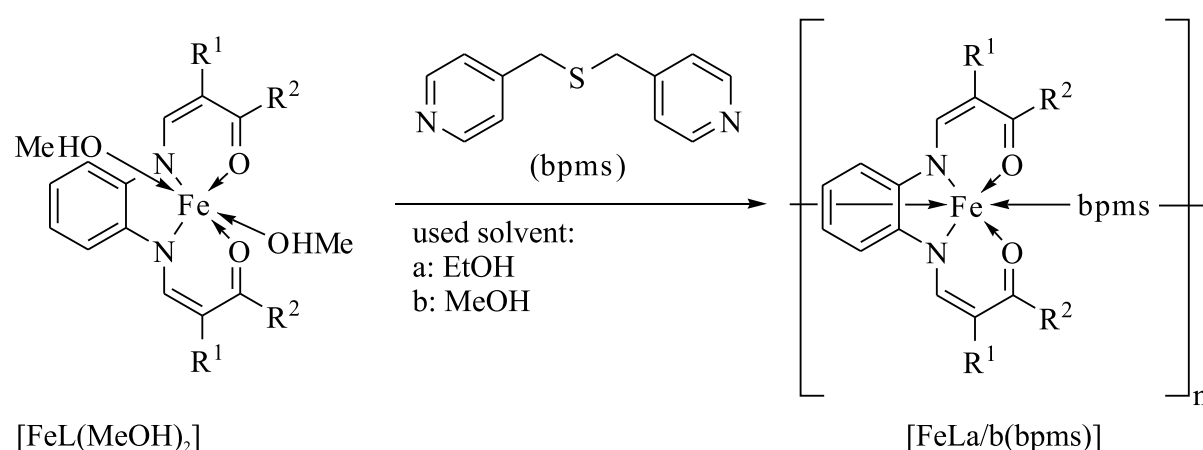
11.1 Introduction

The spin crossover (SCO) phenomenon has been receiving an ongoing interest over decades,^[1] as various applications in information technology^[2] or as sensors^[3] and cool channel control units in food and medical storage^[4] can be envisioned. Especially octahedral iron(II) complexes, which exhibit magnetic and physical changes detectable over the transition between high-spin (HS: $S = 2$) and low-spin (LS: $S = 0$) and coordinative-bridged networks with the objective to enhance communication between the SCO sites^[2,5] and to control the cooperative interactions,^[6,7] have been part of distinctive investigations. Although there is no doubt that the SCO effect is propagated in the solid state by strong cooperative interactions transmitted through hydrogen bonding, π -stacking or van der Waals-interactions from one molecule to another,^[1,7] many open questions still exist. The occurrence of thermal hysteresis loops and its width in SCO materials as well as the reason for stepped or incomplete spin transitions are not yet fully understood. Looking at 1D coordination polymers, we have recently found that the spin crossover behaviour is related to the rigidity of the linker molecule and the intermolecular interactions in such a way, that rigid linkers together with strong cooperativity transmitting interactions more often lead to thermal hysteresis. This was demonstrated for 4,4'-bipyridine linked SCO complexes^[8] and similar observations were made for triply 1,2,4-triazole bridged iron(II) complexes.^[9] In contrast to

this, flexible linkers with pronounced zigzag chain structures result more likely in stepped or incomplete SCO, depending on intermolecular restraining interactions.^[10,11] Moreover, stepped spin transitions in 1D chains are often associated with at least two nonequivalent iron centres, as presented from Neville, Murray and co-workers^[12] or random order-disorder effects of the HS/LS species.^[13]

One reason for the lack of knowledge concerning spin transition behaviour is still the deficiency of detailed structural information upon spin transition within one system, in order to get a deeper insight into the structural changes following the spin state change.

In this paper the synthesis and characterisation of several 1D chain iron(II) compounds (Scheme 1) with the flexible bridging ligand bis(4-pyridylmethyl)sulfane (bpms) is presented. A complete overview is given in Table 1. The tetradentate Schiff base-like equatorial ligands used in this work are partly well established for the syntheses of a multitude of SCO materials (L1, L2)^[8,10,14] or promising new derivatives (L3, L4)^[11,15] of them. Through detailed magnetic (thermal), structural (insofar as possible) and thermodynamic (DSC) analyses of these compounds and comparisons with closely related materials, a relationship between differing intermolecular interactions and the resulting SCO behaviours is drawn.



- L1: $\text{R}^1 = \text{CO}_2\text{Et}$, $\text{R}^2 = \text{Me}$
 L2: $\text{R}^1 = \text{COMe}$, $\text{R}^2 = \text{Me}$
 L3: $\text{R}^1 = \text{CO}_2\text{Me}$, $\text{R}^2 = \text{Me}$
 L4: $\text{R}^1 = \text{CO}_2\text{Et}$, $\text{R}^2 = \text{Ph}$

Scheme 1. General synthesis of the 1D octahedral iron(II) coordination polymers discussed in this work and the used abbreviations.

11. Unusual Stepped Spin Transitions at Iron(II) Coordination Polymers with zigzag-Structure

Table 1. Overview of the Compounds discussed in this work and the used abbreviations.

L _{eq} /solvent	EtOH	MeOH
L1	[FeL1(bpms)] (1a)	[FeL1(bpms)] (1b)
L2	[FeL2(bpms)]·EtOH (2a ·EtOH)	[FeL2(bpms)]·MeOH (2b ·MeOH)
L3	[FeL3(bpms)] (3a)	[FeL3(bpms)]·0.5 MeOH (3b ·0.5 MeOH)
L4	[FeL4(bpms)] (4a)	[FeL4(bpms)] (4b)

11.2 Results

Magnetic measurements: Magnetic susceptibility measurements in a temperature range from 300/350 K to 50 K were used to follow the iron(II) spin state change of all samples. The thermal dependence of the $\chi_M T$ product (with χ_M being the molar susceptibility and T the temperature) for all complexes is given in Figure 1. Comparing the transition curves of the compounds synthesised with ethanol as solvent, **1a** and **3a** show a complete and abrupt SCO, **4a** shows a complete but gradual spin transition behaviour and the SCO of **2a**·EtOH is incomplete, with about three quarters remaining in the HS state. For **1a**, **3a** and **4a**, small plateaus with HS fraction $\gamma_{\text{HS}} \approx 0.1$ can be observed. The transition curves of the compounds using methanol as solvent are quite different from the ethanol samples, with exception of sample **4b**, which shows the identically transition behaviour as **4a**. Compound **1b** shows an incomplete gradual SCO, **2b**·MeOH is a pure HS complex and the SCO of **3b**·0.5 MeOH is complete but also gradual. Thermal hysteresis was not observed for all samples.

11. Unusual Stepped Spin Transitions at Iron(II) Coordination Polymers with zigzag-Structure

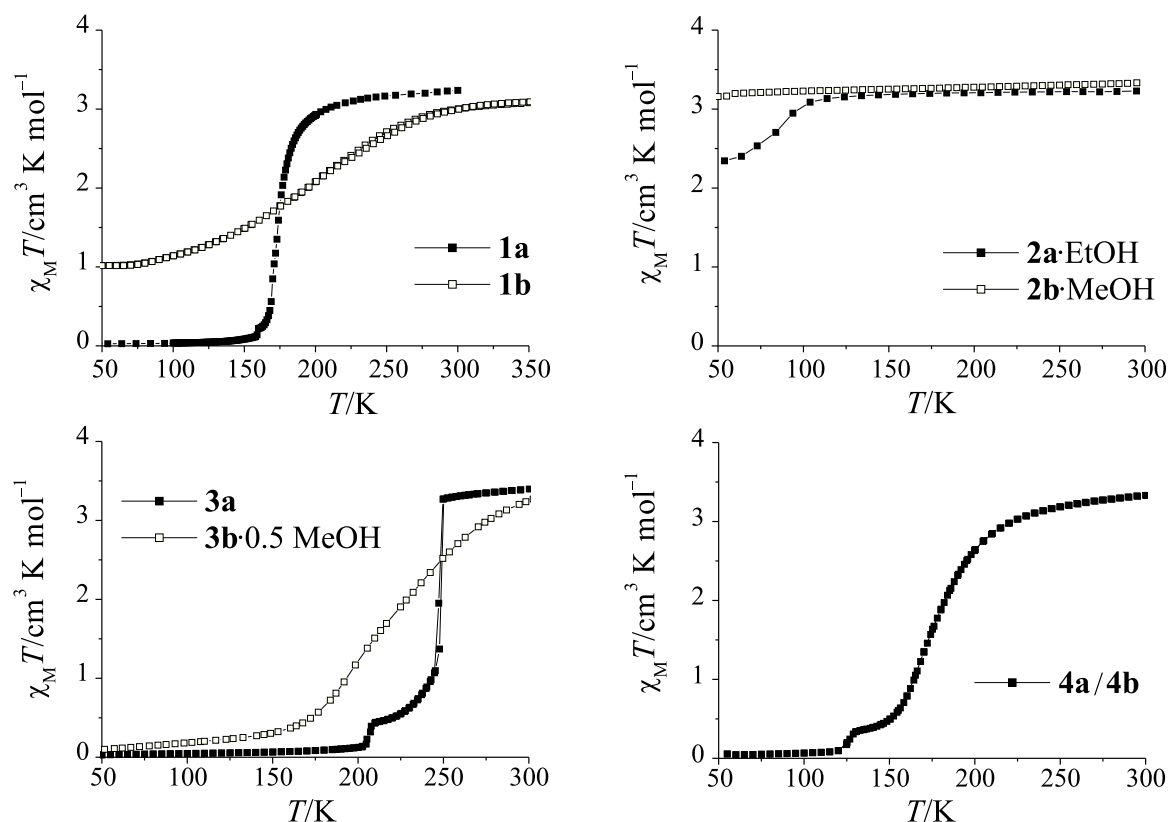


Figure 1. Plots of the $\chi_M T$ product vs. T over the range 50–300 K (350 K) for the compounds discussed in this work and the solvent used for synthesis (filled squares: ethanol, open squares: methanol).

Compound **1a** and **1b** attain maximum $\chi_M T$ values of 3.24 and $3.08 \text{ cm}^3 \text{ K mol}^{-1}$ at 300 K and 350 K, respectively, indicative of HS iron(II). Between 300 and 200 K, the $\chi_M T$ values of **1a** remain approximately constant. Between 200 and 160 K, the $\chi_M T$ values decrease, rapidly then more gradually, to attain a minimum value of $0.22 \text{ cm}^3 \text{ K mol}^{-1}$ ($\gamma_{\text{HS}} = 0.07$). The $T_{1/2}(1)$ value of this step is 175 K. Below 160 K, the $\chi_M T$ values further decrease to attain a minimum value of $0.04 \text{ cm}^3 \text{ K mol}^{-1}$ at 120 K, indicative of iron(II) in the LS state. The $T_{1/2}(2)$ value of this little step is 157.5 K. Below 120 K, the $\chi_M T$ values remain approximately constant. The $\chi_M T$ values of **1b** gradually decrease between 325 and 65 K to attain a minimum value of $1.02 \text{ cm}^3 \text{ K mol}^{-1}$ at 65 K, indicating that one third of the iron(II) sites are still HS. The $T_{1/2}$ value of this SCO is 195 K.

The $\chi_M T$ values for **2a**·EtOH remain approximately constant at $3.20 \text{ cm}^3 \text{ K mol}^{-1}$ between 300 and 135 K, indicative of HS iron(II). Below 135 K, the $\chi_M T$ values gradually decrease to attain a minimum value of $2.40 \text{ cm}^3 \text{ K mol}^{-1}$ at 60 K, indicating that approximately two thirds

of the iron(II) centres remain HS. The $T_{1/2}$ value is 89 K. **2b**·MeOH remains HS in the whole temperature range, with a $\chi_M T$ value of $3.30 \text{ cm}^3 \text{ K mol}^{-1}$ at 300 K.

The $\chi_M T$ values for **3a** remain approximately constant at $3.30 \text{ cm}^3 \text{ K mol}^{-1}$ above 250 K, indicative of iron(II) in the HS state. Over the range 250 to 210 K, the $\chi_M T$ values decrease, first rapidly then gradually, to attain a minimum of $0.43 \text{ cm}^3 \text{ K mol}^{-1}$ at 210 K ($\gamma_{\text{HS}} = 0.13$). The $T_{1/2}(1)$ value of this step is 247 K. Below 210 K, the $\chi_M T$ values decrease, again first rapidly then gradually, to attain a minimum value of $0.08 \text{ cm}^3 \text{ K mol}^{-1}$ at 175 K. The $T_{1/2}(2)$ value of this little step is 205.5 K. Below 175 K, the $\chi_M T$ values remain approximately constant. The $\chi_M T$ values for **3b**·0.5 MeOH gradually decrease from a maximum of $3.27 \text{ cm}^3 \text{ K mol}^{-1}$ at 300 K to a minimum of $0.10 \text{ cm}^3 \text{ K mol}^{-1}$ at 50 K. The $T_{1/2}$ value of this SCO is 216 K.

Compound **4a** attains a maximum $\chi_M T$ value of $3.34 \text{ cm}^3 \text{ K mol}^{-1}$ at 300 K. Below 300 K, the $\chi_M T$ values decrease slowly then, between 230 and 133 K, more rapidly then again gradually to a minimum value of $0.35 \text{ cm}^3 \text{ K mol}^{-1}$ at 133 K ($\gamma_{\text{HS}} = 0.11$). The $T_{1/2}(1)$ value of this step is 179 K. Below 133 K, the $\chi_M T$ values decrease, first rapidly then gradually to attain a minimum of $0.06 \text{ cm}^3 \text{ K mol}^{-1}$ at 95 K. The $T_{1/2}(2)$ value of this little step is 125.5 K. Below 135 K, the $\chi_M T$ values remain approximately constant. The thermal spin transition behaviour of compound **4b** does not differ of that observed for **4a**.

X-Ray structures analysis: Crystals suitable for X-ray analysis of compound **1a** and **4b** were obtained by slow diffusion technique. The crystallographic data are summarised in Supporting Information Table S1. Figure 2 and Figure 3 display the asymmetric units of **1a** and **4b**, respectively. Selected bond lengths and angles around the inner coordination sphere of the iron centres are summarised in Table 2 and Table 3. The determination of the X-ray structure of **1a** in the LS state was not possible, as the crystals crumble while cooling. For compound **4b** it was possible to determine the crystal structure in the HS (**4b**^{HS}) and LS state (**4b**^{LS}).

Both complexes have in common that the iron(II) centres are located in an octahedral coordination sphere consisting of the equatorially coordinated tetradentate Schiff base-like ligand and the axially coordinated bis(monodentate) bridging ligand bpms, bound through terminal 4-pyridyl groups. Each bridging ligand “connects” two iron(II) centres, resulting in the formation of infinite 1D chains as given in Figure 4. Due to the “flexibility” of the axial

ligand with its sulfane bridge, the 1D chains of both compounds propagate in a zigzag-like manner.

Compound **1a** crystallises in the monoclinic space group $P2_1/c$, with four formula units in the unit cell. The observed bond lengths around the iron(II) centre of **1a** are within the range reported for other octahedral iron(II) complexes of this ligand type in the HS state.^[7,16] The average values are 2.08 Å (Fe-N_{eq}), 2.01 Å (Fe-O_{eq}) and 2.27 Å (Fe-N_{ax}). The observed O-Fe-O angle, the so-called bite angle of the ligand, which is typically about 110° for HS iron(II) complexes of this ligand type and about 90° for LS iron(II), is with 107.3° clearly indicative of iron(II) in the HS state. Because of the considerably difference according to the spin state, the bite angle is a characteristic tool for the determination of the spin state.

The parallel 1D chains of **1a** propagate along the [2 0 1] direction and are stacked such that the unit cell contains no residual solvent accessible void volume. The intrachain Fe1 ··· Fe1 separation distance is with 10.02 Å relative short. This highlights the strong twisting of the axially bpms ligand (Figure 4) and the close-packed nature of the chains of **1a** (Figure 6). Such a packing-motif was also found in the crystal structure of the closely related compound [FeL1(bppa)]^[10] (bppa = 1,3-bis(4-pyridyl)propane, Fe1 ··· Fe1 = 10.01 Å), which undergoes an incomplete SCO that stops at an intermediate plateau of 50% HS-fraction. It could be deduced that such mixed HS/LS states are stabilised through restraining intermolecular interactions between the 1D chains, resulting from pronounced zigzag-motifs as well as a dense packing (strong network of intermolecular contacts shorter than the sum of the van der Waals-radii).^[7a,10] For the 1D coordination polymer [FeL2(bipy)]^[8a] (bipy = 4,4'-bipyridine) with its linear chains due to the stiff bridging ligand bipy, an intrachain Fe1 ··· Fe1 separation distance of 11.50 Å was observed.

11. Unusual Stepped Spin Transitions at Iron(II) Coordination Polymers with zigzag-Structure

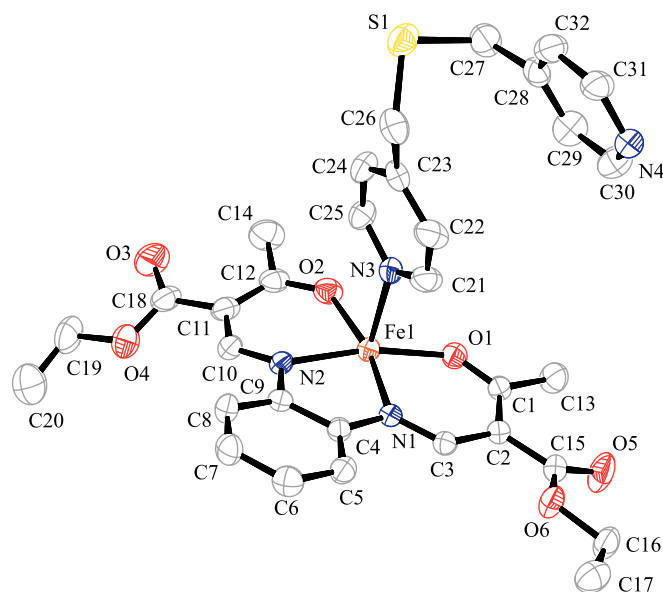


Figure 2. ORTEP drawing of the asymmetric unit of **1a**. Hydrogen atoms were omitted for clarity. Thermal ellipsoids are shown with a 50% probability.

Table 2. Selected bond lengths [Å] and angles [degree] within the inner coordination sphere of the iron(II) coordination polymer **1a**.

	Fe-N _{eq}	Fe-O _{eq}	Fe-N _{ax}	O _{eq} -Fe-O _{eq}	N _{ax} -Fe-N _{ax}
1a	2.083(2)	1.994(2)	2.242(3)	107.33(8)	179.19(9) ^[a]
	2.083(2)	2.016(2)	2.296(3) ^[a]		

Symmetry code: [a] 1 + x, ½ - y, ½ + z.

Compound **4b**^{HS} and **4b**^{LS} crystallise with orthorhombic space group *Pbca*, with eight formula units in the unit cell. The average bond lengths within the first coordination sphere of the iron(II) centres in the HS-structure are 2.08 Å (Fe-N_{eq}), 2.00 Å (Fe-O_{eq}) and 2.23 Å (Fe-N_{ax}). The observed O-Fe-O angle is with 105.2° at the lower limit of the expected HS-values of this ligand type,^[7,16] indicative of a beginning spin transition at slightly lower temperatures. Upon spin transition, a shortening of the bond lengths of about 10% is observed, as discussed for other iron(II) spin crossover complexes in literature.^[1] The average bond lengths in the LS-structure are with 1.92 Å (Fe-N_{eq}), 1.95 Å (Fe-O_{eq}) and 2.01 Å (Fe-N_{ax}) in the typical range. The more pronounced bond-shortening of the axial ligand, which connects the iron centres in the 1D chain, is in agreement with previous findings on mononuclear analogues.^[16] The

11. Unusual Stepped Spin Transitions at Iron(II) Coordination Polymers with zigzag-Structure

observed value of the O-Fe-O angle is with 90.6° clearly indicative of LS iron(II). Together with the bond-shortening, the cell volume shrinks from $8055.4(6)$ to $7675.7(6) \text{ \AA}^3$, comparing the HS- with the LS-structure. Considering the additional contribution of the thermal cell contraction, the observed change of the cell volume ($\Delta V/V = 4.7\%$, $\Delta V = 47.5 \text{ \AA}^3/\text{Fe}$) is in the range expected for an iron(II) SCO complex (sole contribution of the SCO: $\Delta V/V = 3.8\text{--}6\%$; $\Delta V = 25\text{--}35 \text{ \AA}^3/\text{Fe}$)^[1] with no indications of strong cooperative effects.

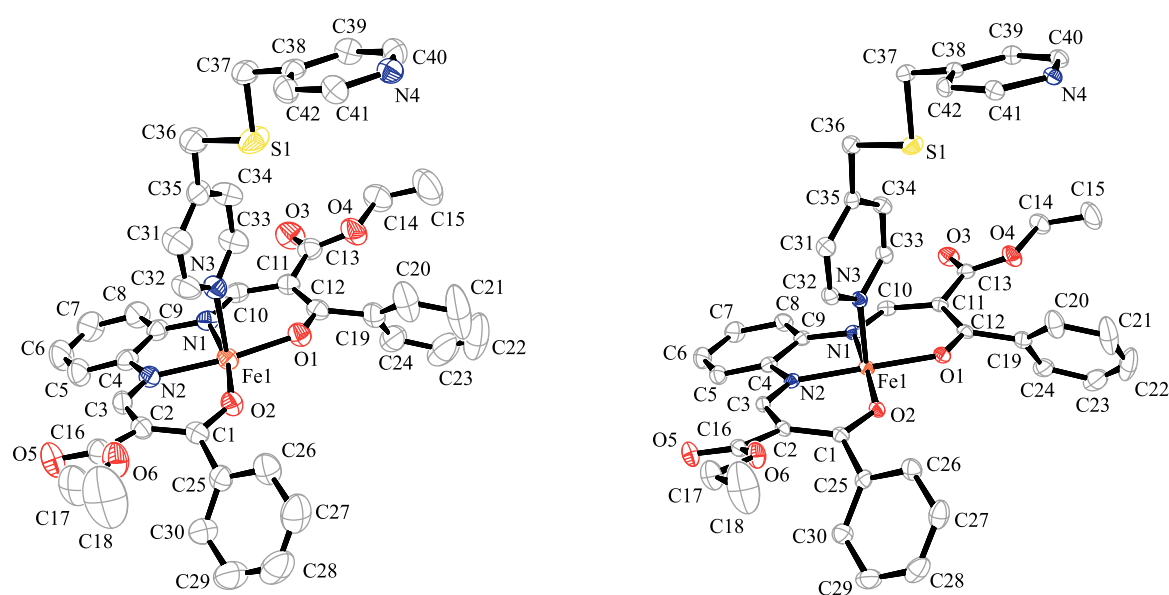


Figure 3. ORTEP drawing of the asymmetric unit of $\mathbf{4b}^{\text{HS}}$ at 250 K (left) and $\mathbf{4b}^{\text{LS}}$ at 125 K (right). Hydrogen atoms were omitted for clarity. Thermal ellipsoids are shown with a 50% probability.

Table 3. Selected bond lengths [\AA] and angles [degree] within the inner coordination sphere of the iron(II) coordination polymers $\mathbf{4b}^{\text{HS}}$ and $\mathbf{4b}^{\text{LS}}$.

	Fe-N _{eq}	Fe-O _{eq}	Fe-N _{ax}	O _{eq} -Fe-O _{eq}	N _{ax} -Fe-N _{ax}
$\mathbf{4b}^{\text{HS}}$	2.082(2)	1.997(1)	2.230(2)	105.16(5)	177.65(6) ^[b]
	2.076(2)	2.007(1)	2.236(2) ^[b]		
$\mathbf{4b}^{\text{LS}}$	1.917(2)	1.942(1)	2.012(2)	90.56(5)	176.81(6) ^[b]
	1.913(2)	1.954(1)	2.023(1) ^[b]		

Symmetry code: [b] $x, \frac{1}{2} - y, -\frac{1}{2} + z$.

11. Unusual Stepped Spin Transitions at Iron(II) Coordination Polymers with zigzag-Structure

The parallel 1D chains of **4b**^{HS} and **4b**^{LS} propagate along the [0 0 1] direction. They are stacked such that there is a total potential solvent accessible void volume of 621.6 and 466.5 Å³, respectively, which is hypothetically enough space for small molecules like toluene. As can be seen from the molecule packing in Figure 5, the porosity results from the arrangement of the chains such that the iron centres together with the equatorial ligands and the axial ligands alternately form layers perpendicular to the [0 0 1] direction. In contrast to **1a**, the axial bridging ligand is not twisted. In line with this finding are the observed intra-chain Fe1···Fe1 separation distances of 12.89 and 12.69 Å for **4b**^{HS} and **4b**^{LS}, respectively, which attests to a straight-lined structure of the axial ligand.

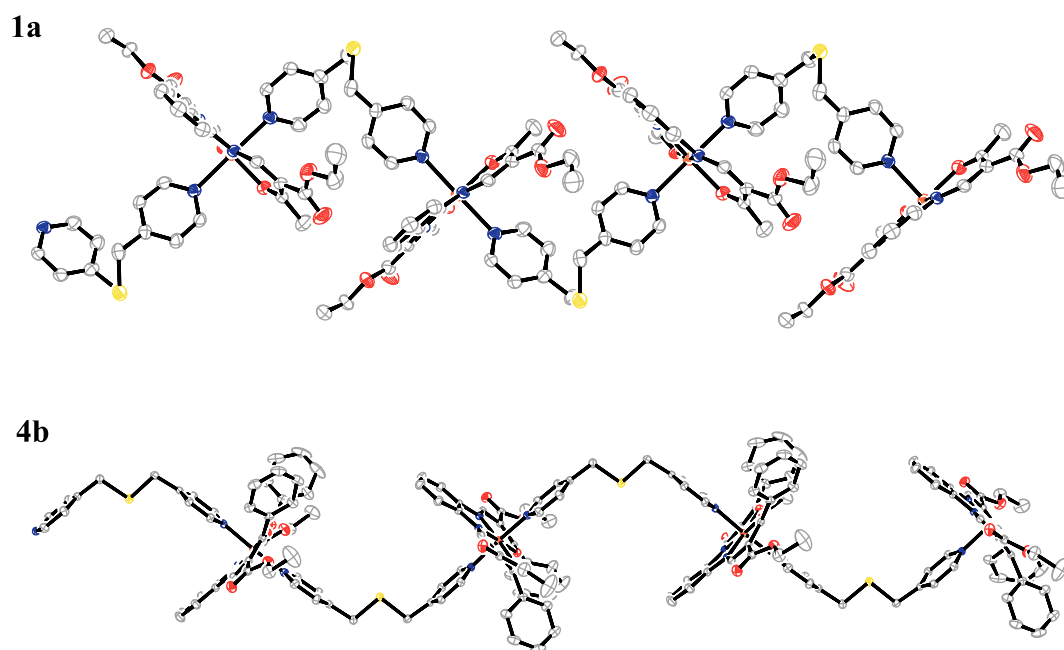


Figure 4. Top: excerpt of the 1D chain of compound **1a** in the crystal. Zigzag motif due to twisted bridging ligand. Bottom: excerpt of the zigzag 1D chain of compound **4b** in the crystal (shown at the example of **4b**^{LS}). Hydrogen atoms were omitted for clarity.

Intermolecular interactions: The investigation of intermolecular interactions is of great significance for an understanding of the magnetic properties. In Table 4 and Table 5 short intermolecular contacts of the complexes discussed in this work are summarised. In Figure 5 and Figure 6 excerpt of the molecule packing of the complexes are shown.

Due to the close packing of **1a**, numerous short interchain contacts in form of non-classical hydrogen bonds can be found (Figure 5). The strongest interactions can be observed between the hydrogen atoms H26 and H32, belonging to the same axial ligand and the carbonyl oxygen atoms O5 and O3, located at different equatorial ligands of adjacent chains, overall building up a 3D network of short contacts. Moreover the sulphur atom acts as acceptor of hydrogen atom H13B of the methyl group of the equatorial ligand.

In comparison to **1a**, the HS-structure of compound $[\text{FeL1}(\text{bppa})]^{[10]}$ provides a higher number of intermolecular interactions. A structure analysis at the intermediate plateau revealed that the relocation of the bridging ligands towards the smaller LS iron(II) centre, which is in general involved by a HS-LS transition,^[7a,17] could not follow the Fe-L bond decrease. Quite the contrary, every second Fe···Fe distance along a chain was even increased. Unfortunately a more profound discussion concerning the different spin transition behaviour of both samples is not possible, as the LS-structure of **1a** is not available.

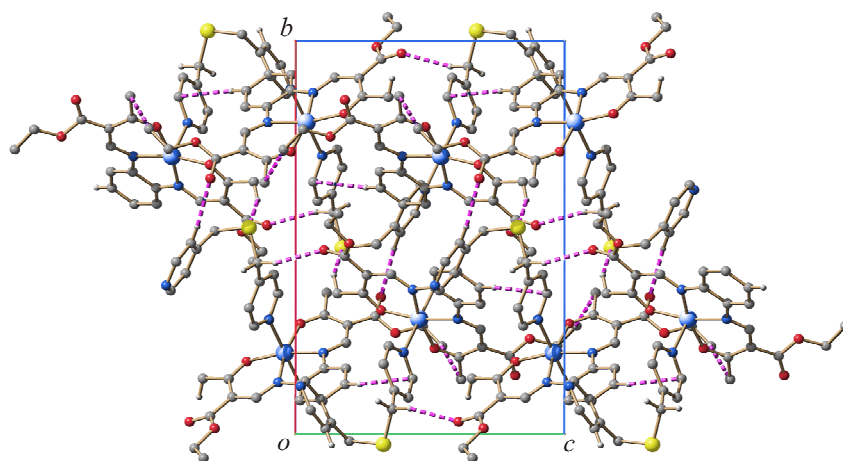


Figure 5. Molecule packing of compound **1a** in the crystal view along [1 0 0]. Intermolecular interactions less than the sum of the van der Waals Radii are depicted in dashed bonds. Hydrogen atoms which do not participate in short contacts have been omitted for clarity.

11. Unusual Stepped Spin Transitions at Iron(II) Coordination Polymers with zigzag-Structure

Table 4. Analysis of short intermolecular contacts [\AA] less than the sum of the van der Waals Radii, $d(\text{I} \cdots \text{J}) < R(\text{I}) + R(\text{J})$, of **1a**.

I	J	$d(\text{I} \cdots \text{J})$	$R(\text{I}) + R(\text{J})$	Δ
H26	O5 ^[a]	2.45	2.72	-0.27
H32	O3 ^[b]	2.54	2.72	-0.18
H20C	C14 ^[a]	2.76	2.90	-0.14
H13B	S1 ^[c]	2.94	3.00	-0.06
H7	C25 ^[a]	2.86	2.90	-0.04
H14A	H20 ^[a]	2.37	2.40	-0.03

Symmetry codes: [a] $x, \frac{1}{2} - y, \frac{1}{2} + z$; [b] $2 - x, -y, 1 - z$; [c] $2 - x, \frac{1}{2} + y, \frac{1}{2} - z$.

The interchain contacts of **4b**^{HS} are less numerous compared to **1a** and overall only a 2D network of interactions can be observed, which is spread through the layers build up of equatorial ligands. This is probably the reason for the more gradual SCO of compound **4b**. Two non-classical hydrogen bonds, involving the iron-coordinating oxygen atoms O1 and O2 of the equatorial ligand and the hydrogen atoms H37A and H37B of a secondary CH₂ group located at the axial ligand of an adjacent chain, can be seen as structure-bearing, as they obviously define the straight-lined arrangement of the chains (Figure 6). Moreover, carbonyl oxygen O5 acts as acceptor for hydrogen H40 belonging to a CH group of a pyridyl ring. When going from **4b**^{HS} to the LS-structure **4b**^{LS}, the number of short intermolecular contacts increases, as expected, but the additionally found contacts, besides the interactions already characterised at **4b**^{HS}, only facilitate the 2D network mentioned above.

The closely related compound [FeL4(bppa)]·0.5 MeOH^[11] we recently investigated, provides a very similarly structure motif: this compound undergoes an incomplete spin transition that rests at an intermediate plateau at 50% HS-fraction and shows a 5 K wide thermal hysteresis loop. Other than **4b**, a 3D network of intermolecular contacts could be observed already for the HS-structure of [FeL4(bppa)]·0.5 MeOH,^[11] which increases the total communication of elastic interactions. Of course the half-occupied methanol molecule plays an important role considering this. The stabilisation of the mixed HS/LS state through the whole low-temperature range was mainly explained by π -stacking of the 1,2-disubstituted benzene-rings of the equatorial ligand of two adjacent chains and the upcoming restraining interaction for

11. Unusual Stepped Spin Transitions at Iron(II) Coordination Polymers with zigzag-Structure

the ligand relocation. This effect is significantly weaker for $\mathbf{4b}^{\text{HS}}$ than for the HS-structure of $[\text{FeL4}(\text{bppa})]\cdot 0.5 \text{ MeOH}$ ($\text{C} \cdots \text{C} = 3.55$ relative to 3.43 \AA).

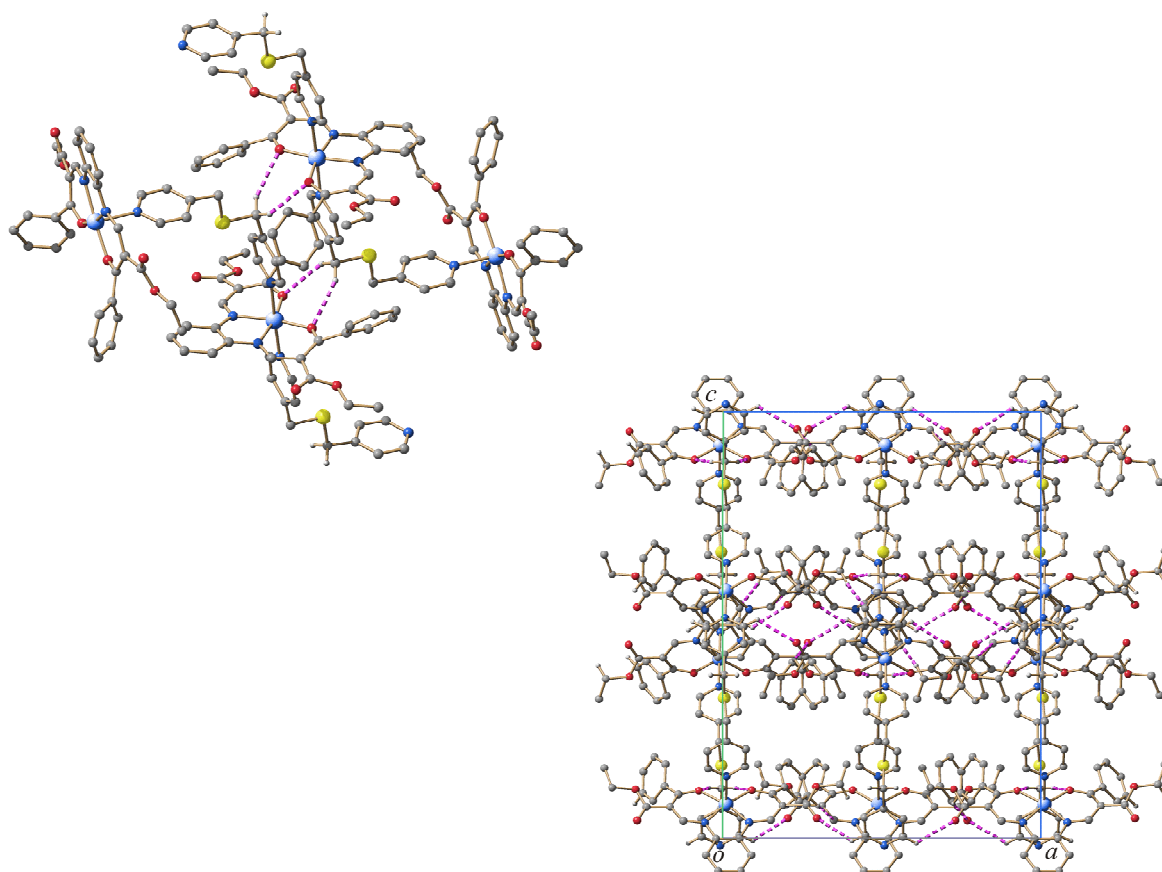


Figure 6: Left: illustration of structure-bearing interchain contacts of $\mathbf{4b}^{\text{HS}}$. Right: molecule packing of compound $\mathbf{4b}^{\text{LS}}$ in the crystal at 125 K, view along $[0\ 1\ 0]$. Intermolecular interactions less than the sum of the van der Waals Radii (dashed bonds) can be only observed within layers formed by equatorial ligands. Hydrogen atoms which do not participate in short contacts have been omitted for clarity. Porous structure created by straight-lined arrangement of the 1D chains.

11. Unusual Stepped Spin Transitions at Iron(II) Coordination Polymers with zigzag-Structure

Table 5. Analysis of short intermolecular contacts [\AA] less than the sum of the van der Waals Radii, $d(\text{I} \cdots \text{J}) < R(\text{I}) + R(\text{J})$, of $\mathbf{4b}^{\text{HS}}$ and $\mathbf{4b}^{\text{LS}}$.

	I	J	$d(\text{I} \cdots \text{J})$	$R(\text{I}) + R(\text{J})$	Δ
$\mathbf{4b}^{\text{HS}}$	H37B	O1 ^[a]	2.58	2.72	-0.14
	H37A	O2 ^[a]	2.60	2.72	-0.12
	H40	O5 ^[b]	2.60	2.72	-0.12
$\mathbf{4b}^{\text{LS}}$	H40	O5 ^[b]	2.51	2.72	-0.21
	H37A	O2 ^[a]	2.55	2.72	-0.17
	H37B	O1 ^[a]	2.56	2.72	-0.16
	H37A	C26 ^[a]	2.80	2.90	-0.10
	H41	O3 ^[d]	2.63	2.72	-0.09
	H36A	C20 ^[a]	2.84	2.90	-0.06
	H37B	C19 ^[a]	2.85	2.90	-0.05
	H17A	C8 ^[e]	2.85	2.90	-0.05
	H23	O3 ^[f]	2.67	2.72	-0.05
	H21	C27 ^[b]	2.87	2.90	-0.03

Symmetry codes: [a] $-x, -\frac{1}{2} + y, \frac{1}{2} - z$; [b] $-\frac{1}{2} + x, y, \frac{1}{2} - z$; [c] $\frac{1}{2} + x, \frac{1}{2} - y, -z$; [d] $\frac{1}{2} + x, y, \frac{1}{2} - z$; [e] $\frac{1}{2} + x, \frac{1}{2} - y, -z$; [f] $-\frac{1}{2} - x, \frac{1}{2} + y, z$.

Crystal contact index: We recently established a correlation between the cooperative effects of some monomeric, dimeric and 1D polymeric coordination SCO compounds and their structural properties derived from X-ray structure analysis, the so-called crystal contact index (CCI).^[11] Up to small hysteresis loops this correlation is in agreement with the model of elastic interactions mediating the structural rearrangements during the cooperative spin transition in the solid phase. It provides a good estimation to accompany the structural interpretation of spin transition properties. The CCI of compound **1a** is with 0.31 relatively small, indicating that low cooperativity can be expected what is in line with results of the magnetic measurement, as thermal hysteresis was not observed. For compound $\mathbf{4b}^{\text{HS}}$ the CCI value is with 0.14 even lower, which is in line with the presumption that the 2D network of intermolecular contacts is responsible for the more gradual SCO behaviour in contrast to abrupt spin transition of compound **1a**. Upon cooling the CCI value increases to 0.36 ($\mathbf{4b}^{\text{LS}}$), indicating that the number of short contacts has increased. In comparison with the observed

CCI of 2.0 for compound $[\text{FeL4}(\text{bppa})]\cdot 0.5 \text{ MeOH}^{[11]}$, the difference seems enormous, but one has to keep in mind that the half-occupied methanol molecule participates in numerous strong interactions. A modulation of the CCI, which not considers interactions of the solvent molecule, resulted in a value of 0.5, which is not this long way off and highlights how huge the influence of solvent molecules can be.

11.3 Conclusion

The combination of four different tetradentate equatorial ligands LX (with X = 1–4), bpms as bridging ligand and methanol or ethanol as solvent led to a series of 1D chain iron(II) compounds of the general formula $[\text{FeLX}(\text{bpms})]\cdot \text{solvent}$, whose synthesis and characterisation is described in this paper. The magnetic measurements exhibit complete spin transitions and unusual intermediate plateaus at $\gamma_{\text{HS}} \approx 0.1$ for compounds **1a**, **3a** and **4a/4b**. On the one side, the results from crystal structure analysis of **1a** and **4b^{HS}/4b^{LS}** are consistent with the outcomes of magnetic measurements, as the interchain contacts of **4b^{HS}** are less numerous relative to **1a** and thus the ST of **1a** is steeper. This is reflected by the lower CCI value of **4b^{HS}** (0.14 relative to 0.31), which indicates weaker cooperative effects within the crystal. On the other side, X-ray analysis reveals pronounced zigzag structures for the chains of both compounds, however, the recently developed concept that zigzag structures in combination with several interchain contacts result in stepwise spins transitions,^[10] cannot be given as an explanation for the unusual stepped ST without a doubt. So far, this phenomenon was only observed in combination with the bpms ligand and thus some ligand-specific effects are very likely. To clarify this, further examples and investigations are necessary.

11.4 Experimental Section

Magnetic measurements: Magnetic susceptibility data were collected by using a Quantum Design MPMSR-2 SQUID magnetometer under an applied field of 0.5 T over the temperature range 50–300 K and 50–350 K for **1b**. The samples were placed in gelatine capsules held within a plastic straw. The data were corrected for the diamagnetic magnetisation of the ligands by using tabulated Pascal's constants, and of the sample holder.

X-Ray crystallography: The intensity data of **1a** and **4b** were collected on an Oxford XCalibur diffractometer by using graphite-monochromated MoK_α radiation. The data were corrected for Lorentz and polarisation effects. The structure was solved by direct methods (SIR-97)^[18] and refined by full-matrix least-square techniques against F_0^2 (SHELXL-97^[19]). The hydrogen atoms were included at calculated positions with fixed displacement parameters. ORTEP-III was used for structure representation,^[20] SCHAKAL-99 to illustrate molecule packings.^[21] The crystallographic data are summarised in Supporting Information Table S1.

Synthesis: All syntheses were carried out under argon by using Schlenk tube techniques. All solvents were purified as described in literature and distilled under argon.^[22] The syntheses of the methanol containing complexes $[\text{FeLX}(\text{MeOH})_2]$ (with X = 1,^[23] 2,^[23] 3,^[15b] 4,^[24] Scheme 1) and anhydrous iron(II) acetate^[25] as starting material are described in literature. 4-(Chloromethyl)pyridine hydrochloride was purchased from Fluka and sodium sulfide hydrate (65%) was purchased from Acros Organics. Both were used as received.

Bis(4-pyridylmethyl)sulfane (bpms): To a solution of 4-(chloromethyl)pyridine hydrochloride (4.00 g, 24.4 mmol) and sodium hydroxide (0.98 g, 24.4 mmol) in water (45 mL) was slowly added a solution of sodium sulfide hydrate (1.46 g, 12.2 mmol) in water (30 mL). The resulting dark red mixture was heated to 80 °C for 2 h and then stirred at room temperature for 24 h. Afterwards the reaction mixture was extracted several times with diethyl ether and the combined organic phases were dried over MgSO_4 . Removal of solvent left the product as a red oily residue which was solidified at -26 °C (yield: 1.61 g, 61%). ¹H NMR (400 MHz, CDCl_3 , 25 °C, TMS): δ = 8.57–8.60 (m, 4H, Ar-NCH), 7.28–7.31 (m, 4H, Ar-CH), 3.59 ppm (s, 4H; CH_2); MS (DEI(+), 70 eV): m/z (%): 216 (84) [M^+], 124 (45)

[C₆H₆NS⁺], 93 (100) [C₆H₆N⁺], 65 (31) [C₅H₅⁺]; elemental analysis calcd (%) for C₁₂H₁₂N₂S (216.30): C 66.63, H 5.59, N 12.95; found: C 66.72, H 5.81, N 13.05.

[FeL1(bpms)] (1a): A solution of [FeL1(MeOH)₂] (0.43 g, 0.85 mmol) and bpms (0.92 g, 4.25 mmol) in ethanol (50 mL) was heated to reflux for 4 h. After cooling to room temperature, black crystals of **1a** formed within 24 h which were filtered off, washed with ethanol (2 × 5 mL) and dried *in vacuo* (yield 0.42 g, 75%). IR (KBr): $\tilde{\nu}$ = 1676(vs) (COO), 1564(vs) cm⁻¹ (CO); MS (DEI(+), 70 eV): *m/z* (%): 443 (32) [FeL1⁺ + H], 442 (100) [FeL1⁺], 397 (28), 354 (30), 309 (28), 216 (15) [bpms⁺]; MS (ESI): *m/z* (%): 874 (9) [M⁺ + bpms], 658 (23) [M⁺], 442 (15) [FeL1⁺], 217 (100) [bpms⁺ + H]; elemental analysis calcd (%) for C₃₂H₃₄FeN₄O₆S (658.55): C 58.36, H 5.20, N 8.51; found: C 58.35, H 5.25, N 8.50.

Crystals of **1a** were obtained by slow diffusion between a solution of [FeL1(MeOH)₂] (0.18 g, 0.35 mmol) in ethanol (15 mL) and a solution of bpms (0.08 g, 0.39 mmol) in ethanol (15 mL). After two weeks **1a** was obtained as black crystals.

[FeL1(bpms)] (1b): A solution of [FeL1(MeOH)₂] (0.42 g, 0.83 mmol) and bpms (1.55 g, 6.94 mmol) in methanol (30 mL) was heated to reflux for 1 h. After cooling to room temperature, **1b** precipitated as black fine crystalline solid within 24 h, which were filtered off, washed with methanol (2 × 5 mL) and dried *in vacuo* (yield 0.27 g, 49%). Elemental analysis calcd (%) for C₃₂H₃₄FeN₄O₆S (658.55): C 58.36, H 5.20, N 8.51; found: C 58.26, H 5.29, N 8.50.

[FeL2(bpms)]·EtOH (2a·EtOH): A solution of [FeL2(MeOH)₂] (0.33 g, 0.86 mmol) and bpms (0.93 g, 4.32 mmol) in ethanol (50 mL) was heated to reflux for 4 h. After cooling to room temperature, black crystals of **2a·EtOH** formed within 24 h, which were filtered off, washed with ethanol (2 × 5 mL) and dried *in vacuo* (yield 0.20 g, 36%). IR (KBr): $\tilde{\nu}$ = 1636(vs) (CO), 1559(vs) cm⁻¹ (CO); MS (DEI(+), 70 eV): *m/z* (%): 382 (99) [FeL2⁺], 367 (41), 340 (23), 354 (30), 216 (49) [bpms⁺], 93 (100); MS (ESI): *m/z* (%): 814 (5) [M⁺ + bpms], 581 (10) [M⁺], 382 (40) [FeL2⁺], 217 (100) [bpms⁺ + H]; elemental analysis calcd (%) for C₃₂H₃₆FeN₄O₅S (644.56): C 59.63, H 5.63, N 8.69; found: C 59.53, H 5.34, N 8.97.

[FeL2(bpms)]·MeOH (2b·MeOH): A solution of [FeL2(MeOH)₂] (0.28 g, 0.63 mmol) and bpms (0.68 g, 3.14 mmol) in methanol (17 mL) was heated to reflux for 1 h. After cooling to room temperature, **2b·MeOH** precipitated immediately as black powder which was filtered

off, washed with methanol (2×5 mL) and dried *in vacuo* (yield 0.21 g, 53%). Elemental analysis calcd (%) for $C_{31}H_{34}FeN_4O_5S$ (630.54): C 60.20, H 5.05, N 9.36; found: C 58.89, H 5.21, N 8.95.

[FeL3(bpms)] (3a): A solution of $[FeL3(MeOH)_2]$ (0.24 g, 0.50 mmol) and bpms (0.54 g, 2.51 mmol) in ethanol (30 mL) was heated to reflux for 4 h. After cooling to room temperature, a fine crystalline black precipitate of **3a** was formed immediately which was filtered off, washed with ethanol (2×5 mL) and dried *in vacuo* (yield 0.20 g, 63%). IR (KBr): $\tilde{\nu} = 1680$ (vs) (CO), 1566 (vs) cm^{-1} (CO); MS (DEI(+), 70 eV): m/z (%): 414 (100) $[FeL4^+]$, 383 (17), 340 (23), 309 (22), 216 (83) $[bpms^+]$, 93 (85); elemental analysis calcd (%) for $C_{30}H_{30}FeN_4O_6S$ (630.49): C 57.15, H 4.80, N 8.89; found: C 57.04, H 4.86, N 8.86.

[FeL3(bpms)]·0.5 MeOH (3b·0.5 MeOH): A solution of $[FeL3(MeOH)_2]$ (0.20 g, 0.61 mmol) and bpms (0.65 g, 3.00 mmol) in methanol (20 mL) was heated to reflux for 1 h. After cooling to room temperature, **3b·0.5 MeOH** precipitated immediately as black fine crystalline solid which was filtered off, washed with methanol (2×5 mL) and dried *in vacuo* (yield 0.25 g, 66%). Elemental analysis calcd (%) for $C_{30.5}H_{32}FeN_4O_{6.5}S$ (646.52): C 56.66, H 4.99, N 8.67; found: C 56.13, H 4.81, N 8.71.

[FeL4(bpms)] (4a): A solution of $[FeL4(MeOH)_2]$ (0.19 g, 0.30 mmol) and bpms (0.33 g, 1.51 mmol) in ethanol (30 mL) was heated to reflux for 4 h. After cooling to room temperature, a fine crystalline black precipitate of **4a** was formed immediately which was filtered off, washed with ethanol (2×5 mL) and dried *in vacuo* (yield 0.18 g, 77%). IR (KBr): $\tilde{\nu} = 1678$ (s) (CO), 1554 (s) cm^{-1} (CO); MS (DEI(+), 70 eV): m/z (%): 566 (100) $[FeL3^+]$, 521 (17), 369 (16), 216 (33) $[bpms^+]$, 93 (41); elemental analysis calcd (%) for $C_{42}H_{38}FeN_4O_6S$ (782.68): C 64.45, H 4.89, N 7.16; found: C 64.19, H 5.00, N 7.17.

[FeL4(bpms)] (4b): A solution of $[FeL4(MeOH)_2]$ (0.13 g, 0.21 mmol) and bpms (0.24 g, 1.00 mmol) in methanol (20 mL) was heated to reflux for 1 h. After cooling to room temperature, **4b** precipitated immediately as black powder which was filtered off, washed with methanol (2×5 mL) and dried *in vacuo* (yield 0.15 g, 90%). Elemental analysis calcd (%) for $C_{42}H_{38}FeN_4O_6S$ (782.68): C 64.45, H 4.89, N 7.16; found: C 63.91, H 4.85, N 7.08. Crystals of **4b** were obtained by slow diffusion between a solution of $[FeL4(MeOH)_2]$ (0.07 g, 0.11 mmol) in methanol (15 mL) and a solution of bpms (0.13 g, 0.60 mmol) in methanol (15 mL). After one week **4b** was obtained as black crystals.

11.5 References

- [1] a) H.A. Goodwin, *Coord. Chem. Rev.*, **1976**, *18*, 293; b) E. König, *Struct. Bonding (Berlin)* **1991**, *76*, 51; c) P. Gütllich, A. Hauser, H. Spiering, *Angew. Chem. Int. Ed. Engl.* **1994**, *33*, 2024, and references therein; d) P. Gütllich, H.A. Goodwin (Eds.), *Spin Crossover in Transition Metal Compounds I–III, Topics in Current Chemistry*, Springer, Berlin, Heidelberg, New York, **2004**; e) J.A. Real, A.B. Gaspar, M.C. Munoz, *Dalton Trans.* **2005**, 2062; f) K. Nakano, N. Suemura, K. Yoneda, S. Kawata, S. Kaizaki, *Dalton Trans.* **2005**, 740; g) O. Sato, J. Tao, Y.-Z. Zhang, *Angew. Chem.* **2007**, *119*, 2200; *Angew. Chem. Int. Ed.* **2007**, *46*, 2152; h) J.A. Kitchen, S. Brooker, *Coord. Chem. Rev.* **2008**, *252*, 2072; i) K.S. Murray, *Eur. J. Inorg. Chem.* **2008**, 3101; k) M.A. Halcrow, *Coord. Chem. Rev.* **2009**, 2059; l) S. Brooker, J.A. Kitchen, *Dalton Trans.* **2009**, 7331; m) C.J. Kepert, *Aust. J. Chem.* **2009**, *62*, 1079; n) K.S. Murray, *Aust. J. Chem.* **2009**, *62*, 1081; o) A.B. Koudriavtsev, W. Linert, *J. Struct. Chem.* **2010**, *51*, 335.
- [2] a) O. Kahn, C. Jay Martinez, *Science* **1998**, *279*, 44; b) O. Kahn, C. Jay, J. Kröber, R. Claude, F. Grolière, *Patent EP0666561* **1995**; c) J.-F. Létard, O. Nguyen, N. Daro, *Patent FR0512476* **2005**; d) J.-F. Létard, P. Guionneau, L. Goux-Capes, *Topics in Current Chemistry, Vol. 235* (Eds.: P. Gütllich, H.A. Goodwin), Springer, Wien, New York, **2004**, 221; e) A. Galet, A.B. Gaspar, M.C. Munoz, G.V. Bukin, G. Levchenko, J.A. Real, *Adv. Mater.* **2005**, *17*, 2949.
- [3] Y. Garcia, V. Kseofontov, P. Gütllich, *Hyperfine Interact.* **2002**, *139/140*, 543.
- [4] Y. Garcia, V. Kseofontov, S. Mentior, M.M. Dîrtu, C. Gieck, A. Bhatthacharjee, P. Gütllich, *Chem. Eur. J.* **2008**, *14*, 3745.
- [5] Y. Garcia, V. Niel, M.C. Munoz, J.A. Real, *Topics in Current Chemistry, Vol. 233* (Eds.: P. Gütllich, H.A. Goodwin), Springer, Wien, New York, **2004**, 195.
- [6] J.A. Real, A.B. Gaspar, V. Niel, M.C. Munoz, *Coord. Chem. Rev.* **2003**, *236*, 121.
- [7] a) B. Weber, *Coord. Chem. Rev.* **2009**, *253*, 2432; b) B. Weber, E.-G. Jäger, *Eur. J. Inorg. Chem.* **2009**, 465.

- [8] a) B. Weber, R. Tandon, D. Himsl, *Z. Anorg. Allg. Chem.* **2007**, 633, 1159; b) B. Weber, E.S. Kaps, C. Desplanches, J.-F. Létard, *Eur. J. Inorg. Chem.* **2008**, 2963.
- [9] M.M. Dîrtu, C. Neuhausen, A.D. Naik, A. Rotaru, L. Spinu, Y. Garcia, *Inorg. Chem.* **2010**, 49, 5723.
- [10] W. Bauer, W. Scherer, S. Altmannshofer, B. Weber, *Eur. J. Inorg. Chem.* **2011**, 2803.
- [11] T. M. Pfaffeneder, S. Thallmair, W. Bauer, B. Weber, *New J. Chem.* **2011**, 35, 691.
- [12] S.M. Neville, B.A. Leita, G.J. Halder, C. Kepert, B. Moubaraki, J.-F. Létard, K.S. Murray, *Chem. Eur. J.* **2008**, 14, 10123.
- [13] J.A. Rodriguez-Velamazán, M. Castro, E. Palacios, R. Burriel, T. Kitazawa, T. Kawasaki, *J. Phys. Chem. B* **2007**, 111, 1256.
- [14] a) B. Weber, W. Bauer, J. Obel, *Angew. Chem.* **2008**, 20, 10252; *Angew. Chem. Int. Ed.* **2008**, 47, 10098; b) B. Weber, E. Kaps, J. Weigand, C. Carbonera, J.-F. Létard, K. Achterhold, F.G. Parak, *Inorg. Chem.* **2008**, 47, 487.
- [15] a) T. Pfaffeneder, W. Bauer, B. Weber, *Z. Anorg. Allg. Chem.* **2010**, 636, 183; b) W. Bauer, T. Ossiander, B. Weber, *Z. Naturforsch. B* **2010**, 65, 323.
- [16] a) B. Weber, E.S. Kaps, J. Obel, W. Bauer, *Z. Anorg. Allg. Chem.* **2008**, 1421; b) B. Weber, C. Carbonera, C. Desplanches, J.-F. Létard, *Eur. J. Inorg. Chem.* **2008**, 1589; c) B. Weber, E.S. Kaps, C. Desplanches, J.-F. Létard, K. Achterhold, F.G. Parak, *Eur. J. Inorg. Chem.* **2008**, 4891.
- [17] a) A.B. Koudriavtsev, A.F. Strassen, J.G. Haasnoot, M. Grunert, P. Weinberger, W. Linert, *Phys. Chem. 5* **2003**, 3676; b) A.B. Koudriavtsev, A.F. Strassen, J.G. Haasnoot, M. Grunert, P. Weinberger, W. Linert, *Chem. Phys. 5* **2003**, 3666.
- [18] A. Altomare, M.C. Burla, G.M. Camalli, G. Cascarano, C. Giacovazzo, A. Guagliardi, A.G.G. Moliterni, G. Polidori, R. Spagna, SIR-97, University of Bari, Bari (Italy), **1997**; *J. Appl. Crystallogr.* **1999**, 32, 115.
- [19] G.M. Sheldrick, SHELXL-97, University of Göttingen, Göttingen (Germany), **1997**.

- [20] C.K. Johnson, M.N. Burnett, ORTEP-III, Oak-Ridge National Laboratory, Oak-Ridge, TN (USA) **1996**; L. J. Farrugia, *J. Appl. Crystallogr.* **1997**, 30, 565.
- [21] E. Keller, SCHAKAL-99, University of Freiburg, Freiburg (Germany), **1999**.
- [22] Team of authors: *Organikum*, Johann Ambrosius Barth Leipzig, Berlin, Heidelberg **1993**.
- [23] E.-G. Jäger, E. Häussler, M. Rudolph, M. Rost, *Z. Anorg. Allg. Chem.* **1985**, 525, 67.
- [24] a) B. Weber, H. Görls, M. Rudolf, E.-G. Jäger, *Inorg. Chim. Acta* **2002**, 337, 247; b) B. Weber, PhD thesis, University of Jena (Germany), **2002**; Der Andere Verlag, Osnabrück, **2003**.
- [25] B. Weber, R. Betz, W. Bauer, S. Schlamp, *Z. Anorg. Allg. Chem.* **2011**, 673, 102.

11. Unusual Stepped Spin Transitions at Iron(II) Coordination Polymers with zigzag-Structure

11.6 Supporting Information

Table S1. Crystallographic data of the iron(II) complexes discussed in this work.

compound	1a	4b^{HS}	4b^{LS}
formula	C ₃₂ H ₃₄ FeN ₄ O ₆ S	C ₄₂ H ₃₈ FeN ₄ O ₆ S	C ₄₂ H ₃₈ FeN ₄ O ₆ S
M_r / g mol ⁻¹	658.54	782.67	782.67
crystal system	monoclinic	orthorhombic	orthorhombic
space group	<i>P</i> 2 ₁ / <i>c</i>	<i>Pbca</i>	<i>Pbca</i>
a / Å	12.164(7)	19.2017(5)	18.8103(9)
b / Å	19.0805(11)	16.2729(8)	16.0825(7)
c / Å	16.115(7)	25.7799(15)	25.3728(13)
α / °	90.00	90	90
β / °	125.95(3)	90	90
γ / °	90.00	90	90
V / Å ³	3028(2)	8055.4(6)	7675.7(6)
Z	4	8	8
ρ / g cm ⁻³	1.445	1.291	1.355
μ / mm ⁻¹	0.619	0.477	0.501
crystal size	0.49 × 0.44 × 0.41	0.30 × 0.26 × 0.23	0.46 × 0.36 × 0.27
T / K	225(2)	250(2)	125(2)
diffractometer	Oxford XCalibur	Oxford XCalibur	Oxford XCalibur
λ (MoK α) / Å	0.71073	0.71073	0.71073
θ -range / °	3.78–26.31	4.24–26.27	4.22–26.27
reflns. collected	57671	32198	21310
indep. reflns. (R_{int})	6157 (0.0604)	8144 (0.0376)	7753 (0.0292)
mean $\sigma(I) / I$	0.0292	0.0625	0.0537
reflns. with $I \geq 2\sigma(I)$	4539	4323	4851
x, y (weighting scheme)	0.0492, 2.0115	0.0408, 0	0.0394, 0
parameters	401	489	489
restraints	0	0	0
$R(F)$ (all data) ^[a]	0.0363 (0.0571)	0.0346 (0.0815)	0.0324 (0.0625)
$wR(F^2)$ ^[b]	0.1097	0.0815	0.0771
$Goof$	1.064	0.823	0.878
shift/error _{max}	0.000	0.000	0.001
max., min. resd. dens. / e Å ⁻³	0.458, -0.435	0.388, -0.255	0.407, -0.341

[a] $R(F) = \sum ||F_o| - |F_c|| / \sum |F_o|$. [b] $wR(F^2) = [\sum [w(F_o^2 - F_c^2)^2] / \sum w(F_o^2)^2]^{1/2}$, $w = 1 / [\sigma^2(F_o^2) + (aP)^2 + bP]$, where $P = [F_o^2 + 2(F_c^2)] / 3$.

12 Increasing the Hysteresis Width of Iron(II) SCO Compounds in a Crystal Engineering-like Approach

Wolfgang Bauer^[a] and Birgit Weber*^[a]

Inorganic Chemistry II, Universität Bayreuth, Universitätsstraße 30, NW I, 95440 Bayreuth, Germany. Fax: +49-92155-2157, E-mail: weber@uni-bayreuth.de

Keywords: Iron, Magnetism, X-ray structure, Hysteresis, Crystal Engineering

Manuscript in preparation.

12.1 Introduction

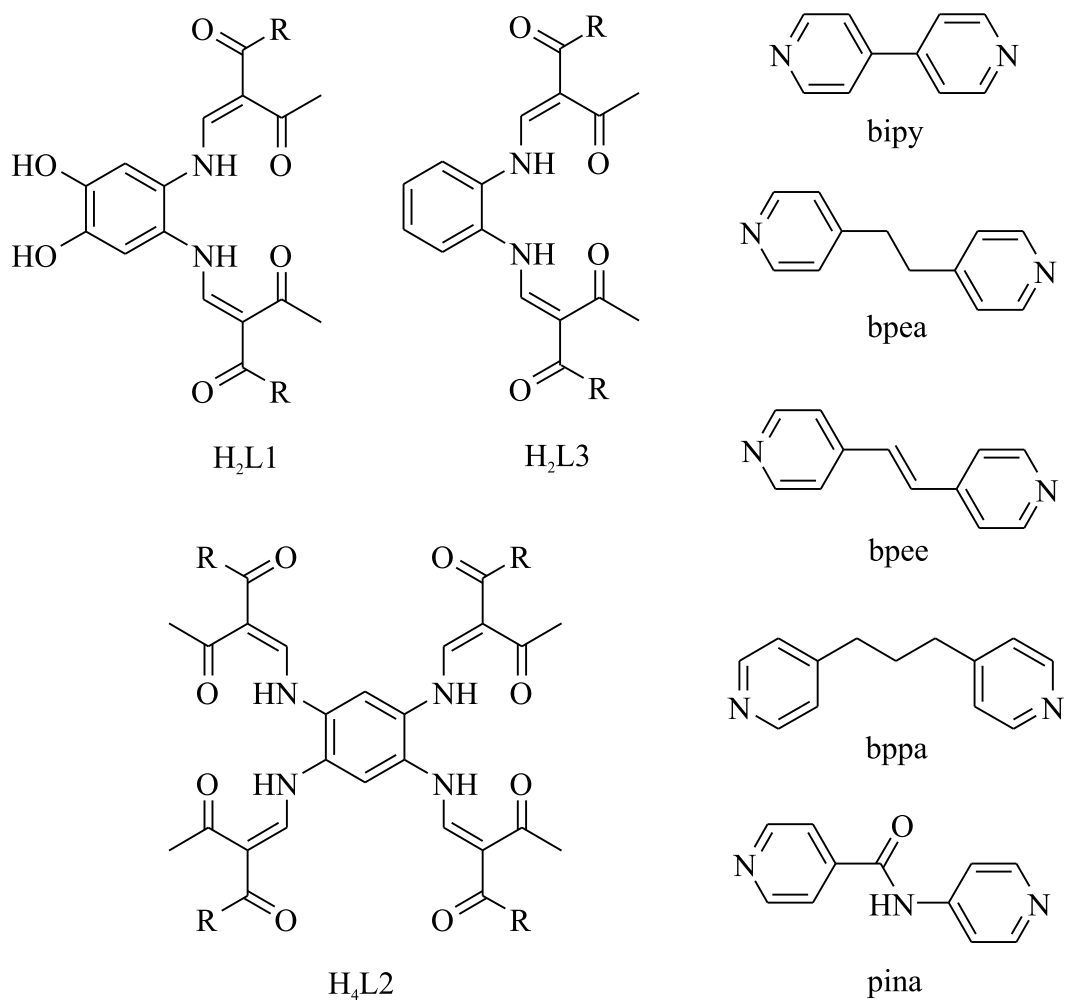
The spin crossover (SCO) phenomenon has been receiving an ongoing interest over decades,^[1] as various applications in information technology^[2] or as sensors^[3] and cool channel control units in food and medical storage^[4] can be envisioned. To meet the requirements, in the recent past much of the focus of interest in SCO research has directed onto the bistability of highly cooperative systems (hysteresis, memory effect), as such materials can exist in two different electronic states, depending on the history of the system.

The ideas of crystal engineering can be easily associated with the aims of spin crossover research, as they have a great deal in common concerning fundamental concepts and strategies. Desiraju defined crystal engineering as “the understanding of intermolecular interactions in the context of crystal packing and in the utilisation of such understanding in the design and new solids with desired physical and chemical properties”.^[5] The desired properties include chemical reactivity as well as optical, magnetic or electronic properties, only to mention some examples.^[6] All these physical properties are affected upon the spin transition as well. The starting point for the investigation of coordination polymers as a branch of crystal engineering was set in the late 1980s by studies about interpenetrating frameworks at scaffolding-like materials.^[7] Nowadays, the two most commonly used strategies in crystal engineering are based on coordination complexation and hydrogen

bonding.^[6] We recently reported of compound [FeL3a(HIm)₂] (HIm = imidazole) with its 70 K wide thermal hysteresis loop due to a 3D hydrogen bond network.^[8] It is our aim to combine attributes of crystal engineering with the syntheses of our SCO complexes to get beyond the classical trial-and-error lead-finding. With a crystal engineering-like approach we try to systematically improve the spin transition behaviour of our compounds by the means of cooperative effects via the interplay of coordination bonding, hydrogen bonding and network design.

With the example of complex [FeL3b(1-meim)₂] (1-meim = 1-methylimidazole),^[9] which exhibits a 2 K hysteresis loop, we could demonstrate that the transition from monomeric ligand systems to dimeric systems leads to an improvement in cooperativity in this case, as compound [Fe₂L2b(1-meim)₄] \cdot 1-meim shows a 21 K wide hysteresis loop.^[9] The next step, the implementation of covalent linker molecules between the metal centres of monomer complexes, especially of that kind which lead to 1D coordination polymers, yielded to a various amount of compounds exhibiting thermal hysteresis loops up to 30 K, as the conditions for intermolecular interactions are improved on this way.^[10,11] With introduction of the bridging ligand *N*-(4-pyridyl)isonicotinamide (pina) to 1D systems, which seems to be highly suitable for hydrogen bonding due to its peptide bond, we managed to support our theory by intensifying the formation of intermolecular interactions: as a result, we obtained the 1D chain compound [FeL3b(pina)] \cdot *x* MeOH that shows up to 90 K wide hysteresis loop around room temperature. Further possibilities to create better conditions for hydrogen bonding are given through specific variations at the equatorially ligand system: through the introduction of two hydroxy groups at the phenyl ring as realised at the ligand system H₂L1,^[12] we obtained a series of new 1D chain compounds of which some exhibit hysteresis. The successful transition from mononuclear to dinuclear systems and one-dimensional coordination polymers motivated the connection of dinuclear systems with suitable bidentate bridging ligands in order to get dimeric coordination polymers and thus further optimise the intermolecular interactions. With compound [Fe₂L2a(bpee)] \cdot 1.5 tol exhibiting a ladder-like 1D structure and a 34 K wide hysteresis loop we are able to show for the first time that this strategy can be expanded this far.

12. Increasing the Hysteresis Width of Iron(II) SCO Compounds in a Crystal Engineering-like Approach



H₂L1a/H₄L2a/H₂L3a: R = OCH₂CH₃

H₂L1b/H₄L2b/H₂L3b: R = CH₃

Scheme 1. Axial and equatorial ligands used in this work for the syntheses of mono- and dinuclear iron(II) coordination polymers.

12.2 Results

Synthesis of the complexes: The axial and equatorial ligands used in this work for the syntheses of mono- and dinuclear iron(II) coordination polymers are depicted in Scheme 1. All compounds were obtained in a two-pot reaction. In a first step, the mononuclear iron complexes $[\text{FeL1a/b}(\text{MeOH})_2]$ and $[\text{FeL3a/b}(\text{MeOH})_2]$, respectively, or the dinuclear iron complexes $[\text{Fe}_2\text{L2a/b}(\text{MeOH})_4]$ were prepared by converting anhydrous iron(II) acetate with the corresponding equatorial ligand $\text{H}_2\text{L1a/b}$, $\text{H}_4\text{L2a/b}$ or $\text{H}_2\text{L3a/b}$ in methanol as solvent. In a second step, these “precursors” were converted with the bidentate axial ligand bipy, bpea, bpee or pina. Overviews of the synthesised compounds ordered by the particular equatorial ligand systems are given in Table 1, 5 and 7.

For the syntheses using $[\text{FeL1a}(\text{MeOH})_2]$ as precursor, toluene (tol) was also used as a solvent, besides methanol. Compared to related 1D iron(II) compounds, in conjunction with the $\text{H}_2\text{L1}$ ligand quite often complexes that additionally contain uncoordinated molecules of the axial ligand were obtained, in line with the results from elemental analysis. The synthesis of $[\text{FeL1a}(\text{bpee})]$ in methanol as solvent was not successful, as well as syntheses of $[\text{FeL1a/b}(\text{bppa})]$. For the complex syntheses using $[\text{Fe}_2\text{L2a}(\text{MeOH})_4]$ as precursor, toluene and dimethylformamide (DMF) were used as solvent; DMF and acetonitrile (ACN) for the complex syntheses with $[\text{Fe}_2\text{L2b}(\text{MeOH})_4]$, respectively. All attempts to synthesise the compounds $[\text{Fe}_2\text{L2b}(\text{bpee})_2]$ and $[\text{Fe}_2\text{L2b}(\text{bppa})_2]$ from suspensions of $[\text{Fe}_2\text{L2b}(\text{MeOH})_4]$ with bpee and bppa in DMF, ACN or MeOH were unsuccessful and only fragmentary coordinated products were obtained. In conjunction with the $\text{H}_4\text{L2}$ ligand system quite often compounds with additional solvent molecules were obtained, as the results from elemental analysis show. The precursor $[\text{FeL3a}(\text{MeOH})_2]/[\text{FeL3b}(\text{MeOH})_2]$ were only converted with the axial ligand pina, as all other thinkable compounds were published before.

All compounds were characterised by elemental analysis, IR and mass spectroscopy as well as *T*-dependent magnetic susceptibility measurement and X-ray crystallography if possible.

12.2.1 The Ligand System H₂L1

Table 1. Overview of the compounds with the H₂L1 ligand system discussed in this work and the used abbreviations.

L _{ax}	solvent	L1a	L1b
bipy	MeOH	[FeL1a(bipy)]·MeOH (1 ·MeOH)	[FeL1b(bipy)]·(0.5 bipy)(MeOH) (4 ·(0.5 bipy)(MeOH))
	toluene	[FeL1a(bipy)] (1)	/
bpea	MeOH	[FeL1a(bpea)]·0.3 bpea (2 ·0.3 bpea)	[FeL1b(bpea)]·0.5 bpea (5 ·0.5 bpea)
	toluene	[FeL1a(bpea)]·(0.5 bpea)(0.5 tol) (2 ·(0.5 bpea)(0.5 tol))	/
bpee	MeOH	/	[FeL1b(bpee)]·(bpee) (MeOH) (6 ·(bpee)(MeOH))
	toluene	[FeL1a(bpee)]·(0.7 bpee)(0.7 tol) (3 ·(0.7 bpee)(0.7 tol))	/

Magnetic measurements of the compounds with ligand system H₂L1: Characteristic values of the thermal dependence of the $\chi_M T$ product (with χ_M being the molar susceptibility and T the temperature) for all iron(II) compounds of this ligand-type are given in Table 2. With exception of **4**·(0.5 bipy)(MeOH) and **6**·(bpee)(MeOH), the room temperature $\chi_M T$ values of these compounds are in the range of 3.13–3.55 cm³ K mol⁻¹ and therefore typical for iron(II) complexes in the high-spin (HS) state. For compound **4**·(0.5 bipy)(MeOH), the room temperature $\chi_M T$ value is 2.03 cm³ K mol⁻¹, indicative of a mixed HS/LS state. For compound **6**·(bpee)(MeOH), the room temperature moment is with 0.39 cm³ K mol⁻¹ indicative of low-spin (LS) iron(II), but upon heating to 400 K, the moment increases to reach a maximum HS $\chi_M T$ value of 3.05 cm³ K mol⁻¹.

Upon cooling (starting from the pure HS state), various types of spin transitions can be observed. For compound **1** and **2**·0.3 bpea a gradual but incomplete SCO is observed with a

remaining HS fraction of $\gamma_{\text{HS}} = 0.35$ and 0.48 at 50 K, respectively, indicative of a mixed HS/LS state. Compound **4**·(0.5 bipy)(MeOH) stays in a mixed HS/LS state in the range 50 – 320 K, then, above 320 K, the $\chi_{\text{M}}T$ values increase to attain a maximum value of $3.41 \text{ cm}^3 \text{ K mol}^{-1}$ at 400 K. For compound **2**·(0.5 bpea)(0.5 tol) an abrupt spin transition is observed. The $\chi_{\text{M}}T$ values remain approximately constant at $3.50 \text{ cm}^3 \text{ K mol}^{-1}$ between 300 and 240 K. Between 240 and 180 K, the $\chi_{\text{M}}T$ values decrease rapidly then, below 180 K, gradually to attain a minimum $\chi_{\text{M}}T$ value of $0.31 \text{ cm}^3 \text{ K mol}^{-1}$ at 50 K, indicative of iron(II) in the LS state. The $T_{1/2}$ value of this ST is 204 K. In Figure 1, the $\chi_{\text{M}}T$ products vs. T of the compounds which exhibit a hysteresis loop are plotted.

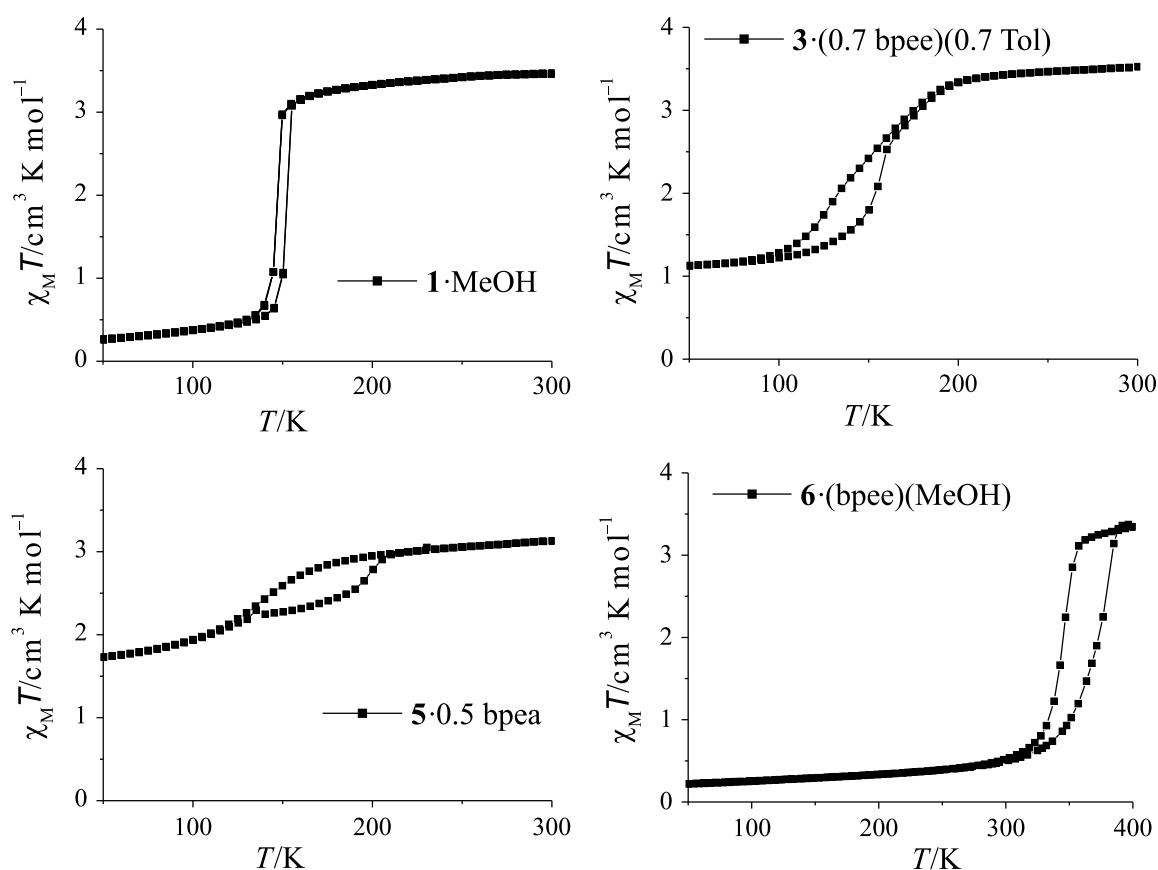


Figure 1. Plots of the $\chi_{\text{M}}T$ product vs. T for the compounds **1**·MeOH, **3**·(0.7 bpee)(0.7 tol), **5**·0.5 bpea and **6**·(bpee)(MeOH).

For **1**·MeOH, between 300 and 155 K, the $\chi_{\text{M}}T$ values remain approximately constant above $3.0 \text{ cm}^3 \text{ K mol}^{-1}$, then, below 155 K, the $\chi_{\text{M}}T$ values rapidly decrease to attain a value of $0.50 \text{ cm}^3 \text{ K mol}^{-1}$ at 130 K. Upon further cooling, the $\chi_{\text{M}}T$ values slightly decrease to attain a minimum value of $0.26 \text{ cm}^3 \text{ K mol}^{-1}$ at 50 K. The $T_{1/2}^{\downarrow}$ value is 146 K. Upon heating a rapid increase of the $\chi_{\text{M}}T$ values can be observed between 136 and 161 K, resulting in a 6 K broad hysteresis loop. The $T_{1/2}^{\uparrow}$ value is 152 K. Compound **3**·(0.7 bpee)(0.7 tol) shows a gradual spin transition between 200 and 95 K in the cooling mode and a minimum $\chi_{\text{M}}T$ value of $1.13 \text{ cm}^3 \text{ K mol}^{-1}$ at 50 K ($\gamma_{\text{HS}} = 0.32$). The $T_{1/2}^{\downarrow}$ value of this SCO is 144 K. In the heating mode, the $\chi_{\text{M}}T$ values remain approximately constant up to 115 K. Between 115 and 160 K the $\chi_{\text{M}}T$ values increase more rapidly than the values in the cooling mode. Between 160 and 200 K, the $\chi_{\text{M}}T$ values of both modes are identical and the transition curves proceed with the same slope. The $T_{1/2}^{\uparrow}$ value is 157 K. The maximum width of the hysteresis loop is 24 K at $1.80 \text{ cm}^3 \text{ K mol}^{-1}$. The magnetic measurement of compound **5**·0.5 bpea reveals a very gradual SCO in the cooling mode, too, with a remaining γ_{HS} value of 0.55 at 50 K and a $T_{1/2}^{\downarrow}$ value of 139 K. Upon heating, the $\chi_{\text{M}}T$ values gradually increase up to $2.30 \text{ cm}^3 \text{ K mol}^{-1}$ at 135 K, followed by a decrease to a minimum $\chi_{\text{M}}T$ value of $2.24 \text{ cm}^3 \text{ K mol}^{-1}$ at 140 K. Above 140 K, the $\chi_{\text{M}}T$ values increase gradually again, until both transition curves meet at 210 K. The $T_{1/2}^{\uparrow}$ value of this SCO is 179 K. The resulting oval hysteresis loop exhibits a maximum width of 43 K. Compound **6**·(bpee)(MeOH) undergoes a spin transition above room temperature. In the temperature range of 50–300 K, the $\chi_{\text{M}}T$ values slightly increase from a $\chi_{\text{M}}T$ value of $0.22 \text{ cm}^3 \text{ K mol}^{-1}$ to $0.51 \text{ cm}^3 \text{ K mol}^{-1}$, indicative of iron(II) in the LS state. Upon heating above 300 K, the $\chi_{\text{M}}T$ values increase, gradually then more rapidly, to attain a maximum value of $3.35 \text{ cm}^3 \text{ K mol}^{-1}$ at 400 K, indicative of iron(II) in HS state. The $T_{1/2}^{\uparrow}$ value of this SCO is 372 K. In the cooling mode, the $\chi_{\text{M}}T$ values decrease, first gradually then, below 365 K, rapidly then again gradually, to attain the LS state again. The $T_{1/2}^{\downarrow}$ value of this spin transition is 344 K, resulting in a 28 K wide hysteresis loop.

12. Increasing the Hysteresis Width of Iron(II) SCO Compounds in a Crystal Engineering-like Approach

Table 2. Overview of the SCO behaviour, characteristic $\chi_M T$ values [$\text{cm}^3 \text{K mol}^{-1}$], the HS residues (γ_{HS}) at 50 K and the $T_{1/2}$ values [K] of the 1D coordination polymers with $\text{H}_2\text{L1}$.

compound	SCO	$\chi_M T$ (50 K)	$\chi_M T$ (300 K)	γ_{HS}	$T_{1/2}$
1 ·MeOH	abrupt, 6 K hysteresis	0.26	3.46	/	↓ 146, ↑ 152
1	gradual, incomplete	1.19	3.44	0.35	180
2 ·0.3 bpea	gradual, incomplete	1.71	3.55	0.48	210
2 ·(0.5 bpea)(0.5 tol)	abrupt, complete	0.31	3.50	/	204
3 ·(0.7 bpee)(0.7 tol)	gradual, hysteresis, incomplete	1.13	3.51	0.32	↓ 144, ↑ 157
4 ·(0.5 bipy)(MeOH)	gradual, incomplete	1.59	3.42 ^[a]	0.47	350
5 ·0.5 bpea	gradual, incomplete, hysteresis	1.73	3.13	0.55	↓ 139, ↑ 179
6 ·(bpee)(MeOH)	abrupt, 28 K hysteresis	0.22	3.34 ^[a]	/	↓ 344, ↑ 372

[a] $\chi_M T$ value at 400 K.

X-Ray structure analysis of the compounds with ligand system H₂L1: From the syntheses with the monomeric ligands H₂L1a and H₂L1b, crystals suitable for X-ray analysis were obtained for compounds **1**·3 MeOH and **4**·(0.5 bipy)(2 MeOH). These crystal structures describe the first examples with those kinds of equatorial ligands and therefore are especially interesting. However, for both compounds, it was not possible to do further analyses as they lose some methanol while drying and become compounds **1**·MeOH and **4**·(0.5 bipy)(MeOH). The crystallographic data and refinement details are summarised in Supporting Information Table S1.1. Selected bond lengths and angles within the first coordination sphere of the iron centres are summarised in Table 3. ORTEP drawings of the asymmetric units of the compounds are given in Figure 2.

The iron(II) centre of **1**·3 MeOH is located in an octahedral coordination sphere, consisting of the equatorially coordinated tetradentate Schiff base-like ligand L1a²⁻ and the axially coordinated bridging ligand bipy, bound through terminal 4-pyridyl groups. Each bridging ligand “connects” two iron(II) centres, resulting in the formation of infinite 1D chains. An excerpt of the molecule packing is shown in Figure 3. Due to the “rigidity” of the axial ligand, the crystal structure reveals parallel linear 1D chains which propagate along the [1 0 0] direction.

Compound **1**·3 MeOH crystallises with the monoclinic space group *P*2₁/*c*, with four formula units in the unit cell. The observed bond lengths around the iron(II) centre of the complex are within the range reported for other octahedral iron(II) complexes of this ligand type in the LS state.^[8–11,13] The average values are 1.89 Å (Fe-N_{eq}), 1.94 Å (Fe-O_{eq}) and 2.00 Å (Fe-N_{ax}). The observed O-Fe-O angle, the so-called bite angle of the ligand, which is typically about 110° for HS iron(II) complexes of this ligand type and about 90° for LS iron(II), is with 88.5° clearly indicative of iron(II) in the LS state.

An analysis of polymeric structures reveals an infinite one-dimensional chain with the base vector: [1 0 0].

12. Increasing the Hysteresis Width of Iron(II) SCO Compounds in a Crystal Engineering-like Approach

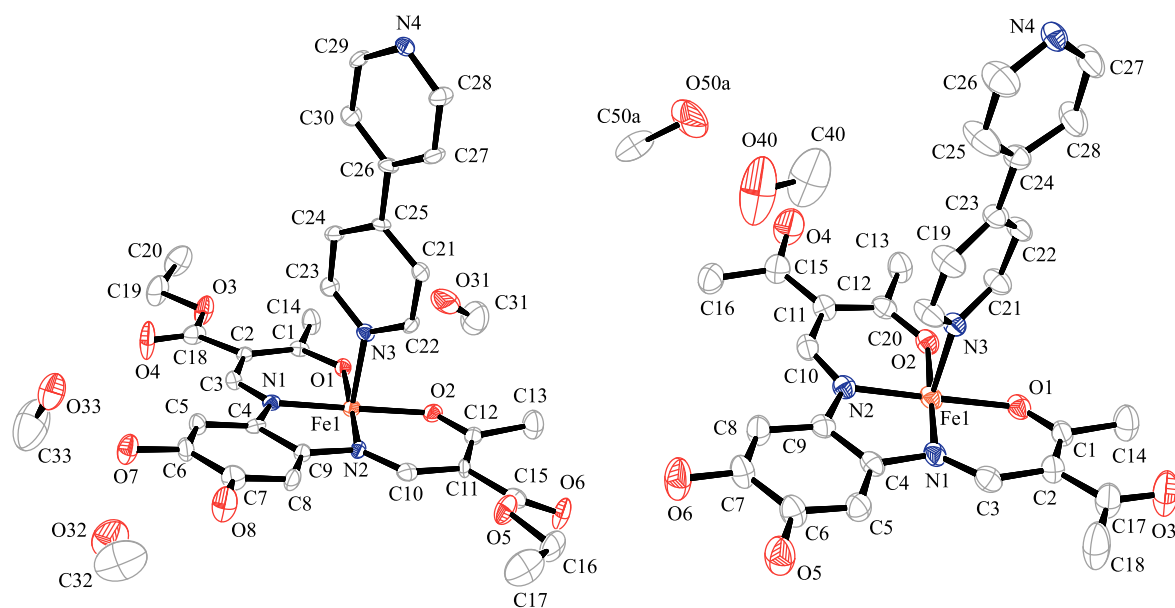


Figure 2. ORTEP drawing of the asymmetric units of **1**·3 MeOH and **4**·(0.5 bipy)(2 MeOH). Hydrogen atoms were omitted for clarity, as well as the half bipy molecule for **4**·(0.5 bipy)(2 MeOH). Thermal ellipsoids are shown with a 50% probability.

Table 3. Selected bond lengths [Å] and angles [degree] within the inner coordination sphere of the 1D iron(II) coordination polymers with the ligand system H₂L1.

compound	Fe-N _{eq}	Fe-O _{eq}	Fe-N _{ax}	O _{eq} -Fe-O _{eq}	N _{ax} -Fe-N _{ax}
1 ·3 MeOH	1.893(2)	1.941(2)	2.004(3)	88.47(8)	178.75(10) ^[a]
	1.891(2)	1.936(2)	1.995(3) ^[a]		
4 ·(0.5 bipy) (2 MeOH)	1.902(4)	1.944(4)	1.989(5)	86.92(16)	177.17(17) ^[b]
	1.906(4)	1.942(4)	2.002(5) ^[b]		

Symmetry codes: [a] $-1 + x, y, z$; [b] $1 + x, y, z$.

The asymmetric unit additionally contains 3 methanol molecules, bound through hydrogen bonds to the complex: methanol 1 (C31-O31) bonds to the iron-coordinating oxygen atoms O1 and O2, which act as acceptors, whereas the methanol hydroxy group O31-H31 is the donor group. Moreover, oxygen atom O31 is the acceptor of the donor hydroxy group O33-H33, belonging to methanol 3 (C33-O33). This solvent molecule builds a further hydrogen bond to one of the hydroxy groups of the equatorial ligand O7-H7, which is the donor group, whereas methanol oxygen O33 is the acceptor. Methanol 2 (C32-O32) also participates in two hydrogen bonds: on the one side, O32 is the acceptor and bonds to the second hydroxy group of the equatorial ligand, namely O8-H8; on the other side, the methanol hydroxy group O32-H32 is the donor group and bonds to acceptor carbonyl oxygen atom O6, which is part of an ethoxy carbonyl group of the equatorial ligand. Moreover two hydrogen bonds of the kind C-H...O (non-classical hydrogen bond) can be found involving the carbonyl oxygen atoms O4 and O6 of both ethoxy carbonyl side groups and two CH groups of bipyridine rings of adjacent chains. In Table 4 a summary of the intermolecular hydrogen bonds is given. An analysis of intermolecular polymeric hydrogen bond structures reveals, that methanol 1 forms an infinite 1D chain with base vector $[2 \bar{1} 1]$ and methanol 3 is part of an infinite 2D network in the plane $(1 0 \bar{2})$ with base vectors $[0 1 0]$ and $[2 0 1]$.

Compound **4**·(0.5 bipy)(2 MeOH) crystallises with the triclinic space group $P\bar{1}$, with two formula units in the unit cell. The observed bond lengths around the iron(II) centre of the complex are also within the range of iron(II) in the LS state. The average values are 1.90 Å (Fe-N_{eq}), 1.94 Å (Fe-O_{eq}) and 1.99 Å (Fe-N_{ax}). The observed O-Fe-O angle is with 86.9° indicative of LS iron(II) as well.^[8-11,13]

The asymmetric unit of **4**·(0.5 bipy)(2 MeOH) additionally contains half of a bipy molecule and two methanol molecules, of which one is disordered. These molecules are all part of hydrogen bonds. The nitrogen atom N30 of the bipy molecule bonds to hydroxy group O5-H5 located at the phenyl ring of the equatorial ligand. Methanol 1 (C40-O40) participates in two hydrogen bonds: on the one side, the hydroxy group O40-H40A acts as a donor group and is bound to the acceptor O4, a carbonyl oxygen part of an acetyl side group of the equatorial ligand; on the other side O40 is the hydrogen bond acceptor and bonds the hydroxy group O50A/B-H50A/E of disordered methanol 2 (C50A/B-O50A/B). In addition, an intermolecular hydrogen bond can be observed between the second hydroxy group at the phenyl ring of the

equatorial ligand, O6-H6, and carbonyl oxygen O3, located at an acetyl side group of an adjacent equatorial ligand. An analysis of intermolecular polymeric hydrogen bond structures reveals that an infinite one-dimensional chain with the base vector: $[0\ 1\ 0]$ exists, formed between adjacent equatorial ligands and not involving the intercalated molecules.

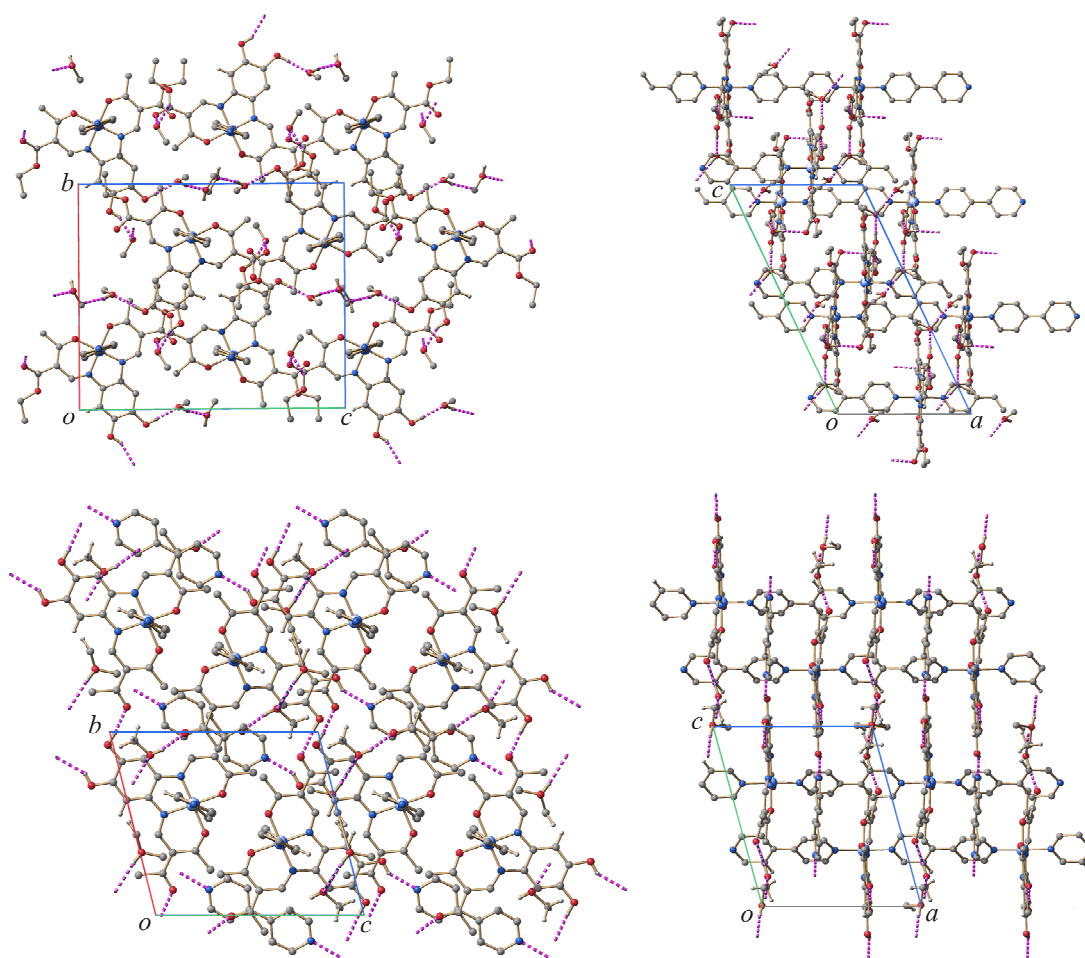


Figure 3. Excerpts of the molecule packing of $1 \cdot 3 \text{ MeOH}$ along the a (top left) and b axis (top right) and of $4 \cdot (0.5 \text{ bipy})(2 \text{ MeOH})$ along the a (bottom left) and b axis (bottom right).

12. Increasing the Hysteresis Width of Iron(II) SCO Compounds in a Crystal Engineering-like Approach

Table 4. Summary of the intermolecular hydrogen bonds of compounds **1**·3 MeOH and **4**·(0.5 bipy)(2 MeOH) with $d(\text{D} \cdots \text{A}) < R(\text{D}) + R(\text{A}) + 0.50$, $d(\text{H} \cdots \text{A}) < R(\text{H}) + R(\text{A}) - 0.12 \text{ \AA}$, $\text{D-H} \cdots \text{A} > 100.0^\circ$.

compound	D	H	A	D-H	H \cdots A	D \cdots A	D-H \cdots A
1 ·3 MeOH	O7	H7	O33	0.84	1.85	2.687(3)	178
	O8	H8	O32	0.84	1.89	2.655(3)	151
	O31	H31	O1	0.84	2.25	2.945(3)	140
	O31	H31	O2	0.84	2.34	3.091(3)	148
	O32	H32	O6 ^[a]	0.84	2.08	2.889(3)	162
	O33	H33	O31 ^[b]	0.84	1.89	2.728(3)	171
	C21	H21	O4 ^[c]	0.95	2.35	3.198(3)	148
	C30	H30	O6 ^[d]	0.95	2.38	3.255(3)	152
4 ·(0.5 bipy) (2 MeOH)	O5	H5	N30 ^[e]	0.84	2.05	2.797(7)	147
	O6	H6	O3 ^[f]	0.84	1.81	2.647(6)	172
	O40	H40	O4	0.84	1.90	2.727(8)	169
	O50A	H50A	O40	0.84	2.12	2.951(9)	171
	O50B	H50E	O40	0.84	2.11	2.951(9)	175
	C22	H22	O40 ^[g]	0.95	2.59	3.153(9)	118
	C50A	H50D	O50A ^[h]	0.95	1.81	2.733(9)	156

Symmetry codes: [a] $1 - x, -y, -z$; [b] $2 - x, -\frac{1}{2} + y, \frac{1}{2} - z$; [c] $x, \frac{1}{2} - y, -\frac{1}{2} + z$; [d] $1 + x, \frac{1}{2} - y, \frac{1}{2} + z$; [e] $x, y, 1 + z$; [f] $x, -1 + y, z$; [g] $-x, -y, 1 - z$; [h] $-x, -1 - y, -z$.

12.2.2 The Ligand System H₄L₂

Table 5. Overview of the synthesised compounds with the H₄L₂ ligand system and the used abbreviations.

L _{ax}	solvent	L2a	L2b
bpee	toluene	[Fe ₂ L2a(bpee) ₂]·1.5 tol (7 ·1.5 tol)	/
	DMF	[Fe ₂ L2a(bpee) ₂]·1.5 DMF (7 ·1.5 DMF)	/
bipy	toluene	[Fe ₂ L2a(bipy) ₂]·tol (8 ·tol)	/
	DMF	[Fe ₂ L2a(bipy) ₂] (8)	[Fe ₂ L2b(bipy) ₂]·1.5 DMF (11 ·1.5 DMF)
	ACN	/	[Fe ₂ L2b(bipy) ₂]·1.5 ACN (11 ·1.5 ACN)
bpea	toluene	[Fe ₂ L2a(bpea) ₂]·2 tol (9 ·2 tol)	/
	DMF	[Fe ₂ L2a(bpea) ₂]·2 DMF (9 ·DMF)	[Fe ₂ L2b(bpea) ₂]·2 DMF (12 ·2 DMF)
	ACN	/	[Fe ₂ L2b(bpea) ₂]·1.5 ACN (12 ·1.5 ACN)
bppa	toluene	[Fe ₂ L2a(bppa) ₂]·2.5 tol (10 ·2.5 tol)	/
	DMF	[Fe ₂ L2a(bppa) ₂]·2.5 DMF (10 ·2.5 DMF)	/

Magnetic measurements of the compounds with ligand system H₄L₂: Characteristic values of the thermal dependence of the $\chi_M T$ product for all dinuclear iron(II) compounds are given in Table 6. The room temperature $\chi_M T$ values of these compounds are in the range of 5.60–7.10 cm³ K mol⁻¹ and therefore typical for dinuclear iron(II) complexes in the high-spin (HS) state.^[9] With exception of compounds **8** and **8**·tol, which are HS complexes in the whole temperature range investigated, all compounds show spin transition. The SCO of compounds **7**·1.5 DMF, **10**·2.5 DMF, **11**·1.5 DMF and **11**·1.5 ACN is gradual and incomplete, with $\gamma_{HS} > 0.50$, indicating that over 50% of the iron centres are still in the HS state at 50 K. Compounds **10**·2.5 tol and **12**·1.5 ACN also show an gradual and incomplete SCO, but with γ_{HS} values of

0.28 and 0.39, respectively, the remaining HS fraction is only about one-third. In Figure 4, the $\chi_M T$ product vs. T of the compounds **7**·1.5 tol, **9**·2 tol, **10**·2.5 tol and **12**·2 DMF are plotted.

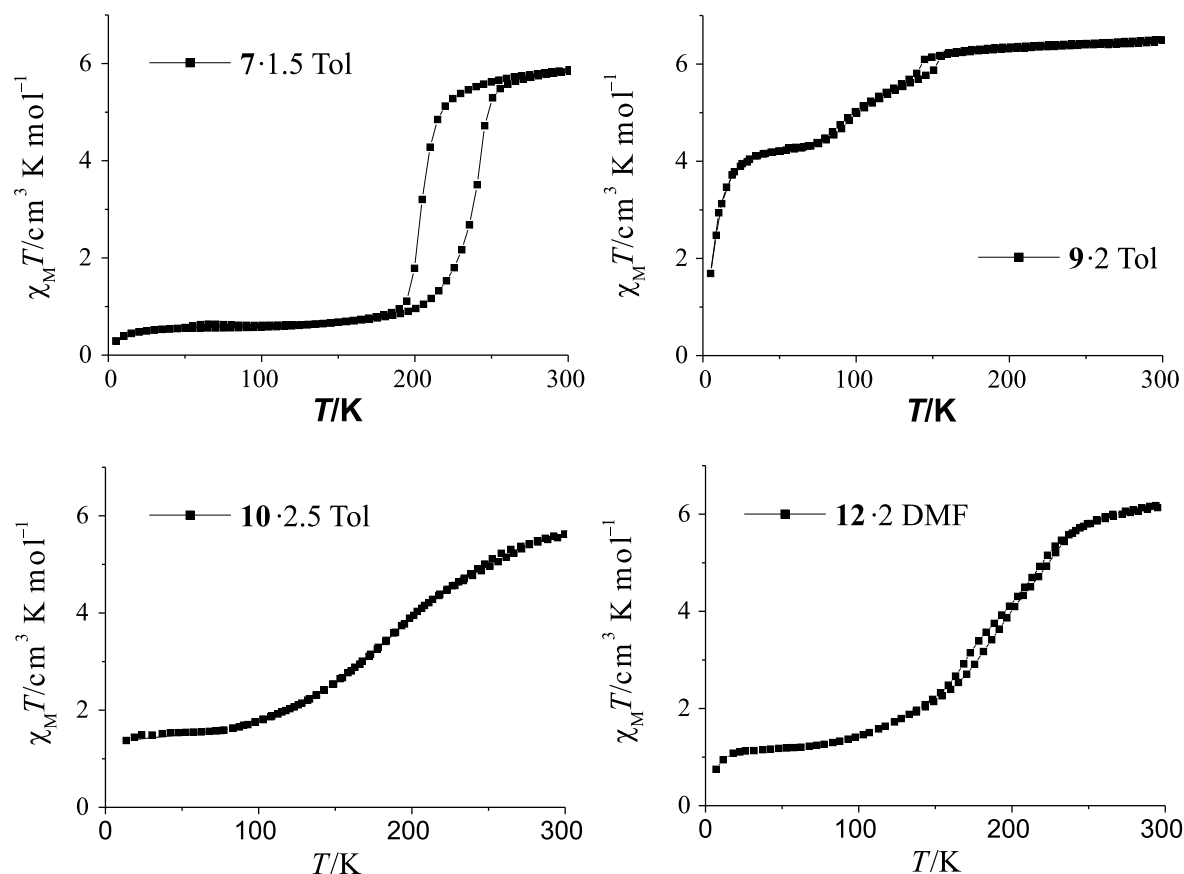


Figure 4. Plots of the $\chi_M T$ product vs. T for the compounds **7**·1.5 tol, **9**·2 tol, **10**·2.5 tol and **12**·2 DMF.

Compound **9**·DMF shows a triangular thermally induced hysteresis loop besides a gradual and incomplete spin transition. In the cooling mode, the $\chi_M T$ values remain approximately constant at $7.00 \text{ cm}^3 \text{ K mol}^{-1}$ between 300 and 200 K. Below 200 K, the $\chi_M T$ values decrease rapidly down to 170 K, then gradually to attain a minimum value of $3.86 \text{ cm}^3 \text{ K mol}^{-1}$ at 50 K. The $T_{1/2}$ value of this SCO is 180 K. Upon heating the $\chi_M T$ values increase gradually between 50 and 214 K to the initial value, building the triangular hysteresis loop which has a maximum width of 13 K at $6.18 \text{ cm}^3 \text{ K mol}^{-1}$. Compound **9**·2 tol shows a similar SCO behaviour, but the transition temperature is moved to lower temperatures. This can be seen by comparing the $T_{1/2}$ value, which is 115 K for **9**·2 tol. A triangular hysteresis loop can be

12. Increasing the Hysteresis Width of Iron(II) SCO Compounds in a Crystal Engineering-like Approach

observed as well, but its maximum width is with 10 K at $5.88 \text{ cm}^3 \text{ K mol}^{-1}$ a bit smaller. The $\chi_{\text{M}}T$ values of compound **12**·2 DMF decrease gradually between 300 and 50 K down to $\gamma_{\text{HS}} = 0.19$. The $T_{1/2}^{\downarrow}$ value of this SCO is 185 K. In the heating mode the $\chi_{\text{M}}T$ values increase slightly smoother so that the $T_{1/2}^{\uparrow}$ value is reached at 191 K, resulting in a small 6 K hysteresis loop. The most interesting spin transition is provided by compound **7**·1.5 tol. The $\chi_{\text{M}}T$ values decrease gradually between 300 and 235 K. Between 235 and 185 K, the $\chi_{\text{M}}T$ values decrease rapidly to attain a minimum value of $0.85 \text{ cm}^3 \text{ K mol}^{-1}$. Below 185 K, the $\chi_{\text{M}}T$ values remain approximately constant down to 50 K. The $T_{1/2}^{\downarrow}$ value of this SCO is 205 K. Upon heating, the $\chi_{\text{M}}T$ values are identical between 50 and 185 K. Above 185 K, the $\chi_{\text{M}}T$ values increase, gradually then rapidly then again gradually to attain the maximum value of $5.90 \text{ cm}^3 \text{ K mol}^{-1}$ at 300 K. The $T_{1/2}^{\uparrow}$ value is 239 K, resulting in a 34 K wide hysteresis loop.

Table 6. Overview of the SCO behaviour, characteristic $\chi_{\text{M}}T$ values [$\text{cm}^3 \text{ K mol}^{-1}$] at 50 K and 300 K the HS residues (γ_{HS}) at 50 K and the $T_{1/2}$ values [K] of the coordination polymers with H₄L2.

compound	SCO	$\chi_{\text{M}}T$ (50 K)	$\chi_{\text{M}}T$ (300 K)	γ_{HS}	$T_{1/2}$
7 ·1.5 tol	abrupt, 34 K hysteresis	0.55	5.90	0.09	↓ 205, ↑ 239
7 ·1.5 DMF	gradual, incomplete	3.19	6.29	0.51	196
8 ·tol	HS	/	6.20	/	/
8	HS	/	7.10	/	/
9 ·2 tol	gradual, hysteresis, incomplete	4.21	6.49	0.64	115
9 ·DMF	gradual, hysteresis, incomplete	3.86	7.00	0.55	180
10 ·2.5 tol	gradual, incomplete	1.54	5.60	0.28	188
10 ·2.5 DMF	gradual, incomplete	3.60	6.00	0.60	171
11 ·1.5 DMF	gradual, incomplete	4.06	6.57	0.61	123
11 ·1.5 ACN	gradual, incomplete	3.08	6.00	0.51	164
12 ·2 DMF	gradual, hysteresis, incomplete	1.24	6.44	0.19	↓185, ↑191
12 ·1.5 ACN	gradual, incomplete	2.45	6.23	0.39	175

X-Ray structure analysis of the compounds with ligand system H₄L2: Great efforts were done to get crystals of sufficient quality for X-ray analysis from the syntheses with the dinuclear ligands H₄L2a and H₄L2b, but this turned out to be very difficult as all compounds are hardly soluble in any solvent. In fact, we only succeeded in the crystallisation of compound **9**·x MeOH by applying a slow diffusion technique, but the quality of the orthorhombic crystals was inferior so we can only speak of a structure motif. The crystal data are summarised in Supporting Information Table S1.1. This is also the reason why the number of solvent molecules intercalated in the crystal structure is not clear. Nonetheless, this motif describes the first structural example of a dinuclear coordination polymer with SCO behaviour and gives an answer to the up to date unknown question, if a two-dimensional sheet structure (staggered arrangement of the dinuclear ligands) or a one-dimensional chain structure (ladder-like, stacked arrangement) is preferred.

All iron centres are crystallographically equal and clearly in the HS state.^[8–11,13] The average bond lengths within the inner coordination sphere are 2.10 Å (Fe-N_{eq}), 2.03 Å (Fe-O_{eq}) and 2.28 Å (Fe-N_{ax}) and the observed O-Fe-O angle is 113°. As can be seen from Figure 5, infinite one-dimensional ladder-like chains are formed, with the base vector [1 0 0]. Within the ladders, the backbones of the dinuclear ligands (the “rungs of the ladders”) are not perpendicular to the axial ligands. The molecule packing displayed in Figure 6 reveals that the chains form parallel layers in the *ab*-plane.

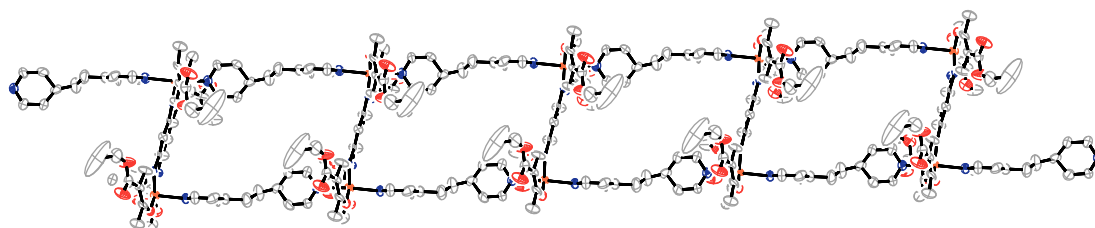


Figure 5. Excerpt of the infinite one-dimensional ladder-like chain structure of compound **9**·x MeOH.

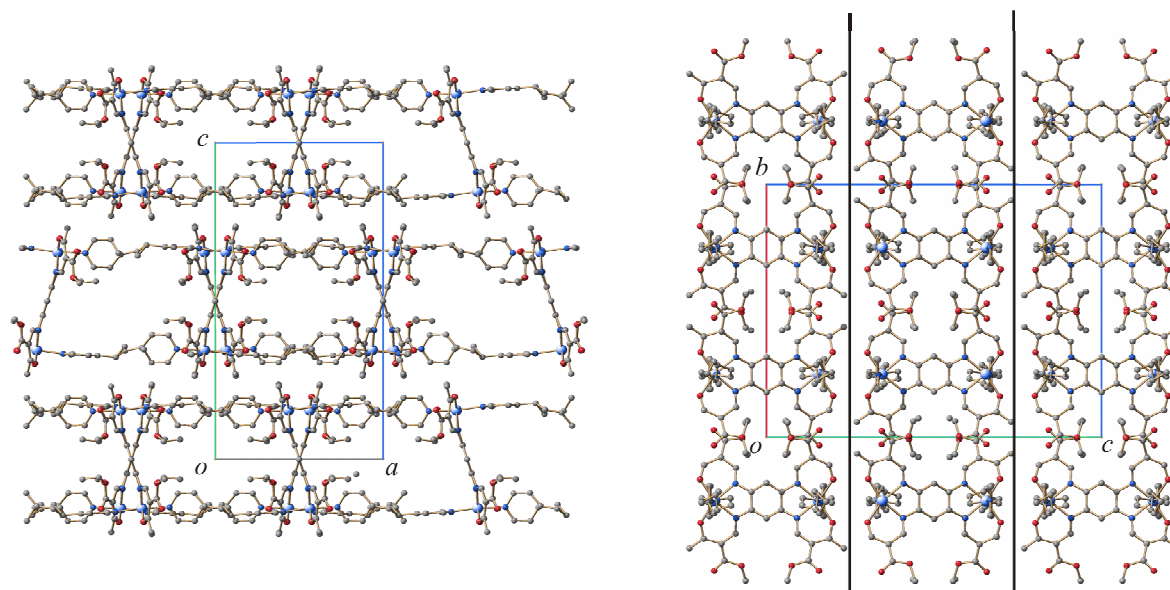


Figure 6. Excerpts of the molecule packing of $9 \cdot x$ MeOH in the ac - (left) and bc -plane (right). The formation of layers in the ab -plane is indicated.

12.2.3 The Ligand System H_2L3

Table 7. Overview of the synthesised compounds with the H_2L3 ligand system and the used abbreviations.

L_{ax}	L3a	L3b
pina	[FeL3a(pina)] (13)	[FeL3b(pina)]·0.5 MeOH (14 ·0.5 MeOH)
	[FeL3a(pina)]·0.5 MeOH (13 ·0.5 MeOH)	[FeL3b(pina)]· x MeOH (14 · x MeOH)
	MeOH)	

Magnetic measurements of the compounds with ligand system H_2L3 : Characteristic values of the thermal dependence of the $\chi_M T$ product for the mononuclear iron(II) coordination polymers are given in Table 8. The maximum $\chi_M T$ values of these compounds at 300 and 350 K, respectively, are in the range of 3.33–3.64 cm³ K mol⁻¹ and therefore typical for iron(II) complexes in the high-spin (HS) state. The powder sample **13**, the crystalline sample **13**·0.5 MeOH as well as the microcrystalline sample of **14**·0.5 MeOH are pure HS compounds in the whole temperature range investigated. An interesting SCO behaviour, with

wide thermal hysteresis loops, was observed for compounds **14**·x MeOH and **14**·2 MeOH, as can be seen in Figure 7. The exact composition of compound **14**·x MeOH is not clear, as the results from elemental analysis are ambiguous and no further analysis was possible due to the small amount of product. The overall measurement consists of two loops within the temperature ranges 350 to 150 K (loop 1) and 400 to 150 K (loop 2). Starting with loop 1, in the temperature range 350 to 270 K, the χ_{MT} values are approximately constant at $3.49 \text{ cm}^3 \text{ K mol}^{-1}$, indicative of iron(II) in the HS state. Between 270 and 194 K, the χ_{MT} values rapidly decrease to attain a minimum of $0.83 \text{ cm}^3 \text{ K mol}^{-1}$. Below 194 K, the χ_{MT} values are approximately constant again. The $T_{1/2}^{\downarrow}$ value of this step is 240 K. With $\gamma_{\text{HS}} = 0.2$, there is still a significant HS fraction left over. Upon heating, an increase of the χ_{MT} values is not observed below 319 K. Between 319 and 336 K, the χ_{MT} values rapidly increase and become identical with the values of the cooling-mode above 336 K. The $T_{1/2}^{\uparrow}$ value of this step is 328 K, resulting in an enormous 88 K wide hysteresis loop. The magnetic measurement of loop 2 starts at 400 K. The shape of the hysteresis loop is the same as for loop 1, but the observed $T_{1/2}$ values are shifted 15 K in average to lower temperatures ($T_{1/2}^{\downarrow}$: 224 K, $T_{1/2}^{\uparrow}$: 316 K). It can only be assumed that the loss of solvent is responsible for this finding.

The results of the magnetic measurement of compound **14**·2 MeOH are quite different compared to **14**·x MeOH. The overall measurement consists of three loops within the temperature ranges 350 to 200 K (loop 1), 400 to 150 K (loop 2) and 350 to 50 K (loop 3). Looking at loop 1, a complete spin transition from the HS to the LS state (see Table 4) with a decrease of the χ_{MT} values between 309 and 214 K can be observed in the cooling mode, whereas a rapid increase can be observed between 265 and 335 K in the heating mode. The $T_{1/2}$ values are 272 (down) and 306 K (up), resulting in a 34 K wide hysteresis loop. The shape of the hysteresis of loop 2 is similar compared to that of loop 1. However, the transition temperatures are significantly shifted to lower temperatures (loop 2: $T_{1/2}^{\downarrow}$: 245 K, $T_{1/2}^{\uparrow}$: 296 K) and the hysteresis width increases from 34 to 51 K. This behaviour could be associated with the loss of solvent molecules, as the measurement temperature was raised to 400 K in the meantime, but loop 3 reveals that something more is going on. Although solvent effects can be excluded, the transition temperatures are shifted downwards again (loop 2: $T_{1/2}^{\downarrow}$: 236 K, $T_{1/2}^{\uparrow}$: 281 K) and a shrinking of the hysteresis width is observed to 45 K.

12. Increasing the Hysteresis Width of Iron(II) SCO Compounds in a Crystal Engineering-like Approach

Much of the SCO behaviour of compounds **14**·x MeOH and **14**·2 MeOH is still not fully understood but it can be said that solvent effects play an important, but not the only role for the wide hysteresis loops of these materials.

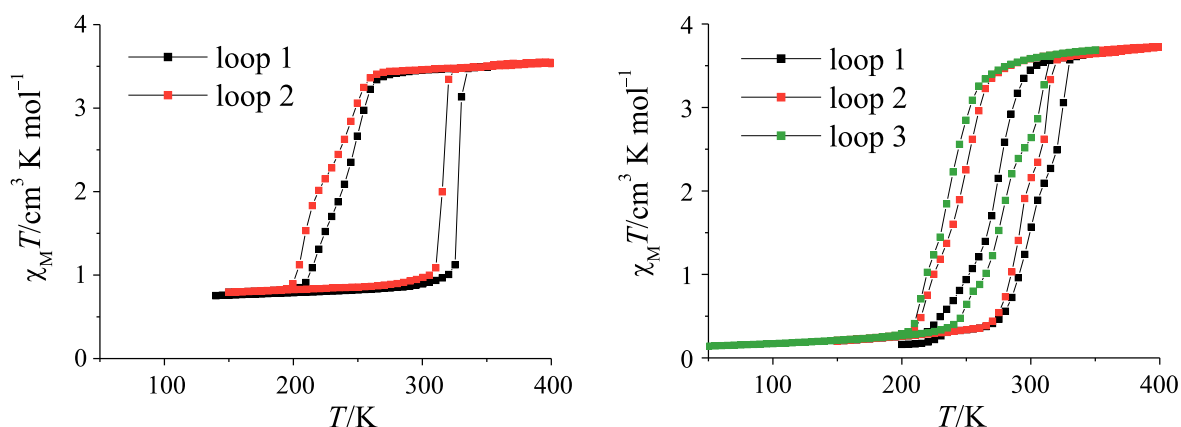


Figure 7. Plots of the $\chi_M T$ product vs. T for the compounds **14**·x MeOH (left) and **14**·2 MeOH (right).

Table 8. Overview of the SCO behaviour, characteristic $\chi_M T$ values [$\text{cm}^3 \text{K mol}^{-1}$], the HS residue (γ_{HS}) at 150 K and the $T_{1/2}$ values [K] of the 1D coordination polymers with $\text{H}_2\text{L3}$ and pina.

compound	sample	SCO	$\chi_M T$	$\chi_M T$	γ_{HS}	$T_{1/2}$
			(150 K)	(300 K)		
13	powder	HS	/	3.33	/	/
13 ·0.5 MeOH	crystal	HS	/	3.19	/	/
14 ·0.5 MeOH	powder	HS	/	3.30	/	/
14 ·x MeOH	crystal	hysteresis, 88 K ^[b] , 92 K ^[c]	0.76	3.49 ^[a]	0.2	↓ 240, ↑ 328 ^[b] ↓ 224, ↑ 316 ^[c]
14 ·2 MeOH	crystal	complete, hysteresis 34 K ^[b] , 51 K ^[c] , 45 K ^[d]	0.2	3.64 ^[a]	/	↓ 272, ↑ 306 ^[b] ↓ 245, ↑ 296 ^[c] ↓ 236, ↑ 281 ^[d]

[a] $\chi_M T$ value at 350 K; [b] magnetic measurement: loop 1; [c] loop 2; [d] loop 3.

X-Ray structure analysis of the compounds with ligand system H₂L3: From the syntheses with the axial bridging ligand pina, crystals were obtained of compounds [FeL3a(pina)]·0.5 MeOH (**13**·0.5 MeOH) and [FeL3b(pina)]·2 MeOH (**14**·2 MeOH). These crystal structures describe the first examples with those kinds of axial ligands and therefore are especially interesting. The crystallographic data and refinement details are summarised in Supporting Information Table S1.2. Selected bond lengths and angles within the first coordination sphere of the iron centres are summarised in Table 9. ORTEP drawings of the asymmetric units of the compounds are given in Figure 8.

Compound **13**·0.5 MeOH crystallises with the monoclinic space group $P2_1/c$. The observed bond lengths around the iron(II) centre of the complex are within the range reported for other octahedral iron(II) complexes of this ligand type in the HS state.^[8–11,13] The average values are 2.01 Å (Fe-N_{eq}), 2.05 Å (Fe-O_{eq}) and 2.25 Å (Fe-N_{ax}). The observed O-Fe-O angle is with 112.0° clearly indicative of iron(II) in the HS state. An analysis of polymeric structures reveals an infinite one-dimensional chain with the base vector: [0 1 0].

The asymmetric unit additionally contains a disordered half occupied methanol molecule, which is bound through van der Waals interactions to the complex. Moreover, a disorder was found for the bridging ligand pina, too, mainly concerning the asymmetric peptide bond. At both disordered structures the carbonyl bond points into the same direction.

Looking at the molecule packing, an interesting arrangement of chains can be found, as displayed in Figure 9. Two adjacent chains, which run in the opposite direction, form pairs of molecules and are held tightly together by intermolecular hydrogen bonds between the NH group of the peptide bond and oxygen atom O2, which is also coordinated to the iron(II) centre. All intermolecular contacts are listed in Table 10. The average interchain distances of 3.5 Å is relative short. This is possible because the flat open chain sites of the equatorial ligands within the chain-pairs point to each other, whereas the bulky backbones point outwards and interact with the backbones of other chain-pairs.

12. Increasing the Hysteresis Width of Iron(II) SCO Compounds in a Crystal Engineering-like Approach

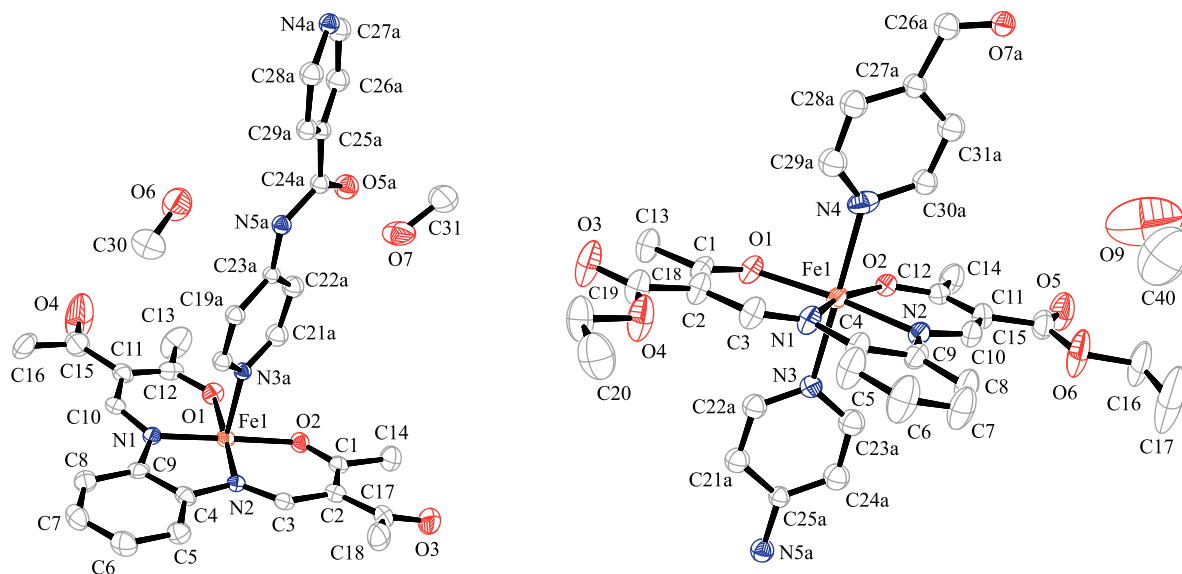


Figure 8. ORTEP drawing of the asymmetric units of **13**·0.5 MeOH (right) and **14**·2 MeOH (left). Hydrogen atoms were omitted for clarity, as well as the disorders of the pina ligands. Thermal ellipsoids are shown with a 50% probability.

Table 9. Selected bond lengths [Å] and angles [degree] within the inner coordination sphere of the 1D iron(II) coordination polymers with the bridging ligand pina.

compound	Fe-N _{eq}	Fe-O _{eq}	Fe-N _{ax}	O _{eq} -Fe-O _{eq}	N _{ax} -Fe-N _{ax}
13 ·0.5 MeOH	2.105(3)	2.026(2)	2.245(3)	111.96(9)	173.99(11)
	2.108(3)	2.070(2)	2.248(3)		
14 ·2 MeOH	1.904(3)	1.940(2)	2.026(13) ^[a]	88.89(10)	174.4(3) ^{[a],[c]}
			1.93(3) ^[b]		
	1.898(3)	1.947(2)	2.008(11) ^[a]		172.6(8) ^{[b],[c]}
			2.05(3) ^{[b],[c]}		

[a] related to N3A; [b] related to N3B; symmetry code: [c] 1 + x, y, z.

Compound **14**·2 MeOH crystallises with the monoclinic space group $P2_1/c$. The observed bond lengths around the iron(II) centre of the complex (Table 9) are within the range reported for other octahedral iron(II) complexes of this ligand type in the LS state.^[8–11,13] The average values are 1.90 Å (Fe-N_{eq}), 1.94 Å (Fe-O_{eq}) and 2.01 Å (Fe-N_{ax}). The observed O-Fe-O angle is with 88.9° clearly indicative of iron(II) in the LS state. An analysis of polymeric structures reveals an infinite one-dimensional chain with the base vector: [1 0 0]. The pina ligand is

12. Increasing the Hysteresis Width of Iron(II) SCO Compounds in a Crystal Engineering-like Approach

disordered in the same way as observed for **13**·0.5 MeOH, with the carbonyl groups of the disordered peptide bonds pointing in the same direction.

The asymmetric unit additionally contains two methanol molecules, each bound through hydrogen bonds to the peptide bond (Table 10). In one case, the hydroxy group of methanol is the donor group (O7-H7A) and the carbonyl oxygen of the peptide bond the acceptor (O5). In the other case, methanol is the acceptor (O6) of the N-H group of the peptide bond (N5-H5). This solvent molecule moreover participates in a second hydrogen bond between its hydroxy group (O6-H6A) and the carbonyl group (O3) of an adjacent equatorial ligand and, thus, is part of an infinite one-dimensional hydrogen bond chain (base vector: [0 0 1]) (Figure 9).

Table 10. Summary of the intermolecular hydrogen bonds of compounds **13**·0.5 MeOH and **14**·2 MeOH with $d(D \cdots A) < R(D) + R(A) + 0.50$, $d(H \cdots A) < R(H) + R(A) - 0.12 \text{ \AA}$, $D-H \cdots A > 100.0^\circ$.

compound	D	H	A	D-H	H···A	D···A	D-H···A
13 ·0.5 MeOH	N5A	H5A	O2 ^[a]	0.88	2.20	2.941(6)	141
	C13A	H13A	O7A ^[a]	0.98	2.43	3.397(7)	168
14 ·2 MeOH	N5A	H5A	O6	0.88	2.19	3.008(6)	155
	N5B	H5B	O6	0.88	2.16	2.893(13)	141
	O7	H7A	O5A	0.84	2.09	2.887(7)	159
	O7	H7A	O5B	0.84	1.94	2.771(13)	169
	O6	H6A	O3 ^[b]	0.84	2.04	2.865(4)	169
	C18	H18A	O7 ^[c]	0.98	2.58	3.458(7)	149
	C18	H18C	O6 ^[d]	0.98	2.59	3.327(5)	132
C20A	H20A	O3 ^[c]	0.95	2.50	3.217(10)	132	

Symmetry codes: [a] $-x, -\frac{1}{2} + y, \frac{1}{2} - z$; [b] $x, -\frac{1}{2} - y, \frac{1}{2} + z$; [c] $-x, \frac{1}{2} + y, -\frac{1}{2} - z$; [d] $x, -\frac{1}{2} - y, -\frac{1}{2} + z$.

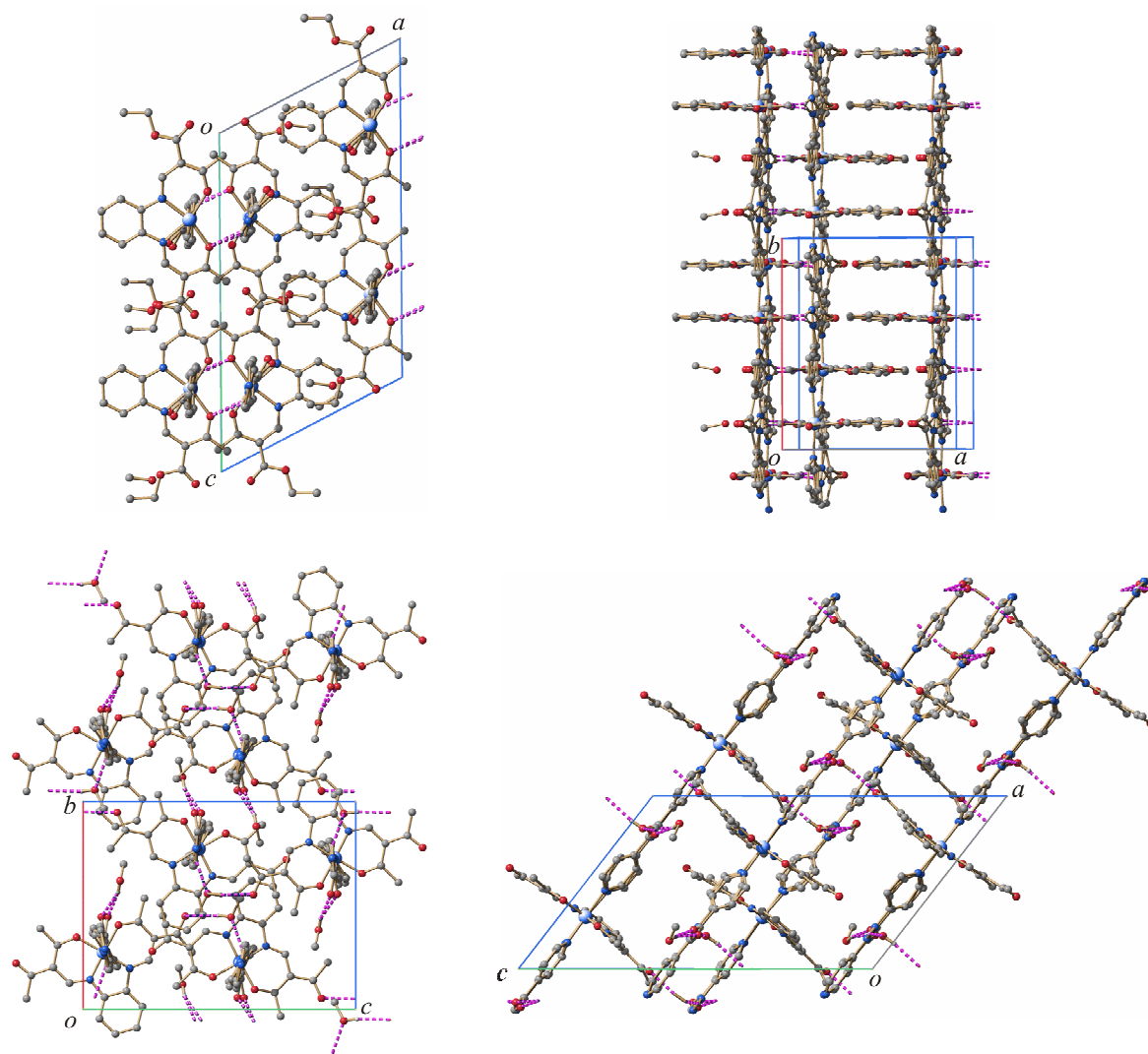


Figure 9. Excerpts of the molecule packing of **13**·0.5 MeOH in the *ac*- (top left) and *ab*-plane (top right) and of **14**·2 MeOH in the *bc*- (bottom left) and *ac*-plane (bottom right).

12.3 Discussion

The crystal engineering concept: Figure 10 displays that, with the principles of coordination bonding through the application of covalent linkers, the cooperative interactions during the spin transition can be systematically increased in a crystal engineering-like approach. Starting with monomeric compounds like $[\text{FeL3b}(\text{py})_2]$ (py = pyridine)^[14] or $[\text{FeL3b}(1\text{-meim})_2]$ (1-meim = 1-methylimidazole)^[9] (Figure 10), 2 K wide hysteresis loops are observed due to two-dimensional networks of weak van der Waals interactions. In the case of 1-meim, the transition from a mono- to a dinuclear complex $[\text{Fe}_2\text{L2b}(1\text{-meim})_4]\cdot 1\text{-meim}$ leads to an improvement of the cooperative effects, as this compound shows a 21 K wide hysteresis loop due to a three-dimensional network of short intermolecular contacts.^[9]

The implementation of covalent linker molecules, finally leading to the formation of 1D coordination polymers, yields to compounds with nearly 30 K wide hysteresis loops, as the conditions for intermolecular interactions are improved on this way.^[11] For compound $[\text{FeL3b}(\text{bipy})]$ (Figure 10), for example, a multitude of short contacts between the chains are found to be responsible for its 18 K wide hysteresis loop,^[10] for compounds $[\text{FeL3a}(\text{bpea})]\cdot (\text{MeOH})$ (hysteresis 27 K)^[11] and $\mathbf{6}\cdot(\text{bpee})(\text{MeOH})$ (hysteresis: 28 K) in addition to that, the cooperativity is further improved by hydrogen bond networks. Compound $\mathbf{6}\cdot(\text{bpee})(\text{MeOH})$ is a perfect example that specific variations at the equatorially ligand system, *e.g.* the introduction of hydroxy groups, can intensify the formation of intermolecular interactions. It is not yet clear if compound $\mathbf{14}\cdot x \text{ MeOH}$ falls into this category, too. We recently showed in our group that unusual wide hysteresis loops are not solely caused by hydrogen bond networks, but direct influences of hydrogen bonds on the ligand field strength at the central ion.^[15]

The combination of both linker-strategies finally leads to the connection of dimeric complexes with covalent bridging ligands in order to get dinuclear coordination polymers and thus further improve the cooperativity. The results show that this strategy absolutely works, as the ladder-like 1D double-strand compound $\mathbf{7}\cdot 1.5 \text{ tol}$ exhibits a 34 K wide hysteresis loop. This finding makes it worth to thoroughly investigate any possibilities for extending and improving this strategy of target-orientated optimisation of intermolecular interactions following the concepts of crystal engineering.

12. Increasing the Hysteresis Width of Iron(II) SCO Compounds in a Crystal Engineering-like Approach

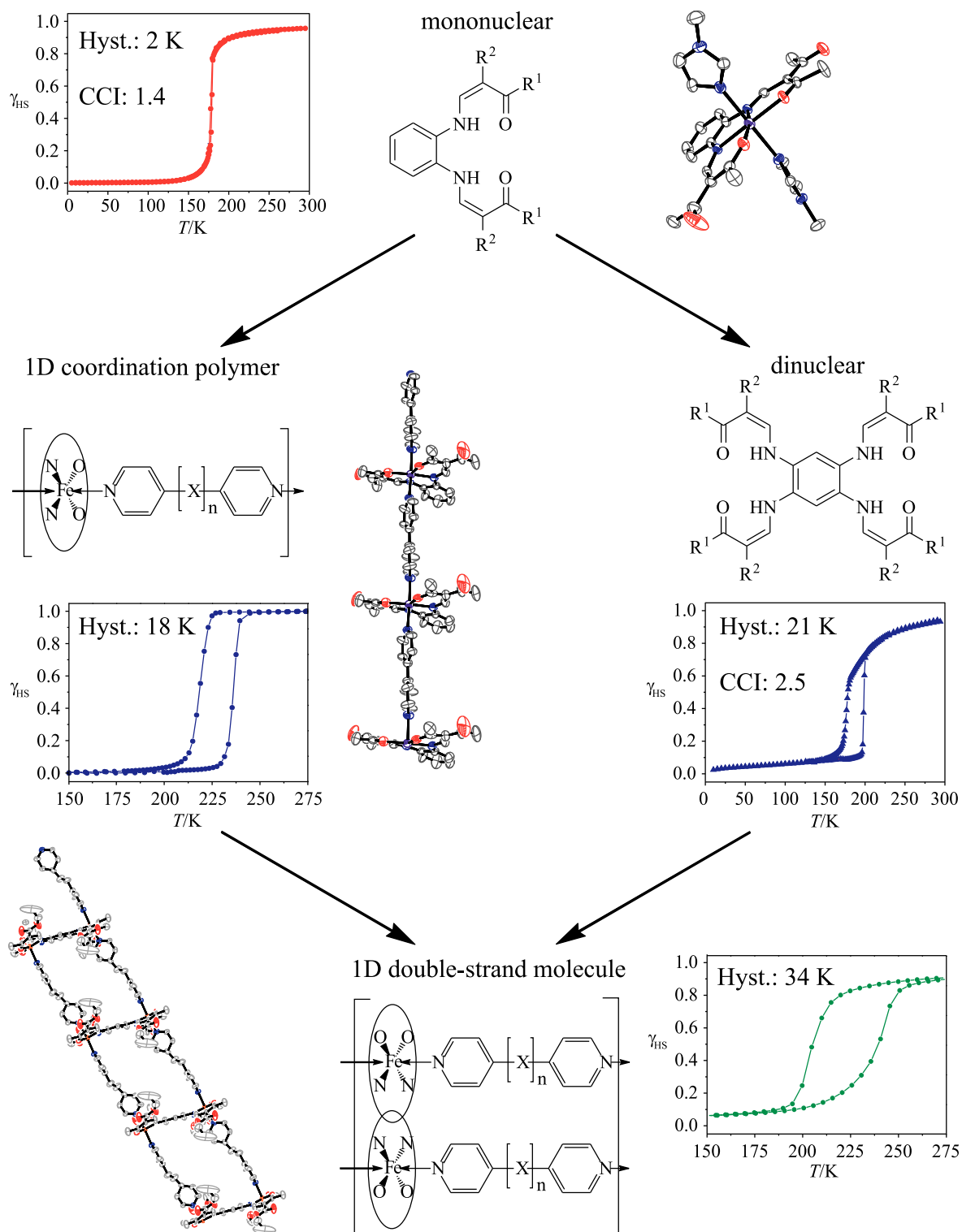


Figure 10. Transition from mononuclear to polynuclear systems. Schematic representation of the synthesis strategy to systematically increase the cooperativity of the iron(II) SCO compounds by increasing their covalent character in a crystal engineering-like approach.

12.4 Conclusion

With the crystal structures of compounds **1**·3 MeOH and **4**·(0.5 bipy)(2 MeOH), as well as the structure motif of **7**·1.5 tol, we have got a first view to the “inner life” of these particular complex systems that gives some useful hints for an understanding of the intermolecular interactions. Talking of the H₂L1 ligand system, we now know for sure that the hydroxy groups take part in hydrogen bonds either to solvent molecules (*e.g.* **1**·3 MeOH) or, as expected, to adjacent complex molecules (*e.g.* **4**·(0.5 bipy)(2 MeOH)) and build up hydrogen bond networks. Moreover, we have got the confirmation that uncoordinated ligand molecules may intercalate in the crystal lattice as predicted from elemental analysis. Talking about the dinuclear coordination polymers, we now know that a one-dimensional ladder-like structure with stacked arrangement of the dinuclear ligands is preferred for this type of complexes in comparison to a two-dimensional sheet structure with staggered arrangement.

12.5 Experimental Section

Magnetic measurements: Magnetic susceptibility data were collected by using a Quantum Design MPMSR-2 SQUID magnetometer under an applied field of 0.5 T over the temperature range 2 to 400 K in the settle mode. The samples were placed in gelatine capsules held within a plastic straw. The data were corrected for the diamagnetic magnetisation of the ligands by using tabulated Pascal's constants and of the sample holder.

X-Ray structure determination: The intensity data were collected on an Oxford XCalibur diffractometer (**1**·3 MeOH, **14**·2 MeOH) or a Nonius Kappa CCD diffractometer (**4**·(0.5 bipy) (2 MeOH), **9**·x MeOH, **13**·0.5 MeOH) by using graphite-monochromated MoK $_{\alpha}$ radiation. The data were corrected for Lorentz and polarisation effects. The structures were solved by direct methods (SIR-97)^[16] and refined by full-matrix least-square techniques against $F_o^2 - F_c^2$ (SHELXL-97).^[17] All hydrogen atoms were calculated in idealised positions with fixed displacement parameters. ORTEP-III^[18] was used for the structure representation, SCHAKAL-99^[19] to illustrate molecule packings. The crystallographic data are summarised in Supporting Information Table S1.1 and S1.2. The quality of the data of **9**·x MeOH is inferior. The remaining residue densities cannot be assigned to any solvent molecules. The highest symmetrical orthorhombic space group suggested (*Ibam*) is not stable upon refinement. We will therefore only be publishing the conformation of the molecule and the crystal data.

Synthesis: All syntheses of the iron(II) complexes were carried out under argon by using Schlenk tube techniques. All solvents were purified as described in literature and distilled under argon.^[20] The syntheses of anhydrous iron(II) acetate,^[21] the ligands H₂L1,^[12] H₄L2a,^[22] H₄L2b,^[23] H₂L3^[24] and the precursors [FeL1(MeOH)₂]^[12] and [FeL3(MeOH)₂]^[25] were published before. The pina ligand was synthesised in two steps: firstly, isonicotinoylchloride hydrochloride was synthesised.^[26a] The second step was the conversion to *N*-(4-pyridyl)isonicotinamide.^[26b]

***N*-(4-Pyridyl)isonicotinamide (pina):** Thionylchloride (60 mL) was added carefully to a stirred mixture of isonicotinic acid (24.6 g, 0.2 mol) and dimethylformamide (1 mL). After 30 min. all of the acid had gone into solution. Excess thionylchloride was removed *in vacuo* and

diethyl ether (200 mL) was stirred into the residue. The crude product was filtered, washed with diethyl ether and dried *in vacuo*. Without further purification the isonicotinic acid in form of the chloride hydrochloride was reacted with 4-aminopyridine (18.8 g, 0.2 mmol) in pyridine (400 mL) at ambient temperature for five days. The product separated with pyridine hydrochlorid. After filtration the solid was suspended in water (1.5 L) to give a colourless material. The product was dissolved in ethanol (300 mL) and 5% sodium bicarbonate solution (200 mL), and on addition of water (1.5 L), gave a colourless flocculent product which was recrystallised from water (approximately 300 mL) (yield: 22.8 g, 57%). ¹H NMR (400 MHz, CDCl₃, 25 °C, TMS): δ = 8.8 (m, 2H, CO-Ar-H), 8.6 (m, 2H, N-Ar-H), 8.0 (s, 1H, NH), 7.7 (m, 2H, CO-Ar-H), 7.6 ppm (m, 2H, N-Ar-H); elemental analysis calcd (%) for C₁₁H₉N₃O (199.21): C 66.3, H 4.6, N 21.1; found: C 65.9, H 4.6, N 21.0.

[FeL1a(bipy)]·MeOH (1·MeOH): A solution of [FeL1a(MeOH)₂] (0.22 g, 0.46 mmol) and bipy (0.36 g, 2.31 mmol) in methanol (25 mL) was heated to reflux for 1 h. After cooling to room temperature, the brown precipitate was filtered off, washed with methanol (2 × 5 mL) and dried *in vacuo* (yield 0.26 g, 89%). IR (KBr): $\tilde{\nu}$ = 1683(s) (COO), 1572(s) cm⁻¹ (CO); MS (FAB-(+), 70 eV): *m/z* (%): 474 (23) [FeL1a⁺], 157 (24) [bipy⁺ + H], 154 (100); elemental analysis calcd (%) for C₃₁H₃₄FeN₄O₉ (662.47): C 56.2, H 5.2, N 8.5; found: C 55.8, H 4.8, N 8.8.

[FeL1a(bipy)]·3 MeOH (1·3 MeOH): Crystals of sufficient quality for X-ray analysis were obtained by applying a slow diffusion technique using a Schlenk tube which is, to a certain height, separated into two chambers by a dividing wall. Into one chamber [FeL1a(MeOH)₂] (0.09 g, 0.17 mmol) was placed, into the other chamber bipy (0.13 g, 0.84 mmol). Solvent methanol was carefully filled up just as high to allow slow diffusion at one point of contact above the dividing wall. Within a couple of days 1·3 MeOH was obtained as black thin needles.

[FeL1a(bipy)] (1): A suspension of [FeL1a(MeOH)₂] (0.18 g, 0.31 mmol) and bipy (0.48 g, 3.07 mmol) in toluene (20 mL) was heated to reflux for 2 h. After cooling to room temperature, the dark brown precipitate was filtered off, washed with diethyl ether (2 × 5 mL) and dried *in vacuo* (yield 0.09 g, 46%). Elemental analysis calcd (%) for C₃₀H₃₀FeN₄O₈ (630.43): C 57.2, H 4.8, N 8.9; found: C 56.8, H 4.8, N 8.8.

[FeL1a(bpea)]·0.3 bpea (2·0.3 bpea): A solution of [FeL1a(MeOH)₂] (0.21 g, 0.44 mmol) and bpea (0.41 g, 2.20 mmol) in methanol (25 mL) was heated to reflux for 1 h. After cooling to room temperature, the black precipitate was filtered off, washed with methanol (2 × 5 mL) and dried *in vacuo* (yield 0.21 g, 73%). IR (KBr): $\tilde{\nu}$ = 1682(vs) (COO), 1571(s) cm⁻¹ (CO); MS (FAB-(+), 70 eV): *m/z* (%): 474 (40) [FeL1a⁺], 185 (100) [bpea⁺ + H]; elemental analysis calcd (%) for C₃₆H₃₈FeN_{4.7}O₈ (719.89): C 60.1 H 5.3, N 9.1; found: C 59.9, H 5.4, N 9.2.

[FeL1a(bpea)]·(0.5 bpea)(0.5 tol) (2·(0.5 bpea)(0.5 tol)): In toluene (20 mL) a suspension of [FeL1a(MeOH)₂] (0.17 g, 0.30 mmol) and bpea (0.55 g, 2.98 mmol) was heated to reflux for 2 h. After cooling to room temperature, the dark green precipitate was filtered off, washed with diethyl ether (2 × 5 mL) and dried *in vacuo* (yield 0.11 g, 46%). Elemental analysis calcd (%) for C_{41.5}H₄₄FeN₅O₈ (796.67): C 62.6, H 5.6, N 8.8; found: C 62.7, H 5.8, N 8.6.

[FeL1a(bpee)]·(0.7 bpee)(0.7 tol) (3·(0.7 bpee)(0.7 tol)): In toluene (20 mL) a solution of [FeL1a(MeOH)₂] (0.18 g, 0.31 mmol) and bpee (0.57 g, 3.15 mmol) was heated to reflux for 2 h. The formation of a violet precipitate was observed in the boiling heat. After cooling and filtration, the precipitate was washed with diethyl ether (2 × 5 mL) and dried *in vacuo* (yield 0.09 g, 35%). IR (KBr): $\tilde{\nu}$ = 1687(s) (COO), 1572(vs) cm⁻¹ (CO); MS (FAB-(+), 70 eV): *m/z* (%): 474 (12) [FeL1a⁺], 183 (60) [bpee⁺ + H] 154 (100); elemental analysis calcd (%) for C_{44.7}H₄₄FeN_{5.3}O₈ (839.37): C 63.9 H 5.3, N 8.9; found: C 63.9, H 5.3, N 8.9.

[FeL1b(bipy)]·(0.5 bipy)(MeOH) (4·(0.5 bipy)(MeOH)): A solution of [FeL1b(MeOH)₂] (0.25 g, 0.56 mmol) and bipy (0.44 g, 2.80 mmol) in methanol (40 mL) was heated to reflux for 3 h. The black crystals that precipitated within 2 days were filtered off, washed with methanol (2 × 5 mL) and dried *in vacuo* (yield 0.23 g, 71%). IR (KBr): $\tilde{\nu}$ = 1634(s) (CO), 1559(s) cm⁻¹ (CO); MS (FAB-(+), 70 eV): *m/z* (%): 414 (3) [FeL1b⁺], 157 (24) [bipy⁺ + H], 154 (100); elemental analysis calcd (%) for C₃₄H₃₄FeN₄O₇ (680.51): C 59.9 H 5.2, N 10.3; found: C 59.4, H 5.1, N 10.3.

Crystals with the composition [FeL1b(bipy)]·(0.5 bipy)(2 MeOH) (4·(0.5 bipy)(2 MeOH)), suitable for X-ray analysis, were obtained out of the mother liquor.

[FeL1b(bpea)]·0.5 bpea (5·0.5 bpea): A solution of [FeL1b(MeOH)₂] (0.32 g, 0.72 mmol) and bpea (0.66 g, 3.59 mmol) in methanol (30 mL) was heated to reflux for 3 h. After cooling to room temperature, the black precipitate was filtered off, washed with methanol (2 × 5 mL) and dried *in vacuo* (yield 0.30 g, 60%). IR (KBr): $\tilde{\nu}$ = 1636(s) (CO), 1561(s) cm⁻¹ (CO); MS

12. Increasing the Hysteresis Width of Iron(II) SCO Compounds in a Crystal Engineering-like Approach

(FAB-(+), 70 eV): m/z (%): 414 (1) [FeL1b⁺], 185 (100) [bpea⁺ + H]; elemental analysis calcd (%) for C₃₆H₃₆FeN₅O₆ (690.55): C 62.6 H 5.3, N 10.1; found: C 62.3, H 5.4, N 10.2.

[FeL1b(bpee)]·(bpee)(MeOH) (6·(bpee)(MeOH)): A solution of [FeL1b(MeOH)₂] (0.30 g, 0.67 mmol) and bpee (0.61 g, 3.36 mmol) in methanol (30 mL) was heated to reflux for 3 h. After cooling to room temperature, the black precipitate was filtered off, washed with methanol (2 × 5 mL) and dried *in vacuo* (yield 0.28 g, 57%). IR (KBr): $\tilde{\nu}$ = 1636(s) (CO), 1561(s) cm⁻¹ (CO); MS (FAB-(+), 70 eV): m/z (%): 414 (1) [FeL1b⁺], 185 (100) [bpea⁺ + H]; elemental analysis calcd (%) for C₄₃H₄₂FeN₆O₇ (810.67): C 63.7 H 5.2, N 10.4; found: C 63.4, H 5.2, N 10.3.

[Fe₂L2a(MeOH)₄]: A solution of iron(II) acetate (2.60 g, 14.8 mmol) and H₄L2a (4.00 g, 6.30 mmol) in methanol (200 mL) was heated to reflux for 4 h. After 24 h at 4°C, the light brown precipitate was filtered off, washed with methanol (2 × 5 mL) and dried *in vacuo* (yield 4.52 g, 76%). Elemental analysis calcd (%) for C₃₈H₅₄Fe₂N₄O₁₆ (934.54): C 48.9 H 5.8, N 6.0; found: C 49.3, H 5.2, N 6.4.

[Fe₂L2b(MeOH)₄]: A solution of iron(II) acetate (1.96 g, 11.3 mmol) and H₄L2b (2.40 g, 4.18 mmol) in methanol (200 mL) was heated to reflux for 4 h. After 24 h at 4°C, the dark brown precipitate was filtered off, washed with methanol (2 × 5 mL) and dried *in vacuo* (yield 1.85 g, 54%). Elemental analysis calcd (%) for C₃₄H₄₆Fe₂N₄O₁₂ (818.44): C 50.1 H 5.7, N 6.6; found: C 49.4, H 5.8, N 6.6.

[Fe₂L2a(bpee)₂]·1.5 tol (7·1.5 tol): A suspension of [Fe₂L2a(MeOH)₄] (0.27 g, 0.29 mmol) and bpee (0.79 g, 4.33 mmol) in toluene (30 mL) was heated to reflux for 1 h. After cooling to room temperature, the green precipitate was filtered off, was washed with toluene (2 × 5 mL) and dried *in vacuo* (yield 0.27 g, 80%). IR (KBr): $\tilde{\nu}$ = 1688(s) (COO), 1572(s) cm⁻¹ (CO); MS (FAB-(+), 70 eV): m/z (%): 806 (13) [FeL2a⁺], 183 (50) [bpee⁺ + H]; 154 (100), 136 (71); elemental analysis calcd (%) for C_{68.5}H₇₀Fe₂N₈O₁₂ (1309.03): C 62.8, H 5.4, N 8.6; found: C 62.6, H 5.5, N 8.1.

[Fe₂L2a(bpee)₂]·1.5 DMF (7·1.5 DMF): A solution of [Fe₂L2a(MeOH)₄] (0.11 g, 0.18 mmol) and bpee (0.43 g, 2.35 mmol) in DMF (15 mL) was heated to reflux for 4 h. After cooling to room temperature, the dark green precipitate was filtered off, washed with diethyl

12. Increasing the Hysteresis Width of Iron(II) SCO Compounds in a Crystal Engineering-like Approach

ether (2 × 5 mL) and dried *in vacuo* (yield 0.08 g, 60%). Elemental analysis calcd (%) for C_{62.5}H_{68.5}Fe₂N_{9.5}O_{13.5} (1280.46): C 58.6, H 5.4, N 10.4; found: C 58.3, H 5.4, N 10.1.

[Fe₂L2a(bipy)₂]·tol (8·tol): A suspension of [Fe₂L2a(MeOH)₄] (0.22 g, 0.24 mmol) and bipy (0.55 g, 3.53 mmol) in toluene (30 mL) was heated to reflux for 1 h. After cooling to room temperature, the brown precipitate was filtered off, washed with toluene (2 × 5 mL) and dried *in vacuo* (yield 0.19 g, 71%). IR (KBr): $\tilde{\nu}$ = 1690(s) (COO), 1573(s) cm⁻¹ (CO); MS (FAB-(+), 70 eV): *m/z* (%): 806 (2) [FeL2a⁺], 157 (9) [bipy⁺ + H]; 154 (100), 136 (68); elemental analysis calcd (%) for C₆₁H₆₂Fe₂N₈O₁₂ (1210.88): C 60.5, H 5.2, N 9.3; found: C 60.7, H 5.2, N 9.4.

[Fe₂L2a(bipy)₂] (8): A solution of [Fe₂L2a(MeOH)₄] (0.10 g, 0.11 mmol) and bipy (0.33 g, 3.53 mmol) in DMF (15 mL) was heated to reflux for 4 h. After cooling to room temperature, the brown precipitate was filtered off, washed with diethyl ether (2 × 5 mL) and dried *in vacuo* (yield 0.08 g, 72%). Elemental analysis calcd (%) for C₅₄H₅₄Fe₂N₈O₁₂ (1118.26): C 58.0, H 4.9, N 10.0; found: C 58.0, H 4.9, N 10.1.

[Fe₂L2a(bpea)₂]·2 tol (9·2 tol): A suspension of [Fe₂L2a(MeOH)₄] (0.27 g, 0.29 mmol) and bpea (1.06 g, 5.78 mmol) in toluene (25 mL) was heated to reflux for 1 h. After cooling to room temperature, the yellow ochre precipitate was filtered off, washed with toluene (2 × 5 mL) and dried *in vacuo* (yield 0.36 g, 91%). IR (KBr): $\tilde{\nu}$ = 1690(s) (COO), 1574(s) cm⁻¹ (CO); MS (FAB-(+), 70 eV): *m/z* (%): 806 (14) [FeL2a⁺], 185 (9) [bpea⁺ + H]; 154 (100), 136 (70); elemental analysis calcd (%) for C₇₂H₇₈Fe₂N₈O₁₂ (1359.13): C 63.6, H 5.8, N 8.2; found: C 62.9, H 5.7, N 8.1.

[Fe₂L2a(bpea)₂]·x MeOH (9·x MeOH): Brown crystals of the composition 9·x MeOH were obtained by slow diffusion techniques of [Fe₂L2a(MeOH)₄] (0.10 g, 0.12 mmol) and bpea (0.44 g, 2.39 mmol) in methanol solution after three weeks.

[Fe₂L2a(bpea)₂]·DMF (9·DMF): A solution of [Fe₂L2a(MeOH)₄] (0.10 g, 0.11 mmol) and bpea (0.39 g, 2.14 mmol) in DMF (15 mL) was heated to reflux for 4 h. After cooling to room temperature, the fine crystalline precipitate was filtered off, washed with diethyl ether (2 × 5 mL) and dried *in vacuo* (yield 0.11 g, 88%). Elemental analysis calcd (%) for C₆₁H₆₅Fe₂N₉O₁₃ (1247.94): C 58.7, H 5.6, N 10.1; found: C 58.8, H 5.5, N 10.0.

12. Increasing the Hysteresis Width of Iron(II) SCO Compounds in a Crystal Engineering-like Approach

[Fe₂L2a(bppa)₂]·**2.5 tol (10**·**2.5 tol):** A solution of [Fe₂L2a(MeOH)₄] (0.22 g, 0.24 mmol) and bppa (0.70 g, 3.53 mmol) in toluene (30 mL) was heated to reflux for 1 h. The formation of a brown precipitate was observed in the boiling heat. After cooling and filtration, the precipitate was washed with toluene (2 × 5 mL) and dried *in vacuo* (yield 0.10 g, 29%). IR (KBr): $\tilde{\nu}$ = 1689(s) (COO), 1571(s) cm⁻¹ (CO); MS (FAB-(+), 70 eV): *m/z* (%): 806 (14) [FeL2a⁺], 199 (100) [bpea⁺ + H]; elemental analysis calcd (%) for C_{77.5}H₈₆Fe₂N₈O₁₂ (1433.25): C 65.0, H 6.1, N 7.8; found: C 65.2, H 6.1, N 7.8.

[Fe₂L2a(bppa)₂]·**2.5 DMF (10**·**2.5 DMF):** A solution of [Fe₂L2a(MeOH)₄] (0.11 g, 0.18 mmol) and bppa (0.47 g, 2.35 mmol) in DMF (15 mL) was heated to reflux for 1 h. After cooling to room temperature, the black microcrystalline precipitate was filtered off, washed with diethyl ether (2 × 5 mL) and dried *in vacuo* (yield 0.09 g, 59%). Elemental analysis calcd (%) for C_{67.5}H_{83.5}Fe₂N_{10.5}O_{14.5} (1385.63): C 58.5, H 6.1, N 10.6; found: C 58.3, H 6.0, N 10.6.

[Fe₂L2b(bipy)₂]·**1.5 DMF:** A suspension of [Fe₂L2b(MeOH)₄] (0.14 g, 0.17 mmol) and bipy (0.53 g, 3.44 mmol) in DMF (20 mL) was heated to reflux for 3 h. The formation of a light brown precipitate was observed in the boiling heat. After cooling and filtration, the precipitate was washed with diethyl ether (2 × 5 mL) and dried *in vacuo* (yield 0.07 g, 36%). IR (KBr): $\tilde{\nu}$ = 1640(s) (CO), 1563(s) cm⁻¹ (CO); MS (FAB-(+), 70 eV): *m/z* (%): 686 (10) [FeL2b⁺], 157 (35) [bipy⁺ + H], 154 (100), 136 (68); elemental analysis calcd (%) for C₅₆H₆₀Fe₂N₁₀O₁₀ (1144.82): C 58.7, H 5.3, N 12.2; found: C 58.3, H 5.3, N 11.9.

[Fe₂L2b(bipy)₂]·**1.5 ACN (11**·**1.5 ACN):** A suspension of [Fe₂L2b(MeOH)₄] (0.35 g, 0.61 mmol) and bipy (1.42 g, 9.08 mmol) in ACN (30 mL) was heated to reflux for 4 h. After cooling to room temperature, the black solid was filtered off, washed with diethyl ether (2 × 5 mL) and dried *in vacuo* (yield 0.29 g, 43%). Elemental analysis calcd (%) for C₅₆H_{51.5}Fe₂N_{9.5}O₈ (1097.3): C 61.3, H 4.7, N 12.1; found: C 61.0, H 4.8, N 12.0.

[Fe₂L2b(bpea)₂]·**2 DMF:** A suspension of [Fe₂L2b(MeOH)₄] (0.19 g, 0.23 mmol) and bpea (0.86 g, 4.66 mmol) in DMF (20 mL) was heated to reflux for 3 h. After cooling to room temperature, the yellow ochre precipitate was filtered off, washed with diethyl ether (2 × 5 mL) and dried *in vacuo* (yield 0.09 g, 33%). IR (KBr): $\tilde{\nu}$ = 1641(s) (CO), 1564(s) cm⁻¹ (CO); MS (FAB-(+), 70 eV): *m/z* (%): 686 (2) [FeL2b⁺], 185 (19) [bpea⁺ + H], 154 (100), 136

(65); elemental analysis calcd (%) for $C_{60}H_{68}Fe_2N_{10}O_{10}$ (1200.93): C 60.0, H 5.7, N 11.7; found: C 58.5, H 5.8, N 11.5.

[Fe₂L2b(bpea)]₂·1.5 ACN (12·1.5 ACN): A suspension of [Fe₂L2b(MeOH)₄] (0.24 g, 0.42 mmol) and bpea (1.15 g, 6.23 mmol) in ACN (30 mL) was heated to reflux for 4 h. After cooling to room temperature, the black solid was filtered off, washed with diethyl ether (2 × 5 mL) and dried *in vacuo* (yield 0.37 g, 79%). Elemental analysis calcd (%) for $C_{57}H_{58.5}Fe_2N_{9.5}O_8$ (1116.3): C 61.4, H 5.3, N 11.9; found: C 62.1, H 5.4, N 11.9.

[FeL3a(pina)] (13): A solution of [FeL3a(MeOH)₂] (0.55 g, 1.09 mmol) and pina (1.08 g, 5.43 mmol) in methanol (45 mL) was heated to reflux for 1 h. The formation of a dark violet precipitate was observed in the boiling heat. After cooling and filtration, the precipitate was washed with methanol (2 × 5 mL) and dried *in vacuo* (yield: 0.51 g, 74%). IR (KBr): $\tilde{\nu} = 3232(w)$ (NH), 1688(s) (COO), 1569(s) cm^{-1} (CO); MS (DEI-(+), 70 eV): m/z (%): 442 (100) [FeL3a⁺], 199 (48) [pina⁺], 106 (43); elemental analysis calcd (%) for $C_{31}H_{31}FeN_5O_7$ (641.45): C 58.0, H 4.9, N 10.9; found: C 57.7, H 4.9, N 10.8.

[FeL3a(pina)]·0.5 MeOH (13·0.5 MeOH): Violet crystals of sufficient quality for X-ray analysis were obtained by slow diffusion techniques of [FeL3a(MeOH)₂] (0.12 g, 0.23 mmol) and pina (0.23 g, 1.18 mmol) in methanol solution after two weeks. Elemental analysis calcd (%) for $C_{31.5}H_{33}FeN_5O_{7.5}$ (657.48): C 57.5, H 5.1, N 10.7; found: C 57.6, H 4.9, N 10.8.

[FeL3b(pina)] (14·0.5 MeOH): A solution of [FeL3b(MeOH)₂] (0.35 g, 0.78 mmol) and pina (0.78 g, 3.92 mmol) in methanol (30 mL) was heated to reflux for 1 h. The formation of a precipitate was observed in the boiling heat. After cooling and filtration 14·0.5 MeOH was obtained as dark violet microcrystalline solid that was washed with methanol (2 × 5 mL) and dried *in vacuo* (yield: 0.35 g, 77%). IR (KBr): $\tilde{\nu} = 3229(w)$ (NH), 1687(m) (CO), 1647(s) (CO), 1560(vs) cm^{-1} (CO); MS (DEI-(+), 70 eV): m/z (%): 382 (70) [FeL3b⁺], 199 (97) [pina⁺], 106 (100); elemental analysis calcd (%) for $C_{29.5}H_{29}FeN_5O_{5.5}$ (597.15): C 59.3, H 4.7, N 11.4; found: C 59.3, H 4.9, N 11.7.

[FeL3b(pina)]_x MeOH (14_x MeOH): Amorphous black crystals of the composition 14_x MeOH were obtained by slow diffusion techniques of [FeL3b(MeOH)₂] (0.11 g, 0.25 mmol) and pina (0.24 g, 1.23 mmol) in methanol solution after two weeks. Elemental

12. Increasing the Hysteresis Width of Iron(II) SCO Compounds in a Crystal Engineering-like Approach

analysis calcd (%) for $C_{30}H_{31}FeN_5O_6$ (613.44): C 58.7, H 5.1, N 11.4; found: C 58.5, H 4.9, N 11.7.

[FeL3b(pina)]·2 MeOH (14·2 MeOH): Violet crystals of sufficient quality for X-ray analysis were obtained by slow diffusion techniques of [FeL3b(MeOH)₂] (0.12 g, 0.27 mmol) and pina (0.27 g, 1.34 mmol) in methanol solution after one week. Elemental analysis calcd (%) for $C_{31}H_{35}FeN_5O_7$ (645.49): C 57.7, H 5.5, N 10.9; found: C 57.4, H 5.0, N 10.8.

12.6 References

- [1] a) H.A. Goodwin, *Coord. Chem. Rev.* **1976**, *18*, 293; b) E. König, *Struct. Bonding (Berlin)* **1991**, *76*, 51; c) P. Gütllich, A. Hauser, H. Spiering, *Angew. Chem. Int. Ed. Engl.* **1994**, *33*, 2024, and references therein; d) P. Gütllich, H.A. Goodwin (Eds.), *Spin Crossover in Transition Metal Compounds I–III, Topics in Current Chemistry*, Springer, Berlin, Heidelberg, New York **2004**; e) J.A. Real, A.B. Gaspar, M.C. Munoz, *Dalton Trans.* **2005**, 2062; f) K. Nakano, N. Suemura, K. Yoneda, S. Kawata, S. Kaizaki, *Dalton Trans.* **2005**, 740; g) O. Sato, J. Tao, Y.-Z. Zhang, *Angew. Chem.* **2007**, *119*, 2200; *Angew. Chem. Int. Ed.* **2007**, *46*, 2152; h) J.A. Kitchen, S. Brooker, *Coord. Chem. Rev.* **2008**, *252*, 2072; i) K.S. Murray, *Eur. J. Inorg. Chem.* **2008**, 3101; k) M.A. Halcrow, *Coord. Chem. Rev.* **2009**, 2059; l) S. Brooker, J.A. Kitchen, *Dalton Trans.* **2009**, 7331; m) C.J. Kepert, *Aust. J. Chem.* **2009**, *62*, 1079; n) K.S. Murray, *Aust. J. Chem.* **2009**, *62*, 1081; o) A.B. Koudriavtsev, W. Linert, *J. Struct. Chem.* **2010**, *51*, 335.
- [2] a) O. Kahn, C. Jay Martinez, *Science* **1998**, *279*, 44; b) O. Kahn, C. Jay, J. Kröber, R. Claude, F. Grolière, *Patent* EP0666561 **1995**; c) J.-F. Létard, O. Nguyen, N. Daro, *Patent* FR0512476 **2005**; d) J.-F. Létard, P. Guionneau, L. Goux-Capes, *Topics in Current Chemistry, Vol. 235* (Eds.: P. Gütllich, H.A. Goodwin), Springer, Wien, New York, **2004**, 221; e) A. Galet, A.B. Gaspar, M.C. Munoz, G.V. Bukin, G. Levchenko, J.A. Real, *Adv. Mater.* **2005**, *17*, 2949.
- [3] Y. Garcia, V. Kseofontov, P. Gütllich, *Hyperfine Interact.* **2002**, *139/140*, 543.
- [4] Y. Garcia, V. Kseofontov, S. Mentior, M.M. Dîrtu, C. Gieck, A. Bhatthacharjee, P. Gütllich, *Chem. Eur. J.* **2008**, *14*, 3745.
- [5] G.R. Desiraju, *Crystal engineering: The design of organic solids*, Elsevier, Amsterdam, **1989**.
- [6] G.R. Desiraju, *J. Chem. Sci.* **2010**, *122*, 667.
- [7] A) O. Ermer, *J. Am. Chem. Soc.* **1988**, *110*, 3747 b) B.F. Hoskins, R. Robson, *J. Am. Chem. Soc.* **1990**, *112*, 1546.

- [8] B. Weber, W. Bauer, J. Obel, *Angew. Chem.* **2008**, *120*, 10252; *Angew. Chem., Int. Ed.* **2008**, *47*, 10098
- [9] B. Weber, E. Kaps, J. Obel, K. Achterhold, F.G. Parak, *Inorg. Chem.* **2008**, *47*, 10779.
- [10] B. Weber, R. Tandon, D. Himsl, *Z. Anorg. Allg. Chem.* **2007**, *633*, 1159; b) b) B. Weber, E. Kaps, C. Desplanches, J.-F. Létard, *Eur. J. Inorg. Chem.* **2008**, 2963.
- [11] W. Bauer, W. Scherer, S. Altmannshofer, B. Weber, *Eur. J. Inorg. Chem.* **2011**, 2803.
- [12] B. Weber, J. Obel, *Z. Anorg. Allg. Chem.* **2009**, *635*, 2474.
- [13] a) B. Weber, E.-G. Jäger, *Eur. J. Inorg. Chem.* **2009**, 465; b) B. Weber, E. Kaps, J. Obel, W. Bauer, *Z. Anorg. Allg. Chem.* **2008**, 1421; c) B. Weber, C. Carbonera, C. Desplanches, J.-F. Létard, *Eur. J. Inorg. Chem.* **2008**, 1589; d) B. Weber, E. Kaps, C. Desplanches, J.-F. Létard, K. Achterhold, F.G. Parak, *Eur. J. Inorg. Chem.* **2008**, 4891; e) W. Bauer, B. Weber, *Inorg. Chim. Acta* **2009**, *362*, 2341; e) B. Weber, E. Kaps, *Heteroatom. Chem.* **2005**, *16*, 391.
- [14] B. Weber, E. Kaps, J. Weigand, C. Carbonera, J.-F. Létard, K. Achterhold, F.G. Parak, *Inorg. Chem.* **2008**, *47*, 487.
- [15] B. Weber, W. Bauer, T. Pfaffeneder, M.M. Dîrtu, A.D. Naik, A. Rotaru, Y. Garcia, *Eur. J. Inorg. Chem.* **2011**, DOI: 10.1002/ejic.201100394.
- [16] A. Altomare, M.C. Burla, G.M. Camalli, G. Cascarano, C. Giacovazzo, A. Guagliardi, A.G.G. Moliterni, G. Polidori, R. Spagna, SIR-97, University of Bari, Bari (Italy), **1997**; *J. Appl. Crystallogr.* **1999**, *32*, 115.
- [17] G.M. Sheldrick, SHELXL-97, University of Göttingen, Göttingen (Germany), **1997**.
- [18] C.K. Johnson, M.N. Burnett, ORTEP-III, Oak-Ridge National Laboratory, Oak-Ridge, TN (USA), **1996**; L.J. Farrugia, *J. Appl. Crystallogr.* **1997**, *30*, 565.
- [19] E. Keller, SCHAKAL-99, University of Freiburg, Freiburg (Germany), **1999**.
- [20] Team of authors: *Organikum*, Johann Ambrosius Barth Leipzig, Berlin, Heidelberg, **1993**.
- [21] B. Weber, R. Betz, W. Bauer, S. Schlamp, *Z. Anorg. Allg. Chem.* **2011**, *673*, 102.

- [22] a) G. Leibelng, PhD thesis, University of Jena (Germany), **2003**; b) E.-G. Jäger, *Chemistry at the Beginning of the Third Millennium* (Eds.: L. Fabbrizzi, A. Poggi); Springer, Berlin, **2000**, pp. 103.
- [23] E.F. Hasty, T.J. Colburn, D.N. Hendrickson, *Inorg. Chem.* **1973**, *12*, 2414.
- [24] L. Wolf, E.-G. Jäger, *Z. anorg. allg. Chem.* **1966**, *346*, 76.
- [25] E.-G. Jäger, E. Häussler, M. Rudolph, A. Schneider, *Z. Anorg. Allg. Chem.* **1985**, *525*, 67.
- [26] a) J.B. Christensen, *Molecules* **2001**, *6*, 47; b) T.S. Gardner, E. Wenis, J. Lee, *J. Org. Chem.* **1954**, *19*, 753.

12. Increasing the Hysteresis Width of Iron(II) SCO Compounds in a Crystal Engineering-like Approach

12.7 Supporting Information

Table S1.1. Crystallographic data of 1·3 MeOH and 4·(0.5 bipy)(MeOH). For the structure motive of 9·x MeOH only the crystal date are given..

compound	1·3 MeOH	4·(0.5 bipy) (2 MeOH)	9·x MeOH
formula	C ₃₃ H ₄₂ FeN ₄ O ₁₁	C ₃₅ H ₃₈ FeN ₅ O ₈	
$M_r / \text{g mol}^{-1}$	726.56	712.55	
crystal system	monoclinic	triclinic	orthorhombic
space group	$P2_1/c$	$P\bar{1}$	
$a / \text{Å}$	11.1275(18)	11.1228(9)	13.7279(9)
$b / \text{Å}$	16.408(2)	11.8129(9)	19.5972(13)
$c / \text{Å}$	21.317(3)	13.3170(9)	25.8758(13)
$\alpha / ^\circ$	90	102.269(5)	90
$\beta / ^\circ$	115.206(11)	103.440(4)	90
$\gamma / ^\circ$	90	95.947(4)	90
$V / \text{Å}^3$	3521.5(9)	1641.3(2)	6961.3(7)
Z	4	2	
$\rho / \text{g cm}^{-3}$	1.370	1.442	1.203
μ / mm^{-1}	0.492	0.521	0.481
crystal size	0.23 × 0.07 × 0.03	0.19 × 0.07 × 0.04	0.14 × 0.07 × 0.05
T / K	173(3)	173(2)	293(2)
diffractometer	Oxford XCalibur	KappaCCD	KappaCCD
$\lambda (\text{MoK}\alpha) / \text{Å}$	0.71073	0.71073	0.71073
θ -range / °	4.22–26.14	3.24–25.19	
reflns. collected	12551	10103	
indep. reflns. (R_{int})	5806 (0.0487)	5799 (0.072)	
mean $\sigma(I) / I$	0.1784	0.0993	
reflns. with $I \geq 2\sigma(I)$	2722	3892	
x, y (weighting scheme)	0.0082, 0	0.0558, 4.6271	
parameters	448	474	
restraints	0	31	
$R(F)$ (all data) ^[a]	0.0411 (0.1101)	0.0699 (0.1140)	
$wR(F^2)$ ^[b]	0.0518	0.1853	
$Goof$	0.690	1.064	
shift/error _{max}	0.001	0.000	
max., min. resd. dens. / e Å ⁻³	0.42, -0.38	0.60, -0.73	

[a] $R(F) = \sum ||F_o| - |F_c|| / \sum |F_o|$. [b] $wR(F^2) = [\sum [w(F_o^2 - F_c^2)^2] / \sum w(F_o^2)^2]^{1/2}$, $w = 1 / [\sigma^2(F_o^2) + (aP)^2 + bP]$, where $P = [F_o^2 + 2(F_c^2)] / 3$.

12. Increasing the Hysteresis Width of Iron(II) SCO Compounds in a Crystal Engineering-like Approach

Table S1.2. Crystallographic data of [FeL3a(pina)]·0.5 MeOH (**13**·0.5 MeOH) and [FeL3b(pina)]·2 MeOH (**14**·2 MeOH).

compound	13 ·0.5 MeOH	14 ·2 MeOH
formula	C _{31.44} H _{32.76} FeN ₅ O _{7.44}	C ₃₁ H ₃₅ FeN ₅ O ₇
$M_r / \text{g mol}^{-1}$	655.55	645.49
crystal system	monoclinic	monoclinic
space group	$P2_1/c$	$P2_1/c$
$a / \text{Å}$	12.4271(2)	13.3304(11)
$b / \text{Å}$	13.7853(2)	12.9564(11)
$c / \text{Å}$	20.6941(3)	21.5188(15)
$\alpha / ^\circ$	90	90
$\beta / ^\circ$	117.3780(10)	127.769(5)
$\gamma / ^\circ$	90	90
$V / \text{Å}^3$	3148.05(8)	2937.9(4)
Z	4	4
$\rho / \text{g cm}^{-3}$	1.383	1.459
μ / mm^{-1}	0.535	0.571
crystal size	0.21 × 0.19 × 0.17	0.32 × 0.19 × 0.11
T / K	200(2)	173(2)
diffractometer	KappaCCD	Oxford XCalibur
$\lambda (\text{MoK}\alpha) / \text{Å}$	0.71073	0.71073
θ -range / $^\circ$	3.32–25.35	4.19–25.38
reflns. collected	20881	11924
indep. reflns. (R_{int})	5747 (0.0249)	5286 (0.0391)
mean $\sigma(I) / I$	0.0200	0.0837
reflns. with $I \geq 2\sigma(I)$	5008	3309
x, y (weighting scheme)	0.0202, 6.4748	0.0690, 0
parameters	405	391
restraints	0	24
$R(F)$ (all data) ^[a]	0.0541 (0.0614)	0.0516 (0.0924)
$wR(F^2)$ ^[b]	0.1232	0.1316
$Goof$	1.171	0.960
shift/error _{max}	0.000	0.000
max., min. resd. dens. / e Å^{-3}	0.450, -0.400	1.104, -0.582

[a] $R(F) = \sum ||F_o| - |F_c|| / \sum |F_o|$. [b] $wR(F^2) = [\sum [w(F_o^2 - F_c^2)^2] / \sum w(F_o^2)^2]^{1/2}$, $w = 1 / [\sigma^2(F_o^2) + (aP)^2 + bP]$, where $P = [F_o^2 + 2(F_c^2)] / 3$.

Danksagung

Frau Prof. Dr. Birgit Weber möchte ich für die sehr gute Betreuung (auch bei einer Entfernung von über 200 km) und ihren wissenschaftlichen Ehrgeiz danken, welcher mir das Mitwirken an zahlreichen Publikationen sowie Teilnahmen an nationalen und internationalen Tagungen ermöglichte. Des Weiteren möchte ich mich für die interessante Themenstellung und den gewährten wissenschaftlichen Freiraum bedanken, außerdem für ihr Verständnis und ihre Bemühungen, mir den Abschluss meiner Promotion in München zu gewährleisten.

Den Mitgliedern des Arbeitskreises in München, insbesondere Jarka Obel und Stephan Schlamp, möchte ich für die gute Zusammenarbeit, das angenehme Arbeitsklima und die schöne Zeit danken. Aus dem Arbeitskreis in Bayreuth möchte ich Dr. Peter Thoma für seine mentale Unterstützung danken.

Mein Dank geht auch an alle Mitarbeiter der Analytikabteilung, die unzählige Messungen an meinen Proben durchgeführt haben. Großer Dank gilt auch Dr. Peter Mayer und den Leuten vom Röntgen-Team für ihre Bemühungen beim Aufsetzen meiner Kristalle und alle wichtigen Hinweise zum Lösen von Problemstrukturen: Sandra Albrecht, Anna Filser, Helene Giglmeier, Tobias Kerscher, Phillip Lorenz und Moritz Reichvilser.

Bei Herrn Prof. Dr. Peter Klüfers und seinem gesamten Arbeitskreis möchte ich mich dafür bedanken, dass ich auch als „externes AK-Mitglied“ weiterhin am Geschehen des Arbeitskreises teilnehmen durfte.

Ich danke allen Mitgliedern des AK Klüfers des Weiteren für die Unterstützung, die angenehme Atmosphäre, die anregenden fachlichen Diskussionen, die geselligen Runden und die schöne Zeit: Sandra Albrecht, Thorsten Allscher, Richard Betz, PD Dr. Hans-Christian Böttcher, Anna Filser, Natascha Ghaschghaie, Helene Giglmeier, Kathrin Gilg, Philipp Grimminger, David Heß, Lida Holowatyj-den Toom, Sarah Illi, Xaver Kästele, Tobias Kerscher, Leonie Lindner, Phillip Lorenz, Tobias Mayer, Christine Neumann, Maximilian Pfister, Moritz Reichvilser, Felix Roeßner, Johanna Schulten, Thomas Schwarz, Martin Steinborn, Markus Wolf, Xaver Wurzenberger, Anna Zangl.

Ich danke auch meinen Bachelorstudenten und Forschungspraktikanten Rosanna Burford, Tanja Ossiander, Toni Pfaffeneder, Sebastian Thallmair und Sabrina Walser für ihr Interesse und ihre wertvolle Mitarbeit.

Herrn Prof. Dr. T. Fässler von der Fakultät für Chemie der TU München möchte ich für die Möglichkeit zur Mitbenutzung des SQUIDs danken, ebenso Bele Boeddinghaus für die reibungslose Organisation der Messzeiten sowie ihre unerschöpfliche Hilfsbereitschaft bei sämtlichen Problemen.

Herrn Prof. Dr. Yann Garcia von der Université Catholique de Louvain danke ich für die Durchführung der kalorimetrischen Messungen, den wissenschaftlichen Anregungen und den fachlichen Austausch.

Herrn Dr. Klaus Achterhold von der Fakultät für Physik der TU München danke ich für die Messung der Mössbauerproben sowie die gute Zusammenarbeit.

Ein besonderer Dank gilt auch denjenigen, die mir bei der Abfassung dieser Arbeit durch Anregungen und Korrekturlesen zur Seite standen: Tobias Mayer und Stephan Schlamp.

Der größte Dank gebührt jedoch meiner Familie, in besonderem Maße meinen Eltern, denen diese Arbeit gewidmet ist. Ohne Eure bedingungslose Unterstützung, die Aufmunterung und das mir entgegengebrachte Vertrauen wäre das alles nicht möglich gewesen!

Publikationsliste

Wissenschaftliche Publikationen

1. W. Bauer, B. Weber: „Magnetism and Crystal Structure of an N₃O₃ Coordinated Iron(II) Complex“ *Acta Cryst. C* **2008**, C64, m237–m239.
2. B. Weber, E. Kaps, J. Obel, W. Bauer: „Synthesis and Magnetic Properties of new Octahedral Iron(II) Complexes“ *Z. Anorg. Allg. Chem.* **2008**, 634, 1421–1426.
3. B. Weber, W. Bauer, J. Obel: „An Iron(II) Spin Crossover Complex with 70 K wide Thermal Hysteresis Loop due to a 2D Hydrogen Bond Network“ *Angew. Chem. Int. Ed.* **2008**, 47, 10779–10787; *Angew. Chem.* **2008**, 120, 10252–10255.
4. W. Bauer, B. Weber: „X-Ray Structure and Magnetic Properties of Dinuclear and Polymer Iron(II) Complexes“ *Inorg. Chim. Acta* **2009**, 362, 2341–2346.
5. S. Thallmair, W. Bauer, B. Weber: „Strategies Towards the Purposeful Design of Longrange Ferromagnetic Ordering Due to Spin Canting“ *Polyhedron* **2009**, 28, 1796–1801.
6. B. Weber, J. Obel, D. Henner-Vasquez, W. Bauer: „Two new Iron(II) Spin Crossover Complexes with N₄O₂ Coordination Sphere and Spin Transition around Room Temperature“ *Eur. J. Inorg. Chem.* **2009**, 5527–5534.
7. B. Weber, J. Obel, L.-R. Lorenz, W. Bauer, L. Carrella, E. Rentschler: „Control of Exchange Interactions in Trinuclear Complexes based on Orthogonal Magnetic Orbitals“ *Eur. J. Inorg. Chem.* **2009**, 5535–5540.
8. T. Pfaffeneder, W. Bauer, B. Weber: “X-Ray Structure and Magnetic Properties of two new iron(II) 1D Coordination Polymers with Bis(imidazolyle)methane as bridging ligand” *Z. Anorg. Allg. Chem.* **2010**, 636, 183–187.
9. W. Bauer, T. Ossiander, B. Weber: “A Promising New Schiff Base-like Ligand for the Synthesis of Octahedral Iron(II) Spin Crossover Complexes” *Z. Naturforsch. B* **2010**, 65, 323–328.
10. B. Weber, R. Betz, W. Bauer, S. Schlamp: “Crystal Structure of Iron(II) Acetate” *Z. Anorg. Allg. Chem.* **2011**, 673, 102–107.

11. T. Pfaffeneder, S. Thallmair, W. Bauer, B. Weber: "Complete and Incomplete Spin Transitions in 1D Chain Iron(II) Compounds" *New J. Chem.* **2011**, 35, 691–700.
12. W. Bauer, W. Scherer, S. Altmannshofer, B. Weber: "Two-Step *versus* One-Step Spin Transitions in Iron(II) 1D Chain Compounds" *Eur. J. Inorg. Chem.* **2011**, 2803–2818.
13. W. Bauer, T. Pfaffeneder, K. Achterhold, B. Weber: "Complete Two-Step Spin-Transition in a 1D Chain Iron(II) Complex with 110 K wide Intermediate Plateau" *Eur. J. Inorg. Chem.* **2011**, DOI: 10.1002/ejic.201100224.
14. B. Weber, W. Bauer, T. Pfaffeneder, M.M. Dîrtu, A.D. Naik, A. Rotaru, Y. Garcia: "Influence of Hydrogen Bonding on the Hysteresis Width in Iron(II) Spin Crossover Complexes" *Eur. J. Inorg. Chem.* **2011**, DOI: 10.1002/ejic.201100394.

Vorträge

1. „Spin Crossover an Eisen(II)-Koordinationspolymeren – Synthese und Modelle“, 7. Koordinationschemie-Treffen, Universität Stuttgart, Stuttgart, Deutschland, 27.02.–01.03.2011. Ausgezeichnet als bester Vortrag.

Beiträge zu nationalen und internationalen Konferenzen

1. B. Weber, E. Kaps, W. Bauer: „New Iron(II) Spin Crossover Complexes—About the Influence of Covalent Linkers on Cooperative Interactions“, 11th International Conference on Molecule-based Magnets, ICMM 2008, Florenz, Italien, 20.09.–24.09.2008. Ausgezeichnet als bestes Poster.
2. W. Bauer, B. Weber: „New Iron(II) Spin Crossover Coordination Polymers“, 14. Vortragstagung der Wöhler-Vereinigung für Anorganische Chemie, München/Garching, Deutschland, 08.10.–10.10.2008.
3. W. Bauer, B. Weber: „Synthesis of New Iron(II) Spin Crossover Polymers“, Synthesefest 2009, München/Großhadern, Deutschland, 17.03.–18.03.2009.
4. B. Weber, W. Bauer: „Iron(II) Spin Crossover Complexes—Molecular Switches with Memory Effect“, 44th EUCHEM Conference on Stereochemistry, Bürgenstock/Brunnen, Schweiz, 17.05.–22.05.2009.

5. W. Bauer, B. Weber: „Mössbauer Spectroscopy on Iron(II) Spin Crossover Coordination Polymers”, International Conference on the Application of the Mössbauer Effect, ICAME 2009, Wien, Österreich, 19.07.–24.07.2009.

Lebenslauf

Name	Wolfgang Bauer
Geburtsdatum	31.07.1981
Geburtsort	Landsberg am Lech
Staatsangehörigkeit	deutsch

Berufserfahrung

seit 04/2008	Wissenschaftlicher Angestellter am Department Chemie und Biochemie der LMU München
--------------	--

Hochschulausbildung

seit 04/2008	Anfertigung der vorliegenden Dissertation unter Anleitung von Prof. Dr. B. Weber
09/2007–03/2008	Diplomarbeit unter Anleitung von Prof. Dr. B. Weber Abschluss: Diplom-Chemiker Univ.
10/2004–09/2007	LMU München Hauptstudium im Fach Chemie
10/2002–10/2004	LMU München Grundstudium in den Fächern Chemie und Biochemie

Wehrdienst

10/2001–09/2002	Grundwehrdienst und freiwillig verlängerter Wehrdienst
-----------------	--

Schulbildung

09/1991–06/2001	Ignaz-Kögler-Gymnasium/Landsberg am Lech Leistungskurse: Chemie, Wirtschaft Abschluss: Allgemeine Hochschulreife
-----------------	--

Preise und Auszeichnungen

10/2009	Preis der Dr. Klaus Römer Stiftung
---------	------------------------------------